5-1-2016

EPISODIC UPLIFT OF THE ROCKY MOUNTAINS: EVIDENCE FROM U-PB DETRITAL ZIRCON GEOCHRONOLOGY AND LOW-TEMPERATURE THERMOCHRONOLOGY WITH A CHAPTER ON USING MOBILE TECHNOLOGY FOR GEOSCIENCE EDUCATION

Maria Magdalena Donahue

Maria Magdalena Sandoval Donahue
Candidate

Earth & Planetary Sciences
Department

This dissertation is approved, and it is acceptable in quality and form for publication:

Approved by the Dissertation Committee:

Dr. Karl E. Karlstrom , Chairperson

Dr. Laura Crossey

Dr. Gary Weissmann

Dr. Louis Scuderi

Dr. Shari Kelley

EPISODIC UPLIFT OF THE ROCKY MOUNTAINS:

EVIDENCE FROM U-PB DETRITAL ZIRCON GEOCHRONOLOGY AND

LOW-TEMPERATURE THERMOCHRONOLOGY

WITH A CHAPTER ON

USING MOBILE TECHNOLOGY FOR GEOSCIENCE EDUCATION

by

MARIA MAGDALENA SANDOVAL DONAHUE

B.S. Geological Sciences, University of Oregon, 2005
B.S. Fine Arts, University of Oregon, 2005
M.S. Earth & Planetary Sciences, University of New Mexico, 2007

DISSERTATION

Submitted in partial Fulfillment of the
Requirements for the Degree of

Doctor of Philosophy
Earth & Planetary Sciences

The University of New Mexico
Albuquerque, New Mexico

May 2016

DEDICATION

To my husband, John,

who has encouraged, supported me

who has been my constant inspiration, source of humor,

& true companion and partner in this endeavor.

To our daughters, MariaElena and Penélope,

that one day, you may explore these landscapes yourselves.

ACKNOWLEDGEMENTS

The ideas and research presented in this dissertation is the work of many people. My advisor, Karl Karlstrom, has been a source of inspiration and knowledge, and who was always available to offer guidance, manuscript revision, and generous funding. Karl Karlstrom has been exceptional in his unfailing support for my unique combination of life and academics that includes professional distance running, creative side projects, growing a family in addition to the rigors of academia; for this flexibility in approach, I am forever grateful. My committee members Gary Weissmann, Louis Scuderi and Shair Kelley have provided balance, support, and insight as my education has taken shape. Coauthors Shari Kelley, Mark Pecha, David Gonzales, and Jason Ricketts contributed hugely in field, analytical, and writing efforts. Field work was assisted by friends and colleagues Rachel Price, Kirt Kempter, and John Donahue.

Development and presentation of ideas regarding *Field Play* were supported by Vanessa Svhilla; I thank her for her enthusiastic willingness to discuss interdisciplinary educational ideas.

The Department of Earth & Planetary Sciences generously provided financial support, a setting in which I was able to both take and teach a variety of courses, and find many lasting friendships. The New Mexico Geological Society provided me scholarship funds, for analytical purposes. Additional funding from the Alfred P. Sloan Minority Ph.D. Program, the University of New Mexico Graduate and Professional Association and Office of Graduate Studies, Colorado Geological Society, and many other smaller sources have made this dissertation possible.

Most importantly, I thank my husband John Donahue for his love, inspiration, patience, and partnership in this journey.

EPISODIC UPLIFT OF THE ROCKY MOUNTAINS: EVIDENCE FROM U-PB DETRITAL ZIRCON GEOCHRONOLOGY AND LOW-TEMPERATURE THERMOCHRONOLOGY WITH A CHAPTER ON USING MOBILE TECHNOLOGY FOR GEOSCIENCE EDUCATION

By

Maria Magdalena Sandoval Donahue

B.S. Geological Sciences, University of Oregon, 2005

B.S. Fine Arts, University of Oregon, 2005

M.S. Earth & Planetary Sciences, University of New Mexico, 2007

Ph.D. Earth & Planetary Sciences, University of New Mexico, 2016

ABSTRACT

The timing and processes of development of the high topography and high relief of the southern Rocky Mountains of Wyoming, Colorado and New Mexico has been controversial for over a hundred years. The Mesozoic and Paleozoic rocks in the region formed a 3-4 km thick sub-horizontal stratigraphy that resided at elevations of zero to minus 4 km at the end of the Cretaceous. These units have been differentially uplifted/subsided and are presently at elevations of -10 to 4 km elevations, and have been eroded from above the core of many Precambrian basement cored uplifts exposed in > 4 km peaks.

This study applies several different methodologies towards understanding the timing and relative importance of the events that uplifted and shaped the Rocky Mountains. These studies include incision studies (Chapter 1), detrital zircon analysis of Cenozoic fluvial deposits resting on the "Rocky Mountain Erosion Surface (Chapter 2), and low temperature apatite fission track (AFT) and U-Th/He (AHe) low temperature thermochronology to look at differential cooling histories across the Rockies (Chapter 3). Chapter 4 investigates a project in which I designed and deployed a mobile device application for enhancing the traditional geoscience field education and research experience.

Incision studies (Chapter 1) investigated the timing and rate of incision of the Black Canyon of the Gunnison by the Gunnison River. Canyon geometry is shaped by a headward-migrating knickzone presently located within the Painted Wall section of the Black Canyon. Average bedrock incision rates over the last 0.64 Ma surrounding the knickpoint vary from 150 m/Ma (downstream), to 400-550 m/Ma (within), to 90-95 m/Ma (upstream), suggesting it is a transient feature. Lava Creek B ash constrains strath terraces along a paleo-profile of the river. Within the paleo-Bostwick River tributary, we determine an incision rate of 400-550 m/Ma, reflecting incision at 2-3 times regional incision rates. We interpret this to be incision response to a headward-migrating wave of transient incision, potentially initiated by downstream base level fall during abandonment of Unaweep Canyon at about 1 Ma. Rate extrapolation indicates that the ~700 m depth of Black Canyon has been eroded since 1.3 – 1.75 Ma. The Black Canyon knickpoint overlies a strong gradient between low velocity mantle under the Colorado Rockies and higher velocity mantle of the Colorado Plateau. We interpret drainage

reorganization and transient incision of both the Gunnison and upper Colorado River systems to be responding to mantle-driven epeirogenic uplift of the southern Rockies in the last 10 Ma.

This study (Chapter 2) investigates the timing of erosion and deposition of several fragmented and little-understood conglomerate and sedimentary units, which are then used to better understand the timing of formation of the enigmatic Rocky Mountain Erosion Surface. Detrital zircon studies reclassify the Telluride Conglomerate and Blanco Basin Formation as being of Oligocene age, with maximum depositional ages of 30±3 Ma. This requires new understanding of the uplift of the San Juan Mountain regions, as we interpret these units to be the conglomeratic/sedimentary response to pre-volcanic epeirogenic doming and unroofing. This study also expands into New Mexico to investigate the depositional timing of the Paleocene-Eocene age McDermott, Galisteo and Baca Formations, and the Oligocene-age El Rito Formation and Ritito Conglomerate; each of these units rests upon the diachronous Rocky Mountain Erosion Surface and grades upward into volcanic deposits; these units are interpreted to be a sedimentary record of the multi-stage uplift of the Rocky Mountains. At each age, these units record the repeated process of doming and unroofing of basement rocks accompanying magmatism, deposition of thin gravel-sand sheets above regional unconformities, deposition of voluminous volcaniclastic aprons. This study suggests that relief has increased through time as the Rocky Mountain headwater regions of the fluvial systems that deposited progressively younger units of this study have gained in absolute elevation, while the ultimate base levels have remained the same or very similar.

The third study (Chapter 3) moves to larger scales of both time and space in order to investigate uplift and exhumation histories on the regional scale. This study included a literature review and compilation of all published low-temperature thermochronology data (apatite fission track and apatite (U-Th)/He) (AHe) for the southern Rocky Mountain region and adds new apatite (U-Th)/He data on selected conglomeratic/sedimentary units to both add richness to the data base and to attempt to better constrain Oligocene burial histories. This study reinforces interpretations of a multi-stage uplift history to the Rocky Mountains by identifying regional episodes of rapid cooling that was driven by regional exhumation and differential uplift. Laramide cooling is investigated in compiled AFT and AHe data and age-elevation transects across the region. We notice spatial preservation of Laramide ages in Rocky Mountain thrust uplifts and elevation differences between the base of the Laramide-age AFT partial annealing zone, reinforcing models suggesting that Laramide cooling was driven by thrust uplifts that have not been reheated since uplift. New AHe data show that the Oligocene fluvial deposits were covered by ~1 km of volcaniclastic debris that likely extended westward onto the Colorado Plateau, refining understanding of the geometry and extent of the San Juan volcaniclastic apron. A delay of ~10 Ma between Oligocene magmatism and regional cooling through the 110-50ºC (AFT-AHe system) implies that post-Oligocene denudation was driven by erosional denudation following Oligocene surface uplift. Case studies highlight the semi-steady cooling of Oligocene plutons from ~30-15 Ma, followed by a potential ~20-10 Ma acceleration in cooling perhaps due to local faulting and/or uplift associated with Rio Grande rifting. Post-10 Ma cooling in areas not associated with the Rio Grande rift is compatible with models that incorporate

regional integration of the Colorado River and Rio Grande to cause differential incision and localized rapid cooling.

The fourth study highlights a project called Field Play. Our current human interaction with these landscapes is also of importance. The communication of science and education of Rockies both academic and public populations is of great importance as we have unprecedented access to information and rapidly evolving digital technologies. This project utilizes mobile technologies (smartphones, tablets) to augment the field experience. The goal of this project is to create a personalized, scalable and interactive educational learning environment which facilitates user exploration and access to robust geologic information. This project was featured in the New Mexico Geological Society's 2014 Fall Field Conference, as well as being used in my own teaching of introductory environmental science classes. This project is ongoing.

TABLE OF CONTENTS

LIST OF FIGURES

Chapter 1

Chapter 2

Chapter 3

LIST OF TABLES

Chapter 2

Chapter 3

INTRODUCTION

This dissertation is divided into four chapters, each using a different analytical technique and methodology to understand the tectonic and geomorphic evolution of topography in the southern Rocky Mountains. The final chapter discusses an innovative project that incorporates mobile technology into to field-based geoscience education. Each of the first three chapters are intended to be coauthored journal articles. Each of these chapters is written to stand alone but each addresses topics of tectonics, geomorphology, and geochronology within the Rocky Mountains; thus, there is some minor - though necessary - redundancy in geologic background and associated reference materials between chapters. Major funding sources for each of these projects are noted in the chapter.

The first chapter builds on work begun in my M.S. studies (University of New Mexico, 2007). This dissertation publication added significantly to the MS work by incorporating new geochronologic and tephrachronologic analytical work and revision of geophysical imaging. Field mapping and sampling was conducted with coauthors Karl Karlstrom and Andres Aslan. Cosmogenic burial geochronological work was conducted at the Purdue University PRIME laboratory under the direction of coauthor Darryl Granger and with the consultation of coauthor Andrew Darling. Tephrachronologic work was conducted at the United States Geological Survey laboratory under the guidance of coauthor Elmira Wan. Geophysical analysis was conducted by coauthor Steven Hansen (University of New Mexico).This paper was published in the journal Geosphere in 2013.

Chapter two, focusing on the timing of erosion and deposition of conglomeratic and sedimentary units in the San Juan Mountains and in north-central New Mexico, is a multi-disciplinary approach to better constraining erosion, deposition, and the timing of the formation of the regional Rocky Mountain Erosion Surface. The present draft of this manuscript is being reviewed by coauthors and will be submitted to journal Geosphere or Lithosphere this fall 2015, pending coauthor comments. This study builds on extensive work done in the San Juan Basin and Rio Grande rift areas, adding a new dataset: detrital zircon data done in the context of sedimentology analysis of units. As this work was evolving, I became aware of new paleo-botanical studies and paleoelevation interpretations and these were incorporated along with addition of Stephanie Zaborac-Reed as coauthor. This study involved extensive field sampling, done by Maria Magdalena Sandoval Donahue, her committee members, and coauthors. Original investigation of the Telluride Conglomerate was undertaken by coauthor David Gonzales (Fort Lewis College, CO), his colleagues and undergraduate students, especially the undergradiuate thesis of C. Harraden (2007). Assessment of Cretaceous to Eocene sedimentary units of the San Juan Basin builds on work begun by coauthor Mark Pecha (University of Arizona, AZ), and utilizes the extensive stratigraphic work done by previous workers, particularly Steven Cather (New Mexico Bureau of Geology). Steve Cather also provided one sample of the Baca Formation that is included in this study. Detrital zircon analyses were conducted by Maria Magdalena Sandoval Donahue at the University of Arizona LaserChron Center (University of Arizona, AZ), under the direction of Mark Pecha. Undergraduate mentee, Rachel Price (University of New Mexico) also assisted with analyses at the LaserChron Center.

Chapter three, focusing on large-scale spatio-temporal patterns in low-temperature thermochronologic cooling histories of the Rocky Mountains, began with an extensive literature review and compilation of published low-temperature thermochronology data. This study builds upon this substantial collation of data by adding new data in areas of sparse thermochrnonologic data (e.g., the San Juan Mountains, northern New Mexico), and investigates large-scale patterns in Cenozoic cooling. Much of the apatite fission track data used in this study is the work of coauthor Shari Kelley (New Mexico Bureau of Geology). One of the important pieces of this study is the combined use of both apatite fission track and apatite (U-Th)/He in locations where both sample types exist. This allows a sample to be tracked from the AFT system at a depth of ~3 km (assuming a ~30ºC/km geotherm) to near-surface exposures using the AHe system to temperatures of~50 ºC, or 1-2 km dept. When then paired with local and regional incision rate data, this enables the tracking of cooling and exhumation of units from depth to surface exposure. This work discusses the important contributions of former students Rebecca Garcia and Joshua Feldman (New Mexico Institute of Mining and Technology (NM Tech)), Ryan McKeon (Lehigh University), and Jason Ricketts (UNM); all of whom were co-advised by Shari Kelley and are coauthors to this chapter. Apatite grains were separated at the University of Arizona LaserChron Center and then picked and packaged by Maria Magdalena Sandoval Donahue under the guidance of Shari Kelly at NM Tech. Samples were irradiated and original sample reports were generated at the University of Arizona's Arizona Radiogenic Helium Dating Laboratory under the direction of Peter Reiners. Thermal modeling was done by Maria Magdalena

Sandoval Donahue using the HeFTY program. This manuscript will be submitted to Geosphere in 2015-2016 pending coauthor review and comments.

Chapter four focuses on innovations in geoscience education in the project Field Play. The goal of this project is to create a unique and personal educational experience for users of all skills and backgrounds while they are immersed in the field. Field Play utilizes mobile technologies to incorporate audio tours, augmented reality, streams multiple data types, and makes them available and interactive on the mobile device. This project was created by John Donahue and myself. Programming and mobile device interface was done by John Donahue; content and user interface was done by myself. This project was partially funded by a research grant from the New Mexico Geological Society to fund the incorporation of this project into the 2014 Fall Field Conference. This app also served as topic for an invited talk at the National Academy of Sciences (2014) and participation in an EarthCube geoscience-computational field conference (2014). Work on this application is ongoing.

Work presented in this dissertation contributes to a better understanding of timing, location, and driving mechanisms behind the elevation gain and shaping of topography of the southern Rocky Mountains, and to document my effort to improve geoscience education and communication via incorporating modern technologies.

CHAPTER 1 INCISION HISTORY OF THE BLACK CANYON OF THE GUNNISON, COLORADO, OVER THE PAST ~1 MA INFERRED FROM DATING OF FLUVIAL GRAVEL DEPOSITS

Magdalena S. Donahue[1], Karlstrom, K.E.[1], Aslan, A. [2], Darling[3], A., Granger, D.[4], Wan, E.[5], and Dickinson, R.[6], Kirby, E.[7]

(Published in Geosphere, 2013)

[1]Department of Earth and Planetary Sciences, Northrop Hall, University of New Mexico, Albuquerque, New Mexico 87131, USA

[2] Physical and Environmental Sciences, 1100 North Avenue, Colorado Mesa University, Grand Junction, Colorado 81501, USA

[3] School of Earth and Space Exploration, Arizona State University, Tempe, Arizona 85287, USA

[4] Department of Earth and Atmospheric Sciences, Purdue University, West Lafayette, Indiana 47907, USA

[5] U.S. Geological Survey, MS 975, Menlo Park, California 94205, USA

[6] Department of Geosciences, University of Arizona, Tucson, Arizona 85718, USA

[7] Department of Geosciences, Pennsylvania State University, 336 Deike Building, University Park, PA, 16802, USA

ABSTRACT

Spatio-temporal variability in fluvial incision rates in bedrock channels provides data regarding uplift and denudation histories of landscapes. The longitudinal profile of the Gunnison River, tributary to the Colorado River, contains a prominent knickzone with 800 m of relief across it within the Black Canyon of the Gunnison. Average bedrock incision rates over the last 0.64 Ma surrounding the knickpoint vary from 150 m/Ma (downstream), to 400-550 m/Ma (within), to 90-95 m/Ma (upstream), suggesting it is a transient feature. Lava Creek B ash constrains strath terraces along a paleo-profile of the river. An isochron cosmogenic burial date in the Paleo Bostwick River of 870±220 ka is consistent with the presence of 0.64 Ma Lava Creek B ash in locally derived, stratigraphically younger sediment. With 350 m of incision since deposition, we determine an incision rate of 400-550 m/Ma, reflecting incision through resistant

basement rock at 2-3 times regional incision rates. Such contrast is interpreted to a wave of transient incision, potentially initiated by downstream base level fall during abandonment of Unaweep Canyon at about 1 Ma. Rate extrapolation indicates that the ~700 m depth of Black Canyon has been eroded since 1.3 – 1.75 Ma. The Black Canyon knickpoint overlies a strong gradient between low velocity mantle under the Colorado Rockies and higher velocity mantle of the Colorado Plateau. We interpret recent reorganization and transient incision of both the Gunnison and upper Colorado River systems to be a response to mantle-driven epeirogenic uplift of the southern Rockies in the last 10 Ma.

INTRODUCTION

Three major orogenic plateaus on Earth include the Tibetan Plateau, Altiplano-Puna Plateau of South America, and the Colorado Plateau of the western United States. In tectonically active regions such as Tibet and the Andes, the complex interactions between dynamically uplifting plateaus and geomorphic evolution are recorded in deep bedrock gorges commonly located at the edges of these uplifted plateaus (Schlidgen et al., 2007). Rivers on the eastern margin of the Tibetan Plateau such as the Yalong, Dadu and Yangtze rivers and tributaries (Kirby et al., 2003, Ouimet et al., 2010; Kirby and Ouimet, 2011) and exiting the Altiplano (Schildgen et al., 2007) are interpreted to be adjusting to tectonic forcings because of the youthfulness of these mountain belts that give rise to the dramatic landscapes. Spectacular bedrock gorges also exist in the western U.S. associated with the Sierra Nevada (House et al., 2001; Ducea et al., 2003), Hells Canyon and associated Wallowa Mountains uplift (Hales et al., 2005), the edge of the Colorado Plateau in Grand Canyon (Karlstrom et al., 2008), and the Rocky

Mountains (Karlstrom et al., 2012). However, in the case of the western U.S., there is ongoing debate about the extent to which these rugged gorges and landscapes are due to active tectonics (Epis and Chapin, 1975; McMillan et al., 2002, 2006; Karlstrom et al., 2008; 2012; Eaton 2009; Aslan et al., 2010) and/or influenced more by climatic forcing and isostatic adjustments to denudation (Gregory and Chase, 1992, 1994; Pederson et al., 2002; Molnar, 2004; Roy et al., 2004, 2009).

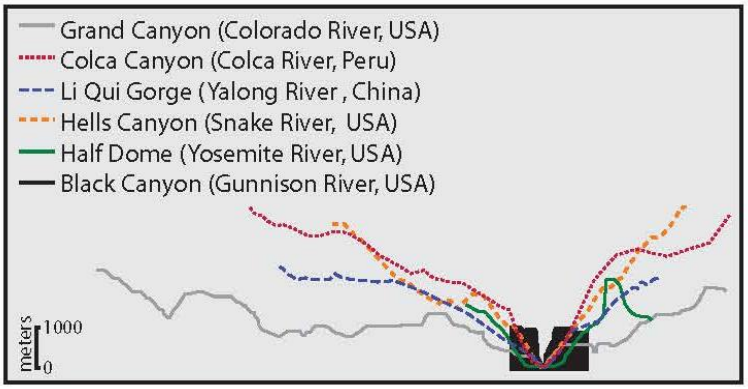

Figure 1-Error! No text of specified style in document.**-1** Canyon comparisons showing high depth:width ratio as compared to many of the world's most iconic bedrock canyons. The Black Canyon of the Gunnison shows remarkable depth and narrowness when compared to other major canyons.

Figure 1 shows comparative profiles of deep bedrock canyons from the areas mentioned above. Compared to other bedrock canyons in the western U.S. and other orogenic plateau, Black Canyon is not the widest or deepest, but its depth-to-width ratio is among the highest of the world's bedrock gorges. In the western U.S., Grand Canyon and Hells Canyon, both carved mainly in the last 5-6 Ma due to mantle-driven uplift (Hales, et al., 2005; Karlstrom et al., 2008) are much wider overall, but their inner bedrock gorges are less deep and less steep-walled. Yosemite, primarily a glacial valley, is a much broader canyon. Incision rates are anomalously high on rivers that exit the three main orogenic plateaus of the world: Tibetan river gorges incise at rates of 300-

500 m/Ma or more (Ouimet et al., 2010; Dortch et al., 2011) and incision in the Bolivian Andes has been measured at 1350 m/Ma (Safran et al., 2005). In the western U.S., Black Canyon incision rates are locally 400-550 m/Ma (Aslan et al., 2008; this paper). These are high incision rates in spite of the fact that the river is carving through resistant Precambrian basement rocks including the unfoliated and sparsely jointed Vernal Mesa granite (Hansen, 1965).

The goals of this paper are to integrate new geomorphic, geochronologic, and geophysical data and methodologies to understand the incision history of Black Canyon of the Gunnison. This work builds on the work of Wallace Hansen (1965, 1967, 1971 and 1987), who pioneered study of many of the geologic and geomorphic relationships explored here. To this geologic context, we bring several new analyses including: 1) analysis of the Gunnison River system longitudinal profiles (e.g., Wobus et al., 2006; Aslan et al., 2008; Darling et al., 2009; Kirby and Whipple, 2012); 2) synthesis of new and previously published river incision rate data on the Gunnison River and its tributaries, 3) sampling and characterization of a key Lava Creek B ash locality for tephrochronologic or confirmation of ages, and 4) mapping and cosmogenic ^{26}Al and ^{10}Be dating of terrace deposits associated with the Gunnison River. Collectively, these new observations and data allow us to evaluate possible driving mechanisms for incision of Black Canyon.

BACKGROUND

Pre-10 Ma origin and history of the Gunnison River system

The Gunnison River follows the crest of the Laramide anticlinal Gunnison Uplift uplift as it flows to the west-northwest across the western slope of the Colorado Rockies

(Hansen, 1965). This Laramide uplift is within the broader Pennsylvanian-age Uncompahgre Uplift of the Ancestral Rockies. During the late Cretaceous, these Precambrian-cored uplifts were mantled by about 2 km of sedimentary rocks that became broadly flexed and uplifted into the Gunnison uplift starting about 70 Ma (Hansen, 1965). There is little record of the paths of early post-Laramide rivers, but modern river courses seem unaffected by Laramide structures (e.g. Uinta, Uncompahgre, Gunnison uplifts), suggesting that river courses meandered across low relief surfaces at higher stratigraphic levels and became superimposed on the uplifts during regional exhumation (e.g. Hansen, 1956; Hunt, 1969; Douglas et al., 2009). In contrast, modern rivers flow around Tertiary laccoliths, suggesting the influence of mid-Tertiary volcanic constructional topography (e.g. San Juan volcanic field, Elk and West Elk laccoliths; Hunt, 1969). Hence, the modern drainage system likely initiated with magmatic and tectonic events associated with the Oligocene ignimbrite flare up (Lipman, 2007) resulting from the detachment of the Farallon flat slab from the base of North America (Humphreys, 2003).

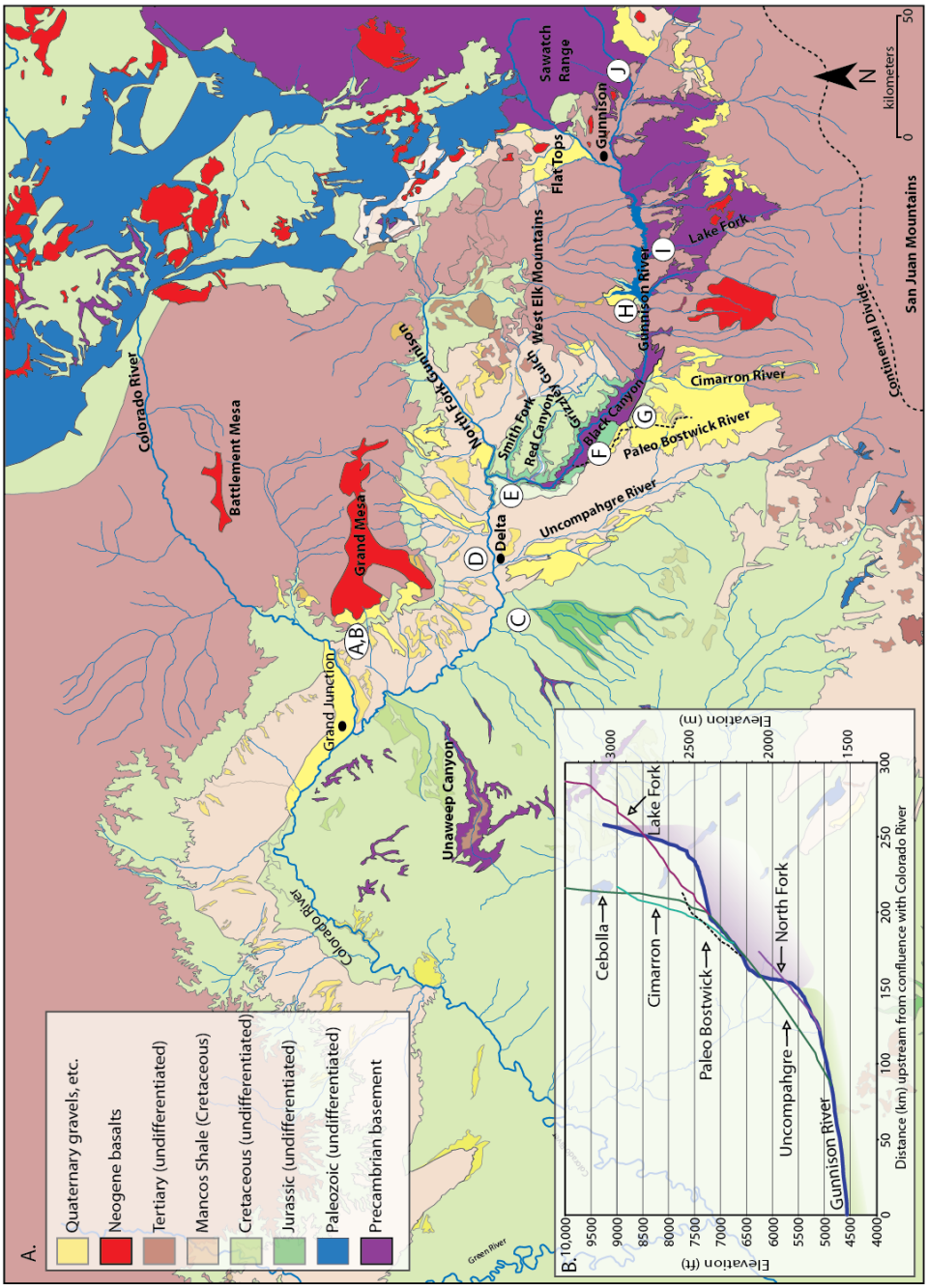

Figure 1-Error! No text of specified style in document.**-2** A. Simplified geologic map of the western slope of the Rocky Mountains showing dated sample (Lava Creek B or cosmogenic burial date) locations (letters), Quaternary faults, and other features discussed in text with letters corresponding to Table 1 and Fig. 3. Nested longitudinal profiles of the Gunnison River system with generalized rock type information (purple= basement along Gunnison river).

A paleo-Gunnison River in about the same location as the modern river emerged in the Oligocene from ca. 35-29 Ma (Hansen, 1965), when drainage was constrained

between volcanic topography of the West Elk Mountains to the north and the San Juan volcanic field to the south (Fig. 2A; Lipman, 2007). Eruptive sheets from these two volcanic centers thicken into an E-W paleovalley in approximately the same location as the modern Gunnison River course, pinning drainage between the two constructional edifices (Hansen, 1965). In particular, of the thickening of the 28.5 Ma Blue Mesa Tuff in the paleovalley axis, with its base contoured by Hansen (1971), indicates the paleo-Gunnison flowed into an E-W oriented valley between these volcanic edifices. Figure 3 shows two paleosurfaces for the Oligocene timeframe: the upper profile, modified from Hansen (1971) shows structure contours at the base of the Oligocene Blue Mesa Tuff dipping upstream (28.5 Ma; Lipman, 2007); the lower profile is created from the elevations of Oligocene West Elk Breccia (29-34 Ma; Coven et al., 1999) at their closest and lowest proximity to the current Gunnison River. Both show that the Oligocene paleo-Gunnison was potentially incising into Precambrian bedrock at modern elevations of 7000- 9000 feet (2134-2744 m).

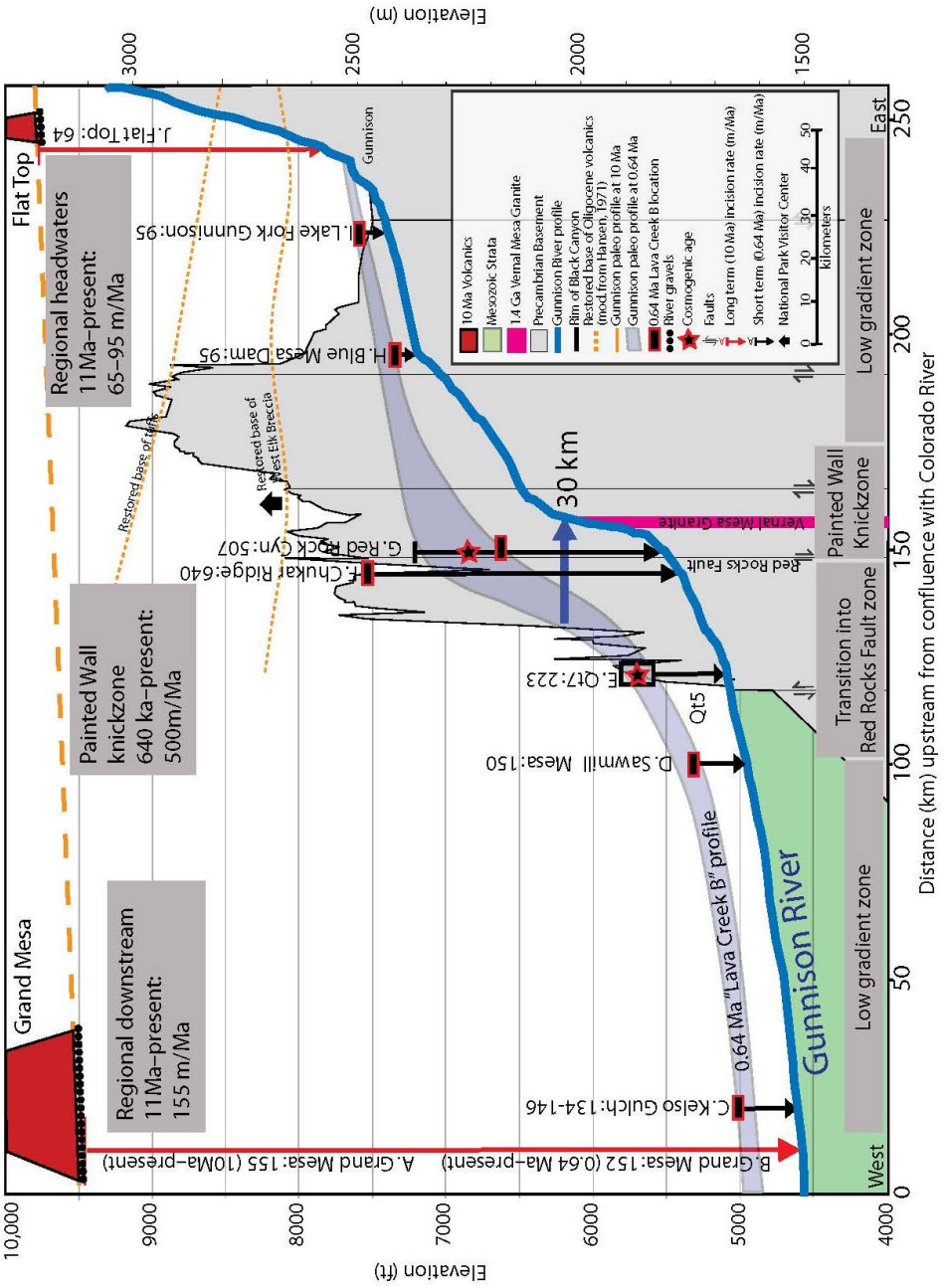

Figure 1-Error! No text of specified style in document.**-3** The modern long profile of the Gunnison River from the confluence with the Colorado River at Grand Junction through the Black Canyon of the Gunnison and into its headwaters (thick blue line) upstream from the town of Gunnison with generalized geology and a composite (black line) of the highest points of the north and south rims of the Black Canyon. Primary geologic units are the Precambrian basement (gray) and 1.4 Ga Vernal Mesa Granite (pink). Ten-to-eleven Ma basalts are shown in solid red, underlain by river gravels and 10-11 Ma paleo river strath (long orange dash). Base of Oligocene volcanics are shown in small orange dash. Black/red stars indicate locations of cosmogenic ages; black/red boxes indicate Lava Creek B locations. Letters correspond to incision data points whose locations are shown in Fig. 2. Blue arrow shows 30km of upstream knickpoint migration in last 0.64 Ma

GUNNISON RIVER PROFILE AND INCISION RATES

Longitudinal River Profiles

The longitudinal profiles of the Gunnison River and its tributaries are shown in Fig. 2B. The modern profile, from headwaters to confluence with the Colorado River, displays a striking convexity associated with the Painted Wall-Chasm View reach of the Black Canyon (Fig. 3). This knickzone is indicative of a disequilibrium river profile (Mackin, 1948) and separates two generally concave portions of the river that have different incision histories. The main features of the Gunnison profile relative to rock type are shown in Fig. 3: 1) a low gradient (1.25 m/km) western reach in erodible Cretaceous and Jurassic rocks, 2) a slight steepening of gradient within basement rocks for ~30 km until the Red Rocks fault zone, 3) a concave river profile inflection marking where the river leaves the trace of the Red Rocks fault zone and transitions into, 4) the high gradient (10 m/km) knickpoint in the Painted Wall reach which is partly within the resistant (sparsely jointed and unfoliated) Vernal Mesa Granite (red stripe in Fig. 3). Above this, the river returns to a lower gradient (5 m/km) above Blue Mesa reservoir while still in Precambrian basement. Finally, the river steepens into the basement-cored Sawatch Range in its high headwaters (as the East River). In summary, while the shallowest reaches are floored by soft rocks (Mancos Shale) and the steepest partly in basement (Vernal Mesa granite), there are both steep and gentle reaches that do not correspond to these rock types. Thus, we infer that the profile geometry is only partly attributable to erodibility of the substrate, in keeping with incision rate evidence that the steepest reach is rapidly incising and hence likely a transient knickpoint.

Modern tributaries to the Gunnison River include the Uncompahgre, North Fork of the Gunnison, Lake Fork of the Gunnison, and Cimarron Rivers and Cebolla Creek

(Figs. 2A, 2B). The Uncompahgre River drains the San Juan Mountains from the vicinity of Ouray, Colorado, and has formed a broad, low gradient canyon in the Cretaceous rocks flanking the Gunnison Uplift. The North Fork of the Gunnison is the major northern tributary to the Gunnison River, and drains the West Elk Mountains. It is of similar slope to the Uncompahgre River; and upon exiting volcanic strata flows largely on Cretaceous bedrock. The Lake Fork of the Gunnison, Cimarron River, and Cebolla Creek are steep tributaries draining the San Juan Mountains. The the Paleo-Bostwick River, also shown on 2A, is defined by a series of high, grass-covered, low-relief parks underlain by fluvial gravels marking the location of this north-flowing paleo-tributary to the Gunnison River that had its confluence with the Black Canyon of the Gunnison in Red Rock Canyon (Hansen, 1987).

Our conceptual framework for drainage evolution in the Black Canyon region utilizes modern drainages as analogs for past drainages. Paleo-tributaries document drainage reorganization due to tectonic (Hansen, 1965; Steven, 1975) and/or stream piracy geomorphic events (Pederson et al., 2002; Schneeflock et al., 2002; Aslan et al., 2008). Here, stream piracy is considered to be the main mechanism for rapid abandonment of river reaches and drainage reorganization. Grizzly Gulch Creek (2A) is presumed to have been abandoned after headwater capture by Iron Creek (Hansen, 1965), while the Paleo-Bostwick River was captured by Cedar Creek of the Uncompahgre system (Figs. 2A, 4A). The modern Lake Fork of the Gunnison and Cimarron Rivers and Cebolla Creek (Fig. 2B), which drain the San Juan volcanic field and have confluences with the Gunnison River above the knickzone within Black Canyon, are used as proxies for pre-knickpoint gradients. We use these gradients to

project the paleo-Bostwick drainage and former gradient of the Gunnison River.

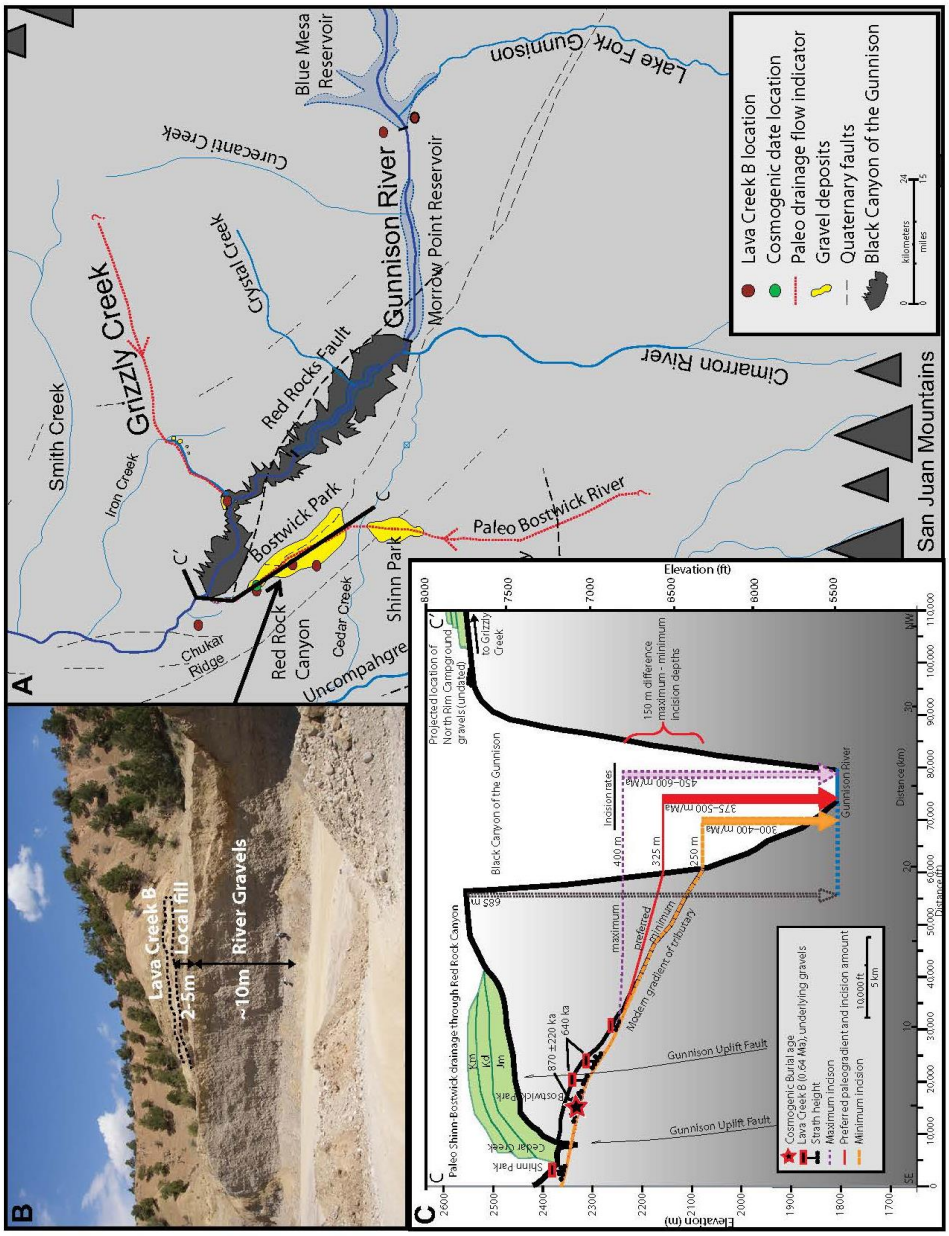

Figure 1-Error! No text of specified style in document.**-4**. A. Generalized map of Black Canyon of the Gunnison region, highlighting Paleo Bostwick and Grizzly Creek rivers, B. River gravel quarry at Bostwick Park, showing gravels overlain by Lava Creek B ash and local fill. C. Cross-sectional view along Paleo Bostwick River through Red Rock Canyon into modern Black Canyon. Possible projections of the tributary into Black Canyon before abandonment of Paleo Bostwick tributary are shown with resulting incision rates, bracketing the potential age of Black Canyon.

Differential Incision Rate Data

Knickpoints and convexities in river profiles are often attributed to relative base-level lowering within the stream system (Gardner, 1983; Burbank and Anderson, 2001; Whipple, 2004), and/or fluvial response to variable rock strengths or erodibility (Burbank and Anderson, 2001; Berlin and Anderson, 2007). Incision rate data across knickpoints provide an avenue to evaluate the extent to which convexities and knickzones may be due to resistant bedrock versus transient incision pulses that may be impeded by hard bedrock. If knickpoints primarily a response of the fluvial profile to incise into resistant bedrock, incision rates should be broadly similar below, within, and above the knickpoint (Gilbert, 1877; Stock and Montgomery, 1999; Phillips et al., 2003; Duvall et al., 2004). Alternatively, in transient knickzones, rates are expected to be highest within the knickzone as the river adjusts and restores towards equilibrium after a change in local base level. Such disequilibrium conditions may be prevalent at the edges of uplifted plateaus or following a change in uplift rate within an active region (Bishop et al., 2005; Goldrick and Bishop, 2007; Whipple, 2004), near a tectonic drop in base-level (Karlstrom et al., 2008), or due to drainage reorganization such as stream capture or even bedrock meander cutoff events at small scales (Finnegan and Dietrich, 2011).

Figure 3 shows the best-constrained Gunnison River region incision rates (vertical arrows) displayed on a longitudinal profile that extends from the confluence with the Colorado River at Grand Junction to the headwaters of the Gunnison River. A summary of incision rates used in paleo-profile reconstruction is listed in Table 1, including previously published as well as new data points (new data points in bold).

TABLE 1. NEW REGIONAL INCISION RATES

Location	Incision rate (m/Ma)	Age of deposit (Ma)	References
Petrie Mesa	**134**	0.64	Sandoval (2007)
North Fork Gunnison	**221**	2.2	Sandoval (2007)
Chukar Ridge	**640**	0.64	Sandoval (2007)
Painted Wall/Red Rock Canyon	**507**	0.64	Sandoval (2007)
Blue Mesa Dam	**95**	0.64	Sandoval (2007)
Lake Fork Gunnison	**90**	0.64	Sandoval (2007)
Flat Top	**55**	10	Sandoval (2007)
Flat Top	64	10	Aslan et al. (2008)
Grand Mesa	142	10	Aslan et al. (2008)
Sawmill Mesa	150	0.64	Darling et al. (2009a, 2009b)

The best-constrained terrace ages are where the 0.64 Ma Lava Creek B ash has been found in association with strath terraces along the Gunnison River and tributaries (Figs 2 and 3). Below the Black Canyon knickzone in the downstream reaches of the Gunnison River, Lava Creek B ash is found on erosional pediments near Grand Junction (Figs. 2 and 3, points A, B), at Kelso Gulch (Figs. 2 and 3, point C) and near the modern river at Sawmill Mesa (Figs. 2 and 3, point D) over the last 0.64 Ma. Incision rates from strath terraces constrained by these ash locations are approximately 130-150 m/Ma, indicating relatively consistent incision throughout this section of the river since ~0.64 Ma.

In contrast, in the upstream portions of the Gunnison River and above the modern knickzone, Lava Creek B ash is found at the Blue Mesa Dam (Figs. 2 and 3, point H) and the Lake Fork of the Gunnison-Gunnison River confluence (Figs. 2 and 3, point I). These two locations give relatively slower incision rates of ~95 m/Ma. The interpretation of these low incision rates is that these reaches of the Gunnison River upstream from the modern knickzone have not yet experienced the base-level fall associated with knickpoint migration.

Incision rates within the Black Canyon knickzone area have been inferred by previous workers (Hansen, 1987; Dethier, 2001; Aslan et al., 2008) to be among the highest rates in the Rockies (Dethier, 2001). Hansen (1987) quoted an incision rate based on projection of the Bostwick paleoriver to where it would have joined the Gunnison River near Red Rocks Canyon (400-500 m/Ma, Figs. 2 and 3, point G and Fig. 4C). His age constraints came from the presence of Lava Creek Bash beds overlying gravels of the Paleo-Bostwick tributary (Hansen, 1987). The combined data led him to infer that Black Canyon has been carved in the last 1-2 Ma. We concur with this conclusion and refine it based on new data presented below. The elevation of the Chukar Ridge Lava Creek B locality (Table 1) provides the highest calculated incision rate in this study (640 m/Ma Figs. 2 and 3, point F). This site is associated with river gravels but is difficult to correlate with other terrace heights.

New Tephrochonology

One of the uncertainties in Hansen's calculation of a 1-2 Ma age of Black Canyon stems from uncertainty of the age of post-abandonment deposits that overlie Bostwick paleo-river gravels in Bostwick Park (Fig. 4A). Dickinson (1956) reported two ashes at different stratigraphic levels in a road cut leading up to the south entrance to Black Canyon (Fig. 5). The upper one was identified as the 0.64 Ma (Lanphere et al., 2002) Yellowstone Lava Creek B ash (Izett and Wilcox, 1985, Hansen, 1987). The lower ash (Fig. 5) was analyzed and reported by Izett (1982) as being similar to the 1.29 Ma Mesa Falls Yellowstone ash (Lanphere et al., 2002), but the correlation was uncertain. Given Hansen's argument that Bostwick paleo-river gravels graded to approximately 350 m down into the depth of the modern Black Canyon, use of the Mesa

Falls age as the minimum age on the gravels led to an inferred rate of 325 m/1.29 Ma= 252 m/Ma necessitating ~2.5 Ma to carve the entire canyon; whereas use of the Lava Creek B age yielded a rate of 507 and a duration of ~1 Ma for carving Black Canyon, assuming steady rates.

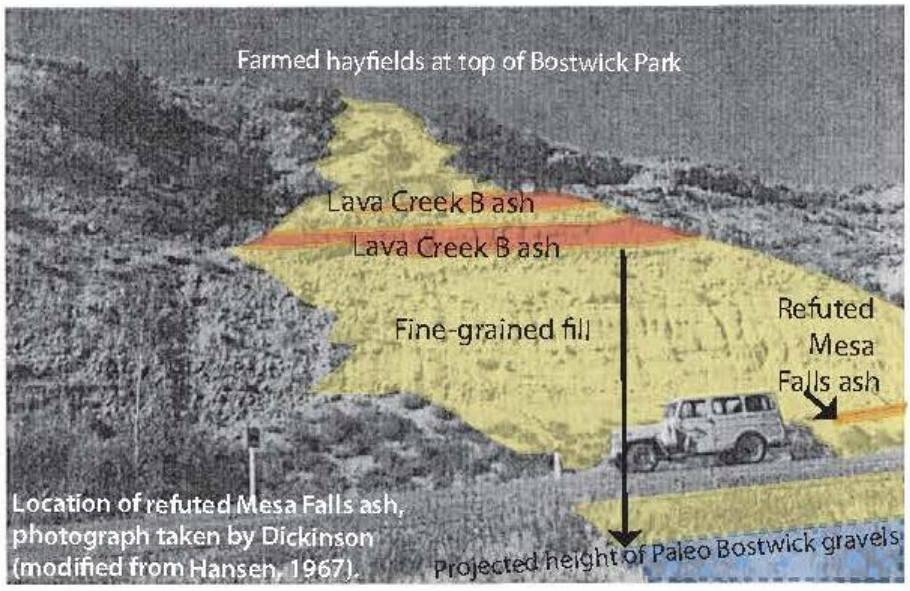

Figure Error! No text of specified style in document.**-5**. Photograph modified from Dickenson (1965) of Lava Creek B and refuted Mesa Falls ash locations at Bostwick Park.

We revisited the site and attempted to resample from the location shown in Fig. 5. Although an extensive excavation was conducted, no ash layer was found in the stratigraphic position of the lower ash noted by Dickinson (1965). Instead, we obtained the original sample (courtesy of Dickinson) and reanalyzed it. Our reanalysis of the Dickinson 'Mesa Falls (?)' ash (Table 2) concludes that while the Mesa Falls correlation is still permissive, there is no positive direct match between the Dickinson ash sample and the Mesa Falls ash. However, there is a positive (>0.95, similarity coefficient) correlation with multiple Lava Creek ash bed samples. The Dickinson sample exhibited a lower iron concentration level that is more similar to Mesa Falls glass shards than

Lava Creek B, as well as the moderate hydration typically seen in older samples. Given that Yellowstone tephra (Huckleberry Ridge, Mesa Falls, and Lava Creek) have overlapping chemistries, the original identification as Mesa Falls ash was likely based on these latter characteristics. Although a Mesa Falls correlation remains possible from the geochemical analysis, new field mapping has failed to reveal a marked unconformity in the few meter thick section of fill between the ashes, therefore, the correlation to Lava Creek B ash is supported by stratigraphic context (Aslan et al., 2008). Thus, based on the new analysis (Table 2) and detailed work on the geology at Bostwick Park that suggest post-abandonment deposits are likely close in age to the gravels (Sandoval, 2007; Aslan et al., 2008), we prefer the 0.64 Ma age as the a minimum age on the Paleo-Bostwick river gravels. We suggest these ashes represent differential erosion and re-deposition of reworked Lava Creek B tephra following abandonment of the Paleo-Bostwick paleovalley.

TABLE 2. U.S. GEOLOGICAL SURVEY (USGS) LABORATORY ANALYSIS OF DICKINSON (1965) BOSTWICK PARK TEPHRA

Sample	Description	Interpretation
K06C03 (suspected Lava Creek B ash)	~95% angular to subangular, lightly to heavily coated (carbonate, organics, clay, and FeO), mostly solid, platy or bw/bwj glass shards	This sample also matches well with a number of the USGS Lab Lava Creek B ash (0.639 Ma, Ar-Ar, sanidine) reference samples. Of specific interest to the investigation could be SL-MM-06-91 (Pop 2), a Lava Creek B ash sample collected by Mike Machette (USGS, Denver, Colorado) from a locality northeast of San Luis, Colorado. In comparison to K06C03, the iron level of SL-MM-06-91 (Pop 2) is slightly higher, and the sodium level is somewhat lower. But the correlation coefficient is still very good at γ 0.98, with and without alkalies.

Note: bw/bwj—bubble walled/bubble walled junction.

Cosmogenic nuclide dating

To further constrain the age of Bostwick gravels and attain additional new incision rate data, we used cosmogenic nuclides (^{10}Be and ^{26}Al) to determine the depositional ages of gravels sampled from two locations: 1) Bostwick quarry and 2) terrace Qt7 (223 m above modern river level) at the North Fork of the Gunnison-Gunnison River confluence (see Figs. 2 and 4 for locations). We used the isochron

burial dating method (Balco and Rovey, 2008) at Bostwick Quarry, and profile dating at terrace Qt7.

Bostwick Quarry The depositional history of these gravels was described by Hansen (1987), Sandoval (2007) and Aslan et al. (2008). About 10 m of coarse gravel was deposited in this Gunnison River paleo-tributary, which had its confluence with the Gunnison through Red Rock Canyon (Fig. 4A). Headward cutting of Cedar Creek, a tributary to Uncompahgre River, then captured the paleo-Bostwick drainage, leaving a largely abandoned canyon with an underfit, ephemeral stream draining through Red Rock Canyon into the Black Canyon. Abandonment triggered the relatively rapid infilling of the canyon with 5-15 m of locally derived "yellow" alluvium that includes proximal deposits composed of reworked Mancos Shale from nearby hill slopes. As mentioned above, the locally derived sediment is interfingered with lenses of reworked Lava Creek B ash that directly overlie the gravel deposit at Bostwick Quarry (Fig. 4B), constraining Bostwick river gravels to older than 0.64 Ma (Aslan et al., 2008).

Cosmogenic nuclide burial dating provides a more direct constraint on the age of these gravels. We obtained a sample from the base of a >10 m thick gravel exposure in the recently excavated Bostwick quarry (Fig. 4B), approximately 1 km east of the road outcrops shown in Fig. 5. Significant shielding here allows the burial age to be interpreted as an accurate (though imprecise) depositional age of the gravels.

The cosmogenic burial analysis was from four quartzite clasts that were collected from the base of the Quarry face approximately 10 meters stratigraphically below Lava Creek B ash. Post-burial shielding from cosmic radiation was thus at least 10 m (thickness of the gravel) and post-abandonment deposits added an additional 3 m of

post-0.64 Ma shielding. Cosmogenic ^{10}Be and ^{26}Al were determined for each clast and analyzed using the isochron method for burial dating (Balco and Rovey, 2008). This method is best executed with clasts collected from the same stratigraphic horizon such that each clast has the same post-burial cosmogenic production history due to similar depth of burial. Each clast has a high probability of having experienced a different exhumation and transport history prior to deposition than the other clasts, such that the initial concentrations of ^{10}Be and ^{26}Al vary. Evolution of these different initial ratios due to radioactive decay after deposition forms an isochron which has an age indicated by its slope and post-burial production indicated indirectly by the y-intercept. Since concentrations of ^{10}Be and ^{26}Al need to be corrected for the post-burial production experienced due to spallation reactions and muons at depth, age determination is necessarily an iterative process (Balco and Rovey, 2008). The isochron date for deposition of the gravel (Fig. 5) is constrained primarily by one data point, and could be improved with further analyses. The best-fit line yielded an age of 870 ± 220 ka (Fig. 6; Darling et al., 2012), compatible stratigraphically with both the Lava Creek B ash minimum age for the gravels and field relationships that suggest the gravel to be older but close in age to the Lava Creek B ash. Thus, the time of major depositional activity of Bostwick paleoriver gravels is constrained to between ~0.87 and 0.64 Ma.

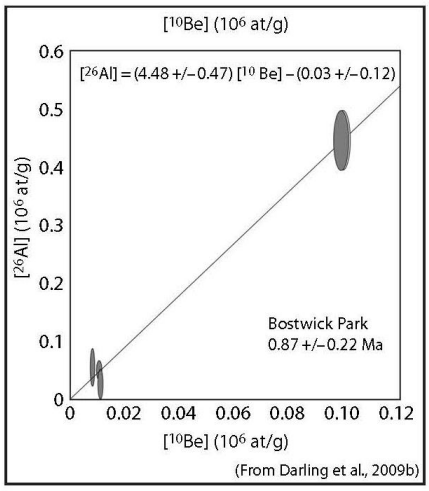

Figure Error! No text of specified style in document.**-6**. Isochron plot of 26Al/10Be data from Darling, et al. (2009) of Bostwick Park quarry.

North Fork of the Gunnison Strath Terraces The North Fork of the Gunnison River is the major northern tributary to the Gunnison River, and joins the Gunnison River below the Black Canyon (Figs. 2 and 7). This tributary junction has migrated down the dip-slope of the underlying Paleo/Mesozoic strata as it has incised, leaving abandoned river drainages (e.g., Smith Fork and Red Canyon) and eleven remnant river terraces abandoned above the present profile (Fig. 7B; Hansen, 1965; Sandoval, 2007). These terrace deposits at the confluence are severely eroded (treads are poorly preserved) and relatively thin (< several meters) implying they represent strath terraces (Sandoval, 2007). The highest terraces are more than 300 m above the modern Gunnison River (Fig. 7B) in this locality. The confluence of the North Fork of the Gunnison with the Gunnison River has apparently maintained its general geometry while the North Fork and the confluence migrated down the dip of the underlying strata and the Cretaceous Dakota escarpment retreated northwards. This is similar to models for

streams “sliding down” the dip slopes of the Uncompahgre Uplift (Aslan, et al., 2008; Darling et al., 2009) and differs from other locations where rivers become entrenched during superposition across basement cored uplifts, as was likely simultaneously occurring on to the east on the Gunnison Uplift (Hansen, 1987). The thickest and most widespread of these deposits, Qt7, with a strath at 223 m above the modern river (Fig. 7B) was chosen for trenching by backhoe and collection of a seven-part vertical profile for cosmogenic profile dating.

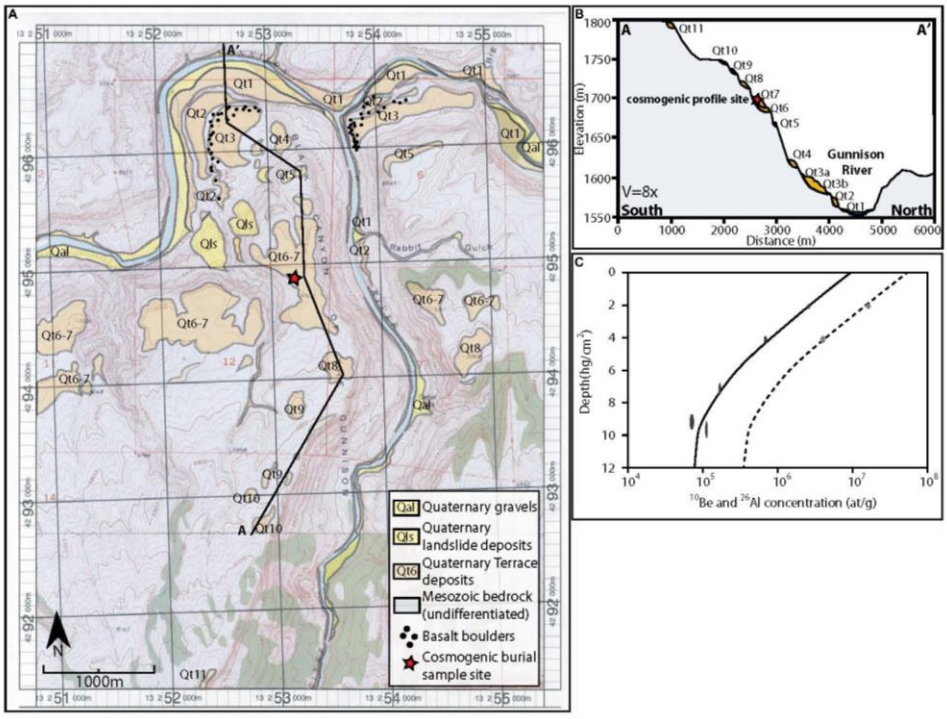

Figure Error! No text of specified style in document.**-7.** A. Simplified geologic map with river terraces at the Gunnison River-North Fork of the Gunnison River confluence, showing Quaternary incision and confluence migration. Red/black star indicate cosmogenic isochron age location. B. Cross sectional view of A-A’ through river terraces. C. Depth vs. concentration plot from Qt7/223: ^{10}Be (solid black line) ^{26}Al (dashed line).

The trench into Qt7/223m terrace was 6.1 m deep; sample depths ranged from 1.4 to 5.6 m. The stratigraphy included an upper 1.1 m of local fine-grained fill overlying pedogenic carbonate atop the gravels. The top of gravel was at 1.4 m depth,

and continued below the base of the excavation, which was limited by the reach of the backhoe. Gravel exposures on the edge of the terrace nearby were approximately 6 m thick suggesting that the bottom of the trench was within 1-2 m of the base of the gravel. The overall stratigraphy seen in the excavation at the confluence is similar to that of Bostwick Quarry, where river gravels are abruptly overlain by fine-grained, yellowish, locally derived colluvium. Five samples consisting of amalgamated gravels or sand were analyzed for ^{10}Be; two of these also yielded meaningful ^{26}Al results. Cosmogenic data are given in Table 3 and Fig. 7C.

TABLE 3. COSMOGENIC NUCLIDE DATA FOR TERRACE QT7/223 M (UTM ZONE 13 253122E, 4295012N)

Sample	Depth (m)	Depth* (g/cm^2)	[^{10}Be]† (10^6 at/g)	[^{26}Al] † (10^6 at/g)
MS-06-18	1.4	205 ± 10	2.635 ± 0.040	15.99 ± 1.05
MS-06-13	2.4	410 ± 20	0.691 ± 0.022	3.95 ± 0.27
MS-06-14	4.0	720 ± 36	0.170 ± 0.003	—
MS-06-15g	4.9	920 ± 46	0.072 ± 0.004	—
MS-06-21g	5.6	970 ± 50	0.112 ± 0.005	—

*Depth calculated for density 1.5 g/cm^2 (0–1.4 m), 1.8 g/cm^2 (1.4–2.75 m), and 1.5 g/cm^2 (>2.75 m).
†^{10}Be and ^{26}Al measured at PRIME Lab, (Purdue University, West Lafayette, Indiana), against standards prepared by Nishiizumi. ^{10}Be was calibrated to values reported in Nishiizumi et al. (2007).

The cosmogenic nuclide data for Qt7 were modeled assuming that the fine-grained overburden has been stable or eroding through time, so that the collection depth of each sample is the shallowest that it has experienced (e.g., Wolkowinski and Granger, 2004). Because each sample was amalgamated from many clasts, they are all assumed to have an identical inherited component at the time of deposition consistent with a condition of steady-state erosion in the source area (Repka et al., 1997). The concentration of cosmogenic *nuclide i* in each sample is calculated using equation (1), where N_i is the concentration of nuclide *i*, P_i is the local production rate, x is depth in cm, t is time since deposition, τ_i is the mean-life of nuclide *i*, E is the terrace erosion rate, ρ is the density of the eroding material (g/cm^3), and L is the penetration length of

secondary cosmic ray neutrons (160 g cm^{-2}). The model is simplified to ignore production by muons, which do not strongly influence the inferred age due to the shallow depth of the profile. While a more complex model including production by muons could be performed (e.g., Granger and Smith, 2000; Hidy et al., 2010), it is not deemed necessary due to the much larger uncertainties in the model associated with terrace erosion..

$$N_i = N_{i,inh} e^{-t/ti} + P_i e^{-x/L} (1/\tau_i + \rho E/L)^{-1} [1 - e^{-(1/ti + rE/L)t}] \quad (1)$$

The model fit to the data is shown in Fig. 7C. The best-fit age is 0.98 ($^{+0.38}/_{-0.07}$) Ma for a local production rate of 12 at/g/yr (^{10}Be) and 82 at/g/yr (^{26}Al).). The knee in the profile is due to the inherited component that dominates at depth but is overprinted by much higher postdepositional production near the surface. The uncertainty in the fit is strongly asymmetric due to the possibility of terrace erosion which increases the model age. The best-fit value for inheritance corresponds to an erosion rate in the source area of 60 m/Ma. The model describes the data well, with a value for reduced χ^2 of 0.85.

DISCUSSION

Knickpoints

Using the model profile age of 980 ka for terrace Qt7 yields an incision rate of 228 (+17/-64) m/Ma. Assuming that the incision rate has been relatively steady, the lower terrace Qt5 (at an elevation of 190 m) probably correlates with the gravels at

Bostwick Quarry and deposition of the Lava Creek B ash at 0.64 Ma. An inferred paleo-profile for this "Lava Creek B" age range is shown as the light purple swath in Fig. 3. This relatively well-constrained paleoprofile mimics the modern river profile and suggests that a steep knickzone existed at 0.64 Ma within but farther west in the Black Canyon, separating low gradient upstream and downstream reaches.

An examination of the relationship of both the modern and the 0.64 Ma knickpoints to changes in bedrock substrate and to the fault-bound Gunnison Uplift supports the hypothesis that the knickpoint is transient, with an upstream propagation rate that has been slowed in the last 0.64 Ma as the knickzone entered basement rocks. The existence of the modern 10 km-long high-gradient reach may be partly explained by the presence of the Vernal Mesa Granite. However, the knickzone extends across and through this resistant rock (Fig. 3), suggesting that bedrock is not the only controlling factor. At 0.64 Ma, the river was just beginning to incise through basement and the top of the steep knickpoint was likely near the Red Rock Canyon confluence. Prior to 0.64 Ma, the knickzone is thought to have moved rapidly through Cretaceous rocks from the Unaweep Canyon area to the Gunnison Uplift (Aslan et al., 2008).

A profile reconstructed from 10 Ma basalts at Grand Mesa and Flat Top Mountain near Almont, Colorado have ancient gravels beneath them (Fig. 3), and suggest that the late Miocene was characterized by a low-relief landscape with an established westward-draining river system. River gravels containing volcanic and basement clasts are found below and incorporated with the basal basalt flows of Grand Mesa (Aslan et al., 2010). Gravels found beneath the ~ 10 Ma Flat Top (north of Gunnison) also contain basement clasts. Grand Mesa and Flat Top Mountain, while

similar in age and in their preservation of gravels from major paleorivers, have very different calculated long-term incision rates. The Grand Mesa basalt flow is 1503 m above the modern Gunnison-Colorado River confluence, while the Flat Top gravels are 639 m above the headwater regions of the Gunnison River. Post-10 Ma incision by the Gunnison and Colorado Rivers in the lower parts of these rivers has removed nearly three times the height of rock from the lower reaches of the Gunnison River, with a regional long term incision rate of 140 m/Ma (Fig. 3, point A; Aslan et al., 2008; Darling et al., 2009). In contrast, the high elevation Rocky Mountain headwater regions of the Gunnison River have been incising through the action of small streams in steep, narrow canyons at 64 m/Ma (Fig. 3, point J) over the same timeframe. The headwaters region is upstream from the modern knickpoint (Fig. 3) and is adjusted to a local base level of the low-gradient upper section of the Gunnison River. This river reach has yet to feel the effects of events that have modified the lower reaches of the river.

Models for drainage evolution

Abandonment of Unaweep Canyon instigating Black Canyon incision:

Unaweep Canyon, a major bedrock gorge now hosting two divergent, underfit streams (Aslan et al., 2008), has been postulated as a possible early path for the Gunnison River as it flowed northwest downstream of the present Black Canyon (Hansen, 1965; Hansen, 1967). The abandonment of Unaweep Canyon at about 1 Ma (Aslan et al., 2008) shows clear evidence of drainage re-organization, probably through stream piracy rerouting the Gunnison River through the Grand Valley. One possibility is that this piracy set-off an incision pulse that is now expressed as the Black Canyon knickzone. Darling et al. (2009) noted that such a transient would have passed rapidly upstream through the weak

Mancos Shale, then more slowly once it encountered Precambrian bedrock of the Gunnison uplift.

Model for mantle processes driving forces driving both drainage reorganization and rapid bedrock incision of Black Canyon Recent tomographic images indicate complex patterns in mantle velocity structure below the Gunnison River (Fig. 8; Karlstrom et al., 2012). Of particular interest, the transition from the low velocity mantle domain beneath the headwaters to higher velocities in the lower reaches of the Gunnison River suggests that buoyant mantle may be driving differential uplift in the Rocky Mountains, and may also be influencing the longitudinal profile of the Gunnison River (Karlstrom et al., 2012). The hypothesis of young uplift in the headwater region of the Gunnison River is supported by apatite fission track and apatite helium cooling ages, which show < 10 Ma AHe cooling ages in the San Juan Mountains to the south (McKeon, 2009) and the West Elk and Elk Ranges to the north (Garcia, 2011) of Black Canyon. This suggests that more than 1 km of material has been eroded off the headwater regions of the Gunnison River in the last 10 Ma. Our hypothesis is that low velocity mantle under these recently exhumed areas may have driven headwater uplift resulting in higher gradients for the Gunnison River, that then facilitated drainage reorganization and upstream knickpoint migration.

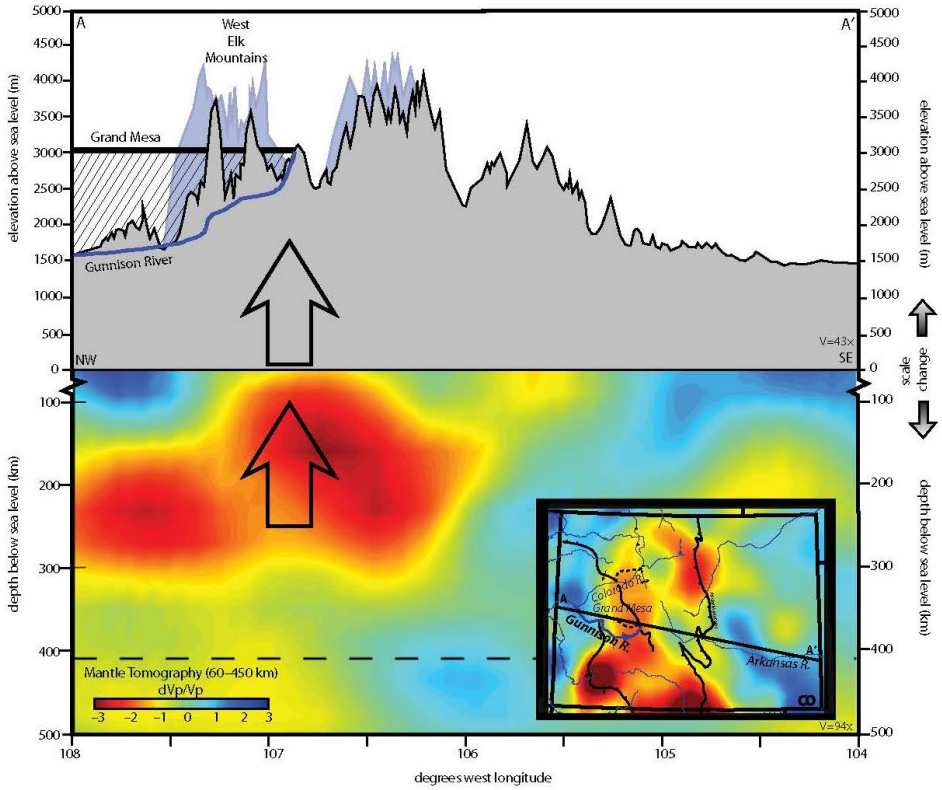

Figure 1-Error! No text of specified style in document.**-8**. Cross sectional view of tomography beneath the general trend of the Gunnison River (A-A' on inset), showing possible influence of buoyant mantle (red areas) affecting topographic behavior in the Gunnison region. Blue line represents the Gunnison River longitudinal profile from headwaters to confluence with the Colorado River. Thick black line is at the elevation of Grand Mesa (black oval on inset), hatched area indicates material removed through erosion since the eruption of Grand Mesa basalts.

An important and often overlooked component of the uplift story involves flexural isostatic rebound driven by erosional denudation of the Rocky Mountain-Colorado Plateau region. Lazear et al. (2013) present calculations of isostatically driven rebound applied to the Gunnison River region that suggest that independent of any tectonic surface uplift, there has been about 200 meters of differential isostatically driven rock uplift of the Gunnison knickpoint region relative to both the Colorado-Gunnison confluence and the headwater regions, including Grand Mesa.

CONCLUSIONS

Our data suggest a very young river system responding to multiple forcings, including downstream drainage reorganization, differential isostatic rock uplift, and possible mantle-driven headwater uplift. New data conclusions are as follows.

***1) Differential incision across a transient knickzone*:** Incision rates downstream of the modern knickpoint are higher (130-150 m/Ma over 0.64 Ma and 140m/Ma over 10 Ma) in comparison to upstream rates (90-100 m/Ma over 0.64 Ma and ~60 m/Ma over 10 Ma). Incision rates within the 10 km-long Painted Wall knickzone are strikingly higher at ~500 m/Ma over 0.64 Ma (Fig. 3, Table 1). This variation in incision rate within a relatively small lateral distance (100 km) and within the hardest rock in the region (Fig. 3) argues that this feature is the transient expression of a stream system adjusting to a downstream drainage reorganization and related regional base level fall/ headwater uplift. Our model also indicates approximately 30 km of upstream knickpoint migration through basement over the past 0.64 Ma, and about 30 km of knickpoint migration from 1.0-0.64 Ma through soft Cretaceous rock. This documents the importance of bedrock erodibility on knickpoint propagation rates.

2) Incision history of Black Canyon of the Gunnison: Projection of the 0.64 Ma Lava Creek B-associated river gravels in the abandoned paleo-Bostwick tributary to its intersection with the Gunnison at Red Canyon is presently the best constraint on the age and rate of incision of Black Canyon. At this location, approximately 350 m of the roughly 700 m total depth of the Black Canyon has been incised in the last 0.64 – 0.87 Ma. We use the Cimarron gradient as a proxy for the paleo-Bostwick to extrapolate preserved and dated straths to their inferred confluence with the river at 350 m above the river. The result is that over the past 0.87-0.64 ka, incision has occurred at the high

average rate of 400-550 m/Ma. If one assumes steady incision rates, this implies the spectacular bedrock Black Canyon was carved within the last 1.3 – 1.75 Ma. However, given that these high rates are only likely to have been active in the Black Canyon reach once the incision transient from Unaweep abandonment arrived near Red Canyon after 1 Ma, rates may have been higher and carving of the entire bedrock canyon in the last ~ 1 Ma seems most likely.

***3) New tephrochronology and cosmogenic burial dating of gravels provide new incision rates*:**

Our new data suggest that the previously reported 1.2 Ma Mesa Falls tuff locality in the Shinn-Bostwick drainages is likely to be the 0.64 Ma Lava Creek B. The new age of the paleo Bostwick gravels below the ash of 870 ±220 Ma precludes this ash being Mesa Falls. This reassignment is also supported by stratigraphic relations, indicating no major unconformity between the two exposed ashes. Cosmogenic dating indicates that terrace Qt7/223 m at the North Fork of the Gunnison -Gunnison River confluence is 0.98 ($^{+0.38}/_{-0.07}$) Ma, yielding an incision rate there of 228 ($^{+17}/_{-64}$) m/Ma.

4) Persistent differential incision in the early Gunnison River: Incision rates calculated from 10 Ma basalts show the same long term differential incision as the younger profiles and suggests that either (a) the knickpoint was already in existence at 10 Ma or (b) that post- 3 Ma incision has created the differential incision rates (our favored hypothesis). The Oligocene profile is near the modern profile in the upper reaches of the Gunnison system, suggesting zero long-term incision—presumably due to a combination of aggradation and surface uplift following the construction of Oligocene-

age volcanics. Erosionally driven isostatic rebound of the region may also have helped focus incision of the Black Canyon of the Gunnison.

AKNOWLEDGEMENTS

This work was supported by the Colorado Rockies Experiment and Seismic Transects (CREST) experiment funded by the National Science Foundation Continental Dynamics Program under award EAR-0607808. Thanks also to David C. Noe and anonymous reviewers for editorial comments, the Alfred P. Sloan Minority Ph.D. Program, and the Mesa State College Research Experience for Undergraduates participants in 2006, who were supported by NSF REU-Site Award EAR-0453264.

REFERENCES CITED

Aslan, A., Karlstrom, K., Hood, W.C., Cole, R.D., Oesleby, T.W., Betton, C., Sandoval, M.M., Darling, A., Kelley, S., Hudson, A. Kaproth, B., Schoepfer, S., Benage, M. and Landman, 2008, River incision histories of the Black Canyon of the Gunnison and Unaweep Canyon: interplay between late Cenozoic tectonism, climate change, and drainage integration in the western Rocky Mountains, *in* Raynolds, Robert G. edl, Roaming the Rocky Mountains and Environs; Geological Field Trips, Geological Society of America Field Guide, 10 p. 175-202.

Aslan, A., Karlstrom, K.E., Crossey, L.J., Kelley, S., Cole, R., Lazear, G., and Darling, A., 2010, Late Cenozoic evolution of the Colorado Rockies: Evidence for Neogene uplift and drainage integration, *in* Morgan, L.A., and Quane, S.L., eds., Through the Generations: Geologic and Anthropogenic Field Excursions in the Rocky Mountains from Modern to Ancient: Geological Society of America Field Guide 18, p. 21–54.

Balco. G., and Rovey, C.W., 2008, An isochron method for cosmogenic nuclide dating of buried soils and sediments: American Journal of Science, v. 308, p. 1083-1114.

Berlin, M. M., and R. S. Anderson, (2007), Modeling of knickpoint retreat on the Roan Plateau, western Colorado, Journal of Geophysical Res., 112, F03S06, doi:10.1029/2006JF000553.

Bishop, P., Honey, T.B., Jansen, J.D., and Artza, I.L., 2005, Knickpoint recession rate and catchment area: the case of uplifted rivers in Eastern Scotland: Earth Surface Processes and Landforms, v. 30, p. 767-778, doi: 10.1002/esp.1191.

Burbank, D.W. and Anderson, R.S., 2001, *Tectonic Geomorphology*, Blackwell Publishing, 161 p.

Cather, S.M., Karlstrom, K.E., Timmons, J.M, and Heizler, M.T., 2006, Palinspatic reconstruction of Proterozoic basement-related aeromagnetic features in north-central New Mexico: Implications for Mesoproterozoic to late Cenozoic tectonism: Geosphere, v.2, no. 6, p299-323, doi: 10.1130/GES00045.1.

Coven, B., Panter, K. and Stork, A., 1999, Ar/Ar age of the West Elk Volcano, Gunnison and Delta counties, Colorado: Geological Society of America Abstracts with Programs, v.31, no. 7, p. 478.

Darling, A., Aslan, A., Betton, C.W., Cole, R.D., Karlstrom, K.E., 2007, Late Quaternary incision rates and drainage evolution of the confluence of the Uncompahgre and Gunnison Rivers based on terraces dated with Lava Creek B ash, Western Colorado: Geological Society of America Abstracts with Programs, v. 39, no. 6, p. 306.

Darling, A., Aslan, A., Cole, R., Karlstrom, K., Betton, C., Wan, E., 2009, Late Quaternary Incision Rates and Drainage Evolution of the Uncompahgre and Gunnison Rivers Calibrated by Lava Creek B Ash, Western Colorado: Rocky Mountain Geology, v. 44, p. 71-83.

Darling, A., Karlstrom, K., Kirby, E., and Ouiment, W., 2009, Comparison of the modern profiles and discharge of the Green and Colorado Rivers and implications for epeirogenic uplift of the Colorado Plateau and Rocky Mountains: Geological Society of America Abstracts with Programs, v. 41, no. 7, p. 306-307.

Darling, A.L., Karlstrom, K.E., Granger, D.E., Aslan, A., Kirby, E., Ouimet, W.B., Lazear, G.D., Coblentz, D.D., Cole, R.D., 2012, New incision rates along the Colorado River system based on cosmogenic burial dating of terraces: implications for regional controls on Quaternary incision: Geosphere, v. 8, no. 5, p. 1020-1041.

Dethier, D.P., 2001, Pleistocene incision rates in the western United States calibrated using Lava Creek B tephra: Geology, v. 29, no. 9, p. 783-786.

Dickinson, R.G., 1965, Geologic map of the Cerro Summit Quadrangle Montrose County, Colorado: U.S. Geological Survey Geological Map Series, No. GGQ0486D, scale 1:24,000, 1 sheet.

Dortch, J.M., Dietsch, C., Owen, L.A., Caffee, M.W., and Ruppert, K., 2011, Episodic fluvial incision of rivers and rock uplift in the Himalaya and Transhimalaya: Journal of the Geological Society, London, Vol. 168, 2011, p. 783–804. doi: 10.1144/0016-76492009-158.

Douglas, J., Meek, N., Dorn, R., and Schmeekle, M., 2009, A criteria-based methodology for determining the mechanism of transverse drainage development, with application to the southwestern United States: GSA Bulletin, March/April, v. 121; no. 3/4; p. 586–598; doi: 10.1130/B26131.1; 6 fi gures; 5 tables; Data Repository item 2008163.

Ducea, M.N., Kidder, S., and Zandt, G., 2003, Arc composition at mid-crustal depths: Insights from the Coast Ridge Belt, Santa Lucia Mountains, California: Geophys. Res. Lett., 30, 1703, doi:10.1029/2002GL016297, 2003

Duvall, R.A., Kirby, E., Burbank, B., 2004, Tectonic and lithologic controls on bedrock channel profiles and processes in coastal California: Journal of Geophysical Research, v. 109: F03002, doi:10.1029/2003JF000086.

Eaton, G.P., 2009, Epeirogeny in the Southern Rocky Mountains region: Evidence and origin: Geosphere, v. 5, p. 408.

Epis, R., and Chapin, C., 1975, Geomorphic and tectonic implications of the post-Laramide, late Eocene erosion surface in the Southern Rocky Mountains Mountains: *in* Curtis, B.F., ed., Cenozoic history of the Southern Rocky Mountains: Geological Society of America Memoir 144, p. 45–74.

Finnegan, N.J. and Dietrich, W.E., 2011, Episodic bedrock strath terrace formation due to meander migration and cutoff: Geology, v. 39, p. 143-146.

Garcia, R.V., 2011, Cenozoic intrusive and exhumation history of the Elk and West Elk Mountain plutons, southwest Colorado: M.S. Thesis, New Mexico Institute of Mining and Technology, Socorro, NM.

Gardner, T.W., 1983, Experimental study of knickpoint and longitudinal profile evolution in cohesive, homogeneous material: Geological Society of America Bulletin, v. 94, p. 664-672.

Gilbert, G.K., 1877, Report on the geology of the Henry Mountains, *in* Powell J.W., ed., United States Geographical and Geological Survey of the Rocky Mountains region, US Government Printing Office: Washington, p. 160.

Goldrick, G., and Bishop, P., 2007, Regional analysis of bedrock stream long profiles: evaluation of Hack's SL form, and formulation and assessment of an alternative (the DS form): Earth Surface Processes and Landforms, v. 32, p. 649-671.

Granger, D. E., and Smith, A. L., 2000, Dating buried sediments using radioactive decay and muogenic production of ^{26}Al and ^{10}Be: Nuclear Instruments and Methods in Physics Research B v. 172, p. 822-826.

Gregory, K.M., and Chase, G.C., 1992, Tectonic significance of paleobotanically estimated climate and altitude of the late Eocene erosion surface, Colorado: Geology, v. 20, p. 581–585.

Gregory, K. M., and Chase, C. G., 1994, Tectonic and climatic significance of a late Eocene low relief, high level geomorphic surface, Colorado: Journal of Geophysical Research, v. 99, pp. 20,141– 20,160.

Hales, T.C., Abt, D.L., Humphreys, E.D., and Roering, J.J., 2005, A lithospheric instability origin for Columbia River flood basalts and Wallowa Mountains uplift in northeast Oregon: Nature, v. *438* p. *842*-845 doi: 10.1038/nature04313.

Hansen, W.R., 1965, The Black Canyon of the Gunnison - today and yesterday: U.S. Geological Survey Bulletin Report B: 1191, 76 p.

Hansen, W.R., 1967, The lower Black Canyon of the Gunnison: National Parks & Conservation Association, Washington, DC, v. 41, no. 238, p.14-19.

Hansen, W.R., 1971, Geologic map of the Black Canyon of the Gunnison River and vicinity, western Colorado: U.S. Geological Survey Miscellaneous Geological Investigations Map I-584, scale: 31,680, 1 map on 2 sheets.

Hansen, W.R., 1987, The Black Canyon of the Gunnison, Colorado, *in* Bues, S., ed., Centenial Field Guide: Boulder, Colorado, Rocky Mountain Section, Geological Society of America, v.2, p. 321-324.

Hidy, A. J., Gosse, J. C., Pederson, J. L., Mattern, J. P., Finkel, R. C., 2010, A geologically constrained Monte Carlo approach to modeling exposure ages from profiles of cosmogenic nuclides: An example from Lees Ferry, Arizona: Geochemistry, Geophysics, Geosystems, v. 11, Q0AA10.

House, M.A., Wernicke, B.P., and Farley, K.A., 2001, Paleo-geomorphology of the Sierra Nevada, California, from (U-Th)/He ages in apatite: American Journal of Science, v. 301, p. 77–102.

Humphreys, E., Hessler, E., Dueker, K., Farmer, G.L., Erslev, E., Atwater, T., 2003, How Laramide-Age Hydration of North American Lithosphere by the Farallon Slab Controlled Subsequent Activity in the Western United States: International Geology Review, vol. 45, p. 1-21.

Hunt, C.B., 1969, Geologic history of the Colorado River *in* The Colorado River Region and John Wesley Powell, USGS Professional Paper 669, p. 59-130.

Izett, G.A. and Wilcox, R.E., 1982, Map showing localities and inferred distributions of the Huckleberry Ridge, Mesa Falls, and Lava Creek ash beds (Pearlette family ash beds) of Pleistocene age in the Western United States and southern Canada, scale 1:4,000,000, 1 sheet.

Karlstrom, K.E., Crow, R., Crossey, L., Coblentz, D., and Van Wijk, J., 2008, Model for tectonically driven incision of the younger than 6 Ma Grand Canyon: Geology, v. 36, no. 11, p. 835–838, doi:10.1130/G25032A.1.

Karlstrom, K.E. Coblentz, D., Ouimet, W., Kirby, E., Van Wijk, J., Schmandt, B., Kelley, S., Lazear, G., Crossey, L. J., Crow, R., Aslan, A, Darling, A., Dueker, K., Aster, R., McCarthy, J., and CREST working group, 2012, Mantle-driven dynamic uplift of the Rocky Mountains and Colorado Plateau and its surface response: Toward a unified hypothesis: Lithosphere, v. 4, no. 1, p.3-22, GSA data repository item 2012041, doi: 10.1130/L150.1

Kirby, E., and Ouimet, W. 2011, Tectonic geomorphology along the eastern margin of Tibet: Insights into the pattern and processes of active deformation adjacent to the Sichuan Basin, *in* Gloaguen R., Ratschbacher L., eds., Growth and collapse of the Tibetan Plateau: Geological Society of London Special Publication 353, p.165–188; doi: 10.1144/SP353.9.

Kirby, E., Whipple, K.X., Wenqing Tang and Zhiliang Chen, 2003, Distribution of active rock uplift along the eastern margin of the Tibetan Plateau: Inferences from bedrock channel longitudinal profiles: Journal of Geophysical Research, v. 108, no. B4, 2217, doi: 10.1029/2001JB000861.

Kirby, E., and Whipple, K.X., 2012, Expression of active tectonics in erosional landscapes: Journal of Structural Geology, v. 44, p. 54-75.

Lanphere, M.A., Champion, D.E., Christiansen, R.L., Izett, G.A., Obradovich, J.D., 2002, Revised ages for tuffs of the Yellowstone Plateau volcanic field: assignment of the Huckleberry Ridge Tuff to a new geomagnetic polarity event: Geological Society of America Bulletin; v. 114; no. 5, p. 559-568.

Lazear, G.D., Karlstrom, K.E., Aslan, A., Kelley, S., 2013, Denudationa dn flexural isostatic response of the Colorado Platea and southern Rocky Mountain region since 10 Ma: Geosphere, v. 9, no. 5, p. 792-814.

Lipman, P.W., 2007, Incremental assembly and prolonged consolidation of Cordilleran magma chambers: Evidence from the Southern Rocky Mountain volcanic field: Geosphere, v. 3, no. 1, p. 42-70.

Mackin, J.H., 1948, Concept of the graded river: Geological Society of America Bulletin, v. 59, no. 5, p. 463–511, doi:10.1130/0016-7606(1948)59[463:COTGR]2.0.CO;2.

McMillan, M.E., Angevine, C.L., Heller, P.L., 2002 Postdepositional tilt of the Miocene-Pliocene Ogallala Group on the western Great Plains: Evidence of late Cenozoic uplift of the Rocky Mountains: Geology, v. 30; no. 1; p. 63–66;

McMillan, M.E., Heller, P.L., Wing, S.L., 2006, History and causes of post-Laramide relief in the Rocky Mountain orogenic plateau: Geological Society of America Bulletin, v. 118, no. 3/4, p. 393-405.

Molnar, P., 2004, Late Cenozoic increase in accumulation rates of terrestrial sediment: How might climate change have affected erosion rates?: Annual Review of Earth and Planetary Science, v. p. 32:67-89.

Molnar, P., and England, P., 1990, Late Cenozoic uplift of mountain ranges and global climate change: chicken or egg?: Nature, v. 346, p 29-34.

Nishiizumi, K., Imamura, M., Caffee, M.W., Southon, J.R., Finkel, R.C., and McAninch, J., 2007, Absolute calibration of 10Be AMS standards: Nuclear Instruments & Methods in Physics Research–Beam Interactions with Materials and Atoms, v. 258B, p. 403–413, doi: 10.1016/j.nimb.2007.01.297.

Ouimet, W., Whipple, K.X., Royden, L., Reiners, P., Hodges, K., and Pringle, M., 2010, Regional incision of the eastern margin of the Tibetan Plateau: Lithosphere, v. 2, no. 1, p. 50-63.

Pederson J.L., Mackley R.D., Eddleman J.L., 2002, Colorado Plateau uplift and erosion evaluated using GIS: GSA Today, Vol. 12, No. 8 p. 4–10.

Pelletier, J.D., 2010, Numerical modeling of the late Cenozoic geomorphic evolution of Grand Canyon, Arizona: Geological Society of America Bulletin, v. 122, no. 3-4, p. 595-608, doi: 10.1130/B26403.1.

Phillips, W.M., Commins, D.C., Gupta, S., 2003, Rates of knickpoint migration and bedrock erosion from cosmogenic Be-10 in a landscape of active normal faulting: Geological Society of America Abstracts with Programs, v. 35, no. 6, p. 63.

Repka, J. L., Anderson, R. S., and Finkel, R. C. 1997, Cosmogenic dating of fluvial terraces Fremont River, Utah: Earth and Planetary Science Letters, v. 152, p. 59-73.

Roy, M., Kelley, S.A., Pazzaglia, F., Cather, S., House, M., 2004, Middle Tertiary buoyancy modification and its relationship to rock exhumation, cooling, and subsequent extension at the eastern margin of the Colorado Plateau: Geology, v. 32; no. 10; p. 925-928.

Roy, M., Jordan, T.H., and Pederson, J., Cenozoic magmatism and rock uplift of the Colorado Plateau by warming of chemically buoyant lithosphere: Nature 459, p. 978-984, doi:10.1038/nature08052 2009

Safran,E.B., Bierman, P.R., Aalto, R., Dunne, T., Whipple, K.X. and Caffee, M., 2005, Erosion rates driven by channel network incision in the Bolivian Andes: Earth Surface Processes And Landforms v. 30, p.1007–1024, doi: 10.1002/esp.1259

Sandoval, M.M., 2007, Quaternary Incision History of the Black Canyon of the Gunnison, Colorado [M.S. Thesis]: Albuquerque, New Mexico, University of New Mexico, 120 p.

Schildgen, T.F., Hodges, K.V., Whipple, K.X., Reiners, P.W. and Pringle, M.S., 2007, Uplift of the western margin of the Andean plateau revealed from canyon incision history, southern Peru: Geology, v. 35, p. 523-526.

Schneeflock, F., Meyer, G., Karlstrom, K., Wagner, S., 2002, Quaternary drainage development and incision history in the Black Canyon of the Gunnison area, Colorado: Geological Society of America Abstracts with Programs, v. 34, no. 6, p. 472.

Steven, T.A., 1975, Middle Tertiary volcanic field in the Southern Rocky Mountains: Cenozoic history of the Southern Rocky Mountains, Geological Society of America Memoir 144, p. 75-94.

Steven, T.A., 2002, Late Cenozoic tectonic and geomorphic framework surrounding the evaporate dissolution area in west-central Colorado, *in* Kirkham, R.M., Scott, R.B., and Jukdins, T.W., eds., Late Cenozoic evaporate tectonism and volcanism in west-central Colorado: Geological Society of America Special Paper 366, p. 15–30.

Stock, J.D., Montgomery, D.R., 1999, Geologic constraints on bedrock river incision using the stream power law: Journal of Geophysical Research, v. 40, Issue B3, p. 4983-4994.

Whipple, K.X., 2004, Bedrock rivers and the geomorphology of active orogens: Annual Review Earth and Planetary Sciences, v. 32, p. 151-185.

Wobus, C.W., Crosby, B.T., and Whipple, K.X., 2006, Hanging valleys in fluvial systems: Controls on occurrence and implications for landscape evolution: Journal of Geophysical Research, v. 111, F02017, doi:10.1029/2005JF000406.

Wolkowinski, A.J., and Granger, D.E., 2004, Early Pleistocene incision of the San Juan River, Utah, dated with 26Al and 10Be: Geology, v. 32, p. 749-752.

CHAPTER 2 DETRITAL ZIRCON ANALYSIS OF EARLY TERTIARY PALEORIVERS IN THE SOUTHERN ROCKY MOUNTAINS: MULTI-STAGE UPLIFT AND EMERGENCE OF MODERN DRAINAGE PATTERNS

Magdalena S. Donahue[1], Mark Pecha[2], Karl E. Karlstrom[1], David Gonzales[3]
[1] Department of Earth and Planetary Sciences, Northrop Hall, University of New Mexico, Albuquerque, New Mexico 87131, USA
[2]Department of Geosciences, University of Arizona, 1040 E. 4th Street, Tucson, AZ 85721, USA
[3]Department of Geosciences, Fort Lewis College, 1000 Rim Drive, Durango, CO 81301, USA

ABSTRACT

The earliest paleoriver deposits that record post-Laramide erosion of the Colorado/ New Mexico Rockies have been historically considered to be of Eocene age and to rest on a widespread Rocky Mountain Erosion Surface (RMES). New detrital zircon dates indicate that these paleorivers range in age from Paleocene (65 Ma McDermott Formation), to Eocene (50-40 Ma Galisteo and Baca Formations), to Oligocene (30- 26 Ma; Telluride, Blanco Basin, El Rito/Ritito conglomerates). McDermott Formation yields age peaks of 1750-1650, 1450-1410, and 65 Ma and records a Paleocene paleoriver system (McDermott-Ojo Alamo-Animas-Nacimiento formations) that flowed south from the emerging Laramide San Juan-La Plata uplift to the San Juan Basin. The Eocene San Jose and Galisteo formations record paleorivers that flowed SE out of the San Juan Basin with prominent peaks at 1700, 1400, 1100, 450, 250, and 95 Ma suggesting continued and more widespread unroofing of the basement- cored, sedimentary-draped San Juan Mountains. Baca Formation has peaks of 1750-1650, 1500-1400, 220-180, and 570 Ma and represents an east-flowing river sourced in the Laramide Mogollon highlands. The Oligocene Telluride and Blanco

Basin paleorivers flowed west and south (respectively) from the uplifting San Juan Mountains. Both have detrital zircon spectra with youngest grain ages of ~ 30 Ma probably derived from the 35-30 Ma calderas of the NE San Juans; Proterozoic grains (1750-1650 and 1,450-1,420 Ma) are similar to dated Proterozoic basement in the Needle Mountains. The dominantly pre-volcanic El Rito (29 Ma max depositional age) and Ritito (27 Ma max depositional age) of New Mexico also have ~ 30 Ma peaks as well as prominent quartzite clasts (from the Tusas Mountains). These Oligocene paleoriver systems are interpreted to have been part of an extensive Blanco Basin- Conejos- El Rito- Ritito- Abiquiu distributed fluvial system with the Telluride as the ancestral San Miguel/Dolores River and the Blanco Basin/El Rito as the ancestral Chama River. The newly dated Oligocene river systems are interpreted to reflect epeirogenic doming and unroofing of the San Juan Mountains during mantle-driven surface uplift associated with early stages of the Oligocene ignimbrite flare-up.

In each age system, pre-volcanic gravels transition upward to volcaniclastic deposits. We infer a common process involving: 1) doming and unroofing of basement rocks accompanying magmatism—Colorado Mineral belt volcanism in the Laramide and ignimbrite flare up in the Oligocene; 2) deposition of relatively thin and widespread gravel/sand sheets above regional unconformities; and 3) deposition of voluminous volcaniclastic aprons around volcanic edifices. This process repeated in the Paleocene, Eocene, and Oligocene, and these successions are interpreted to be syntectonic records of magmatism that accompanied mantle- driven epeirogenic uplift. The different age conglomerates and underlying unconformities resulted in several sub-regional Rocky Mountain erosion surfaces that spanned 70-25 Ma and preserve different components of

the multi-stage uplift of the southern Rocky Mountain region: Laramide, mid-Tertiary, and post 10 Ma.

INTRODUCTION

The topography of the modern southern Rocky Mountains (SRM) began to take shape in the Laramide orogeny (~70-45 Ma), which was characterized by fault-bounded, basement-cored uplifts and basins (Dickinson and Snyder, 1978; Coney and Reynolds, 1977) (Fig.1). The Oligocene ignimbrite flare-up (38-25 Ma) which dramatically re-shaped SRM topography due to voluminous ignimbrites erupted from dozens of calderas in Colorado and New Mexico (Lipman, 2007). Crustal extension associated with the Rio Grande rift (Ricketts et al., 2015), mantle-driven Neogene differential uplift (Karlstrom et al., 2012), and isostatic uplift driven by rebound following differential denudation(Lazear et al., 2013) have also played important roles in shaping the modern topography.Latest Cretaceous paleorivers flowed onto the Colorado Plateau from the south and west toward deltaic systems at the edge of the retreating Cretaceous seaway (Cather et al., 2012). Some Laramide drainages (Paleocene-Eocene) terminated in internally drained basins west of the uplifting Rockies (e.g. Uinta and Claron basins); others flowed east to the Gulf of Mexico (Galloway et al., 2011). The end of the Laramide orogeny was marked by erosional beveling of uplifts and formation of an "Eocene Erosion Surface" (Cross, 1894; Davis, 1911; Atwood and Mather, 1932; Steven, 1968, Epis and Chapin, 1975) that was later re-named the Rocky Mountain

Erosion surface (RMES; (Evanoff and Chapin, 1994; Chapin, C.E., Kelley, 1997; Pazzaglia and Kelley, 1998; Leonard, 2002)).

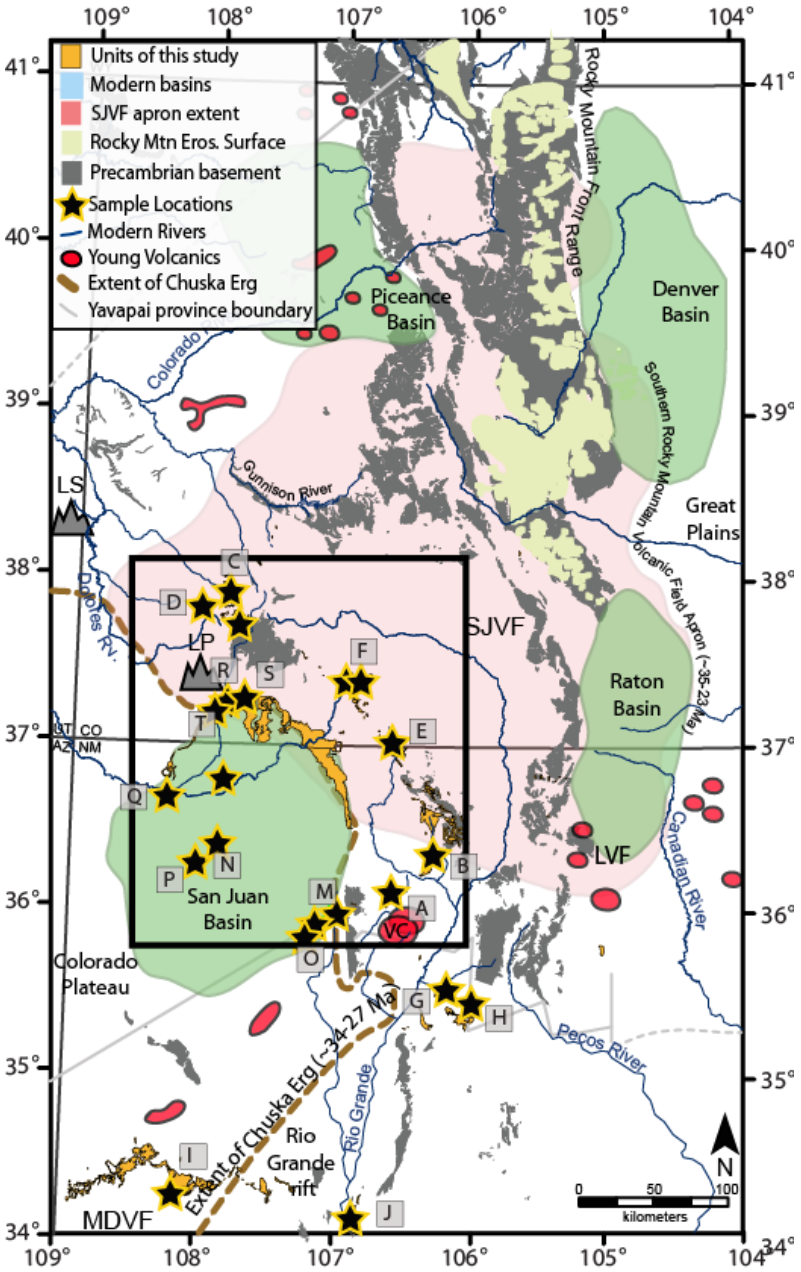

Figure 2-Error! No text of specified style in document.**-1** Location map for southern Rocky Mountain region of Colorado and New Mexico. Major geologic features shown include exposed basement rock, Laramide basins, the extent of the Southern Rocky Mountain Volcanic Field Apron, and conglomeratic/sedimentary units of this study. Detrital zircon sample locations are shown as black/yellow stars; sample location, show by letter in gray box, are keyed by to Table 1. Abbreviations are: LS = La Sal Mountains, LP = La Plata Mountains, SJVF = San Juan Volcanic Field, LVF = Latir

Volcanic Field, VC = Valles Caldera Complex, MDVF = Mogollon Datil Volcanic Field. Black box indicates area expanded in Fig. 4.

This paper focuses on paleoriver systems in the southern Rocky Mountains of Colorado and New Mexico whose deposits unconformably overlie the RMES and have been referred to as the "Eocene" conglomerates. We applied detrital zircon analyses to Tertiary fluvial deposits that have been noted to contain dominantly pre-volcanic clasts, and that have been previously interpreted to record post-Laramide but pre-Oligocene erosional unroofing of the Rockies (Steven and Epis 1968; Cather, et al., 2012). To the extent possible from outcrop preservation and character of fluvial units, we attempt to make the distinction between major trunk rivers with far traveled (> 100 km) gravels versus more localized alluvial fans and distributed fluvial systems (Weissmann et al., 2010) formed near the boundaries between localized uplifts and adjacent basins. Deposition of these widespread conglomerate deposits records a balance between progradation due to increased sediment supply from uplifted source areas and degree of subsidence of the basins (Heller, et al., 2013). We examine the concept that the thin and widespread post-Laramide gravel/sand sheets and underlying unconformities are syntectonic records of diverse styles of tectonism (Heller et al., 2013), not only foreland basins and rift settings, but also more subtle transient mantle- driven epeirogenic uplift (Karlstrom et al., 2011; Cather et al., 2012;).

The first goal of this paper is report 38 detrital zircon and sedimentary analyses of these conglomerate units to help elucidate the age, provenance, and flow path of early Tertiary paleoriver systems in southern Colorado and north-central New Mexico (Fig. 1). Overall, we establish that these conglomerates and the underlying composite RMES

span 70-25 Ma, and preserve a record of the multi-stage uplift of the southern Rocky Mountain region. The second goal is to use the paleorivers to develop a model for changes in local base level, paleoelevation, and relief in the Rockies due to multi-stage Cenozoic surface uplift.

BACKGROUND AND DEPOSITIONAL FRAMEWORK OF SEDIMENTARY UNITS

The Rocky Mountain Erosion Surface

Widespread surfaces of gentle topography and their overlying sedimentary deposits in the SRM region have been interpreted to record post-Laramide periods of extensive erosion (Epis & Chapin, 1975; Dickinson et al., 1988; Erslev, 1993; Pazzaglia & Kelley, 1998). Cross (1894) provided an early detailed geologic map of the San Juan region, and Davis, (1911) proposed this widespread area of gentle topography as a single peneplain, formed by lateral planation by streams at or near sea level. Multiple surfaces were observed, two by Finlay (1916) and Lee (1917, 1922), and as many as eleven by van Tuyl and Lovering (1935). Later workers returned to the idea of a single erosion surface that had undergone subsequent deformation (Mackin, 1947; Wahlstrom, 1947; Moore, 1960). The "late Eocene erosion surface" (Fig. 1) was defined in the classic Epis and Chapin (1975) paper that used geomorphic and geologic evidence (particularly the 36.7 Ma overlying Wall Mountain Tuff) to correlate many of the poorly preserved, extensively faulted and isolated segments of low relief erosion surfaces spanning approximately 10,000km^2 over the Front-, Rampart-, Sawatch-, Sangre de Cristo-, and Wet Mountain Ranges at elevations ranging from 2300-3800m (Pazzaglia and Kelley,

1998). Epis and Chapin (1975) used the overlying volcanics to bracket the age of "the surface" as being older than 38 Ma.

A newer name, "Rocky Mountain Erosion Surface" (RMES), was used to emphasize a diachronous origin for what was still considered a regional erosion surface (Evanoff & Chapin, 1994; Chapin and Kelley, 1997; Cather et al., 2008). Pazzaglia and Kelley (1998) referred to the RMES as an "upland surface of low relief presumably formed by fluvial erosion following Laramide deformation." They discussed whether the surface: 1) was created at near-modern elevations by progressive lowering and rounding of divides of Laramide highlands, 2) was created near sea level with fluvial erosion and rock uplift during Laramide deformation nearly balancing each other, or 3) was created at high elevation with a climate and hydrology favorable to reduction of relief. On the Great Plains, Leonard et al., (2002) described this erosion surface as a low-relief unconformity surface that cuts across mountain ranges as the result of erosion from early Eocene through Miocene, and, is locally still in development on the Great Plains.

The age and paleo-elevation history of Rocky Mountain erosion surfaces remains in debate and is central to interpretations of Rocky Mountain uplift history. Paleobotanists using the late Eocene Florrissant, Oligocene Pitch-Pinnacle, and late Oligocene Creede floras have suggested that low-relief surfaces could have formed either: A) at elevations close to sea level (Leopold, in prep.) requiring significant post-Laramide surface uplift, or B) at elevations equal to or higher than modern elevation of 2.5-2.6 km (Wolfe and Shorn, 1989; Wolfe, 1992; Gregory, et al.,1996; Meyer 2007), requiring no surface uplift since the Laramide. Gregory and Chase (1994) concluded that "the surface" formed in a humid climate characterized by small storm events at

elevations close to its modern elevation, and that regional dissection has resulted from late Cenozoic climate change. In contrast, recent paleobotanical work using the nearest living relative (NRL) method reinforces older interpretations (Axelrod, 1997)that the Florissant fauna, and hence the underlying RMES, formed at low elevations, followed by 2-4 km of post-38 Ma uplift of the region. Variations of this multi-stage uplift interpretation have been supported by geologic (Cather, et al., 2012) and stable isotope (Barton and Fricke, 2006) work. The newer interpretation is compatible with models that combine geomorphic and thermochronologic data and invoke significant mantle-driven surface uplift of the region in the last 10 Ma (Karlstrom et al., 2011; Nereson, et al., 2013; Rosenberg, 2014). Overall, opposing interpretations of paleontological data do not provide resolution of paleoaltimetry and uplift history.

Isostatic rebound studies (Pederson et al., 2002; Roy et al., 2004; Lazear et al., 2013) are in general agreement that ~ 1 km of isostatic uplift due to erosional denudation of the southern Rocky Mountain region has taken place since the Laramide, and that the overall 2-3 km surface elevation gain since the Cretaceous was dominantly of tectonic origin. But models differ in the proposed timing of tectonic surface uplift and resulting erosional isostatic rebound to have been post-Laramide (Pederson, Mackley, et al., 2002), post-Oligocene (Roy et al., 2004), and/or in the last 10 Ma (Lazear et al., 2013).

The multi-stage surface uplift model proposed in this paper builds on the paleontological interpretation for dominantly Neogene surface uplift in the Rockies (Raynolds et al. 2007; Leopold and Zaborac-Reed, in prep., personal communication, 2015). Figure 2 is a summary of the stratigraphic framework of the study region

(adapted from Cather, 2004). Positions of sub-regional erosion surfaces are labeled RMES 1, RMES-2, and RMES-3. Colors of the different ages of conglomerate/sedimentary sections are the same as in Figure 1.

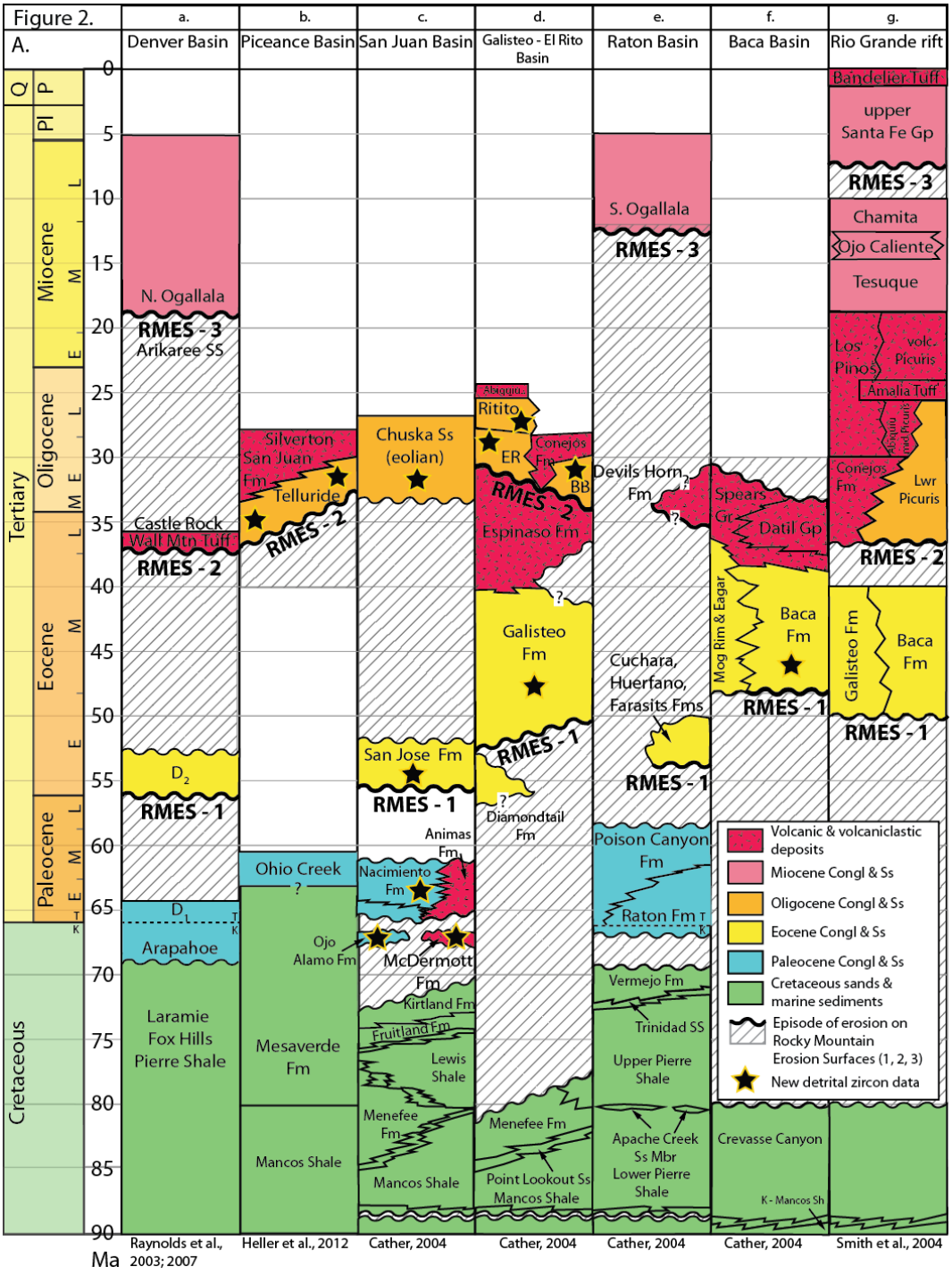

Figure Error! No text of specified style in document.**-2** Age of and post-Laramide stratigraphic units of the southern Rocky Mountains (adapted and expanded from Cather et al., 2012 and Heller et al., 2012). Green = Cretaceous marine sediments, Blue= Paleocene, Yellow= Eocene, Orange= Oligocene, and Pink= Miocene deposits that unconformably overlie older strata and/or diachronous components of the Rocky Mountain Erosion Surface (RMES-1 to RMES-3). Red= volcanic and volcaniclastic units that overlie and/or interfinger with dominantly pre-volcanic conglomerates. Stars= new detrital zircon data discussed in text; diagonal pattern= erosional episodes.

Cretaceous San Juan Basin underpinnings

Cretaceous marine strata document early Laramide basin subsidence in the Denver, Piceance, San Juan and Raton Basins (Fig. 2). These strata formed at sea level (which was ~200 m higher than modern sea level; Cather et al., 2012), as basins subsided and mountains rose. The Late Cretaceous Dakota Formation was deposited ~ 90 Ma on a regional unconformity that beveled across progressively deeper Mesozoic levels to the south, toward the rising Mogollon highlands in southern New Mexico and Arizona (Dickinson, 2013). The thickness of post-Dakota strata reached ~ 3 km in the San Juan basin and rate of sediment accumulation records an early pulse of Laramide orogenic subsidence 75-65 Ma.

Latest Cretaceous- Paleocene McDermott Member and Animas Formation

Following less than ~5 Ma oferosion following the Kirtland Formation (Williamson and Weil, 2008; Lucas et al., 2006), latest Cretaceous and Paleocene strata were deposited in the San Juan basin. The volcaniclastic McDermott Member is located on the northwestern margin of the San Juan Basin (Figs. 2, 3) and is composed of sandstones, shales, and volcaniclastic conglomerate (Gonzales and Gianniny, 2010; Wegert and Parker, 2011) that disconformably overlie the Cretaceous Kirtland Shale and underlie the volcanic-rich Animas Formation. Previous workers have interpreted the age of the McDermott to be Upper Cretaceous (Maastrichtian stage) based on fossils (Reeside and Knowlton, 1924). Suggestions for the depositional setting of this unit range from volcaniclastic (Reeside, J.B., Knowlton, 1924; Barnes, 1953; Kottlowski, 1957; Sikkink, 1987a), a fluvial system intermixed with lahars (O'Shea, 2009), or lahar deposits emplaced during strong Laramide tectonism (Wegert and Parker, 2011). The

unit ranges in thickness from 9-122 m (Reeside, and Knowlton, 1924). Paleocurrent indicators indicate SE and SW-flowing streams (Sikkink, 1987a). Volcaniclastic material within the McDermott includes clasts of diorite, monzonite, and trachyandesite; the source of volcaniclastic material within the McDermott is petrologically and geochemically similar to the 75-65 Ma La Plata laccolithic complex (Lorraine and Gonzales, 2003; Gonzales and Gianniny, 2010; Wegert and Parker, 2011) located on the southwestern part of the Colorado Mineral Belt. Workers have proposed the volcaniclastic conglomerates within the McDermott Member were deposited by debris flows and hyperconcentrated flows perhaps incorporating volcaniclastic material from minor volcanic-flank eruptions and gravity slides associated with over steepening and southern flank-collapse due to the emplacement of extensive sills forming the intrusive complex of the modern La Plata Mountains (Lorraine and Gonzales, 2003). Gonzales and Gianniny (2010) proposed an alternative hypothesis for formation of the unit, suggesting that rapid exposure of the intrusive complex led to erosion of intrusive material, which was subsequently concentrated into S-SW-flowing debris flows and streams, depositing the McDermott Member just SSW of its La Plata source, but not requiring active magmatic activity to be involved in deposition of the unit. This is based on a lack of definitive evidence for a volcanic source in the McDermott and, instead, that the igneous detritus resembles the intrusive rocks of the La Plata Mountains. McDermott is overlain by the volcaniclastic Animas Formation that reaches thicknesses of ~800 m.

Paleocene (66-63 Ma) Ojo Alamo Sandstone and Nacimiento Formations

In the central San Juan basin, the Ojo Alamo Sandstone and overlying Nacimiento Formation represent drainage system reorganization related to continuing Laramide tectonism Cather, 2004). The Ojo Alamo is a thin (6-120 m thick) laterally continuous arkosic sand sheet with minor conglomerate and mudstones. Paleocurrent and lithologic indicators suggest that it was derived from the San Juan Mountains to the northwest (Sikkink, 1987b; Klute, 1986; Powell, 1973). New Ar-Ar detrital sanidine ages indicate it was deposited at 65.7 Ma (Heizler et al., 2013; Heizler, personal communication, 2016). The overlying Nacimiento Formation consists of up to 525 m of finer grained sandstone and mudstone (Smith, 1992b; Williamson, 1996) with numerous paleosol horizons (Hobbs and Fawcett, 2014). Detrital sanidines indicate an age of 65.7-63.0 Ma for this unit (Heizler, personal communication, 2016). Workers have traditionally considered these deposits to be contemporaneous with the volcaniclastic rocks of the McDermott and Animas deposited on the northern edge of the basin (Cather, 2004).

55-40 Ma (Eocene) San Jose, Galisteo, and Baca Formations

As shown in Figure 3, north-central New Mexico has three units of Eocene (55-37 Ma) age as shown by fossil evidence. The San Jose Formation crops out in northwestern New Mexico and southwestern Colorado. It contains the youngest sedimentary bedrock exposed in the San Juan Basin (Smith, 1992a). The Baca Formation (Cather, 2009) crops out in central/ eastern New Mexico, and the Galisteo Formation (Stearns, 1943) crops out in northern New Mexico. These units are both overlain by volcaniclastic strata, the Spears and Espinaso Formations, respectively.

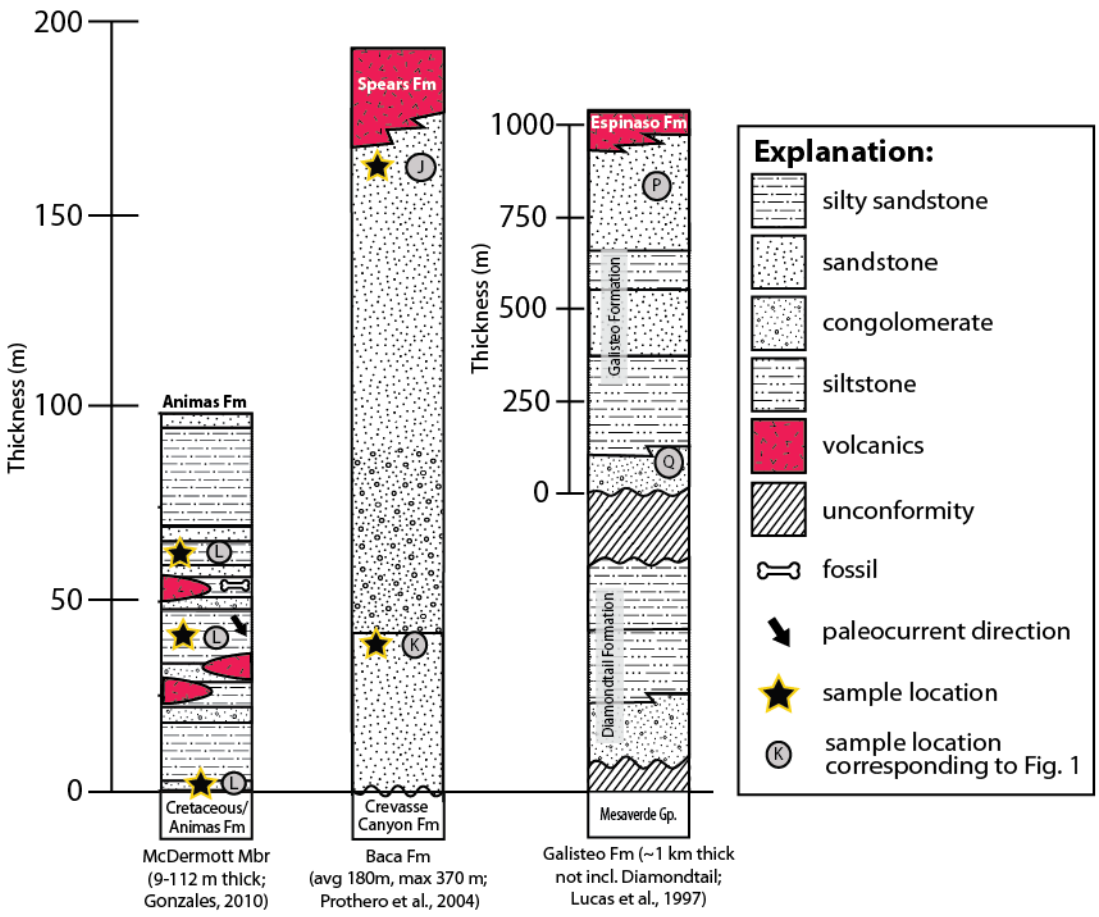

Figure 2-Error! No text of specified style in document.**-3** Stratigraphic columns adapted from previous workers and this study for Paleocene and Eocene-age units of McDermott Member, Baca Formation, and Galisteo Formation. Sample locations within the stratigraphic setting are indicated.

55-48 Ma (Eocene) San Jose Formation

The early Eocene San Jose Formation outcrops throughout the central San Juan Basin and preserves the last episode of Laramide basin sedimentation in northwestern New Mexico and southwestern Colorado. It was deposited by rivers with a general southward paleocurrent direction, though significant variation exists within the formation (Smith, 1992a). Intraformational angular unconformity and reverse faults in the eastern outcrop area show that the San Jose Formation was deposited simultaneous

to deformation along the basin-bounding Nacimiento fault (Smith, 1988; Woodward, 1987). Sedimentary source areas include the San Juan Uplift, Brazos-Sangre de Cristo Uplift, and Nacimiento Uplift (Smith, 1992a). The formation consists of five named members consisting of siliciclastic mudstones, sandstones, and minor conglomerate (Smith, 1992a; Smith and Lucas, 1991). These lithologically defined members represent at least three cycles of tectonically-driven changes in stream power, stream position, sediment supply, and regional slope (Smith, 1992a, 1988).

40-37 Ma (Eocene) Galisteo Formation.

The late Paleocene-Eocene Galisteo Formation contains 37-40 Ma fossils (Lucas and Ingersoll, 1981; Williamson and Lucas, 1992; Ingersoll et al., 1990) and has two main units (Fig. 3). It is concordantly overlain by the ~4 km-thick 36- 27 Ma volcaniclastic Espinaso Formation (Lisenbee, 1999; Connell and Lucas, 2001) or is locally unconformably overlain by Santa Fe Group sequences (Cather, 1992). The Galisteo Formation is thought to be widely sourced from the San Juan Basin region of the Colorado Plateau (Cather, 1992), Sangre de Cristo and Nacimiento uplifts, and sits unconformably on the Mesa Verde Group. The Galisteo consists of two unconformity-bound tectonosequences (the lower Diamond Tail Formation and the upper Galisteo Formation) representing the sedimentary response to two tectonic episodes (Lucas et al., 1982, 1997; Maynard, 2005).

50-40 Ma Baca Formation:

The Eocene-Oligocene fluvial-lacustrine Baca Formation of west-central New Mexico is discontinuously exposed and consists of conglomerate, sandstone, mudstone and claystone (Fig. 3) sourced from the Laramide-age Mogollon Highlands, Sierra,

Montosa, Defiance and Zuni Lucero uplifts (Cather and Johnson, 1984; Cather, 1986, 2009). This unit averages 180 m in thickness (Prothero, et. al., 2004) and disconformably overlies a low-relief erosional surface developed on the late Cretaceous Crevasse Canyon Formation. It is overlain by the ~1 km-thick, ~38.0 Ma Spears Formation (lower part of the Datil Group; Cather et al., 1987; Prothero et al., 2004). The depositional age of the Baca Formation is bracketed between 46-50 Ma by Bridgerian fossils near its base and ~38 Ma volcanciclastic units that overly the unit ((Kelley et al., 2009)). This unit has been interpreted to have been sourced from high topography of the Mogollon highlands to the south that was uplifted in the Laramide Orogeny (Cather, 1982; Dickinson et al., 2012). In that sense, it is broadly correlative with the Mogollon Rim Formation (Potochnik, 1989), Rim Gravels, and Music Mountain Formation (Young and Hartman, 2014). The Baca Formation (Baca Basin) has been linked to the Carthage basin and envisioned as a fluvial system that flowed east from the Springerville region of the Mogollon highlands to the Gulf of Mexico (Galloway et al., 2011).

The overlying Spears Formation is a several hundred meter thick volcaniclastic unit intercalated with Datil Group ignimbrites and lavas. Lower Spears Group was deposited 34-33.5 Ma (Cather and Johnson, 1984) and consists of fluvial and debris flow units in a volcaniclastic apron surrounding the Mogollon Datil volcanic field. In the Springerville area it is overlain by eolian sandstones correlated with the 34-27 Ma Chuska Sandstone (Cather et al., 2008).

Oligocene Telluride and Blanco Basin paleoriver systems

An important contribution of this study is the detrital zircon evidence (presented below) that the Telluride Conglomerate and Blanco Basin Formation, previously considered to be Eocene conglomerates (Cross and Larsen, 1935; Larsen and Cross, 1956; Bromfield and Bush, 1968; Cather, 2004) are Oligocene in age.

~ 30 Ma Telluride Conglomerate.

The Telluride Conglomerate is exposed at elevations ranging from ~9,000-10,000 feet (2743 -3048 m) on the western slopes of the San Juan Mountains (Fig. 4). The Telluride Conglomerate lies unconformably on Precambrian to Mesozoic units and is overlain by the Miocene volcaniclastic San Juan Formation and ~27 Ma (Bove et al., 2001) Silverton Volcanic Group (Burbank and Luedke, 1969). Gradationally, overlying the Telluride Conglomerate, the 27.6-28.3 San Juan Formation (Lipman, 2007) exceeds 1 km in thickness and is subsequently overlain by the 50 m-thick 27.6 Ma Crystal Lake tuff (Burbank and Luedke, 1969) associated with the Silverton caldera. These early pre-caldera volcanicastics and Silverton caldera ignimbrites are subsequently overlain by the

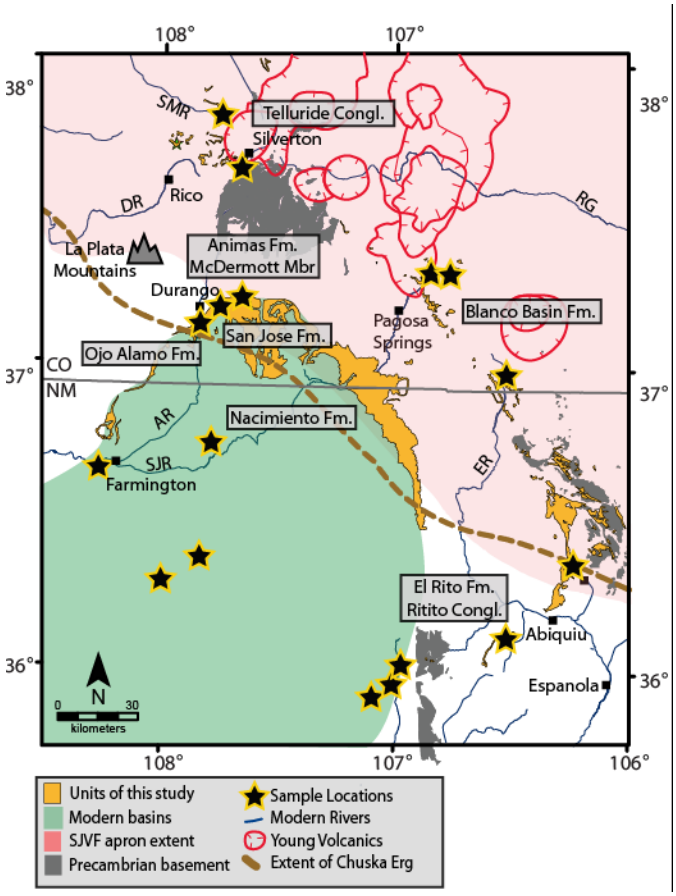

Figure 4-Error! No text of specified style in document.**-4** Location map for southern San Juan Mountains and northwestern New Mexico. Major features shown include exposed basement rock (gray), the San Juan Basin (green), the extent of the Southern Rocky Mountain Volcanic Field Apron (pink), SJVF calderas (red l line), and conglomeratic/sedimentary units of this study (gold). Detrital zircon sample locations are shown as black/yellow stars. Abbreviations of modern rivers are: SMR = San Miguel River, DR = Dolores River, RG = Rio Grande, AR = Animas River, SJR = San Juan River, ER = El Rito.

27.5 Ma Carpenter Ridge Tuff, which contributed an excess of 1000 km^3 volcaniclastic material and in places exceeded 100 m thickness (Lipman, 2007).

The Telluride Conglomerate contains Paleozoic to Tertiary clasts recording unroofing of the nearby Needles Mountains block (Gonzales et al., 2005). Previous workers have postulated that the Telluride Conglomerate was deposited in a lake (Cross and Purington, 1899) or by alluvial processes (Harraden, 2007). We conclude a combination of fluvial processes formed this unit, building upon the previous work of Kray (2004), Gonzales et al., (2005) and Harraden (2007).

The Telluride Conglomerate is a boulder-to-pebble conglomerate with interbedded sandstones and siltstones (Fig. 5) and preserves a regional unroofing sequence (Gonzales et al., 2005). Proximal debris flows in the unit contain poorly-sorted, matrix supported conglomerates and moderately sorted, grain supported

sandstone lenses (Little Molas Lake, town of Telluride). Increasingly fine-grained fluvial characteristics with larger percentage of andesititc to rhyolitic clasts are found at more distal outcrops (Mt. Wilson; just north of town of Telluride). Upper sections of the Telluride Conglomerate at Mt. Wilson that are in contact with overlying volcanic units are metamorphosed. The overlying and widespread 32 Ma San Juan Formation (Lipman et al., 1970) is ~ 2,000 (615 m) in thickness, and consists largely of mudflow deposits, volcaniclastic rocks that interfinger with lava flows (Lipman et al., 1976). The Molas Lake section (Fig. 5) contains a poorly sorted and primarily matrix-supported conglomerate with subrounded to angular clasts of limestone, quartzite, granite, schist-gneiss, siltstones, and sandstones; porphyritic granitic clasts. Limestones and Paleozoic clasts types dominate the lower portions of the conglomerate, and preserve local SE to NW scour channel paleoflow indicators. Upsection, the unit contains increasing proportions of Proterozoic lithologies eroded from the nearby Needle Mountains uplift. Proterozoic clasts exceed 1 m diameter in parts of the outcrop. Especially within the upper 2-5 m of the section, andesitic to rhyolitic volcanic clasts are present indicating temporal overlap of volcanism with fluvial deposition.

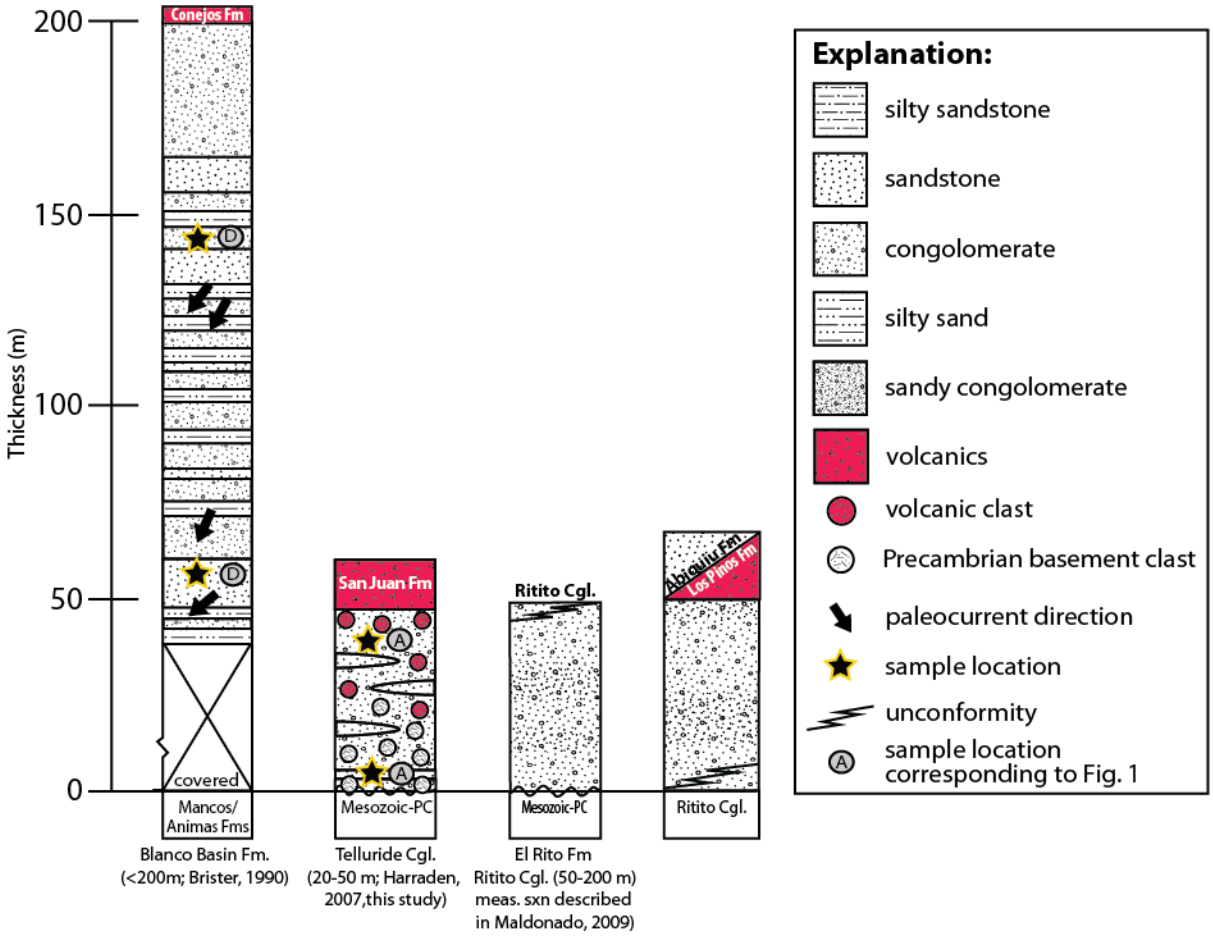

Figure 2-Error! No text of specified style in document.**-5** Stratigraphic columns adapted from previous workers and this study for Oligocene-age units of Blanco Basin Formation, Telluride Conglomerate, El Rito Formation and Ritito Conglomerate. Sample locations within the stratigraphic setting are indicated.

~ 30 Ma Oligocene Blanco Basin Formation.

The Blanco Basin Formation is exposed at 9,000-10,000 ft. (2743 -3048 m) elevation on the southern slopes of the San Juan Mountains (Fig. 4). The thin (<~200 m), mixed unit of conglomerate and sandstone lenses contains mainly of arkosic material sourced from basement rocks, with sedimentary Mesozoic and Tertiary volcaniclastic material intermixed (Brister, 1992). The unit unconformably overlies the Jurassic Morrison Formation, Cretaceous Mancos Shale (90-85 Ma), or Paleocene-Cretaceous Animas Formations. It is overlain by the volcanic units of the~34 Ma

Conejos Formation (Brister, 1992; Lipman and McIntosh, 2008). The Conejos Formation contains early pre-caldera flows from the 28.3-27.8 Ma La Garita cluster; volcaniclastic units thin from ~1.3 km near the caldera center to ~600 m preserved in more distal locations (Lipman, 2000, 2007). The Blanco Basin Formation is locally overlain by reworked Quaternary landslide deposits and Oligocene volcanic units, taking the form of bedded conglomerates and breccias (Lipman and Hall, 1975).

29-26 Ma El Rito Formation and Ritito Conglomerate

The El Rito Formation is found at elevations of 6,000-10,000 ft. (1828-3048 m) in northern New Mexico (Fig. 4). The El Rito Formation is sandstone and conglomeratic (Fig. 5), dominated by Ortega Quartzite basement clasts, with lesser amounts of gneiss, schist and metavolcanics from the Tusas Mountains. It sits unconformably on Precambrian to Mesozoic rocks (Lee et al., 2013) and its upper contact locally interfingers with the Ritito Conglomerate, or is unconformably overlain by the ~400 m thick (Maldonado and Kelley, 2009), 26.0-25.5 Abiquiu Tuff Formation (Koning et al., 2011; Logsdon, 1981). Paleoflow studies indicate the unit was deposited by south-flowing streams (May, 1980, 1984; Ekas et al., 1984; Ingersoll et al., 1990)May. Workers have suggested the El Rito was largely eolian-derived material perhaps sourced from a topographically high volcanic complex or basement rocks of the Tusas and Sangre de Cristo Mountains (Koning et al., 2011) and deposited on a south-sloping distal alluvial slope (Koning et al., 2005) with sediments later reworked by a fluvial system. Several workers use the term Ritito Conglomerate for dominantly non-volcanic clast (basement –derived) conglomerates in the Tusas Mountain region (Maldonado and Kelley, 2009; Koning et al., 2011; Aby, S.B., Kempter, K., Koning, 2011) such that

there is little map or age distinction between El Rito and Ritito conglomerates in the Tusas Mountains.

26 Ma (Latest Oligocene) Ritito Conglomerate.

The Ritito Conglomerate (Fig. 4), a coarse, locally-preserved conglomerate deposited by south-flowing river systems sourced from the Laramide highlands of the Jemez Mountains, Tusas Mountains, and Sierra Nacimiento, overlies the El Rito Formation, Mesozoic or Permian sedimentary rocks or Proterozoic basement and is gradationally overlain by the volcanic Los Pinos Formation (Koning et al., 2011) or Abiquiu Formations (Maldonado and Kelley, 2009). The Ritito Conglomerate is dominated by Proterozoic basement clasts including quartzite, granite, metavolcanics, quartz schists and small amounts of Mesozoic sedimentary units (Fig. 5). Cenozoic volcanic clasts sourced from the San Juan and Latir volcanic fields to the north are minor and found in the uppermost parts of the unit (Kelley et al., 2013) where it transitions into the volcaniclastic dominated Los Pinos Formation (Aby, S.B., Kempter, K., Koning, 2011). The unit has a maximum thickness of 210 m and clasts range from granule to boulder size (Maldonado and Kelley, 2009). A K-Ar age of ca. 27 Ma (Lipman et al., 1970) on a basalt near the base of the Ritito Conglomerate and an assumed ca. 27 Ma age on altered basalt interbedded with the Ritito Conglomerate (Moore, 2000) bracket the Oligocene age of the unit. Paleocurrent directions are largely to the south, following a broad zone of subsidence (Smith et al., 2002). The sub-Ritito/ Abiququ erosion surface suggests an unconformity on top of a convoluted paleotopography (Smith et al., 2002).

METHODS: U-PB DETRITAL ZIRCON GEOCHRONOLOGY

U-Pb detrital zircon geochronology was conducted by laser ablation multicollector inductively coupled plasma mass spectrometry (LA-MC-ICPMS) following the methods of (Miller et al., 2006; Gehrels et al., 2008) and (Dickinson and Gehrels, 2009)**(2009**). U-Pb ages were determined for randomly selected detrital zircon grains. U-Pb data are reported in Appendix 1 and also shown in age-probability plots (Ludwig, 2008) where each grain age and its error is summed into curves with equal areas below the curves for each unit. We report inferred maximum depositional ages as peak ages for the youngest-age curves and discuss provenance ages reported as the ages of the main peaks.

Probability (P) values were also calculated from Kolmogorov-Smirnoff (K-S) statistics (Press et al., 1987). K-S statistics test the null hypothesis that two detrital zircon age populations might have been selected at random from the same parent population (e.g., Dickinson, 2013). If $P > 0.05$, one cannot with 95% confidence reject the null hypothesis that 2 detrital zircon age populations were derived at random from the same parent population. P values > 0.05 give increasingly higher certainty that one can reject the null hypothesis. For example at $P=0.4$, one is 40% certain the distributions could have come from the same source population. At $P = 1.0$, there is statistical identity between populations. This test is a statistically rigorous test, but we find many examples of fluvial samples from the same stratigraphic unit, and even the same stratigraphic horizon may not "pass the test" of being statistically indistinguishable. This is especially true for samples with high number of grains analyzed. Thus, we also compare and contrast samples using the presence and absence of the main age

probability peaks and we lump samples from the same unit even with low p values to help characterize overall variability in a given fluvial succession.

RESULTS: U-PB DETRITAL ZIRCHON GEOCHRONOLOGY

New detrital zircon ages are presented in Table 1 and discussed below from oldest to youngest units. Complete detrital zircon analyses are in Appendix 1. Statistical analyses of units are in Appendix 2.

Table 1. Detrital Zircon Ages

Unit Grp	Loc. ID	Unit Name	Sample Number	UTM	Easting	Northing	Longitude WSGS 84 DD	Latitude WSGS 84 DD	No. grains	Max. Depo. Peak Age (Ma)	Unit Best Depo. Age [range] (Ma)
Oligocene	A	Ritito Formation (El Rito, NM - lower)	MS-11-2	13S	363976	4000888 02	-106.5119	36.1431	92	1690	29.72±0.48
Oligocene	A	Ritito Formation (El Rito, NM - upper)	MS-11-4	13S	363998	4001072	-106.5117	36.1448	91	29.72±0.48	
Oligocene	B	El Rito Formation (near El Rito climbing area, NM)	MS-11-5	13S	388820	4028136	-106.2397	36.3919	97	32.3±6.3	32.3±6.3
Oligocene	A	El Rito Formation (Cerro Pedernal, NM)	MS-11-1	13S	254112	4203426	-106.5234	36.1434	84	187.3±3.6	
Oligocene	C	Telluride Conglomerate (Little Molas Lake - basal)	MS-10-7	13S	0260912	482548	-107.7140	37.7590	98	523.7±4.0	31.3±2.0
Oligocene	C	Telluride Conglomerate (Little Molas Lake - upper)	MS-10-9	13S	0253999	4203164	-107.7110	37.7590	80	31.3±2.0	
Oligocene	D	Telluride Conglomerate (Mt. Wilson - upper)	MSD-CO-2011-17	13S	0236328	4191579	-107.9961	37.8336	89	33.8±0.7	

Unit Grp	Loc. ID	Unit Name	Sample Number	UTM	Easting	Northing	Longitude WSGS 84 DD	Latitude WSGS 84 DD	No. grains	Max. Depo. Peak Age (Ma)	Unit Best Depo. Age [range] (Ma)
Oligocene	D	Telluride Conglomerate (Mt. Wilson - basal)	MSD-CO-2011-18	13S	0236313	4191627	-107.9963	37.8340	95	34.05±0.7	
Oligocene	C	Telluride Conglomerate (upper)	WP42	13S	0255237	4203103	-107.7854	37.9426	85	33.4 ±1.3	
Oligocene	C	Telluride Conglomerate (basal)	WP43	13S	0255019	4203071	-107.7878	37.9422	87	63.0 ±1.3	
Oligocene	C	Telluride Conglomerate	WP52	13S	0254840	4202774	-107.7898	37.9395	100	65.7 ±1.0	
Oligocene	E	Blanco Basin Formation (Chama, NM - middle)	MSD-CO-2011-13	13S	363024	4102024	-106.5405	37.0545	91	33.8±1.1	
Oligocene	E	Blanco Basin Formation (Chama, NM - lower)	MSD-CO-2011-14	13S	363101	4102023	-106.5397	37.0545	57	450	
Oligocene	F	Blanco Basin Formation (Pagosa Springs, CO - upper)	DG-BristerE-PCA-2011	13S	034729	4141134	-106.8673	37.4022	138	160	33.8±1.1
Oligocene	F	Blanco Basin Formation (Pagosa Springs, CO - basal)	DG-BristerE-PC3b-2011	13S	034729	4141134	-106.8673	37.4022	83	227	
Oligocene	F	Blanco Basin Formation (Pagosa Springs, CO - basal)	DG-BristerE-PC5-2011	13S	034729	4141134	-106.7879	37.4033	139	565	
Paleocene-Eocene	G	Galisteo Formation (South of La Cienega, NM)	MSD-NM-2011-23	13S	397607	3935726	-106.1298	35.5599	180	45	
Paleocene-Eocene	H	Galisteo Formation (Galisteo Preserve, NM - upper)	MSD-NM-2011-25	13S	414654	3926576	-105.9408	35.4790	94	170	45-95

Unit Grp	Loc. ID	Unit Name	Sample Number	UTM	Easting	Northing	Longitude WSGS 84 DD	Latitude WSGS 84 DD	No. grains	Max. Depo. Peak Age (Ma)	Unit Best Depo. Age [range] (Ma)
Paleocene-Eocene	H	Galisteo Formation (Galisteo Preserve, NM - lower)	MSD-NM-2011-26	13S	414890	3926385	-105.9381	35.4773	283	95	
Paleocene-Eocene	I	Baca Formation (near Pie Town, NM)	MSD-NM-2012-1	12S	766715	3798370	-108.1023	34.2923	97	69.9±8.4	74.4±2.5 - 69.9±8.4
Paleocene-Eocene	J	Baca Formation (Jornada del Muerto, NM)	SCATH2012-1	13S	334540	3781574	-106.7950	34.1620	99	74.4±2.5	
Paleocene-Eocene	K	San Jose Formation	WP46	13S	02949518	4077581	-107.8079	36.8110	98	71.9 ±3.1	80.0 ±2.6 - 71.9 ±3.1
Paleocene-Eocene	L	San Jose Formation	WP32	13S	0322647	3990366	-106.9687	36.0417	88	80.0 ±2.6	
Paleocene-Eocene	M	Nacimiento Formation	WP26	13S	0318955	3983387	-107.0081	35.9781	84	72.0 ±1.5	72.0 ±1.5 - 69.9 ±3.3
Paleocene-Eocene	N	Nacimiento Formation	WP34	13S	0245147	4033259	-107.8422	36.4107	92	69.9 ±3.3	
Paleocene-Eocene	O	Ojo Alamo Formation	WP27	13S	0311105	3978428	-107.0939	35.9320	109	72.9±3.0	72.9±3.0 - 66.9 ±4.9
Paleocene-Eocene	P	Ojo Alamo Formation	WP36	12S	0768768	4023296	-108.0063	36.3172	92	69.9 ±2.4	
Paleocene-Eocene	Q	Ojo Alamo Formation	WP63a	12S	0747235	4065432	-108.2324	36.7024	91	66.9 ±4.9	
Paleocene-Eocene	R	Animas Formation	WP44	13S	0252661	4129028	-107.7896	37.2750	93	63.6 ±1.2	68.1±1.6 - 63.6 ±1.2
Paleocene-Eocene	S	Animas Formation	WP45	13S	0261466	4132507	-107.6915	37.3086	84	70.4 ±1.5	
Paleocene-Eocene	T	Animas Formation (basal)	WP57	13S	0245949	4123229	-107.8633	37.2210	96	68.9±1.2	
Paleocene-Eocene	T	Animas Formation (basal conglomerate volcanic cobble)	WP57vc	13S	0245949	4123229	-107.8633	37.2210	88	68.1±1.6	
Paleocene-Eocene	T	Animas Formation (basal conglomerate chert cobble)	WP57cc	13S	0245949	4123229	-107.8633	37.2210	10	-	

Unit Grp	Loc. ID	Unit Name	Sample Number	UTM	Easting	Northing	Longitude WSGS 84 DD	Latitude WSGS 84 DD	No. grains	Max. Depo. Peak Age (Ma)	Unit Best Depo. Age [range] (Ma)
Paleocene-Eocene	T	McDermott Formation (Durango, CO - upper)	MS-10-2	13S	245834	4123296	-107.8646	37.2216	90	68.36±0.8	68.3±0.77-69.3±0.7
Paleocene-Eocene	T	McDermott Formation (Durango, CO - basal)	MS-10-4	13S	245834	4123296	-107.8646	37.2216	99	69.5±1.1	
Paleocene-Eocene	T	McDermott Formation (basal)	WP53	13S	0245526	4123391	-107.8681	37.2223	94	69.7±1.1	
Paleocene-Eocene	T	McDermott Formation (single cobble)	WP53b	13S	0245526	4123391	-107.8681	37.2223	55	69.3±0.7	
Paleocene-Eocene	T	McDermott Formation (upper)	WP56	13S	0245937	4123229	-107.8634	37.2210	85	68.3±0.7	

Detrital zircon of the 68-63 Ma McDermott Member and Animas, Ojo Alamo, Nacimiento Formations

Detrital zircon of McDermott Member and Animas Formation

Detrital zircon samples (Fig. 6) were collected basal, middle, and upper parts of the McDermott Member exposed near Durango, Colorado (Fig. 4). The stratigraphic context of the samples is shown in Fig.3. The lower sample (location T) has a 66 Ma peak, with 48 % Proterozoic grains ranging from 1750-1400 Ma. The upper sample has youngest peak at 65 Ma, with an age range of 71-65 Ma. This sample had relatively few Proterozoic grains (11%); those grains are dominated by a peak at 1694 Ma with an age range between 1748-1647 Ma. The McDermott Member has a youngest peak composite spectrum maximum depositional age of 68.3±0.77-69.3±0.7 Ma. We combine all

samples from the McDermott Member (Fig 6; n=426) to better characterize the diverse zircon populations in the provenance for this overall stratigraphic unit. The merged post-100 Ma grain population (Fig 6; n=193) shows a dominant 68.3±0.7 (2σ) Ma peak.

P-values for the four McDermott member samples show low values between samples with the exception of significant values between WP52 and MSD-10-04 (0.097) and WP56-MSD-10-02 (0.522). The Animas Formation shows low P-values between WP44 and all other samples. However, other sample pairs are significant and range between 0.368 and 0.761 (see Appendix 2).

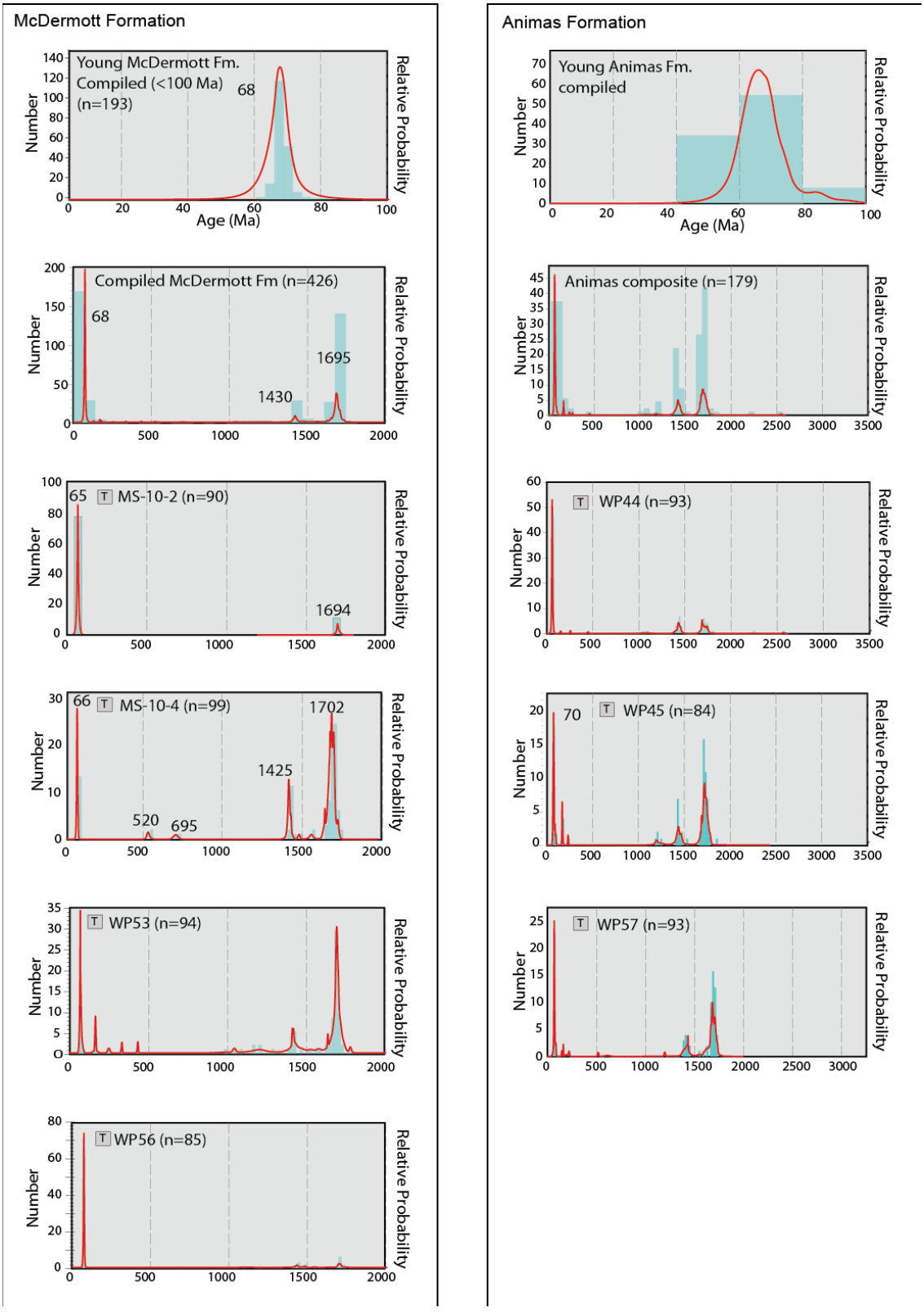
McDermott Formation
Young McDermott Fm.
Compiled (<100 Ma)
(n=193)
68
Number
Relative Probability
Age (Ma)
Compiled McDermott Fm (n=426)
68
1695
1430
MS-10-2 (n=90)
65
1694
MS-10-4 (n=99)
66
1702
1425
520
695
WP53 (n=94)
WP56 (n=85)
Animas Formation
Young Animas Fm.
compiled
Animas composite (n=179)
WP44 (n=93)
WP45 (n=84)
70
WP57 (n=93)

Figure 2-Error! No text of specified style in document.**-6** Detrital zircon spectra for McDermott Member and Animas Formation.

Detrital zircon of Ojo Alamo Formation

Detrital zircon analysis of this unit (n=202) reveals dominant Proterozoic age peaks of ~1730 and ~1400 Ma with 57% of grains between 1400-1750 Ma. Subordinate Jurassic and Cretaceous-age peaks occur at ~160 Ma (7% of grains at 150-170 Ma) and 70-80 Ma (7% of grains). We combine all samples from the Ojo Alamo Formation (Fig 7; n=184) to better characterize the diverse zircon populations in the provenance for this overall stratigraphic unit. The merged post-100 Ma grain population (Fig 7; n=21) shows a dominant 72.9±3.0 (2σ) Ma peak. K-S statistic show P-values for the three Ojo Alamo Formation samples show significant P-values between all three samples: WP36-WP27 (0.396), WP36-WP63A (0.509), and WP36A-WP27 (0.482).

This DZ signature is compatible with reworking of older San Juan basin sedimentary units and a sedimentary source in Proterozoic crystalline basement, all of which were present up gradient from the Paleocene San Juan Basin. The presence of Maastrichtian-aged detrital zircons in the Ojo Alamo Sandstone shows that San Juan Basin paleorivers were also sourcing young shallow magmatic or volcanic units in the earliest Paleocene.

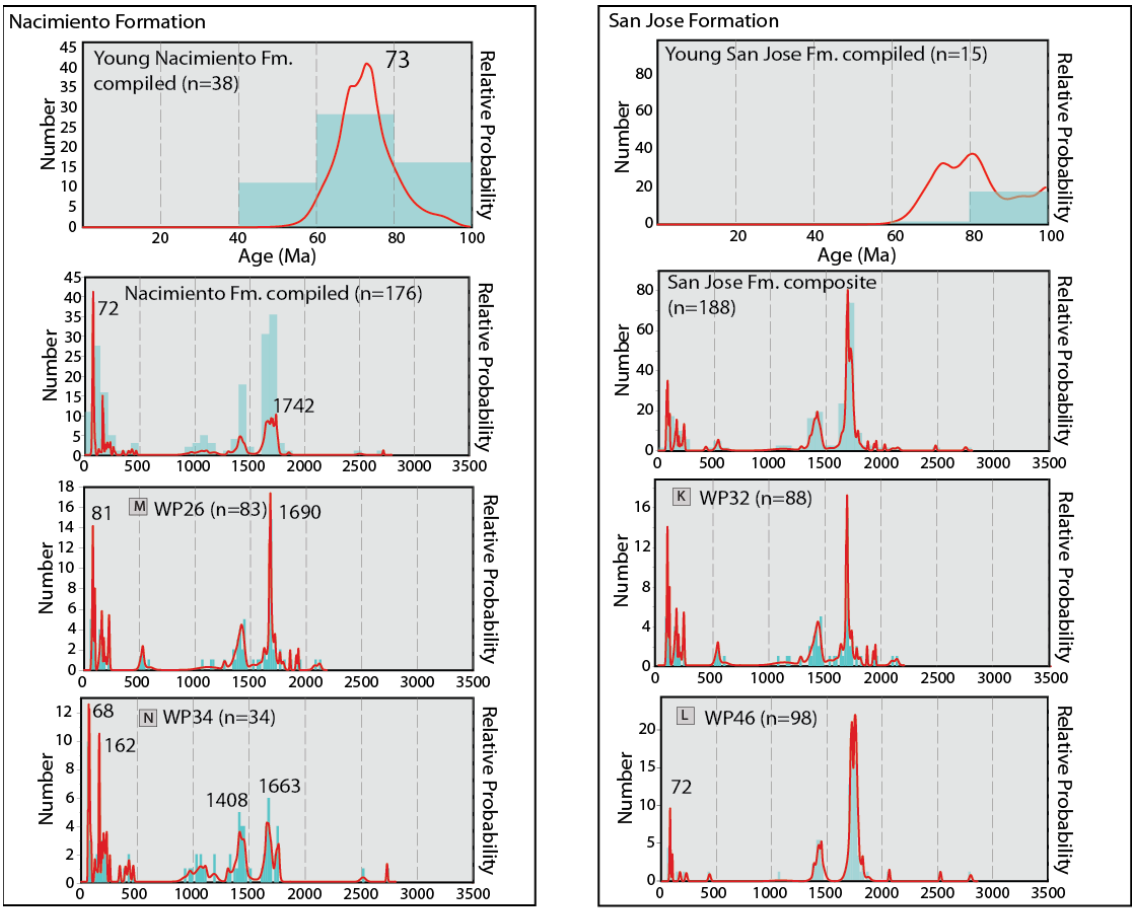
Nacimiento Formation
Young Nacimiento Fm. compiled (n=38)
73
Nacimiento Fm. compiled (n=176)
72
1742
M WP26 (n=83)
81
1690
N WP34 (n=34)
68
162
1408
1663
San Jose Formation
Young San Jose Fm. compiled (n=15)
San Jose Fm. composite (n=188)
K WP32 (n=88)
L WP46 (n=98)
72
Number
Relative Probability
Age (Ma)

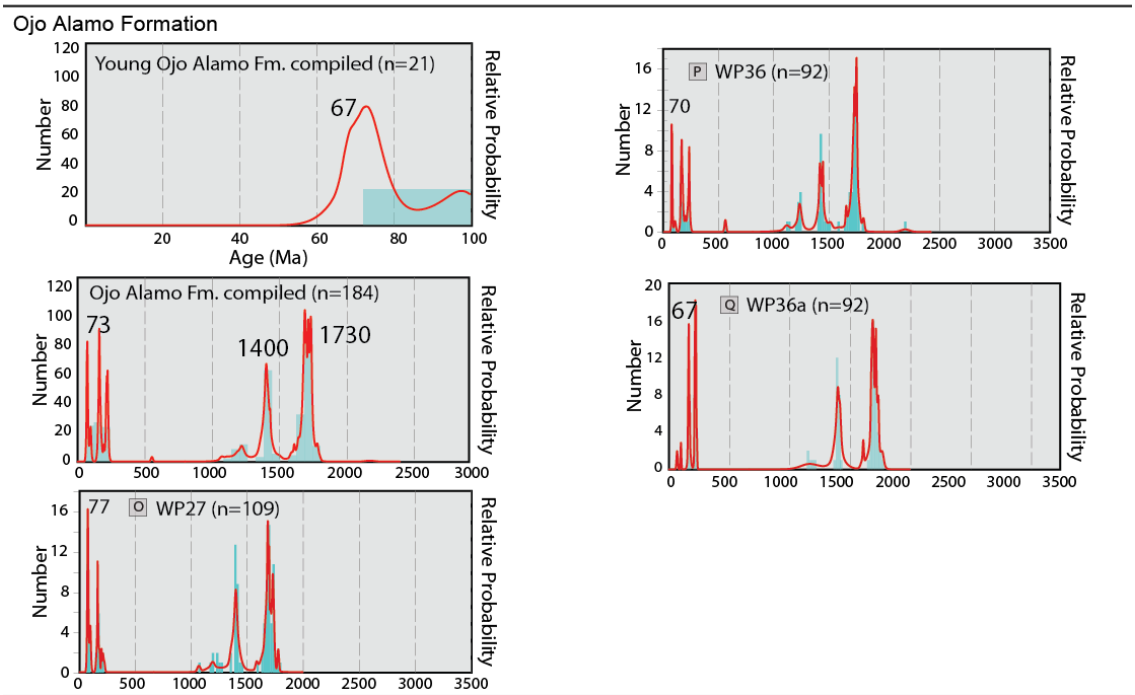
Ojo Alamo Formation
Young Ojo Alamo Fm. compiled (n=21)
67
Ojo Alamo Fm. compiled (n=184)
73
1400
1730
O WP27 (n=109)
77
P WP36 (n=92)
70
Q WP36a (n=92)
67
Number
Relative Probability
Age (Ma)

Figure 2-Error! No text of specified style in document.**-7** Detrital zircon spectra for Nacimiento, San Jose, and Ojo Alamo Formations.

Detrital zircon of Nacimiento Formation

Detrital zircon analysis of this unit (n=176) reveals dominant Proterozoic age peaks with 49% of grains between 1400-1750 Ma. We combine all samples from the Nacimiento Formation (Fig 7; n=176) to better characterize the diverse zircon populations in the provenance for this overall stratigraphic unit. The merged post-100 Ma grain population (Fig 7; n=38) shows a dominant 69.9±3.3 (2σ) Ma peak. K-S statistic show P-values of 0.000 between the two samples. The Nacimiento Formation have low P-values between the two samples (0.000).

This DZ signature is compatible with reworking of older San Juan basin sedimentary units and/or a sedimentary source in Proterozoic crystalline basement. The presence of Maastrichtian-aged detrital zircons in the Nacimiento Formation shows that San Juan Basin paleorivers were also sourcing young shallow magmatic or volcanic units in the early to middle Paleocene.

Detrital zircon of the San Jose Formation:

The early Eocene (~55 Ma) San Jose Formation was deposited unconformably on the Nacimiento Formation and consists of fluvial siliciclastics derived predominantly from the north-northwest. Detrital zircon analysis of this unit (n=188) reveals dominant Proterozoic age peaks of ~1710 and ~1400 Ma and subordinate Jurassic and Cretaceous age peaks at 160, and 72. We combine all samples from the San Jose Formation (Fig 7; n=188) to better characterize the diverse zircon populations in the provenance for this overall stratigraphic unit. The merged post-100 Ma grain population (Fig 7; n=15)

shows a dominant 71.9±3.1 (2σ) Ma peak. This DZ signature is compatible with reworking of older San Juan basin units as well as a sedimentary source in in Proterozoic crystalline basement. Its spectrum is, in turn, similar to the slightly younger Galisteo Formation and K-S statistic show P-values of 0.000.

Detrital zircon of the 40-37 Ma (Eocene) Galisteo Formation.

Samples were collected from the upper Galisteo Formation for detrital zircon analysis but did not sample the lower Diamondtail lithosequence (Fig. 3). Basal (directly above the Diamondtail Formation) and upper samples of the Galisteo Formation were collected in the Galisteo Preserve (Fig. 1). Another upper section sample was collected from the Galisteo Formation near La Cienega, NM. Figure 8 shows the youngest grains and hence the maximum depositional peak ages from detrital zircon analytical method are 94 Ma in the upper section and 170 in the basal portions of the same unit, while the youngest grains from the La Cienega section are 45 Ma. Stratigraphically, these are inconclusive with determining true maximum depositional age. Provenance also shows input from compiled ages (n=557) ranging between the minimum 45-163 Ma in the lower part of the unit while the upper portion of the unit shows a much more uniform source, with spectral peaks dominated by a single young peak at 283 Ma. Older portions of each of the Galisteo Formation sequences show minor but constant input from sources throughout the 1800-1300 Ma timeframe (Fig. 4E). K-S statistics for this sample show low P-values between MSD-NM-2011-25 and MSD-NM-2011-23 (0.001) and MSD-NM-2011-26 (0.046), but high between MSD-NM-2011-26 and MSD-NM-2011-23 (0.358).

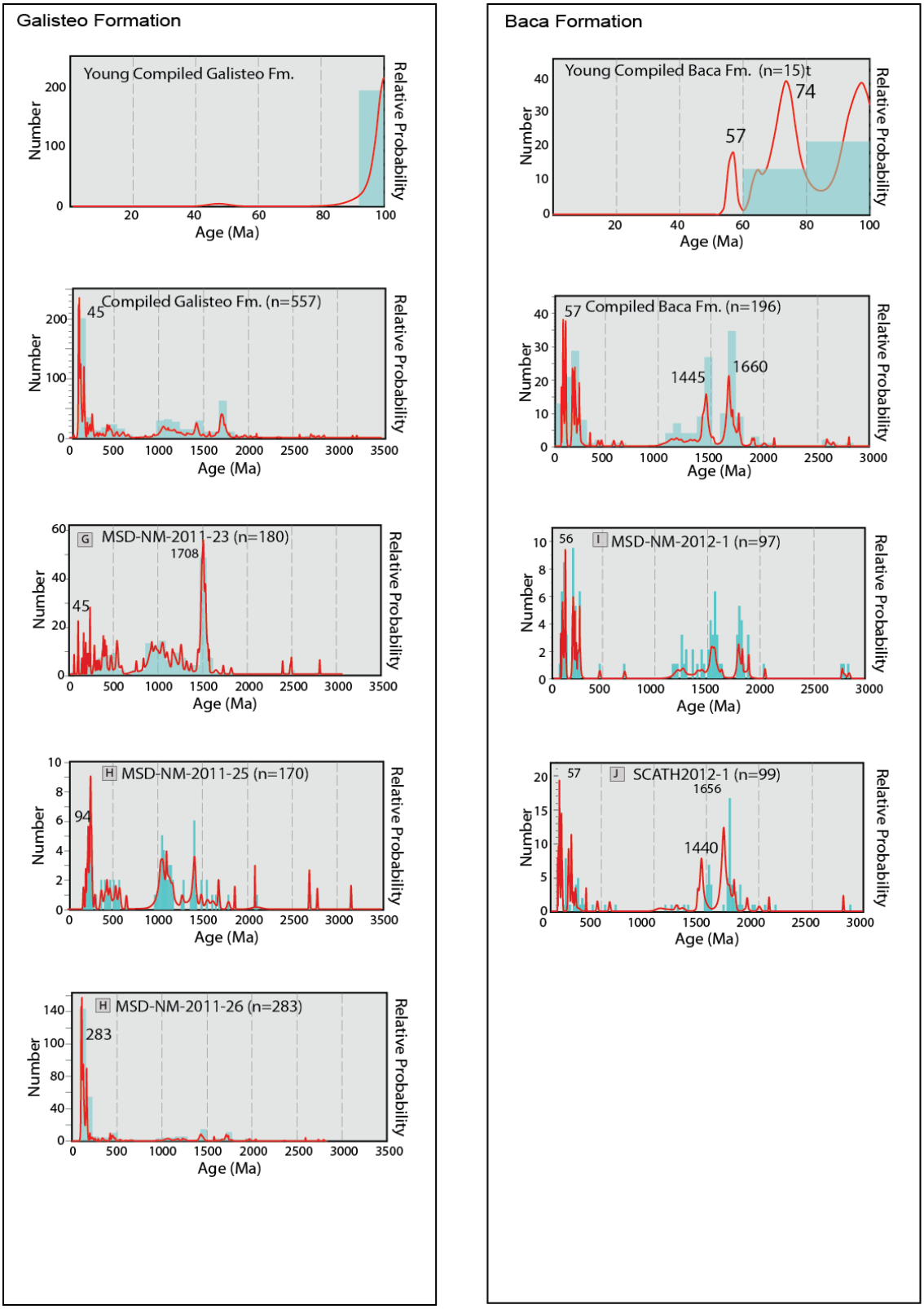

Figure 2-Error! No text of specified style in document.**-8** Detrital zircon spectra for Galisteo and Baca Formations.

Detrital zircon of the 50-40 Ma Baca Formation:

Detrital zircon analyses were conducted on two Baca Formation samples (Fig. 8), an upper section sample from near Pie Town, NM, and a second sample collected from Jornada del Muerto by Steve Cather (pers. comm., 2012) (Fig. 1). Samples show youngest grains of 56-57 Ma compatible with its 40-50 Ma fossil age. We combine all samples from the San Jose Formation (Fig 8; n=196) to better characterize the diverse zircon populations in the provenance for this overall stratigraphic unit. Broad 70-100 and 170-220 distributions suggest extensive sampling of Cordilleran arc magmatism. There are relatively few Paleozoic grains. Precambrian-age spectral peaks range from 1.3-1.5 Ga and 1.65-1.75 Ga, with a general absence of 1.0 Ga grains. The merged post-100 Ma grain population (Fig 8; n=15) shows a youngest peak at 57 Ma. P values for the two Baca Formation samples contain low vales between SCATH2012-1 and MSD-NM-2012-1 of 0.010.

Detrital zircon of the ~ 30 Ma Telluride Conglomerate.

We collected seven detrital zircon samples, from three locations: basal and upper section samples were collected from near Little Molas Lake and Mt. Wilson (Figs. 4, 9) and near the town of Telluride, CO.. These represent proximal and more distal fluvial sections, respectively. The upper section at Little Molas Lake (sample #MS-10-9, location B) yielded the youngest zircon grains at ~30 Ma (MDA = 31.3±2.0 Ma; 15% grains ≤40 Ma). The spectrum also includes peaks at 602 and strong Precambrian peaks at ~1750-1650 and 1400 Ma (63% grains 1400-1750 Ma). Samples from the lower part of the section above Molas Lake (sample #MS-10-7) returned no young grains of < 200 Ma. Instead, the spectrum is dominated by strong peaks at 1455-1427 and 520 as well as

less dominant but steady input of zircons from 1700-1750 Ma (83% grains 1400-1750 Ma).

The thick (nearly 400 m/1300 ft.) Mt. Wilson section of Telluride Conglomerate has been intruded and elevated by large sills including the 27 Ma Mt. Wilson Stock (Gonzales, 2015) and is overlain by thick succession of volcaniclastic rocks. There is minor contact metamorphism of the Telluride Conglomerate where it is in contact with overlying volcanic units.

Samples were taken from unaltered Telluride Conglomerate. The upsection sample from Mt. Wilson (MSD-CO-2011-18) has youngest grains of 33.8±0.7 Ma (19% grains ≤40 Ma) while the basal sample from Mt. Wilson (MSD-CO-2011-18) has MDA = 34.05±0.7 Ma (8% grains ≤40 Ma). Both samples also show a steady but non-single-peak-dominant input of grains ranging from 1750-1600 and 1475-1400 Ma. The combined Little Molas Lake and Mt. Wilson spectrum is dominated by a peak at 34 Ma, with secondary peaks at 65 Ma, and ~1700 Ma (Fig. 5B).

Upper Telluride Conglomerate (WP42) has MDA = 33.4±1.3 Ma (6% grains ≤40 Ma). Telluride Conglomerate samples WP43 and WP 52 return no grains younger than 50 Ma, with MDAs = 63.0±1.3 Ma and 65.7±1.0 Ma, respectively. We combine all samples from the Telluride Conglomerate (Fig 8; n=637) to better characterize the diverse zircon populations in the provenance for this overall stratigraphic unit. The merged post-100 Ma grain population (Fig 7; n=109) shows a dominant 31.3±2.0 (2σ) Ma peak.

P-values for samples used in K-S statistics for the Telluride Conglomerate samples range between 0.0.000-0.491 (Table 2).

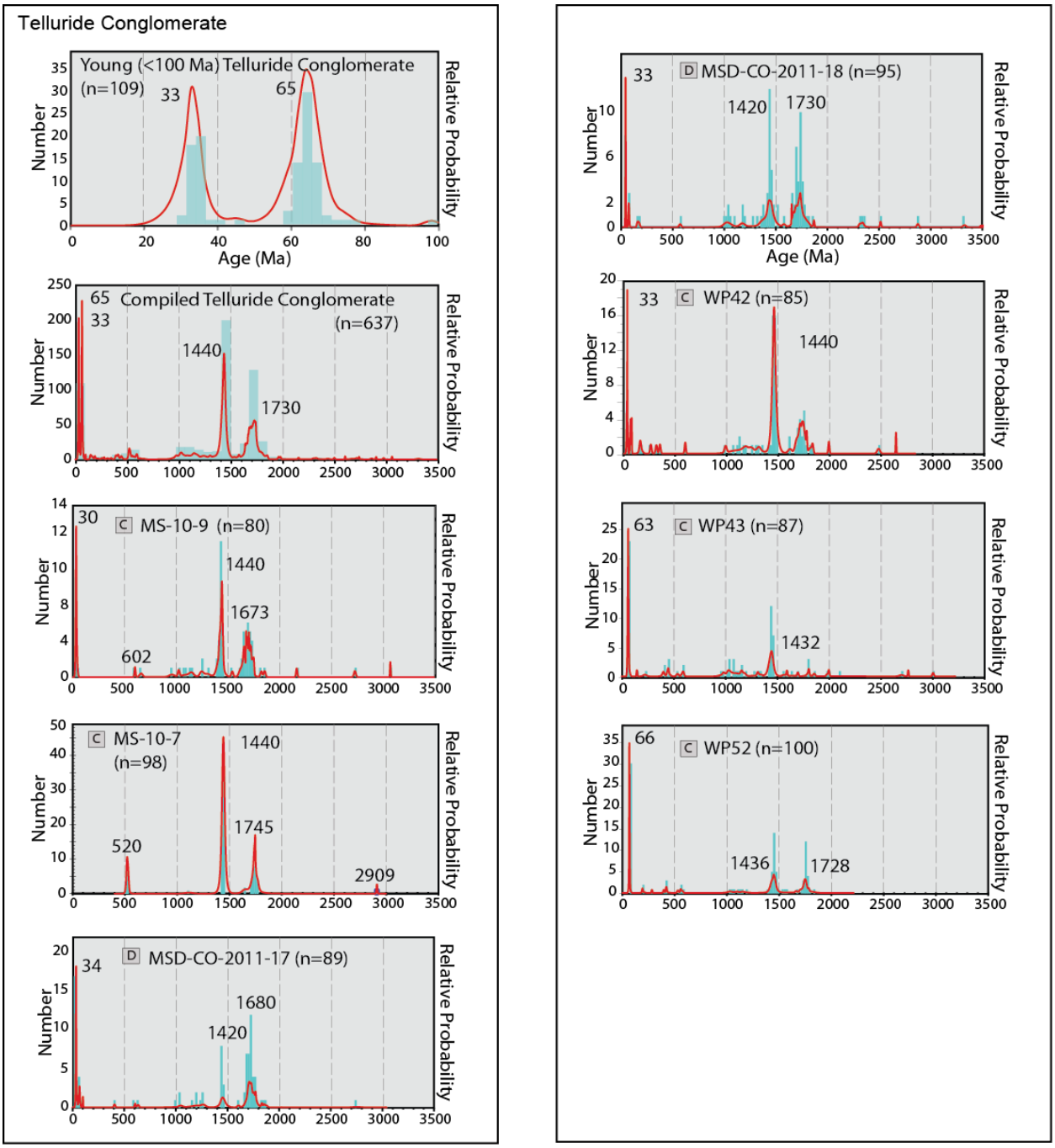

Figure 2-Error! No text of specified style in document.**-9** Detrital zircon spectra for Telluride Conglomerate.

Detrital zircon of the ~ 30 Ma Oligocene Blanco Basin Formation.

New detrital zircon data from two locations (Fig. 4) return a MDA = 33.8±1.1 Ma (4% of grains ≤40 Ma) in the mid-section sample near Chama, NM (1, location E).

None of the other samples have young grain populations of note. The Chama section samples are dominated by peaks at 1690 and 1698 Ma, and notably lack input from the ~1400 Ma grain population. In contrast, the Pagosa Springs samples (Fig. 1, location F) have signatures dominated by peaks in the 1450-1430 Ma range, but are nearly bereft of any of the ~1700 Ma grains so prevalent in the Chama section. We combine all samples from the Blanco Basin Formation (Fig 8; n=638) to better characterize the diverse zircon populations in the provenance for this overall stratigraphic unit. The merged post-100 Ma grain population (Fig 8; n=7) shows a dominant 33 Ma peak.

P-values from the five Blanco Basin samples show low values (0.000) between MSD-CO-2011-13 and the DG-BRISTERE-PC3A, PC3B, and PC5. High correlations exist between DG-BRISTERE-PC3B and DG-BRISTERE-PC5 (1.0), and DG-BRISTERE-PC3B and DG-BRISTERE-PC3A (0.649) and DG-BRISTERE-PC3A and DG-BRISTERE-PC5 (0.311).

Source material is likely similar to that found in the Telluride Conglomerate: the Needles Mountain basement rocks including the ~ 1.8-1.7 Ga Irving Formation and Twilight Gneiss (Gonzales and Van Schmus, 2007), ~1.8-1.4 Ga Uncompahgre Group and Vallecito Conglomerate (Jones et al., 2009), ~1.7 Ga Bakers Bridge and ~1.72 Ga Tenmile Granite the ~1.4 Ga Eolus Granite and Electra Lake Gabbro (Gonzales and Van Schmus, 2007).

Detrital zircon of the 29-26 Ma El Rito Formation and Ritito Conglomerate

This study includes two samples of the El Rito from two locations (Fig. 4): the El Rito climbing area north of Abiquiu (Fig. 1, location B) and near Cerro Pedernal (Fig. 1, location A). Detrital zircon ages indicate the El Rito Formation sample from the El

Rito climbing area (location B, sample #MS-11-5) had 4 young grains: 37.6±2.5, 34.1±2.4, 29.8±2.3, and 28.6±2.5Ma. The next peak ages are 1655+, 1092, 1006, and Ma. The age-probability plot shows a young peak of 29 Ma, with the spectrum otherwise dominated by a range of grains from ~1750-1650 Ma with peaks at 1710 and1688 Ma. The Cerro Pedernal El Rito sample (location A, sample #MS-11-1) lacks young grains otherwise dominated by a range of grains from ~1750-1650 Ma with age peaks at 1695 and 1691 Ma. This syn-rift deposit is likely not long-traveled and sourced from local Precambrian exposures. P-values for the El Rito are low (0.002) between the two samples, suggesting these two sections of the El Rito contain divergent source material.

Detrital zircon of the 26 Ma (Latest Oligocene) Ritito Conglomerate.

Detrital samples from the Ritito Conglomerate in this study are from the basal and upper sections of one outcrop near Cerro Pedernal, NM. The Ritito Conglomerate detrital zircon signature (MDA = 29.72±0.48) is similar to that of the El Rito Formation (MDS = 32.3±6.3, 4% of grains ≤40 Ma). The youngest grains include 5 grains of 26.9-26.3 Ma grains and 21 <40 Ma grains (23% of grains) ~ from the upper part of the Ritito Conglomerate section with the remaining spectrum is dominated by clasts of 1710-1680 Ma age. P-values for K-S statistics are 0.000-0.02 between the four samples from the two units. This is in agreement with evidence for a lobe of the 25 Ma Amalia tuff (Zimmerer and McIntosh, 2012) that overlies the Ritito in the Tusas Mountains.

We combine all samples from the El Rito Formation and Ritito Conglomerate **(F**ig 10; n=364) to better characterize the diverse zircon populations in the provenance

for these overall stratigraphic unit. The merged post-100 Ma grain population (Fig 10; n=4) shows a dominant 28 Ma peak.

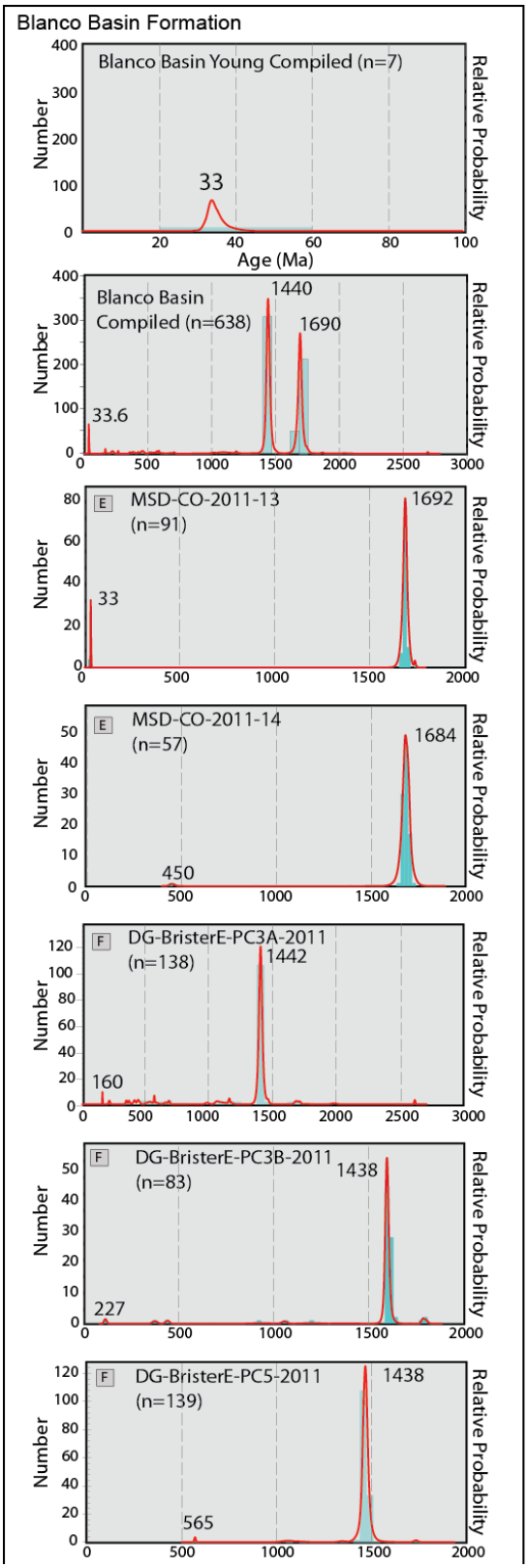
Blanco Basin Formation
Blanco Basin Young Compiled (n=7)
33
Blanco Basin
Compiled (n=638)
1440
1690
33.6
E
MSD-CO-2011-13
(n=91)
1692
33
E
MSD-CO-2011-14
(n=57)
1684
450
F
DG-BristerE-PC3A-2011
(n=138)
1442
160
F
DG-BristerE-PC3B-2011
(n=83)
1438
227
F
DG-BristerE-PC5-2011
(n=139)
1438
565
Number
Relative Probability
Age (Ma)

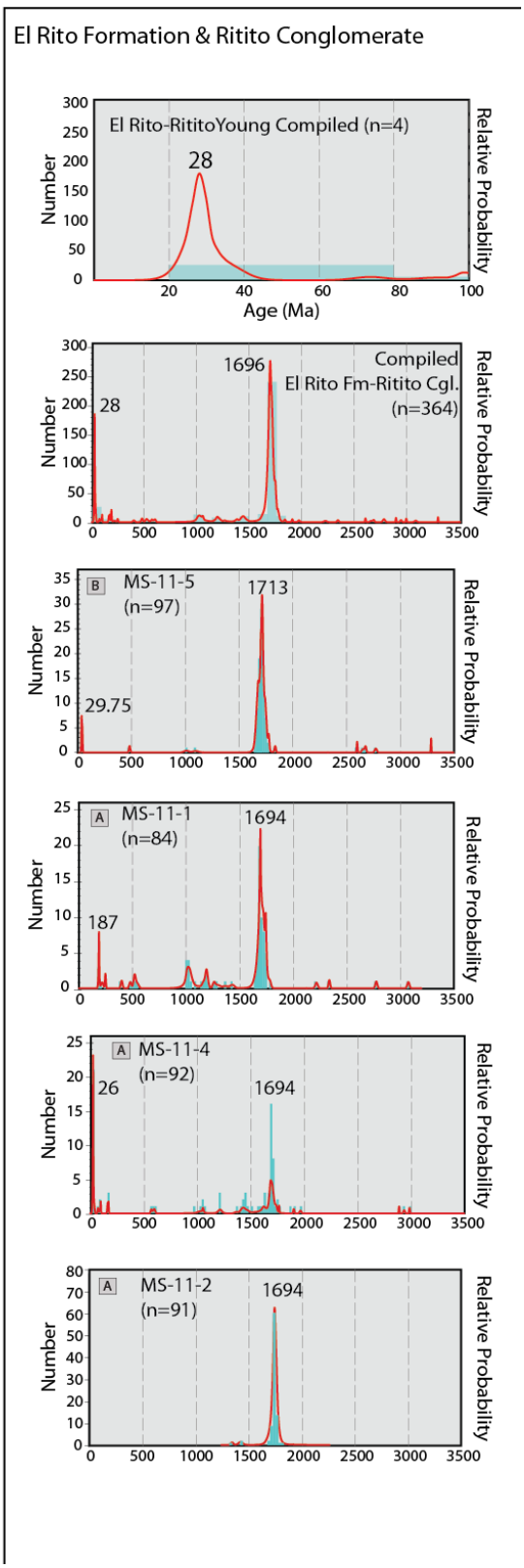
El Rito Formation & Ritito Conglomerate
El Rito-RititoYoung Compiled (n=4)
28
Compiled
El Rito Fm-Ritito Cgl.
(n=364)
1696
28
B
MS-11-5
(n=97)
1713
29.75
A
MS-11-1
(n=84)
1694
187
A
MS-11-4
(n=92)
26
1694
A
MS-11-2
(n=91)
1694
Number
Relative Probability
Age (Ma)

Figure 2-Error! No text of specified style in document.**-10** Detrital zircon spectra for Blanco Basin, El Rito Formations and Ritito Conglomerate.

REGIONAL SYNTHEISS & PROPOSED CORRELATIONS

Figure 11 presents the DZ spectra determine in this study. Spectra for the young (< 100 Ma) grains are normalized to facilitate comparison of units and potential correlations. In each spectrum, the preferred depositional age is shown by a solid black line. We have taken the approach that even if two samples from different levels of the same stratigraphic unit are statistically different from each other, the merged results are nevertheless a better way to characterize the max depo age for chronostratigraphic comparison and potential correlation. In addition, the merged spectrum shows the different provenances available during deposition of the stratigraphic unit for paleogeographic interpretations. Comparison of the spectra for these units leads to several stratigraphic advances.

1) San Juan Basin Cretaceous stratigraphic units have Jurassic and Cretaceous peaks indicating they were sourced from the Cordilleran magmatic arc (possibly the Sierra Nevada, southern Arizona and southwestern New Mexico) deposited by some combination of wind and river transport. Youngest zircon grains track the depositional age determined from fossils and ash bed dating(Peppe et al., 2013; Heizler et al., 2013).

2) Paleocene conglomerates in the San Juan Basin represent a mix of local magmatic sources (La Plata Mountains or Rico complex) related to the southern Colorado Mineral Belt volcanism and continued sources from Cordilleran arc. The 65 Ma McDermott Formation was locally sourced, from the La Plata Mountains, Rico area, or Sawatch Range. Ojo Alamo and Nacimiento Formations contain similar detrital

zircon populations and both contain a strong 65 Ma peak like the McDermott Formation and are considered to be unconformity bound Paleocene facies deposited during Laramide basin subsidence. Our data suggest both Cordilleran magmatic arc and local Colorado Mineral Belt magmatism source regions.

3) Eocene conglomerates studied were the San Jose, Galisteo, and Baca Formations. Each had diverse age rocks exposed in the source regions and we support the view that they reflect deposition related to a widespread erosional episode from 60-50 Ma that caused extensive erosional beveling of the Rocky Mountains and an important episode in formation of the Rocky Mountain erosion surface that we call RMES-1 (Fig. 2A). San Jose and Galisteo have similar age and detrital zircon spectra and may have been part of the same fluvial system. Baca and Galisteo Formations are directly overlain by a volcaniclastic deposits.

4) Newly dated Oligocene conglomerates, previously thought to be Eocene, were deposited on a beveled surface that we call RMES-2 (Fig. 2). Telluride Conglomerate is now constrained to be 31.3±2.0-34.05±0.7 Ma, recording a local-regional unroofing sequence; Blanco Basin Formation is 33.8±1.1 Ma. El Rito Formation is 32.3±6.3 Ma and may be an early pulse of the same unit as the 29.72±0.48 Ma Ritito Conglomerate. Like the Eocene conglomerates, these units are directly overlain by volcaniclastic deposits that prograded over the pre-volcanic conglomerates.

Analysis of Precambrian detrital zircons is difficult because of the nearly ubiquitous 1.7 and 1.4 Ga peaks in nearly all spectra. Figure 1 (light gray line) shows the southern boundary of pre-1.7 Ga crust of the Yavapai province that may be useful although younger 1.7-1.6 Ga crust (Mazatzal age) is present in both provinces. 1.45-1.35

Ga plutons are present in both provinces. 1.1 Ga grains (from recycling of Jurassic erg, Dickinson et al., 2012) often make a third Precambrian peak. Figure 11 shows a normalized plot of these grains.

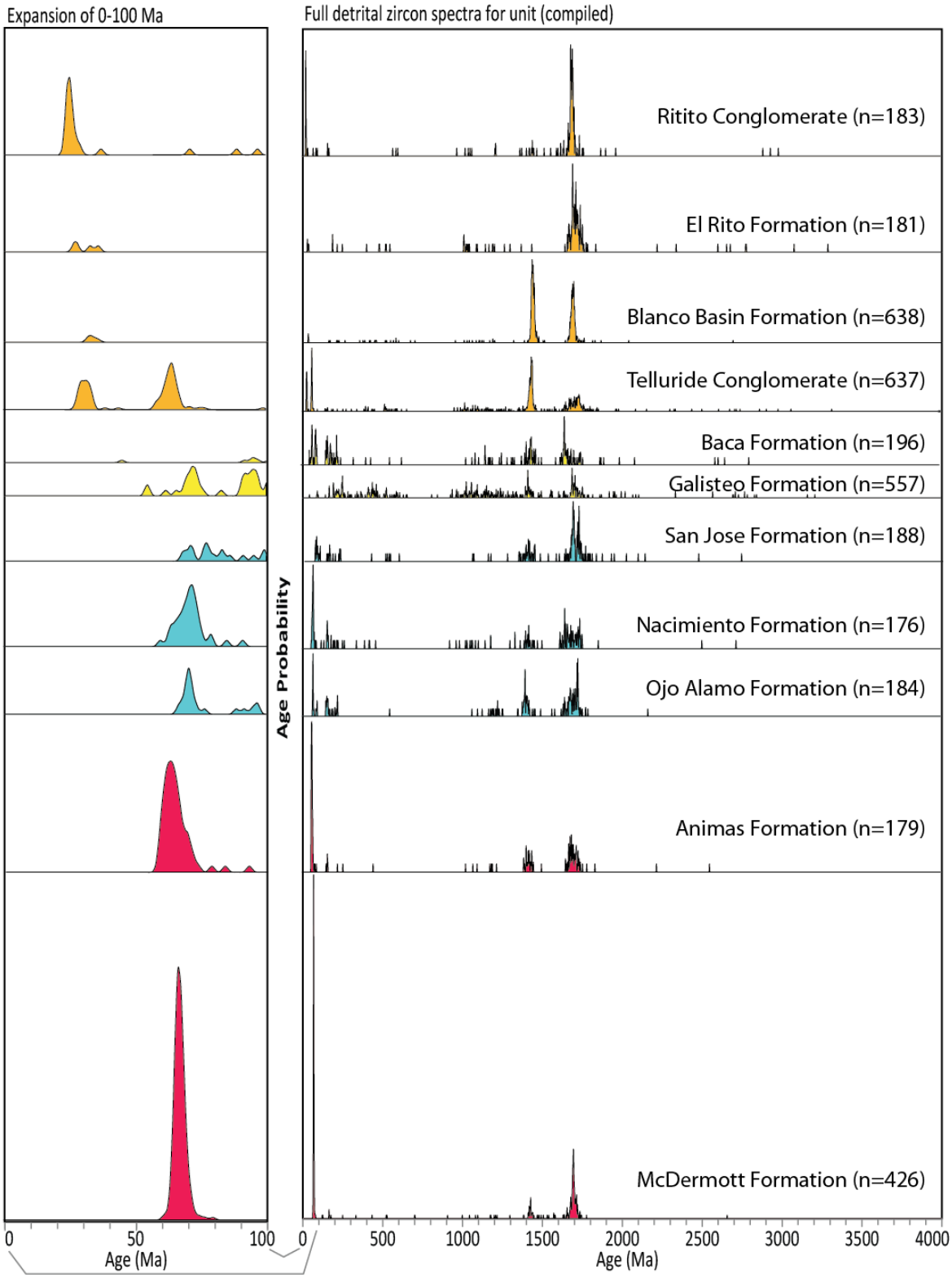
Expansion of 0-100 Ma
Full detrital zircon spectra for unit (compiled)
Ritito Conglomerate (n=183)
El Rito Formation (n=181)
Blanco Basin Formation (n=638)
Telluride Conglomerate (n=637)
Baca Formation (n=196)
Galisteo Formation (n=557)
San Jose Formation (n=188)
Nacimiento Formation (n=176)
Ojo Alamo Formation (n=184)
Animas Formation (n=179)
McDermott Formation (n=426)
Age Probability
0
50
100
Age (Ma)
0
500
1000
1500
2000
2500
3000
3500
4000
Age (Ma)

Figure 2-Error! No text of specified style in document.**-11** Normalized age-probability plots of compiled sample data for units of this study. Left-hand side shows an expansion of 0-100 Ma for each unit; right-hand side shows spectra from 0-4 Ga.

MAGMATIC CONNECTIONS TO ROCKY MOUNTAIN EROSION SURFACE EPSODES

One striking similarity of many of the Paleocene, Eocene, Oligocene and Miocene conglomerate deposits is that they are paired siliciclastic-volcanic successions. Generally pre-volcanic conglomerates containing basement clasts and unroofing successions that are overlain by thick volcaniclastic successions that form aprons around major volcanic centers. Timing of these transitions is as follows: McDermott Formation and Animas Formation at 65 Ma; Galisteo Formation to Espinaso Formation at 40 Ma; Baca Formation to Spears Formation at ~35 Ma; Telluride Conglomerate to San Juan Formation at 32-28 Ma; Blanco Basin to Conejos Formation at 34 Ma; Abiquiu and Lower Picuris Formations to Conejos Formation at 34 Ma; Ritito Conglomerate to Amalia Tuff at 25 Ma (Fig. 2).

Our interpretation for this association at different times and places in the Rocky Mountains attempts to tie together mantle uplift (Heller et al., 2013; Karlstrom et al., 2012) and multiple times of erosion on the RMES. For the Eocene conglomerates, evidence for a two pulses of Colorado Mineral Belt magmatism (~65-40 Ma) separated by a magmatic gap magmatic gap (~56-44 Ma; Feldman, 2010) may provide the best explanation for multiple periods of erosion on the RMES.

PALEODRAINAGES AND PALEOELEVATIONS THROUGH TIME INFERRED

Like numerous previous workers (Pazzaglia and Kelley, 1998; Cather et al., 2012; Heller et al., 2013), this paper uses the stratigraphic record of basement-clast conglomerate and overlying volcaniclastic deposits sheets to evaluate the pre-Miocene history of erosion and associated river systems in the southern Rocky Mountains. We have integrated and synthesized data from preserved remnants of Eocene- Oligocene geomorphic features such as the Rocky Mountain erosion surface, caldera lakes with fossil data, and paleovalleys filled with volcanic deposits. These geomorphic and volcanic features suggest the modern drainage pattern of radial drainage away from the Colorado Rockies became established around Oligocene magmatic centers. Development of Miocene river systems and associated paleoriver deposits are poorly recorded (except in the Rio Grande rift and Ogallala Formation) due to the transition from aggradation to deep erosion (tectonic turn-around of McMillan et al., 2006) that we infer to be due to a Miocene pulse of surface uplift.

Figure 12 describes a speculative model for drainage system evolution and elevation change through time. Paleoelevation history controversial, but we show the present elevation of various deposits and paleogeomorphic features relative to local base level elevations of paleoriver systems of the southern Rocky Mountains at different times. This uplift history is similar to a progressive uplift model proposed by Raynolds et al Raynolds et al. (2007) for the Denver basin. It is also compatible with (calibrated by) interpretations of paleontological data that use comparisons to nearest living relatives (NLR; Axelrod and Bailey, 1976; Axelrod, 1987; Raynolds et al., 2007;Leopold and Zaborac-Reed (personal communication, 2015). This model is an alternative to models for the major pulse of elevation gain in the Laramide followed by

persistent high elevation throughout the Cenozoic (Wolfe, 1992; Wolfe et al., 1998; Gregory et al., 1996).

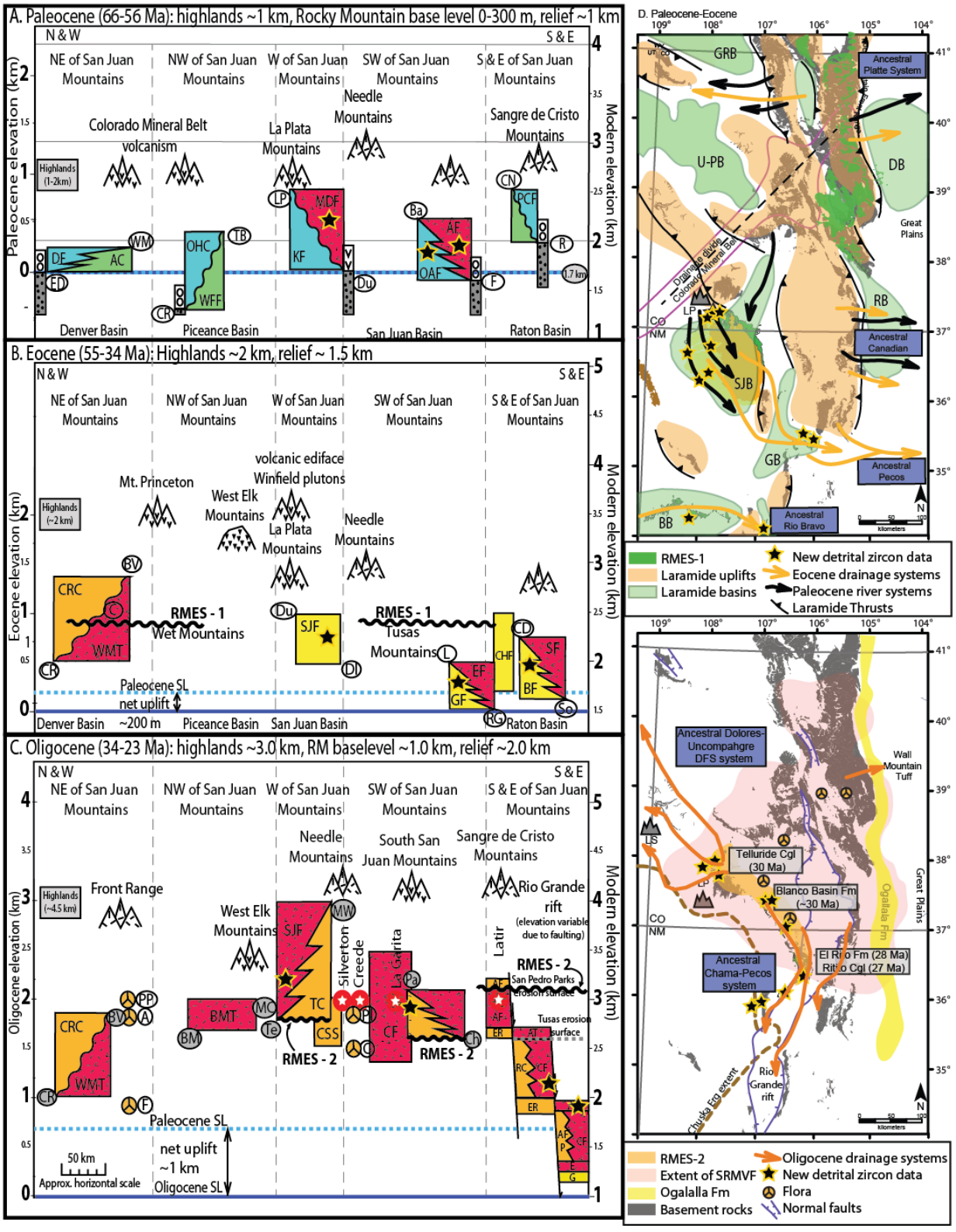
A. Paleocene (66-56 Ma): highlands ~1 km, Rocky Mountain base level 0-300 m, relief ~1 km
N & W
S & E
NE of San Juan Mountains
NW of San Juan Mountains
W of San Juan Mountains
SW of San Juan Mountains
S & E of San Juan Mountains
Colorado Mineral Belt volcanism
La Plata Mountains
Needle Mountains
Sangre de Cristo Mountains
Highlands (1-2km)
Paleocene elevation (km)
Modern elevation (km)
Denver Basin
Piceance Basin
San Juan Basin
Raton Basin
B. Eocene (55-34 Ma): Highlands ~2 km, relief ~ 1.5 km
Mt. Princeton
West Elk Mountains
volcanic ediface
Winfield plutons
RMES - 1
Wet Mountains
Tusas Mountains
Paleocene SL
net uplift
~200 m
Eocene elevation (km)
C. Oligocene (34-23 Ma): highlands ~3.0 km, RM baselevel ~1.0 km, relief ~2.0 km
Front Range
Rio Grande rift
(elevation variable due to faulting)
South San Juan Mountains
RMES - 2
San Pedro Parks
Tusas erosion surface
Paleocene SL
net uplift ~1 km
Oligocene SL
50 km
Approx. horizontal scale
Oligocene elevation (km)
D. Paleocene-Eocene
Ancestral Platte System
Ancestral Canadian
Ancestral Pecos
Ancestral Rio Bravo
Great Plains
Drainage divide Colorado Mineral Belt
RMES-1
Laramide uplifts
Laramide basins
New detrital zircon data
Eocene drainage systems
Paleocene river systems
Laramide Thrusts
Ancestral Dolores-Uncompahgre DFS system
Ancestral Chama-Pecos system
Wall Mountain Tuff
Telluride Cgl (30 Ma)
Blanco Basin Fm (~30 Ma)
El Rito Fm (28 Ma)
Rito Cgl (27 Ma)
Ogallala Fm
Chuska Erg extent
Rio Grande rift
RMES-2
Extent of SRMVF
Ogalalla Fm
Basement rocks
Oligocene drainage systems
New detrital zircon data
Flora
Normal faults

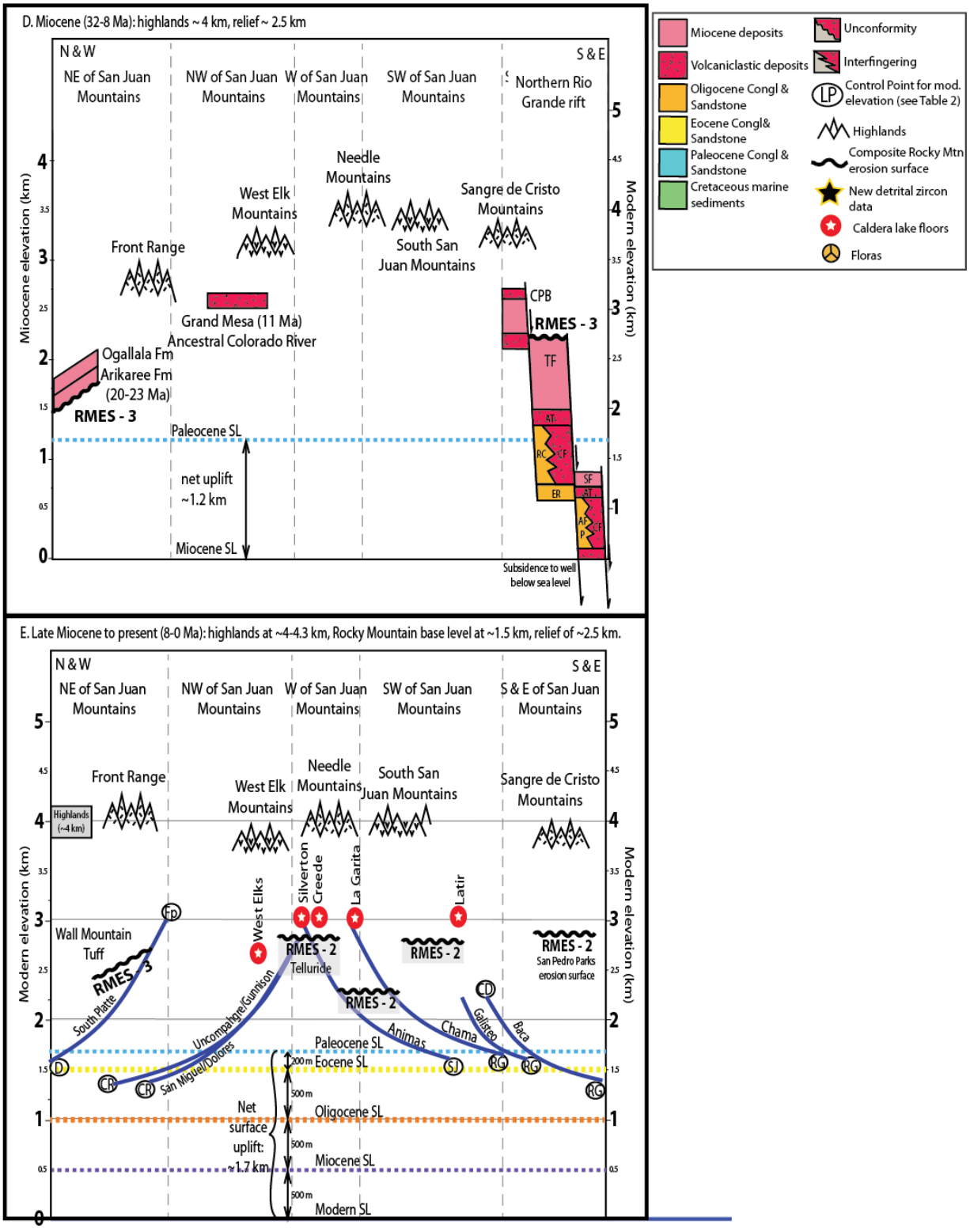

Figure 2-Error! No text of specified style in document.**-12** Current elevation (right axis) and inferred paleoelevation (left axis) of paleoriver deposits (local base level) show model for episodic regional surface uplift and increasing topographic relief through time. A. Paleocene (66-56 Ma) paleorivers were graded to the level of the retreating

Cretaceous seaway (Cretaceous sea level was ~ 200 m above modern sea level; Cather et al., 2012). Paleocene highlands and relief need not have been higher than ~ 1 km. Abbreviations: DF = Denver Fm (67 Ma); AC = Arapahoe Cgl (68 Ma; OHC = Ohio Creek Cgl (60 Ma); WFF = Williams Fork Fm ; MDF = McDermott Fm (67 Ma); KF = Kirtland Fm (~74 Ma); AF= Animas Fm (64-61 Ma); OAF = Ojo Alamo Fm (65 Ma); PCF = Poison Cyn Fm (60-56 Ma). B. Eocene (56-34 Ma) paleoriver deposits include the Castle Rock, San Jose, Cuchara/ Huerfano/Farisita, Galisteo/ Espinaso, Baca/ Spears; preserved geomorphic features include paleovalleys filled with Wall Mountain tuff, volcaniclastics of Castle Rock, and Blue Ridge tuff; and the Eocene erosion surfaces in the Wet Mountains/ Front Range; this component of the Rocky Mountain erosion surface (RMES-1) may reflect syntectonic responses to ~0.5 km of tectonic uplift coincident with Eocene magmatism in the Colorado Mineral Belt (42-38 Ma Winfield/ Echo Canyon plutons of Feldman, 2010). Abbreviations: CRC = Castle Rock Cgl (36 Ma); WMT = Wall Mtn. Tuff (36.7 Ma); SJF = San Juan Fm (~55-28 Ma); GF = Galisteo Fm (54-38 Ma); EF = Espinaso Fm (36 Ma); CHF = Cuchara-Huerfano-Farisita Fms (53-49 Ma); BF = Baca Fm (45-40 Ma); SF = Spears Fm (38 Ma). C. Oligocene (34-23 Ma) paleoriver systems have pre-volcanic gravels overlain by the prograding volcaniclastic apron of the San Juan volcanic field: Telluride/ San Juan; Blanco Basin/ Conejos, El Rito/Ritito/ Conejos. Preserved geomorphic features include caldera complexes, laccoliths, aggradational filling of paleovalleys, and an Oligocene component of erosion (RMES-2) due to epeirogenic (and constructional) uplift. Caldera lakes preserve flora interpreted by Leopold and Axelrod to have been deposited at 1-2 km elevation based on Nearest Living Relative (NLR) analysis: F=Florissant, A= Antero, PP= Pitch Pinnacle, P= Platoro, C= Creede placed as paleoelevations of Leopold and Zaborac-Reed (in prep.). Abbreviations: CRC = Castle Rock Cgl (36 Ma); WMT = Wall Mtn. Tuff (36.7 Ma); BMT = Blue Mesa Tuff (28.5 Ma); SJF= San Juan Fm (28.3 Ma); TC= Telluride Cgl (30 Ma); CSS= Chuska Ss (33-29 Ma); CF = Creede Fm; BBF = Blanco Basin Fm (~30 Ma); CF = Conejos Fm (24 Ma); SF = upper Santa Fe Gp; AF = Abiquiu Fm (30 Ma); P = Lower Picuris Fm (18-34 Ma); AT = Amalia Tuff (25 Ma); ER = El Rito (29 Ma); RC = Ritito Conglomerate (26 Ma); E = Espinaso Fm (36 Ma); G = Galisteo Fm (54-38 Ma). D. Miocene (23-10 Ma) paleoriver deposits are poorly preserved (except in the Rio Grande rift) due to ~0.5 km surface uplift and deep erosion documented by thermochronology and as inferred from Oligocene lake flora. Ogallala Formation represents diachronous aggradation by distributed fluvial systems onto a composite age high level erosion surface (RMES-3). Abbreviations: SF = upper Santa Fe Gp; CPB = Cerro Pedernal basalt (8 Ma); TF = Tesuque Fm (20-10 Ma); AF = Abiquiu Fm (30 Ma); P = Lower Picuris Fm (18-34 Ma); AT = Amalia Tuff (25 Ma); CF = Conejos Fm (24 Ma); ER = El Rito (29 Ma); RC = Ritito Conglomerate (26 Ma); E = Espinaso Fm (36 Ma); G = Galisteo Fm (54-38 Ma). E. Late Miocene to Recent (last 10 Ma) records the incisional history of the modern river system of the Rocky Mountain region at rates of 100-150 m/Ma (Aslan et al., Karlstrom et al., 2011). Differential erosional isostatic rebound of several hundred meters (Lazear et al., 2013) accompanied differential uplift across faults to reverse the apparent gradient of Telluride and ancestral Gunnison paleoprofiles. Neogene and ongoing surface uplift elevate Cretaceous marine deposits to modern elevations of ~ 1.7 km. Location maps at upper-right hand show geographic maps and evolution of river systems during Paleocene (black arrows) and Eocene (gold arrows). Laramide basins (green) and uplifts (tan), RMES-1 (dark green) and Paleocene-Eocene-age detrital zircon samples (black/yellow stars) are indicated. Abbreviations are: GRB = Green River Basin, U-PB = Uinta-Piceance Basin, DB = Denver Basin, RB = Raton Basin, LP = La Plata Mountains, SJB = San Juan Basin, GB = Galisteo Basin, BB = Baca Basin. Location maps at lower-right hand show geographic maps and evolution of river systems during Oligocene (orange arrows). San Juan Volcanic Field Apron extent (pink), flora samples (yellow-black circle symbol), Chuska erg extent (brown dashed line), and Oligocene-age detrital zircon samples (black/yellow stars) are indicated. Abbreviations are: LS=La Sal Mountains, LP = La Plata Mountains.

Stratigraphic columns (Figs. 2, 12) show approximate thicknesses of the gravel sheets, thickness of overlying volcaniclastic sedimentary rocks, where present, and the time of transition from the dominantly pre-volcanic Precambrian clast conglomerates to the time of inundation by aggrading volcaniclastic aprons (e.g., Lipman et al. 2007). The gradients of the pre-volcanic gravels are generally unknown due to fragmentary preservation of river deposits due to subsequent deformation and differential uplift, but a

sense of the elevation of the local base levels is shown based on the lowest and highest present elevations of each units.

We also show inferred paleoriver systems in the map at the right (Fig. 11D, 11E), landscape and geologic features at their modern elevations (right scale of Fig 11), and speculative paleoelevations (left scale). Preserved paleogeomorphic features include paleovalleys, calderas and caldera lakes, shallowly emplaced laccolithic intrusions, and remnants of the underlying Rocky Mountain erosion surface. Modern trunk river systems and highest peaks (hence modern Rocky Mountain relief) are shown with the approximate elevation gradients and flow directions of rivers. Modern drainage flows radially away from central Colorado reflecting that this region is the highest mean elevation region in the conterminous US (Karlstrom et al., 2012). Because of this geometry, the continental divide is shown in the center of the diagram and columns to the left represent areas that presently drain north and west toward Wyoming and the Colorado Plateau and while features to the right drain south and east from the San Juan Mountains to the Great Plains and Gulf of Mexico. Elevations of highest exposed Cretaceous marine units are also shown for reference and to emphasize the overall ~ 2 km scale of surface uplift since ~ 70 Ma.

Paleocene: 66-56 M

Laramide uplift and resulting erosion was dominated by thrust uplifts with relatively modest regional epeirogeny, and magmatic centers along the Colorado mineral belt. Final withdrawal of the Cretaceous seaway took place diachronously between 72 and 64 Ma (Cather et al., 2012). Regional epeirogenic surface uplift (mean value of several hundred m shown in Fig. 12) is required to explain the sub-Dakota erosion

surface that dipped north off of the Mogollon highlands in southern Arizona and New Mexico, and to explain the regional change to non-marine deposition (Dickinson et al., 1968). Mechanisms for such epeirogeny that accompanied thrust uplifts include some combination of: passage of relatively buoyant segments of the Farallon slab (Saleeby, 2003; Liu and Gurnis, 2010; Heller et al., 2013) hydration of the lithosphere by fluids from the subducting Farallon slab (Humphreys et al., 2003), crustal thickening (Erslev, 2005), and building of magmatic highlands of the Laramide component of the Colorado Mineral Belt (Feldman, 2010; this paper).

Figures 12A shows that Paleocene magmatism is recorded along the northeast-trending Colorado Mineral Belt. The Sawatch-Front Range areas have the ~70 Ma Whitehorn Stock and the 56-63 Ma plutons preserved in the Twin Lakes pluton. In the western San Juan Mountains, plutons range from 75-65 Ma (Gonzales, 2015).The expression of the magmatism in the Four Corners region is as shallow level intrusions as laccoliths: 67-75 Ma La Plata Mountains, 64-73 Ma Sleeping Ute Mountain, and 70-74 Ma Carrizo Mountain (Gonzales, 2015). These plutons still preserve parts of their volcanic edifices in the southwest (e.g., present La Plata, Carrizo and Ute Mountain uplifts (Gonzales, 2015) that sourced the McDermott Formation. While there is no definitive evidence of volcanic edifices farther northeast along the CMB, volcanic and plutonic bodies likely existed in this location but these volcanic and plutonic rocks have been eroded by as much as 8 km of subsequent rock uplift due to erosion (Feldman, 2010) and are only preserved in ash and volcaniclastic rocks in basinal deposits (e.g. Denver Basin; Raynolds et al., 2007). This Laramide magmatism along the CMB was followed by a magmatic gap from 54-44 Ma (Feldman, 2010).

Thin Paleocene gravel sheets present across the Colorado Plateau-Rocky Mountain region mark this period of epeirogenic differential uplift (Heller et al., 2013). The distribution and paleoflow indicators from preserved gravels and their inferred rivers from this time period are shown in Fig. 12and 13. Ohio Creek conglomerates were deposited by north-flowing paleorivers; Arapahoe and Raton conglomerates by east-flowing paleorivers, Ojo Alamo and McDermott Formations by southeast-flowing paleorivers. The Galisteo and Baca Formations were deposited by southeast- and east-flowing paleorivers, respectively. During the time of these units' deposition, the continental divide was likely defined in central Colorado by the NE-trending magmatic uplifts of the CMB, with rivers flowing SE toward the Gulf of Mexico (Galloway et al., 2011) and NW toward internally drained basins such as the Claron, Uinta, Piceance, and Green River basins (Fig. 12A). Relief may have been > 1 km, and basement rocks in the Front Range were exhumed from ~ 3 km depths (Kelley, 2002). Paleocene elevations and regional fluvial base level likely remained near Cretaceous sea level (+ 220 m modern sea level elevation; Cather et al., 2012) throughout the Paleocene as shown by warm, rain forest plant physiognomy with estimated mean annual temperatures of 18-26ºC and annual precipitation of 118-233 cm/yr. (Johnson et al., 2003). The Rocky Mountain erosion surface continued to develop from 56-42 Ma during what Cather et al., Cather et al. (2012) propose as a regional erosion period in the southern Rockies. An 8 Ma lacuna in the Denver Basin (64-56 Ma) is overlain by an arkose (D2 sequence of Raynolds et al., 2007), suggesting continued erosion of the Front Ranges with the RMES and associated rivers graded to still low-elevation basins.

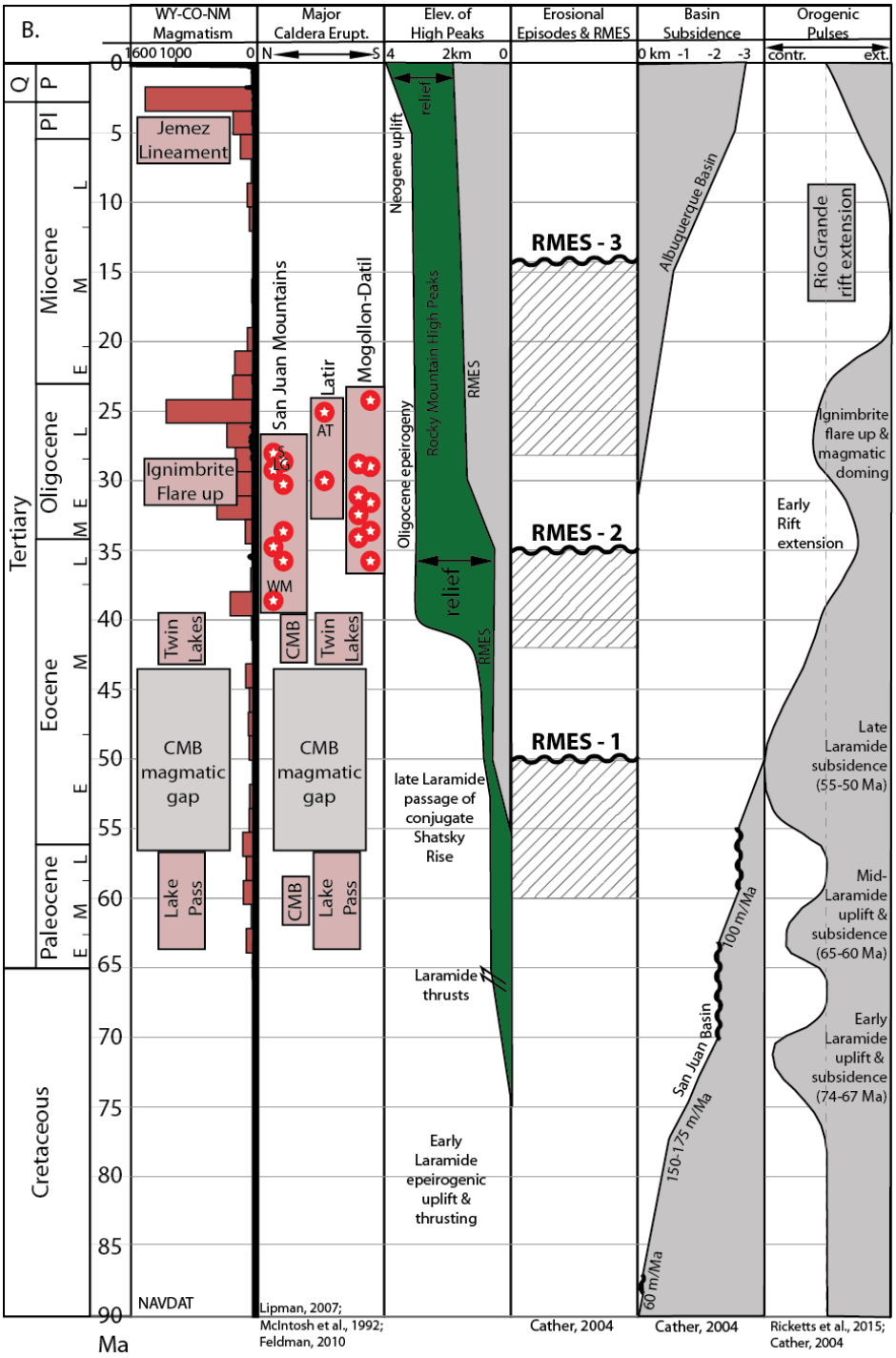

Figure 2-Error! No text of specified style in document.**-13** Major events in the southern Rocky Mountain region are indicated. These include periods of Cenozoic magmatism, major caldera eruptions, speculative elevation of highest peaks through time, regional erosion episodes, basin subsidence curves, andorogenic

Eocene (55-34 Ma)

Figures 12B show that Eocene uplift, erosion, and deposition took place 55-34 Ma. Cather et al. (2012) define an Eocene erosion episode from 42-37 Ma (centered in Wyoming, Montana, and Colorado) that they attribute to the post-Laramide isostatic rebound mechanism. Eocene magmatism includes the 43-39 plutonism of the Twin Lakes pluton that coincides temporally with the erosional event postulated by Cather et al. (2012). Cather et al. (2012) suggest that ~40 Ma Galisteo and Baca gravels reflect deposition or landscape stability in this time window in New Mexico (as reinforced by fossil evidence). Our DZ data are consistent with earlier interpretations for the age, source areas, and paleoflow directions in these systems. In our interpretation, these deposits reflect broad distributed fluvial systems on the flanks of broad uplifts, and view these deposits in terms of continued regional differential uplift following the Laramide due to a combination of mechanisms that added buoyancy, probably including magmatism associated with the Absaroka, Colorado Mineral Belt, and Mogollon highlands volcanic fields (Fig. 14A). The period (42-37 Ma) resulted in formation of the "Eocene" component of the Rocky Mountain erosion surface, although erosional beveling was likely diachronous and goes back earlier to the north (Cather et al., 2012). Several hundred meter deep paleovalleys (600 m in N Colorado, up to 1 km in Arizona) formed before 38 Ma that became filled with Eocene aggradational successions (White River, Castle Rock, Galisteo, Baca, Mogollon Rim Fms). Paleovalleys extended regionally across the northern and southern Rockies and Colorado Plateau, and provide evidence for a minimum headwater uplift of at least 600-1000 m above sea level, as shown in Fig. 12B. In some successions, valley filling and pre-volcanic clast conglomerate deposition foreshadowed deposition of voluminous volcanic-dominated

detritus starting at 38-34 Ma that is interbedded of the Mogollon Rim Formation (38 Ma; (Potochnik, 1989), Baca Formation (38 Ma) and Galisteo Formation (36 Ma). A potential mechanism that may explain this transition is that early buoyancy addition via plutonism in the developing Mogollon Datil and San Juan magmatic centers caused doming, erosion, and pre-volcanic gravel deposition followed by aggradational successions dominated by volcaniclastic sediments that mark the progradation of the volcaniclastic apron of the San Juan and Mogollon Datil volcanic fields beginning about 35 Ma (Ricketts et al., 2015). A pulse of Colorado Mineral Belt plutonism of 44-38 Ma (Feldman, 2010) plausibly drove uplift in central Colorado such that the continental divide likely coincided with the NE-trending Colorado Mineral belt. A magmatic gap from 54-44 Ma based on U-Pb and Ar-Ar cooling data provide evidence that the region remained deep and hot and was affected by reheating events from additional plutonism until after 30 Ma demonstrating long-lived plutonism (~ 40 Ma) at some locations in the Colorado Mineral Belt. Depth of emplacement, constrained by Al in hornblende and metamorphic petrology, shows surprisingly deep emplacement of the Whitehorn batholiths at about 10 km (Feldman, 2010). Unroofing to the surface took place by 37 Ma prior to re-burial by voluminous 37-25 Ma magmatism of the San Juan ignimbrite flare up. The voluminous and well-dated 36.7 ignimbrite Wall Mountain Tuff was erupted from Mt. Princeton (Lipman, 2007).

As shown in Figure 12C, The Oligocene of the southern Rocky Mountain region was a time of culmination of voluminous caldera eruptions in the San Juan and Mogollon Datil volcanic fields (Fig.13). Magmatism began in the San Juan volcanic field from 35-25 Ma (Lipman, 2007; Ricketts et al., 2015). At the same time,

magmatism swept east to west in the Mogollon-Datil field from 38 at Sierra Blanca to 25 Ma in the western Mogollon Datil field. These magmatic sweeps have been interpreted to be due to progressive foundering or delamination of the Farallon slab and asthenospheric result flow that resulted in both magmatism, buoyancy addition, and surface uplift (Karlstrom et al., 2012; Ricketts et al., 2015).

The Telluride and Blanco Basin paleoriver systems, and the parts of the RMES they rest on, are Oligocene in age rather than Eocene. As discussed above, these river systems initially carried dominantly pre-volcanic clasts from unroofing basement cored uplifts of the San Juan Mountains. As pre-caldera stratovolcano edifices grew, early gravels were inundated with volcaniclastic debris of the San Juan and Conejos that were part of an extensive volcaniclastic apron that extended well beyond the present outcrop area of volcanic rocks (Steven and Eaton, 1975; Lipman, 2007). The time of transition from unroofing sequence to volcaniclastic progradation took place 28-24 Ma during eruptions of the largest calderas with the La Garita calderas sourcing Blanco Basin Formation and San Juan-Silverton caldera sourcing the Telluride conglomerate. Uplift of about 0.5 km is inferred to have been driven by lithospheric delamination and asthenospheric return flow (Karlstrom et al., 2012) during this time period (Fig. 12C).

Miocene paleorivers and paleo geomorphic features (32-8 Ma).

Figure 12D shows Rio Grande rifting featured prominently during this time period. Relief increased throughout the region, and the deposition of sedimentary units was especially prevalent in the Rio Grande rift region.

Modern geomorphic features (8-0 Ma)

Modern drainage patterns in the southern Rocky Mountains have emerged from a composite history that was strongly influenced by Oligocene magmatic centers (Fig 12E). Tilted paleoprofiles of Oligocene units require additional differential tectonic uplift of several hundred meters by faulting (e.g., Telluride Conglomerate at Wilson Peak), and differential epeirogenic uplift (Rosenberg, 2014).

CONCLUSIONS

The gravels of this study range widely in age and reflect the evolution of river systems in a dynamic and differentially uplifting landscape. New U-Pb detrital zircon ages elucidate the erosional history of this region. New U-Pb ages constrain provenance and depositional setting for several Tertiary sedimentary units in southern CO and northern NM. Importantly, new ~30 Ma maximum ages for the Telluride Conglomerate and Blanco Basin redefine stratigraphic history for the region. The spatial distribution of these data confirm the composite, diachronous nature of the Rocky Mountain erosion surface. We suggest this feature formed in response to CMB, Laramide and Oligocene ignimbrite magmatism, and associated mantle- driven epeirogenic uplift from 70-25 Ma and this surface reflects the local-to-regional beveling of highlands.

We recognize a repeated pattern of conglomerates overlying the RMES throughout the Cenozoic in southwestern CO and northern NM. We interpret the erosion and subsequent fluvial deposition of the units discussed above NOT to be a result of widespread tectonic quiescence, but rather to record tectono-magmatic driven headwater region uplift relative to basin subsidence. In our model, Oligocene volcanic centers established drainage patterns that persist today (e.g., the drainages of the Telluride Conglomerate and Blanco Basin-El Rito-Ritito Formation paleorivers). Drainages

established around constructional volcanic edifices continue to be modified by young mantle upwelling, volcanism, and faulting.

ACKNOWLEDGMENTS

This work was supported by the Colorado Rockies Experiment and Seismic Transects (CREST) experiment funded by the National Science Foundation Continental Dynamics Program under award EAR-0607808 and NSF-EAR 1032156 for support of the Arizona LaserChron Center. Special thanks to reviewers for editorial comments, support from the Alfred P. Sloan Minority Ph.D. Program, Colorado Scientific Society, New Mexico Geological Society, Geological Society of America, and University of New Mexico Graduate & Professional Student Association. Authors would like to acknowledge the excellent senior thesis by C.L. Harraden and Fort Lewis College's 2012 undergraduate field methods class, and field and laboratory support from Rachel Price and Dr. Kirt Kempter.

REFERENCES CITED

Aby, S.B., Kempter, K., Koning, D., 2011, Recent mapping of the Oligo-Miocene Los Pinos Formation and associated units in the Tusas Mountains, New Mexico Scott, *in* New Mexico Geological Society 62nd Annual Fall Field Conference Guidebook, v. 62, p. 275–280.

Axelrod, D.I., 1997, Paleoelevation Estimated from Tertiary Floras: International Geology Review, v. 39, p. 1124–1133, doi: 10.1080/00206819709465319.

Axelrod, D.I., 1987, The Late Oligocene Creede fl ora, Colorado: University of California Publication of Geological Society, v. 130, p. 1–236.

Axelrod, D.I., and Bailey, H.P., 1976, Tertiary vegetation, climate, and altitude of the Rio Grande depression, New Mexico-Colorado: Paleobiology, v. 2, p. 235–254.

Barnes, H., 1953, Geology of the Ignacio area, Ignacio and Pagosa Springs quadrangles, La Plata and Archuleta Counties, Colorado: US Geological Survey Oil and Gas Investigations Map OM 138, scale 1:63,360,.

Barton, M.A., Fricke, H.C., 2006, Mapping topographic relief and elevation of the Central Rocky Mountain region durin gthe latest Eocene using stable isotope data from mammalian tooth enamel, *in* Geological Society of America Abstracts with Programs, p. 202.

Bove, D.J., Hon, K., Budding, K.E., Slack, P.D., Snee, L.W., and Yeoman, R.A., 2001, Geochronology and geology of late Oligocene through Miocene volcanism and minerialization in the western San Juan Mountains, Colorado: US Geological Survey Professional Paper, v. 1642.

Brister, B.S., 1992, The Blanco Basin Formation (Eocene), San Juan Mountains region, Colorado and New Mexico, *in* New Mexico Geological Society 43rd Annual Field COnference Guidebook, v. 43, p. 321–331.

Bromfield, C.S., and Bush, A.L., 1968, Multiple intrusion in the San Miguel Mountains, Colorado: New Mexico Geological Society 19th field conference,.

Burbank, W., and Luedke, R., 1969, Geology and ore deposits of the Eureka and adjoining districts, San Juan Mountains, Colorado: Geological survey Professional Paper 535, p. 1–73, http://www.getcited.org/pub/101474817.

Cather, S.M., 1982, Lacustrine sediments of Baca Formation (Eocene), western Socorro Country, New Mexico: New Mexico Geology, v. 4 no.1, p. 1–6.

Cather, S.M., 2004, Laramide orogeny in central and northern New mexico and southern Colorado, *in* The Geology of new Mexico, New Mexico Geological Society, p. 203–248.

Cather, S.M., 2009, Stratigraphy and structure of the Laramide Carthage-La Joya Basin, Central New Mexico: New Mexico Geological Society Guidebook 60th Field Conference, p. 227–234.

Cather, S.M., 1992, Suggested revisions to the Tertiary tectonic history of North-central New Mexico: New Mexico Geological Society Guidebook, 43rd Field Conference, v. 43, p. 109–122.

Cather, S.M., 1986, Volcano-sedimentary evolution and tec- tonic implications of the Datil Group (latest Eocene- early Oligocene), west-central New Mexico: University of Texas at Austin, 484 p.

Cather, S.M., Chapin, C.E., and Kelley, S.A., 2012, Diachronous episodes of Cenozoic erosion in southwestern North America and their relationship to surface uplift, paleoclimate, paleodrainage, and paleoaltimetry: Geosphere, v. 8, p. 1177–1206, doi: 10.1130/GES00801.1.

Cather, S.M., Connell, S.D., Chamberlin, R.M., McIntosh, W.C., Jones, G.E., Potochnik, A.R., Lucas, S.G., and Johnson, P.S., 2008, The Chuska erg: Paleogeomorphic and paleoclimatic implications of an Oligocene sand sea on the Colorado Plateau: Geological Society of America Bulletin, v. 120, p. 13–33, doi: 10.1130/1326081.1.

Cather, S.M., and Johnson, G.C., 1984, Eocene tectonics and eopositional setting of west-central New Mexico and eastern Arizona: New Mexico Bureau of Mines and Mineral Resources Circular, v. 192, p. 33.

Cather, S.M., McIntosh, W.C., and Chapin, C.E., 1987, Stratigraphy, age, and rate of deposition of the Datil Group (Upper Eocene-Lower Oligocene), west-central New Mexico: New Mexico Geology, v. 9, p. 50–54, http://medcontent.metapress.com/index/A65RM03P4874243N.pdf\nhttps://geoinfo.

nmt.edu/publications/periodicals/nmg/downloads/9/n3/nmg_v9_n3_p50.pdf.
Chapin, C.E., Kelley, S.A., 1997, The Rocky Mountain Erosion Surface in the Front Range of Colorado, *in* Colorado Front Range Guidebook, Rocky Mountain Association of Geologists, p. 101–113.
Connell, S.D., and Lucas, S.G., 2001, Stratigraphy of the Lower Santa Fe Group, Hagan Embayment, North-Central New Mexico: Preliminary Results, *in* Stratigraphy and Tectonic Development of the Albuquerque Basin, Central Rio Grande rift, p. H–49–H–56.
Cross, W., 1894, Folio 7: Geological Atlas of the United States:.
Cross, W., and Larsen, E.S., 1935, A brief review of the geology of the San Juan region of southwestern Colorado: U.S. Geological Survey Bulletin, p. 138.
Cross, W., and Purington, C.W., 1899, ption of the Telluride quadrangle, Colorado: U.S. Geological Survey Geological Atlas Folio 57:.
Davis, W.M., 1911, The Colorado Front Range : A Study in Physiographic Presentation Author (s): W . M . Davis Source : Annals of the Association of American Geographers , Vol . 1 (1911), pp . 21-83 Published by : Taylor & Francis , Ltd . on behalf of the Association of: Annals of the Association of American Geographers, p. 21–83.
Dickinson, W.R., 2013, Rejection of the lake spillover model for initial incision of the Grand Canyon, and discussion of alternatives: Geosphere, v. 9, p. 1–20, doi: 10.1130/GES00839.1.
Dickinson, W.R., and Gehrels, G.E., 2009, Use of U-Pb ages of detrital zircons to infer maximum depositional ages of strata: A test against a Colorado Plateau Mesozoic database: Earth & Planetary Science Letters, v. 288, p. 115–125.
Dickinson, W.R., Klute, M.A., Hayes, M.J., Janecke, S.U., Lundin, E.R., McKittrick, M.A., and Olivares, M.D., 1988, Paleogeographic and paleotectonic setting of Laramide sedimentary basins in the central Rocky Mountain region: Geological Society of America Bulletin,.
Dickinson, W.R., Lawton, T.F., Pecha, M., Davis, S.J., Gehrels, G.E., and Young, R. a., 2012, Provenance of the Paleogene Colton Formation (Uinta Basin) And Cretaceous-Paleogene provenance evolution in the Utah foreland: Evidence from U-Pb ages of detrital zircons, paleocurrent trends, and sandstone petrofacies: Geosphere, v. 8, p. 854–880, doi: 10.1130/GES00763.1.
Dickinson, R.G., Leopold, E.B., and Marvin, R.F., 1968, Late Cretaceous uplifts and volcanism on the north flank of the San Juan Mountains, Colorado: Quarterly of the Colorado School of Mines, v. 63, p. 125–148.
Ekas, L.M., Ingersoll, R.V., Baldridge, W.S., and Shafiquallah, M., 1984, The Chama-El Rito Member of the Tesuque Formation, Española Basin, New Mexico, in Rio Grande Rift: Northern New Mexico: New Mexico Geological Society 35th Annual Fall Field Conference Guidebook, p. 137–143.
Epis, R.C., and Chapin, C.E., 1975, Geomorphic and tectonic implications of the Post-Laramide, Late Eocene Erosion Surface in the southern Rocky Mountains, *in* Curtis, G.F. ed., Cenozoic history of the southern Rocky Mountains, Geological Society of America Memoir 144, p. 45–74.
Erslev, E., 2005, 2D Laramide Geometries and Kinematics of the Rocky Mountains,

Western U.S.A, *in* The Rocky Mountain Region - An Evolving Lithosphere: Tectonics, Geochemistry, and Geophysics, p. 7–20.
Erslev, E., 1993, Thrusts, back-thrusts, and detachment of Rocky Mountain foreland arches: Geological Society of America Special Paper, v. 280, p. 339–358.
Evanoff, E., and Chapin, C.E., 1994, Composite nature of the "Late Eocene surface" of the Front Range and adjacent regions, Colorado and Wyoming: Geological Society of America Abstracts with Programs, v. 12, p. 12.
Feldman, J.D., 2010, The Emplacement and Exhumation History of the Twin Lakes Batholith and Implications for the Laramide Orogeny and Flat Slab Subduction.
Finlay, G.I., 1916, Description of the Colorado Springs folio: U.S. Geological Survey Folio 203:.
Galloway, W.E., Whiteaker, T.L., and Ganey-Curry, P., 2011, History of Cenozoic North American drainage basin evolution, sediment yield, and accumulation in the Gulf of Mexico basin: Geosphere, v. 7, p. 938–973, doi: 10.1130/GES00647.1.
Gehrels, G.E., Valencia, V. a., and Ruiz, J., 2008, Enhanced precision, accuracy, efficiency, and spatial resolution of U-Pb ages by laser ablation-multicollector-inductively coupled plasma-mass spectrometry: Geochemistry, Geophysics, Geosystems, v. 9, p. n/a–n/a, doi: 10.1029/2007GC001805.
Gonzales, D.A., 2015, New U-Pb Zircon and 40Ar/39Ar age constraints on the Late Mesozoic to Cenozoic plutonic record in the western San Juan Mountains: The Mountain Geologist, v. 52, p. 5–42.
Gonzales, D.A., and Gianniny, G.L., 2010, David A. Gonzales and Gary L. Gianniny The tales of Late Cretaceous to Tertiary gravels in southwestern Colorado (: v. 42, p. 2010–2011.
Gonzales, D.A., Kray, B., and Gianniny, G.L., 2005, Insight into the timing of the Cenozoic uplift in Southwestern Colorado from the Telluride Conglomerate: Geological Society of America Abstracts with Programs, v. 37, p. 16.
Gonzales, D. a., and Van Schmus, W.R., 2007, Proterozoic history and crustal evolution in southwestern Colorado: Insight from U/Pb and Sm/Nd data: Precambrian Research, v. 154, p. 31–70, doi: 10.1016/j.precamres.2006.12.001.
Gregory, K.M., and Chase, C.G., 1994, Tectonic and climatic significance of a late Eocene low-relief , high-level geomorphic surface , Colorado: Journal of Geophysical Research, v. 99, p. 20141–20160.
Gregory, K.M., Mcintosh, W.C., and Range, S., 1996, Paleoclimate and paleoelevation of the Oligocene Pitch-Pinnacle flora, Sawatch Range, Colorado: Geological Society of America Bulletin, v. 108, p. 545–561, doi: 10.1130/0016-7606(1996)108<0545.
Harraden, C.L., 2007, The Deopositional History of the Telluride Conglomerate and Implications for Mid-Tertiary Tectonism in the Western San Juan Mountains, Colorado.
Heizler, M.T., Williamson, T.E., Peppe, D.J., Ramezani, J., Bowring, S.A., and Mason, I., 2013, 40AR/39AR Chronostratigraphy of Cretaceous and Paleocene strata in the San Juan Basin, New Mexico: Accuracy limitation of high precision measurements: Geological Society of America Abstracts with Programs, v. 45, p. 289.
Heller, P.L., Mathers, G., Dueker, K., and Foreman, B., 2013, Far-traveled latest Cretaceous-Paleocene conglomerates of the Southern Rocky Mountains, USA:

Record of transient Laramide tectonism: Bulletin of the Geological Society of America, v. 125, p. 490–498, doi: 10.1130/B30699.1.
Humphreys, E.D., Hessler, E., Dueker, K., Farmer, C.L., Erslev, E., and Atwater, T., 2003, How Laramide-age hydration of North American lithosphere by the Farallon slab controlled subsequent activity in the western United States: International Geology Review, v. 45, p. 575–595.
Ingersoll, R. V., Cavazza, W., Baldridge, W.S., and Shafiqullah, M., 1990, Cenozoic sedimentation and paleotectonics of north-central New Mexico; Implications for initition and evolution of the Rio Grande rift: GSA Bulletin, v. 102, p. 1280–1296, doi: 10.1130/0016-7606(1990)102<1280:CSAPON>2.3.CO;2.
Johnson, K.R., Reynolds, M.L., Werth, K.W., and Thomasson, J.R., 2003, Overview of the Late Cretaceous, early Paleocene, and early Eocene megafloras of the Denver Basin, Colorado: Rocky Mountain Geology, v. 38, p. 101–120, doi: 10.2113/gsrocky.38.1.101.
Karlstrom, K.E., Coblentz, D., Dueker, K., Ouimet, W., Kirby, E., Van Wijk, J., Schmandt, B., Kelley, S., Lazear, G., Crossey, L.J., Crow, R.S., Aslan, A., Darling, A., Aster, R., et al., 2012, Mantle-driven dynamic uplift of the Rocky Mountains and Colorado Plateau and its surface response: Toward a unified hypothesis: Lithosphere, v. 4, p. 3–22, doi: 10.1130/L150.1.
Karlstrom, K.E., Coblentz, D., Dueker, K., Ouimet, W., Kirby, E., Van Wijk, J., Schmandt, B., Kelley, S., Lazear, G., Crossey, L.J., Crow, R., Aslan, a., Darling, a., Aster, R., et al., 2011, Mantle-driven dynamic uplift of the Rocky Mountains and Colorado Plateau and its surface response: Toward a unified hypothesis: Lithosphere, v. 4, p. 3–22, doi: 10.1130/L150.1.
Kelley, 2002, Unroofing of the southern Front Range, Colorado: A view from the Denver Basin: Rocky Mountain Geology, v. 37, p. 189–200.
Kelley, S., and Chapin, C.E., 1997, Internal Structure of the Southern Front Range, Colorado, From an Apatite Fission-Track Thermochronology Perspective, *in* Colorado Front Range Guidebook, Rocky Mountain Association of Geologists, p. 19–30.
Kelley, S.A., Chapin, C.E., Cather, S.M., and Person, M., 2009, Thermal history of the eastern Socorro Basin, Socorro County, New Mexico, based on apatite fission-track thermochronology, *in* New Mexico Geological Society Guidebook, 60th Field Conference, p. 347–358.
Kelley, S.A., Kempter, K.A., McIntosh, W.C., Maldonado, F., Smith, G.A., Connell, S.D., Koning, D.J., and Whiteis, J., 2013, Syndepositional deformation and provenance of Oligocene to Lower Miocene sedimentary rocks along the western margin of the Rio Grande rift, Jemez Mountains, New Mexico, *in* Hudson, M.R., Grauch, V.J.S. ed., New Perspectives on Rio Grande Rift Basins: From Tectonics to Groundwater, Geological Society of America Special Paper 494, v. 494, p. 101–123, doi: 10.1130/2013.2494(05).
Klute, M.A., 1986, Sedimentology and sandstone petrography of the Upper Kirtland Shale and ojo Alamo Sandstone, Cretaceous-Tertiary boundary, western and southern San Juan Basin, New Mexico: American Journal of Science1, v. 286, p. 463–488.

Koning, D., Karlstrom, K., May, J., Skotnicki, S., Horning, R., Newell, D., and Muehlberger, W.R., 2005, Geologic Map of the Ojo Caliente Quadrangle , Rio Arriba and Taos Counties , New Mexico:.

Koning, D.J., Kempter, K., Peters, L., Mciintosh, W.C., and May, S.J., 2011, Miocene-Oligocene volcaniclastic deposits in the northern Abiquiu embayment and southern Tusas Mountains, New Mexico, *in* New Mexico Geological Society Guidebook 62nd Field Conference, p. 251–274.

Kottlowski, F.E., 1957, Mesozoic strata flanking the southwestern San Juan Mountains, Colorado and New Mexico: New Mexico Geological Society 8th Field Conference Guidebook, v. 8, p. 138–153.

Kray, B., 2004, An evaluation of the depositional history and timing of the Tertiary Telluride Conglomerate, Southwest Colorado: Fort Lewis College, Durango, 23 p.

Larsen, E.S., and Cross, W., 1956, Geology and petrology of the San Juan region southwestern Colorado: U.S. Geological Survey Professional Paper, v. 258, p. 303.

Lazear, G., Karlstrom, K., Aslan, A., and Kelley, S., 2013, Denudation and fl exural isostatic response of the Colorado Plateau and southern Rocky Mountains region since 10 Ma: Geosphere, v. 9, p. 792–814, doi: 10.1130/GES00836.1.

Lee, W.T., 1922, Peneplains of the Front Range and Rocky Mountain National Park, Colorado: U.S. Geological Survey Bulletin, v. 730 A, p. 17.

Lee, W.T., 1917, The geologic story of Rocky Mountain National Park, Colorado: U.S. National Park Service, 89 p.

Lee, J.P., Stockli, D.F., Kelley, S.A., Pederson, J.L., Karlstrom, K.E., and Ehlers, T.A., 2013, New thermochronometric constraints on the Tertiary landscape evolution of the central and eastern Grand Canyon , Arizona: Geosphere, doi: 10.1130/GES00842.1.

Leonard, E.M., 2002, Geomorphic and tectonic forcing of late Cenozoic warping of the Colorado piedmont: Geology, v. 30, p. 595–598.

Leonard, E.M., Hubbard, M.S., Kelley, S.A., Evanoff, E., Siddoway, C.S., Charles, G., Heizler, M., Timmons, M., and Oviatt, C.G., 2002, High Plains to Rio Grande Rift : Late Cenozoic Evolution of Central Colorado:, doi: 10.1130/0-8137-0003-5.59.

Lipman, P.W., 2000, Central San Juan caldera cluster: regional volcanic framework: Geological Society of America Special Paper 346, v. 346, p. 9–69.

Lipman, P., 2007, Incremental assembly and prolonged consolidation of Cordilleran magma chambers: Evidence from the Southern Rocky Mountain volcanic field: Geosphere2, v. 3, p. 42–70, doi: 10.1130/GES00061.1.

Lipman, P.W., Fisher, F.S., Mehnert, H.H., Naeser, C.W., Luedke, R.G., and Steven, T.A., 1976, Multiple ages of Mid-Tertiary mineralization and alteration in the western San Juan Mountains, Colorado: Bulletin of the Society of Economic Geologists,.

Lipman, P.W., and Hall, 1975, Reconnaissance geologic map of the Chama Quadrangle: Miscellaneous field studies map MF-682:.

Lipman, P.W., and McIntosh, W.C., 2008, Eruptive and noneruptive calderas, northeastern San Juan Mountains, Colorado: Where did the ignimbrites come from? Geological Society of America Bulletin, v. 120, p. 771–795, doi: 10.1130/B26330.1.

Lipman, P.W., Steven, T.A., and Mehnert, H.H., 1970, Geological Society of America

Bulletin Volcanic History of the San Juan Mountains , Colorado , as Indicated by Potassium − Argon Dating: Geological Society of America Bulletin, doi: 10.1130/0016-7606(1970)81.
Lisenbee, A.L., 1999, Preliminary Geologic Map of the Galisteo Quadrangle , Santa Fe County , New Mexico:.
Liu, L., and Gurnis, M., 2010, Dynamic subsidence and uplift of the Colorado Plateau: Geology, v. 38, p. 663–666.
Logsdon, M.H., 1981, A preliminary basin analysis of the El Rito Formation (Eocene) north-central New Mexico.: Geological Society of America Bulletin, v. 92, p. 968–975, doi: 10.1130/0016-7606(1981)92<968:APBAOT>2.0.CO;2.
Lorraine, M.M., and Gonzales, 2003, Lahars or not lahars? An evaluation of the volcanic connection for the late Cretaceous McDermott Formation near Durango, Colorado: Geological Society of America Rocky Mountain Section Meeting Abstracts with Programs, p. 13–3.
Lucas, S.G., Cather, S.M., Abbott, J.C., and Williamson, T.E., 1997, Stratigraphy and tectonic implications of Paleogene strata in the Laramide Galisteo Basin , north-central New Mexico: New Mexico Geology, p. 89–95.
Lucas, S.G., Hunt, A.P., and Sullivan, R.., 2006, Stratigraphy and age of the Upper Cretaceous Fruitland Formation, west-central San Juan Basin, New Mexico: New Mexico Museum of Natural History and Science Bulletin, v. 35, p. 1–5.
Lucas, S.G., and Ingersoll, R.V., 1981, Cenozoic continental deposits of New Mexico: An overview: Geological Society of America Bulletin,.
Lucas, S.G., Wolberg, D.L., Hunt, A., and Schoch, R.M., 1982, A Middle Eocene Titanothere from the Baca Formation, South-Central new Mexico: Journal of Paleontology, v. 56, p. 542–545.
Ludwig, K.R., 2008, Isoplot 3.6: Berkeley Geochronology Center Special Publication, v. 4, p. 77.
Mackin, J.H., 1947, Altitude and local relief of the Bighorn area during the Cenozoic: Wyoming Geological Association Guidebook, p. 103–120.
Maldonado, F., and Kelley, S.A., 2009, Revisions to the stratigraphic nomenclature of the Abiquiu Formation , Abiquiu and contiguous areas , north-central New Mexico: New Mexico Geology, v. 31, p. 3–8.
May, S.J., 1984, Miocene stratigraphic relations and problems between the Abiquiu, Los Pinos, and Tesuque Formations near Ojo Caliente, northern Espanola Basin: New Mexico Geological Society 35th Annual Fall Field Conference Guidebook, p. 379.
May, S.J., 1980, Neogene geology of the Ojo Caliente-Rio Chama area, Espanola Basin, New Mexico: University of New Mexico, Albuquerque, 204 p.
Maynard, S., 2005, Laccoliths of the Ortiz porphyry belt, Santa Fe County, New Mexico: New Mexico Geology, v. 27, p. 3–21.
McMillan, M.E., Heller, P.L., and Wing, S.L., 2006, History and causes of post-Laramide relief in the Rocky Mountain orogenic plateau -- McMillan et al. 118 (34): 393 -- GSA Bulletin: GSA Bulletin, v. 118, p. 393–405, http://bulletin.geoscienceworld.org/cgi/reprint/118/3-4/393?maxtoshow=&hits=10&RESULTFORMAT=1&author1=mcmillan&andorexacttitle=and&field_name=fulltext&field_value=cenozoic+rocky+mountain&searchi

d=1&FIRSTINDEX=0&sortspec=relevance&fdate=//&tdate=//&resourcetype=HWCIT.
Meyer, H.W., 2007, A Review of Paleotemperature Lapse Rate Methods for Estimating Paleoelevation from Fossil Floras: Reviews in Mineralogy and Geochemistry, v. 66, p. 155–171, doi: 10.2138/rmg.2007.66.6.
Miller, E.L., Toro, J., Gehrels, G., Amato, J.M., Prokopiev, A., Tuchkova, M.I., Akinin, V. V., Dumitru, T. a., Moore, T.E., and Cecile, M.P., 2006, New insights into Arctic paleogeography and tectonics from U-Pb detrital zircon geochronology: Tectonics, v. 25, p. n/a–n/a, doi: 10.1029/2005TC001830.
Moore, F., 1960, Summary of Cenozoic history, southern Laramie Range, Wyoming and Colorado, *in* eology of Colorado: Geological Society of America, Rocky Mountain Association of Geologists, p. 217–222.
Moore, J.D., 2000, Tectonics and volcanism during deposition of the Oligocene–lower Miocene Abiquiu Formation in northern New Mexico: University of New Mexico, 147 p.
O'Shea, C.O., 2009, Volcanic influence over fluvial sedimentation in the Cretaceous McDermott Member, Animas Formation, southwestern Colorado: Bowling Green, Ohio, Bowling Green State University, 90 p.
Pazzaglia, F.J., and Kelley, S., 1998, Large-scale geomorphology and fission-track thermochronology in topographic and exhumation reconstructions of the Southern Rocky Mountains: Rocky Mountain Geology, v. 33, p. 229–257.
Pederson, J.L., Karlstrom, K.E., Sharp, W., and McIntosh, W.C., 2002, Differential incision of the Grand Canyon related to Quaternary faulting - Constraints from U-series and Ar/Ar dating: Geology, v. 30, p. 739–742.
Pederson, J.L., Mackley, R.D., and Eddleman, J.L., 2002, Colorado Plateau uplift and erosion evaluated using GIS: GSA Today,.
Peppe, D.J., Heizler, M.T., Williamson, T.E., Masson, I.P., Brusatte, S., Weil, A., and Secord, R., 2013, New age constraints on the late Cretaceous through early Paleocene rocks in the San Juan basin, New Mexico: GSA abstracts with programs, v. 45.
Potochnik, A.R., 1989, Depositional style and tectonic impli- cations of the Mogollon Rim Formation (Eocene), east- central Arizona: New Mexico Geological Society 40th Annual Field Conference Guidebook, p. 107–118.
Powell, J.S., 1973, Paleontology and sedimentation models of the Kimbeto Member of the Ojo Alamo Sandstone, *in* Fasset, J.E. ed., Cretaceous and Tertiary rocks of the southern Colorado Plateau: Four Corners Geological Society Memoir, p. 111–122.
Press, W., Teukolsky, S., Vetterling, W., Flannery, B., Ziegel, E., Press, W., Flannery, B., Teukolsky, S., and Vetterling, W., 1987, Numerical Recipes: The Art of Scientific Computing: v. 29, 501 p., doi: 10.2307/1269484.
Prothero, D.R., Ludtke, J.A., and Lucas, S.G., 2004, Magnetic stratigraphy of the middle Eocene (Duchesnean) Baca Formation, West-Central New Mexico: New Mexico Museum of Natural History and Science Bulletin, p. 55–58.
Raynolds, R.G., Johnson, K.R., Ellis, B., Dechesne, M., and Miller, I.M., 2007, Earth history along Colorado's Front Range: Salvaging geologic data in the suburbs and sharing it with the citizens: GSA Today, v. 17, p. 4–10, doi:

10.1130/GSAT01712A.1.
Reeside, J.B., Knowlton, F.H., 1924, Upper Cretaceous and Tertiary Formations of the western part of the San Juan Basin Colorado and New Mexico; and Flora of the Animas Formation: v. Profession, p. 117.
Ricketts, J.W., Kelley, S.A., Karlstrom, K.E., Schmandt, B., Donahue, M.S., and van Wijk, J., 2015, Synchronous opening of the Rio Grande rift along its entire length at 25–10 Ma supported by apatite (U-Th)/He and fission-track thermochronology, and evaluation of possible driving mechanisms: Geological Society of America Bulletin, p. B31223.1, doi: 10.1130/B31223.1.
Rosenberg, R., 2014, Late Miocene erosion and evolution of topography along the western slope of the Colorado Rockies: Geosphere, v. 10, p. 641–663, doi: 10.1130/GES00989.1.
Roy, M., Kelley, S., Pazzaglia, F., Cather, S., and House, M., 2004, Middle Tertiary buoyancy modification and its relationship to rock exhumation, cooling, and subsequent extension at the eastern margin of the Colorado Plateau: Geology, v. 32, p. 925, doi: 10.1130/G20561.1.
Saleeby, J., 2003, Segmentation of the Laramide Slab - Evidence from the southern Sierra Nevada region: Bulletin of the Geological Society of America, v. 115, p. 655–668, doi: 10.1130/0016-7606(2003)115<0655:SOTLSF>2.0.CO;2.
Sikkink, P.G.L., 1987a, Lithofacies relationships and depositional environment of the Tertiary Ojo Alamo Sandstone and related strata, San Juan Basin, New Mexico and Colorado: GSA Special Paper, v. 209, p. 81–104.
Sikkink, P.G.L., 1987b, Lithofacies relationships and depositional environment of the Tertiary Ojo Alamo Sandstone and related strata, San Juan Basin, New Mexico and Colorado: Geological Society of America Special Paper, v. 209, p. 81–104.
Smith, L.N., 1988, No Basin analysis of the lower Eocene San Jose Formation, San Juan Basin, New Mexico and Colorado: Albuquerque, University of New Mexico, 166 p.
Smith, L.N., 1992a, Stratigraphy, sediment dispersal and paleogeography of the lower Eocene San Jose Formation, San Juan Basin, New Mexico and Colorado: New Mexico Geological Society Guidebook, v. 43, p. 297–309.
Smith, L.N., 1992b, Upper Cretaceous and Paleogene stratigraphy and sedimentation adjacent to the Nacimiento uplift, southeastern San Juan Basin: New Mexico Geological Society 43rd Annual Field COnference Guidebook, p. 265–296.
Smith, L.N., and Lucas, S.G., 1991, Stratigraphy, sedimentology, and paleontology of the San Jose Formation in the central San Juan Basin, New Mexico: New Mexico Bureau of Mines and Mineral Resources, Bulletin, v. 126, p. 44.
Smith, G.A., Moore, J.D., and McIntosh, W.C., 2002, Assessing roles of volcanism and basin subsidence in causing Oligocene–lower Miocene sedimentation in the northern Rio Grande rift, New Mexico, U.S.A.: Journal of Sedimentary Research, v. 72, p. 836–848.
Stearns, C.E.., 1943, The Galisteo Formation of North-Central New Mexico: Geology, v. 51, p. 301–319.
Steven, T.A., and Eaton, G.P., 1975, Environment of Ore Deposition in the Creede Mining District, San Juan Mountains, Colorado: I. Geologic, Hydrologic, and Geophysical Setting: Economic Geology,.

Steven, T.A., and Epis, R.C., 1968, Oligocene volcanism in south-central Colorado: Colorado School of Mines Quarterly1, v. 63, p. 241–258.
van Tuyl, F.M., and Lovering, T.S., 1935, Physiographic development of the Front Range: Geological Society of America Bulletin, v. 46, p. 1291–1350.
Wahlstrom, E.E., 1947, Cenozoic physiographic history of the Front Range: Geological Society of America Bulletin, doi: 10.1130/0016-7606(1947)58.
Wegert, D., and Parker, D.F., 2011, Petrogenesis of the McDermott Formation trachyandesite, San Juan basin, Colorado and New Mexico: Rocky Mountain Geology, v. 46, p. 183–196, doi: 10.2113/gsrocky.46.2.183.
Weissmann, G.S., Hartley, a. J., Nichols, G.J., Scuderi, L. a., Olson, M., Buehler, H., and Banteah, R., 2010, Fluvial form in modern continental sedimentary basins: Distributive fluvial systems: Geology, v. 38, p. 39–42, doi: 10.1130/G30242.1.
Williamson, T.E., 1996, The beginning of the age of mammals in the San Juan Basin, New Mexico: Biostratigraphy and evolution of Paleocene mammals of the Nacimiento Formation: New Mexico Museum of Natural History and Science Bulletin, v. 8, p. 141.
Williamson, T.E., and Lucas, S.G., 1992, Stratigraphy and mammalian biostratigraphy of the Paleocene Nacimiento Formation, southern San Juan Basin: New Mexico Geological Society 43rd Annual Field COnference Guidebook, p. 265–296.
Williamson, T.E., and Weil, A., 2008, Metatherian mammals from the Naashoibito Member, Kirtland Formation, San Juan Basin, New Mexico and their biochronologic and paleobiogeographic significance: Journal of Vertebrate Paleontology, v. 28, p. 803–815.
Wolfe, J.A., 1992, An analysis of present-day terrestrial lapse rates in the western conterminous United States and their significance to paleoaltitudinal estimates: U.S. Geological Survey Bulletin, v. 1964, p. 35.
Wolfe, J. a., Forest, C.E., and Molnar, P., 1998, Paleobotanical evidence of Eocene and Oligocene paleoaltitudes in midlatitude western North America: Geological Society of America Bulletin, v. 110, p. 664–678, doi: 10.1130/0016-7606(1998)110<0664:PEOEAO>2.3.CO;2.
Woodward, L.A., 1987, Geology and mineral resources of Sierra Nacimiento and vicinity, New Mexico: New Mexico Bureau of Mines and Mineral Resources, Memoir, v. 42, p. 84.
Young, R. a., and Hartman, J.H., 2014, Paleogene rim gravel of Arizona: Age and significance of the Music Mountain Formation: Geosphere, p. 1–22, doi: 10.1130/GES00971.1.
Zimmerer, M.J., and McIntosh, W.C., 2012, The geochronology of volcanic and plutonic rocks at the Questa caldera: Constraints on the origin of caldera-related silicic magmas: Bulletin of the Geological Society of America, v. 124, p. 1394–1408, doi: 10.1130/B30544.1.

CHAPTER 3 TIMING AND DRIVING MECHANISMS FOR MULTI-STAGE UPLIFT OF THE SOUTHERN ROCKY MOUNTAINS: EVIDENCE FROM THERMOCHRONOLOGY

Magdalena S. Donahue[1], J.W. Ricketts[1,2], Rebecca Garcia Trujillo[3], Josh Feldman[3], S.A. Kelley[3], K.E. Karlstrom[1], S. Hansen[1] , Matt Heizler[3]
[1]Department of Earth and Planetary Sciences, Northrop Hall, University of New Mexico, Albuquerque, New Mexico 87131, USA
[2]Department of Geological Sciences, University of Texas at El Paso, 500 W. University Ave., El Paso, TX 79968-0555
[3]Department of Earth and Planetary Science, New Mexico Institute of Mining and Technology, Socorro, NM 87801 USA

ABSTRACT

This paper uses low temperature apatite thermochronology to examine erosionally driven differential cooling of the southern Rocky Mountains. We add 29 new (U-Th)/He thermochronologic analyses to an existing database of 1190 AFT and 903 AHe ages. Analysis of age-elevation transects, paired AFT and AHe data on some samples, and HeFTy modeling reveal striking spatial and temporal patterns in Cenozoic cooling. Most rocks resided for long periods in the partial annealing (AFT) and partial He retention (AHe) zone, with those time periods bracketed by times of more rapid cooling. Different regions preserve different components of a proposed regional episodic uplift and cooling history. Cooling (and inferred uplift) episodes were: 1) 75-45 Ma (Laramide orogeny), 2) 35-25 Ma (ignimbrite flare-up), 3) ~25-10 Ma (Rio Grande rift footwall uplifts), and 4) < 10 Ma (ongoing uplift and exhumation). Apparent exhumation rates (AER) are estimated for each episode using age-elevation transects; cooling rates are estimated from both offset of AFT- AHe ages and HeFTy thermal history models. Paleo geothermal gradients are estimated from the integrated paired AFT and AHe data. Laramide (75-45 Ma) AERs were ~ 70 m/Ma as preserved in

hangingwall blocks of Laramide uplifts. Isotherms were reset during the Late Eocene and Oligocene 45- 35 Ma, during broad epeirogenic uplift and erosion that pre-dated and accompanied 35-25 Ma magmatism. 35-25 Ma reheating associated with ignimbrite volcanism variably overprinted Laramide cooling histories, especially south of the Colorado Mineral Belt. Cooling following this episode had AER of 75-100 m/Ma. Rio Grande rift flank exhumation and cooling took place in rift-flank footwall blocks during a major pulse from 25-10 Ma along the entire length of the Rio Grande rift with AERs of ~150 m/Ma. AHe data from ~ 30 Ma fluvial deposits west of the San Juan Mountains remained above 50ºC and in the AHe partial retention zone until after ~ 15 Ma indicating the presence of a thick (now eroded) volcaniclastic apron that extended onto the eastern Colorado Plateau. Post-10 Ma uplift has ongoing AER 150-300 m/Ma in areas of faulting and in areas overlying sharp mantle velocity transitions and/or where cooling is amplified by river integration and isostatic rebound due to differential erosion. Inferred uplift mechanisms that drove erosional cooling were: Laramide (70-45 Ma) = reverse fault uplift of hangingwalls; mid-Tertiary (35-20 Ma) = ignimbrite flare-up magmatism and long wavelength mantle-driven epeirogenic uplift; Rio Grande rift = 25-10 Ma normal fault footwall uplift; post-10 Ma = continued faulting and mantle-driven magma flux and/or small scale convection. Thermochronologic data in the Rockies are best explained by episodic cooling during and outlasting episodic uplift events that increased both mean surface elevation and mean relief through time and were separated by times of re-equilibration of isotherms.

INTRODUCTION

The Colorado Rocky Mountains form a large region with the highest mean elevation (> 3 km with 550 peaks exceeding 4 km) and highest relief (Karlstrom et al., 2012)in the western United States. The origin and uplift history of this high elevation, high relief region is an ongoing debate. Recent papers have proposed a multi-stage Cenozoic uplift history for the Rocky Mountains based on geologic and thermochronologic arguments (Karlstrom et al., 2012; Cather et al., 2012).

The goal of this paper is to analyze new and compiled low-temperature apatite fission-track (AFT) and apatite (U-Th)/He (AHe) data throughout southwestern Colorado and northern New Mexico (Fig. 1) to better understand variations in the burial and exhumation history from place to place, at different elevations, and through time in the Rockies. This "differential thermochronology" provides a regional dataset to help evaluate linkages between tectonic uplift, erosional denudation, cooling, and isostatic rebound.

New data presented includes: 1) thermochronology of sedimentary units surrounding the San Juan Mountains to evaluate the depth and extent of burial of these units by Oligocene volcanic aprons, 2) comparison of age-elevation relationships and HeFTy models for post-Oligocene cooling of high peaks cored by 35-25 Ma plutons using both AFT and AHe data for selected areas in the West Elk Mountains (Garcia, 2011), Sawatch (Feldman, 2010), and flanks of the Rio Grande rift (Ricketts et al., 2015). We show that age-elevation thermochronologic data using both AFT and AHe data, combined with HeFTy modeling, can provide constraints on apparent exhumation rates (AER), paleo geothermal gradients, and paleo cooling rates.

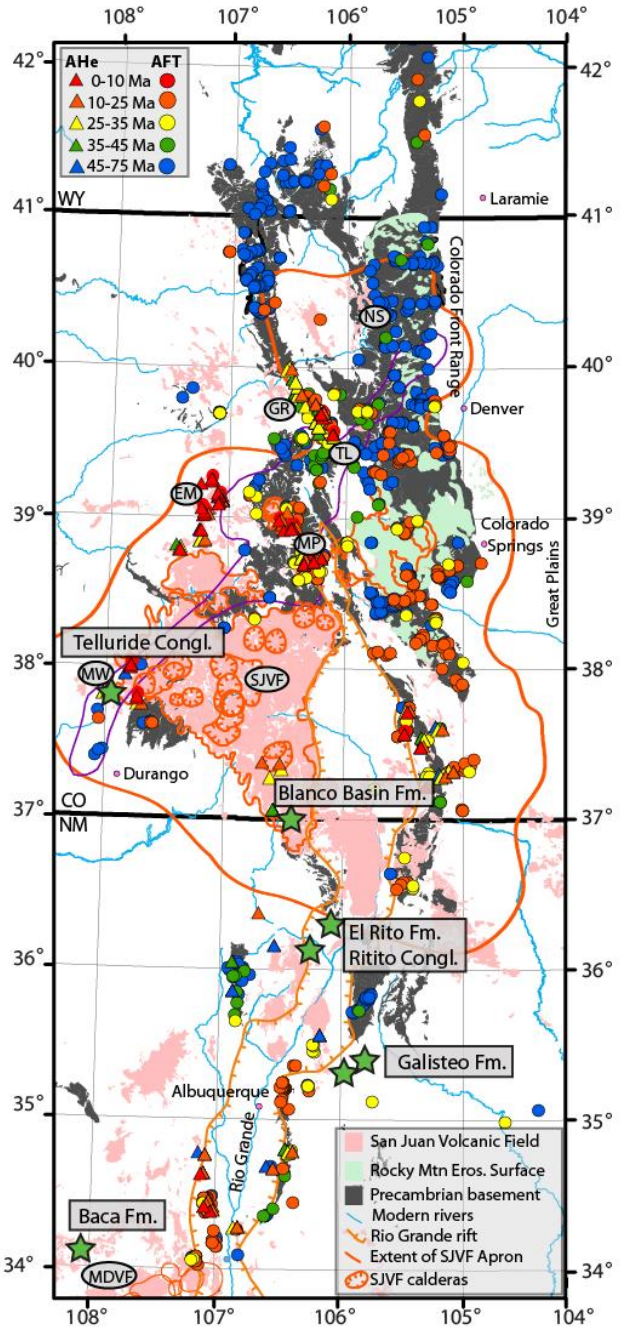

Figure 3-Error! No text of specified style in document.**-1** Spatial distribution of compiled thermochronology data in southern Rocky Mountains. Apatite (U-Th)/He are shown as triangles, apatite fission-track as circles, colored by age: blue = 75-45 Ma, green = 45-35 Ma, yellow = 35-25 Ma, orange = 25-10 Ma, red = <10 Ma. Rocky Mountain Erosion Surface is pale green. The extent of San Juan Volcanic Field Apron (heavy orange line; Lipman, 2007), San Juan volcanic field calderas (orange), Rio Grande rift outline (pale orange) are indicated. Place-name abbreviations in gray ovals: NS = Never Summer Range, GR = Gore Range, TL = Twin Lakes, EM = Elk and West Elk Ranges, MP = Mount Princeton, MW = Mount Wilson, SJVF = San Juan

This paper is organized as follows: The first section explores low-temperature methodologies, and compiles and summarizes all apatite AFT and AHe cooling ages in Colorado to see how well the age data alone support the hypothesis of a multi-stage cooling history. Second, each of the proposed episodes of cooling and inferred uplift are discussed, from oldest to youngest, using both age-elevation transects and HeFTy thermal history modeling to further analyze examples of areas that record one or more episodes well. New datasets are highlighted within each time period and are integrated with the regional compilation. Thirdly, the discussion section then uses the temporal and spatial variations in cooling and exhumation

histories to infer different driving mechanisms for the proposed three different uplift episodes in the Rocky Mountains.

LOW-TEMPTERATURE THERMOCHRONOLOGY METHODS: APATITE FISSION-TRACK AND U(Th/He)

Low-temperature thermochronology using apatite involves two methods: AFT and AHe. Together, these methods can reconstruct a constrained time-temperature history for rocks as they cool from 110ºC to near surface temperatures (15º ± 10ºC). AFT studies provide information on the 110º-60ºC cooling of rocks (Tagami and O'Sulllivan, 2005). At elevated temperatures, fission-tracks formed within a crystal are shortened and eventually erased through annealing (Fleischer et al., 1975). Annealing occurs within the partial annealing zone (PAZ), a temperature bracket of approximately 60-110°C on geologic time scales, below which the system becomes 'closed' and all damage tracks are retained. Compiled AFT Data for this study is found in DR1. AHe analysis is well suited to investigating cooling from ~80º-50ºC. Differential radiation damage in apatite crystals with different U and Th concentrations affects helium diffusion through the crystal lattice such that a positive correlation between AHe ages and effective uranium (eU) suggests prolonged residence in the AHe partial retention zone (~30-90°C) (Flowers et al., 2009).

New data collected as part of this study are from samples from the Telluride Conglomerate, Blanco Basin Formation, El Rito Formation, Ritito Conglomerate, Galisteo Formation and Baca Formation units in Colorado and New Mexico. Apatite separates were made at the University of Arizona LaserChron center, and from these, apatite crystals were selected for AHe dating using a polarizing microscope and chosen

based on crystal size (if possible >70μm when measured perpendicular to the c-axis) and morphology (euhedral crystal shape, lacking inclusions). Crystal lengths and widths were measured to apply an appropriate ejection correction (Ft) (Farley et al., 1996). Individual apatite crystals were then packed in platinum tubes and analyzed at the Arizona Radiogenic Helium Dating Laboratory at the University of Arizona. New AHe data (Appendix 3) were modeled with HeFTy (Ketcham, 2005) to inversely produce continuous time-temperature history paths. Complete AHe data for new samples can be found in DR2. AHe data input into HeFTY includes spherical grain radius and U, Th, and SM concentrations. Grain age uncertainties were all set at 20%, and each model used the radiation damage accumulation and annealing model (RDAAM) (Flowers et al., 2009) and alpha particle stopping distances from Ketcham et al. (2011). In each simulation, 10,000 paths were tried, where resulting "acceptable" paths have a goodness-of-fit parameter >0.05 and "good" paths have a goodness-of-fit parameter of >0.5.

We use HeFTy modeling as a way to generally assess inferred burial depth and subsequent cooling history. Our hypothesis is that each of these units each experienced ~1-3 km burial by their late Eocene-Oligocene volcaniclastic materials shortly after deposition. We use AHe to test whether these units were indeed sufficiently buried (~1-3 km) and heated (above ~ 50°C) to cause release of daughter He. Alternatively, these units may never have been heated above 50°C and hence apatite grains in the conglomerates may retain pre-depositional cooling ages. Our analysis of mid-Cenozoic sedimentary rocks in a later section is similar to the Flowers et al (2008) analysis of the Rim Gravels on the southern Colorado Plateau: as in that study, the depth of burial of

the units of this study is unknown. If the sediments were buried by >1-2 km of volcanic debris from the San Juan volcanic field, the apatites may record a post-30 Ma age and provide a constraint on the thickness of the volcaniclastic apron and the extent and timing of any post -30 Ma erosion. If units are buried too shallowly (<1-2 km), the analysis may reveal the cooling history of detrital grains and instead provide constraints on the pre-30 Ma unroofing of the region.

Constraint boxes were imposed on models only when based on seemingly unequivocal geologic constraints. For Oligocene plutonic rocks, we input a constraint box for the age of emplacement and assign a paleotemperature based on $^{40}Ar/^{39}Ar$ cooling ages. When AFT and AHe data are both available, we modeled both in HeFTy using track length and angle data if such data were reported (e.g. Mt Princeton), or superimposed an AFT constraint box of 120-100ºC (e.g. West Elk Mountains).

For Oligocene sedimentary rocks, models begin with a depositional constraint box of 30 ± 5 Ma. A 5 Ma depositional timeframe determined by detrital zircon geochronology (Donahue et al., Chapter 2) and a surface depositional temperature of 15º ± 10ºC, reflecting likely average surface temperatures. Each model is also constrained to return to this surface temperature as each unit is currently exposed at the surface. Complete HeFTY modeling (Ketcham, 2005) procedures and results for each sample are presented in Figures 2, 3, 4, and 5.

RESULTS

Compilation of Regional-Scale Cooling Patterns and Apparent Exhumation Rates

Compiled new and published AFT and AHe data from the southern Rocky Mountain region is summarized Figure 1 (Appendices 3, 4 and 5, respectively). We combine appreciable age-elevation data with cooling models using all available data. Regional geologic constraints indicate a starting point for uplift studies with the region being at sea level at ca. 75 Ma with basement rocks covered by 0-2 km of Paleozoic rock (thickest in the Ancestral Rocky Mountain basins), and an additional ~ 2 km of Mesozoic rock (Painter and Carrapa, 2013). Underlying assumptions include: 1) regional isotherms were regionally subhorizontal and were re-established between uplift and erosional episodes; 2) differential cooling was due primarily to differential exhumation of the overlying ~ 3-4 km of strata; 3) magmatism perturbed (elevated) isotherms over identifiable large regions surrounding volcanic fields; 4) age-elevation surface transects give "apparent exhumation rates" (AER) in m/Ma if the data are bolstered by similar observations in data gathered from nearby boreholes and/or from modeled cooling paths. The term "apparent" is used in recognition of the complexities in samples suites with a horizontal distribution (e.g., were not collected from a drill hole). These complexities include that isotherms may not have been horizontal and temperatures not constant laterally over the sampling distance, and that both differences in depth of burial, structural complexities, and later heating may complicate cooling patterns.

Figure 1 shows the spatial distribution of apatite thermochologic data in Colorado binned according to the proposed cooling/uplift episodes of earlier workers (Kelley et al., 1992; Kelley and Chapin, 1995; House et al., 2003a; Roy et al., 2004; Kelley and Chapin, 2004; Karlstrom et al., 2012; Cather et al., 2012) and as further

justified in Figure 2. This method of displaying historic compiled and new thermochronologic data includes inherent assumptions that include variable data quality, binning generalizations of potentially time- and location-transgressive geologic events, sample scarcity, and sample location bias due to issues including historical interest and available outcrop/drill core.

AFT ages (Fig. 1) show a strong Laramide mode (75-45 Ma) as well as younger mode centered at ~15-20 Ma. The latter corresponds with the AHe histogram, which shows a strong mode at ~15 Ma. Figure 2C shows a histogram of magmatic rock ages from Colorado ("NAVDAT," 2015). A Laramide pulse of magmatism corresponds to the early Colorado Mineral belt magmatism from 50-75 Ma. The largest mode (Fig.2C) reflects the 35-25 Ma early andesitic stratovolcanos and includes the caldera-related volcanism of the San Juan and Never Summer volcanic fields as well as some laccolithic

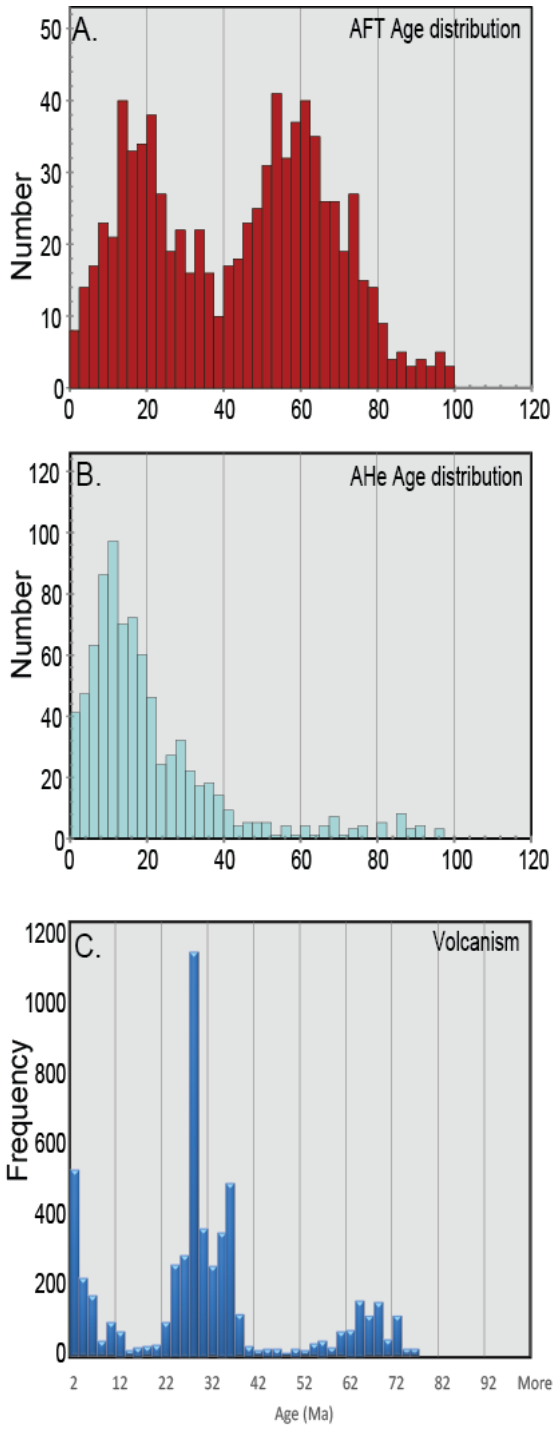

Figure 3-Error! No text of specified style in document.**-2** A. Histogram of compiled AFT data. B. Histogram of compiled AHe data. C. Histogram showing age distribution of volcanism in the southern Rocky Mountain region.

intrusions on and bordering the Colorado Plateau. Although the binning needs further refinement, this composite figure provides initial support for an episodic cooling and justifies the binning of Fig. 1.

A 75-45 Ma cooling pulse (through 110ºC) corresponds in time to the early Laramide deformation and Colorado Mineral Belt magmatism. The 45-35 Ma infrequency of AFT ages corresponds to a time of limited volcanism and also the time of deposition of Eocene conglomerates on the Eocene Rocky Mountain erosion surface (Chapter 2). 35-25 Ma was the time of large volume magmatism that presumably had a strong reheating effect on the Colorado-New Mexico lithosphere. We divide the post-magmatic cooling into 25-10 Ma, which encompasses both the strong AHe major mode, and the major rift-flank uplift of the Rio Grande rift (Kelley et al., 1992; Ricketts

et al., 2015). Post-10 Ma cooling is evident in both AFT and AHe ages, suggesting young cooling that may reflect cooling from young and ongoing denudation caused by Neogene river incision and associated exhumation and tectonism (Kelley and Blackwell, 1990; Karlstrom et al., 2012).

Laramide Cooling

Figure 3 shows age-elevation plots separately for the compiled AFT and AHe ages. Both graphs show samples from elevations that range from the > 4 km peaks to drill hole depths of ~ -4 km. The first-order observation from this plot is that surface rocks at any elevation (1-4 km) can have ages ranging from 0 Ma to > 100 Ma in both the AFT and AHe systems. The modern 110ºC isotherm (zero AFT age) is at depths of 3-4 km below the surface in drill holes, in agreement with modern heat flow measurements for geothermal gradients of 30-40ºC/km (Decker et al., 1988; Kelley and Chapin, 2004). AFT ages older than 75 Ma are preserved in small areas at elevations of 1-4 km compatible with highly variable Cenozoic rock uplift of generally less than ~ 5-6 km in the Rockies. The base of the Laramide (75-45 Ma) AFT partial annealing zone (Laramide 110 ºC isotherm) has been identified in several places and at various elevations: above ~ 3.5-4 km in the Beartooth over thrust, Front Range and Wind River Range (Omar et al., 1994; Kelley and Chapin, 2004; Peyton et al., 2012); Laramie Range (Kelley, 2005); ~3.5 km at Mt Logan and the southern Wet Mountains (Kelley and Chapin, 2004); ~3 km in the Wind River Mountains (Steidtmann et al., 1989; Peyton et al., 2012), ~ 1 km to within the subsurface in drill holes in the MWX well, Wind River Range, Anadarko and Green River Basins (Kelley and Blackwell, 1990; Cerveny and Steidtmann, 1993; Carter et al., 1998; Peyton et al., 2012).These are shown

on Fig. 3 as the simplified kinks in age-elevation transects. The fossil PAZ can be used as a datum for understanding regional post-Laramide denudation of the Rockies, and variation in its current elevation has been interpreted to be due to faulting of pre-Laramide isotherms by Laramide reverse faults (Kelley and Chapin, 2004).

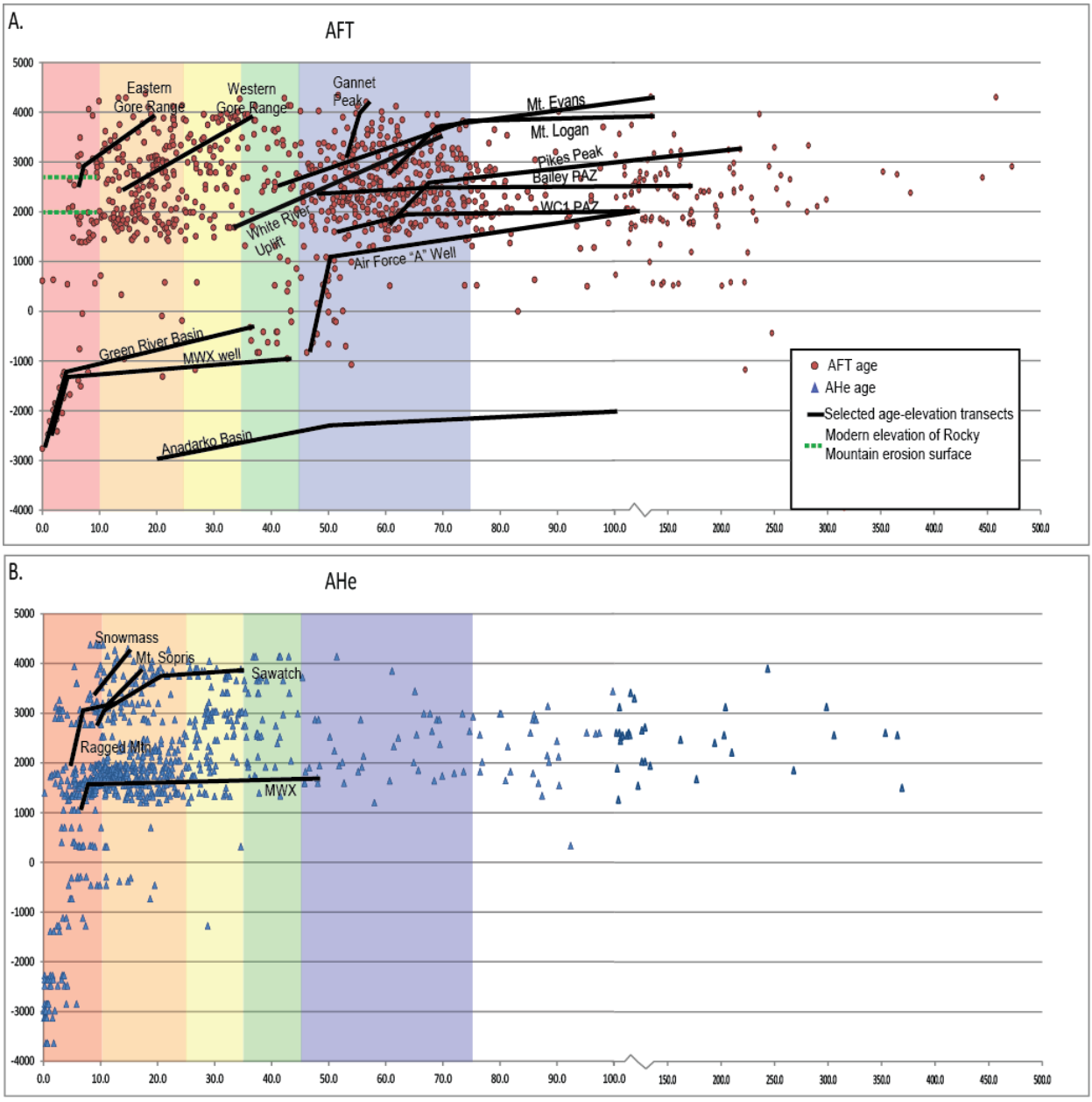

Figure 3-Error! No text of specified style in document.**-3** Age-elevation distribution of compiled AFT (red dots) and AHe (blue triangles) data from 0-500 Ma. Note scale change at 100 Ma. A. AFT Age-elevation regressions from published works highlight cooling rates from the Wet Mountains (modified from Kelley and Chapin, 2004, Fig.10), MWX well (Kelley and Blackwell, 1990); Anadarko Basin (Carter et al., 1998); Gore and Sawatch Ranges (Kelley and Blackwell, 1990; Karlstrom et al., 2012 Fig. 5), Air Force "A" well (Cerveny & Steidtmann, 1993), Gannet Peak and Green River Basin (Peyton and Carrapa, 2012). B. AHe regressions shown from West Elk Mountains (Garcia, 2011); MWX well (Karlstrom et al., 2012 Fig. 5); Sawatch Range (Ricketts et al., 2015 (Fig 3.)).

AFT ages of 75-45 Ma reflect cooling through ~ 110ºC due to erosional removal, during the Laramide orogeny, of a major component of the 3-4 km Phanerozoic section that was present, at sea level, prior to Laramide orogeny (Chapin, C.E., Kelley, 1997; Kelley and Chapin, 2004). Laramide cooling ages are not necessarily spatially associated with magmatism except locally along the Colorado Mineral Belt (Chapin, C.E., Kelley, 1997), implying the erosional denudation was an important process in causing cooling.

Spatial patterns of where Laramide cooling ages (blue dots) are preserved are shown in Fig. 1. Fig.4 shows that the Laramide ages are not (just) in high elevation regions, but are preserved in many regions that were not re-heated or further exhumed during later episodes. Laramide ages are especially common in the Front Range and Wyoming Rockies. Similar cool "sky islands" preserve Laramide AFT (and AHe) ages in hangingwall blocks throughout the Rockies at elevations that range from 2-4 km. Figure 3 summarizes published age –elevation transects (mainly AFT) that record post-Laramide cooling; data is found in DR1 and DR2. The timing of the fast cooling ranges from 70 to 45 Ma, and apparent exhumation rates range from 70-80 m/Ma, with a mean value of about 75 m/Ma.

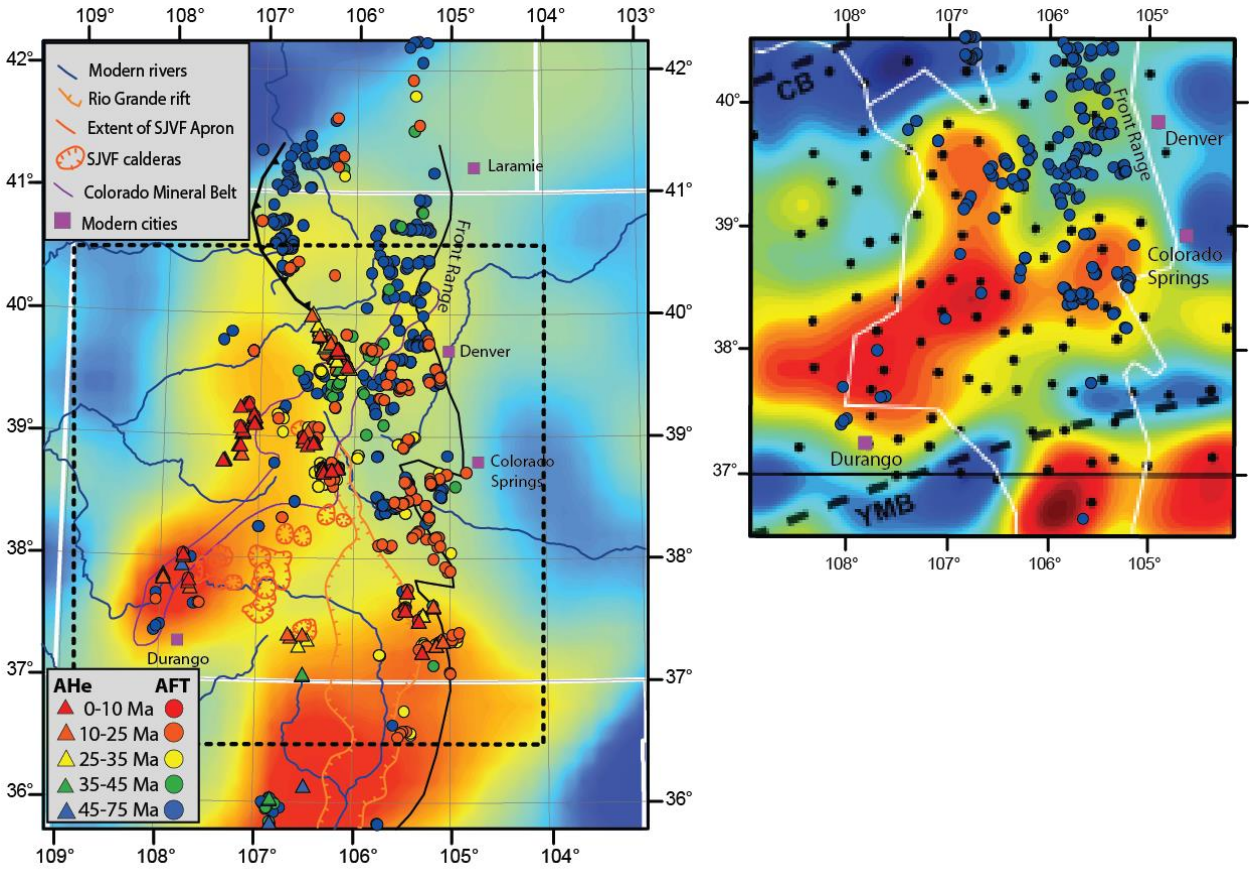

Figure 3-Error! No text of specified style in document.**-4** The central southern Rocky Mountain Region with compiled thermochronologic data. A. Compiled thermochronologic data superimposed on vs/vp tomography at 100 km depth (Schmandt and Humphreys, 2010). Dotted square shows are of Fig. ZB. B. Area of Laramide cooling ages (blue dots) superimposed on crustal temperature (Hansen et al., 2013). White line shows Rocky Mountain outline; black dots represent CREST/TA seismic stations.

Late Eocene (~45-35 Ma) Rocky Mountain Erosion Surface

The Rocky Mountain erosion surface, initially called the Eocene erosion surface (Epis and Chapin, 1975) is a composite set of highland surfaces (Pazzaglia and Kelley, 1998), often capped by thin conglomerate sheets of Late Eocene age such as the Ohio Creek conglomerate of the Piceance basin, Dawson conglomerate of the Denver basin, and Galisteo conglomerate of the Galisteo Basin of New Mexico. The importance for thermochronologic studies is that this was a time that followed a 55-45 Ma magmatic gap (Feldman, 2010) and has been alternately interpreted as a time of tectonic

quiescence (Epis and Chapin, 1975) or broad epeirogenic doming driven by large-scale tectonic events (Heller, et al., 2013; Donahue, Chapter 2) during which regional isotherms had a ~10 Ma time period to relax and restructure, presumably into topography sub-parallel and regionally sub-horizontal surfaces that crossed between Laramide fault block uplifts and basins. It has been proposed that geothermal gradients were relatively low during and after the Laramide (Fitzgerald, e, 2009) due to the presence of the underlying cool Farallon slab. Heat gradients were elevated locally (Decker et al., 1988) , although this would be unlikely to apply in the region of the Colorado Mineral Belt. We speculate that regions where the older RMES are preserved (pale green of Fig. 1) were underlain by normal to somewhat elevated ~25-35 C/km thermal gradients. Younger apatite ages on or near the RMES (yellow and red dots in Fig. 1) are interpreted to represent mid-Tertiary cooling following Oligocene magmatic reheating and/or post-Oligocene uplift/cooling episodes (Kelley and Chapin, 2004). These possibilities are explored in subsequent case by case studies in different regions.

Oligocene (34-21 Ma) Magmatism and Miocene Cooling

Figure 1 shows that Oligocene cooling ages in the AFT system are dominant in the western Gore Range (Naeser et al., 2002; Landman and Flowers, 2013), in the Sawatch and Elk Mountains at the northern end of the San Juan volcanic field (Feldman, 2010; Garcia, 2011), and in some rift flanks of the Rio Grande rift (Ricketts et al., 2015; House et al., 2003b; Kelley and Duncan, 1986; Kelley et al., 1992). These ages are restricted to areas south of the Colorado Mineral Belt but are a surprisingly low percentage of the AFT and AHe histograms (Fig. 2) considering how voluminous the 35-25 Ma magmatism was (Fig. 2C). Like others (House et al., 2003a; Kelley and

Chapin, 2004), we infer from this that the regional Oligocene ignimbrite flare up event elevated and reset regional geotherms in and south of the Colorado Mineral Belt (including the Colorado Plateau), causing regional epeirogenic uplift of the Rocky Mountains relative to both the Great Plains (e.g. Chapin et al., 2014) and Colorado Plateau, potentially due to lithospheric delamination (Karlstrom et al., 2012; Hansen et al., 2013).

The Oligocene plutons are generally shallow level intrusions and include laccoliths of the Colorado Plateau and sills and plutons related to early intermediate composition and later rhyolite caldera volcanism in the San Juan Range. One might expect that thermochronology would show rapid cooling following pluton emplacement to ambient temperatures depending on depth of emplacement. However, thermochronologic data suggest that, in many places, there was a delay between Oligocene magmatism and AFT and AHe ages such that in many places the ages reflect variable amounts of time needed for sufficient post-plutonism denudation to cause rocks to cool through 110ºC AFT and 50ºC AHe temperatures. This is supported in Figure 2 by both AFT and AHe cooling age peaks being "offset" to 20-15 Ma, about 10 Ma after the main 35-25 Ma magmatism. Thus, thermochronology of Oligocene plutons, as summarized below, is useful both for estimating depth of emplacement of plutons and for understanding post-Oligocene differential denudation following magmatism.

Oligocene Plutons & Range-Specific AFT and AHe Results

Sawatch Range, Twin Lakes batholith (Feldman, 2010): Located within the Sawatch Range, the Twin Lakes Pluton was studied by Feldman (2010). An AFT age-elevation transect and HeFTy thermal models are shown in Figure 5. Zircon

crystallization ages are 42 and 44 Ma, biotite Ar ages are ~ 40 Ma, K-spar ages range from 35-30 Ma, and the highest elevation AFT age is 33 Ma. AFT thermal history models determined from track length distributions using HeFTy (Fig. 5A) show fairly rapid cooling from 42- 34 Ma following pluton emplacement for the high elevation sample (H07-HU-001, elevation 4268 m) followed by residence at about 70ºC from 30-13 Ma, then cooling to near surface temperatures from 13-8 Ma. Both AFT age elevation transects and thermal history models using track lengths suggest that lower elevation Huron Peak samples (~ 3 km) show rapid cooling 32-30 Ma, then semi steady cooling 30-23 Ma, then residence at ~ 80ºC from 22-13 Ma and accelerated cooling post-13 Ma. (Fig. 5B). AHe age-elevation data also suggest rapid cooling 13-8 Ma at an apparent exhumation rate of 200 m/Ma. Grizzly Peak and Independence Pass areas have the lowest elevation AHe samples, and yield 8.6 and 16 Ma ages, respectively.

The overall Cenozoic exhumation history of the Twin Lakes Batholith and the larger Sawatch Range region is shown in Fig. 5C. Whitehorn granite near Salida, CO was exhumed from its emplacement depth of ~ 10 km at 70 Ma (based on its metamorphic aureole) to the surface by 36 Ma (based on the depositionally overlying Wall Mountain Tuff). This 10 km of exhumation is compatible with removal of ~ 6 km of Ancestral Rockies sediment in the central Colorado Trough plus 2-3 km of Mesozoic sedimentary rocks between ~ 75-37 Ma at post-Laramide average exhumation rates of rates of 77 m/Ma.

This exhumation reflects a combination of thrust uplift of the Rockies and epeirogenic surface uplift due to buoyancy added to the underlying North American plate via hydration and de-densification of North American lithosphere due to passage

of the Farallon slab (Humphreys et al., 2003). The Twin Lake area may have undergone a lesser degree of post-Laramide denudation and was reheated at 42 Ma during pluton emplacement, then exhumed and cooled ~34-12 Ma. This region thus preserves an excellent record of Oligocene reheating and subsequent exhumation that overprinted (but did not completely obscure) the Laramide exhumation signal. This area also appears to record episodes of rapid cooling within an overall post-Oligocene progressive erosionally driven cooling history.

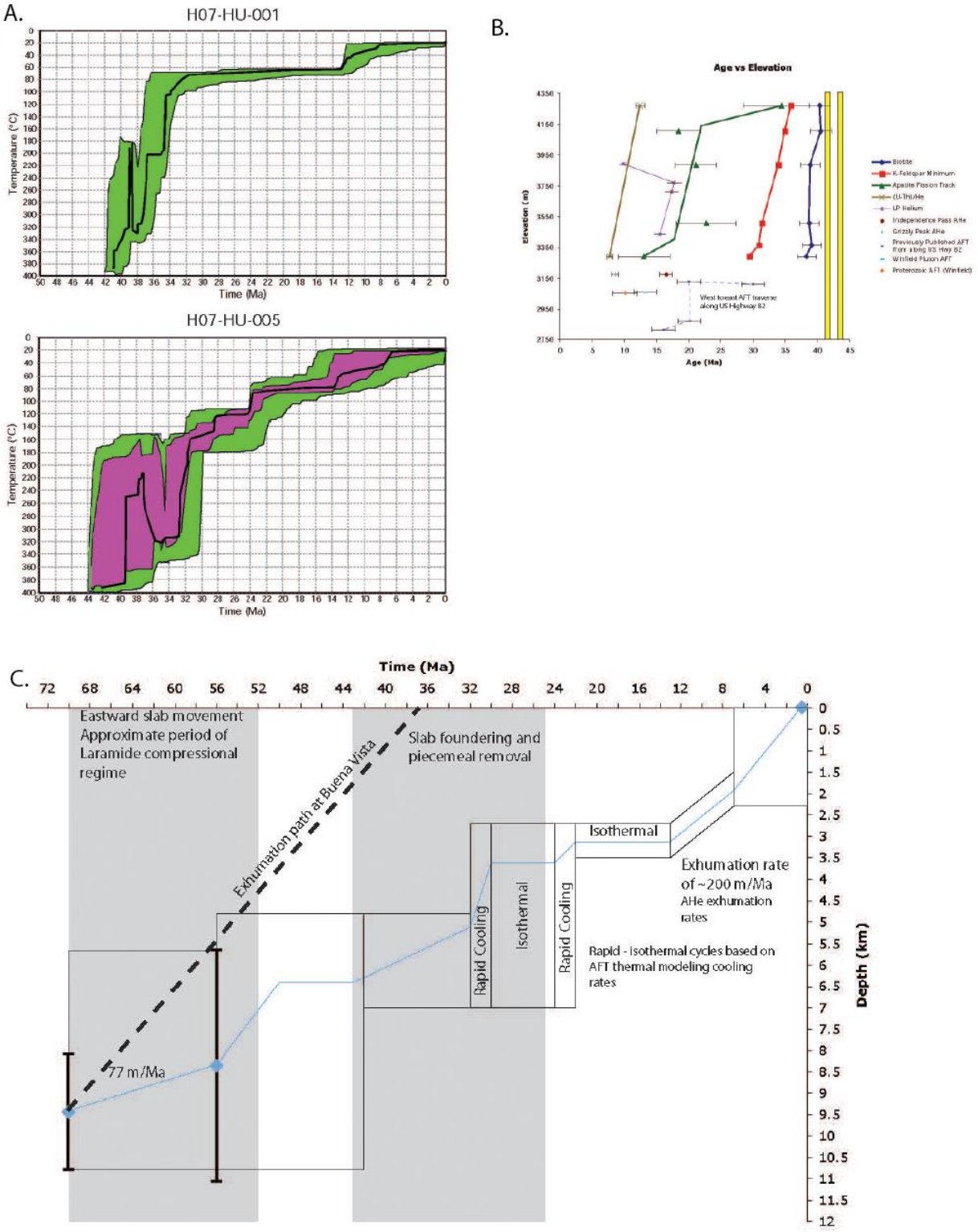
A.
H07-HU-001
Temperature (°C)
Time (Ma)
H07-HU-005
Temperature (°C)
Time (Ma)
B.
Age vs Elevation
Elevation (m)
Age (Ma)
Biotite
K-Feldspar Minimum
Apatite Fission Track
(U-Th)/He
LP Helium
Independence Pass AHe
Grizzly Peak AHe
Previously Published AFT from along US Hwy 82
Winfield Fusion AFT
Proterozoic AFT (Winfield)
West to east AFT traverse along US Highway 82
C.
Time (Ma)
Depth (km)
Eastward slab movement Approximate period of Laramide compressional regime
Slab foundering and piecemeal removal
Exhumation path at Buena Vista
77 m/Ma
Rapid Cooling
Isothermal
Rapid Cooling
Isothermal
Exhumation rate of ~200 m/Ma AHe exhumation rates
Rapid - Isothermal cycles based on AFT thermal modeling cooling rates

Figure 3-Error! No text of specified style in document.**-5** Thermal models and regional cooling history for Twin Lakes region (Feldman, 2010).

Miocene – Recent cooling: Mt. Princeton (Ricketts et al., 2015): Mount Princeton is on the eastern side of the Sawatch Range and also in the rift flank uplift of the northern Rio Grande rift. AFT ages increase westward and at high elevations and combined AFT and AHe constrained HeFTy models are shown in Fig. 3 of Ricketts et al., (2015) show that, following pluton emplacement at 36.6 Ma, high elevation samples (~ 4 km) cooled through AFT closure temperatures of ~ 110ºC at 23 Ma and cooled rapidly to near surface temperatures by 20 Ma. Lower elevation samples (~ 3 km) have AFT ages of 10-20 Ma and AHe ages of < 10 Ma. Thermal models suggest rapid cooling 10-20 Ma, similar to many other footwall uplifts of the Rio Grande rift, was interpreted to record cooling due to exhumation in uplifted footwall blocks. The youngest AHe ages of 2-3 Ma and AFT results (Kelley et al., 1992) may indicate at least partial resetting of the AFT/AHe systems due to geothermal activity at Mt. Princeton hot springs associated with rift-bounding faults.

West Elk Mountains (Garcia, 2011): Garcia (2011) conducted Ar-Ar, AFT, and AHe analyses, including age-elevation transects, on Oligocene plutons of the West Elk Mountains (Fig. 1). These plutons are felsic plutons that were emplaced as laccoliths into different levels of the Paleozoic and Mesozoic strata on the eastern edge of the Colorado Plateau/western edge of the Rocky Mountains. Northern plutons intrude Paleozoic strata and southern plutons intrude Mesozoic and early Tertiary strata. Figure 6 shows a N-S cross section that links the plutons; this shows that plutonism intruded across the Laramide Elk Range thrust fault, took advantage of and perhaps accentuated Laramide

anticlines in Paleozoic strata, and have sill-like or laccolith inflational geometries in the upper Cretaceous rocks.

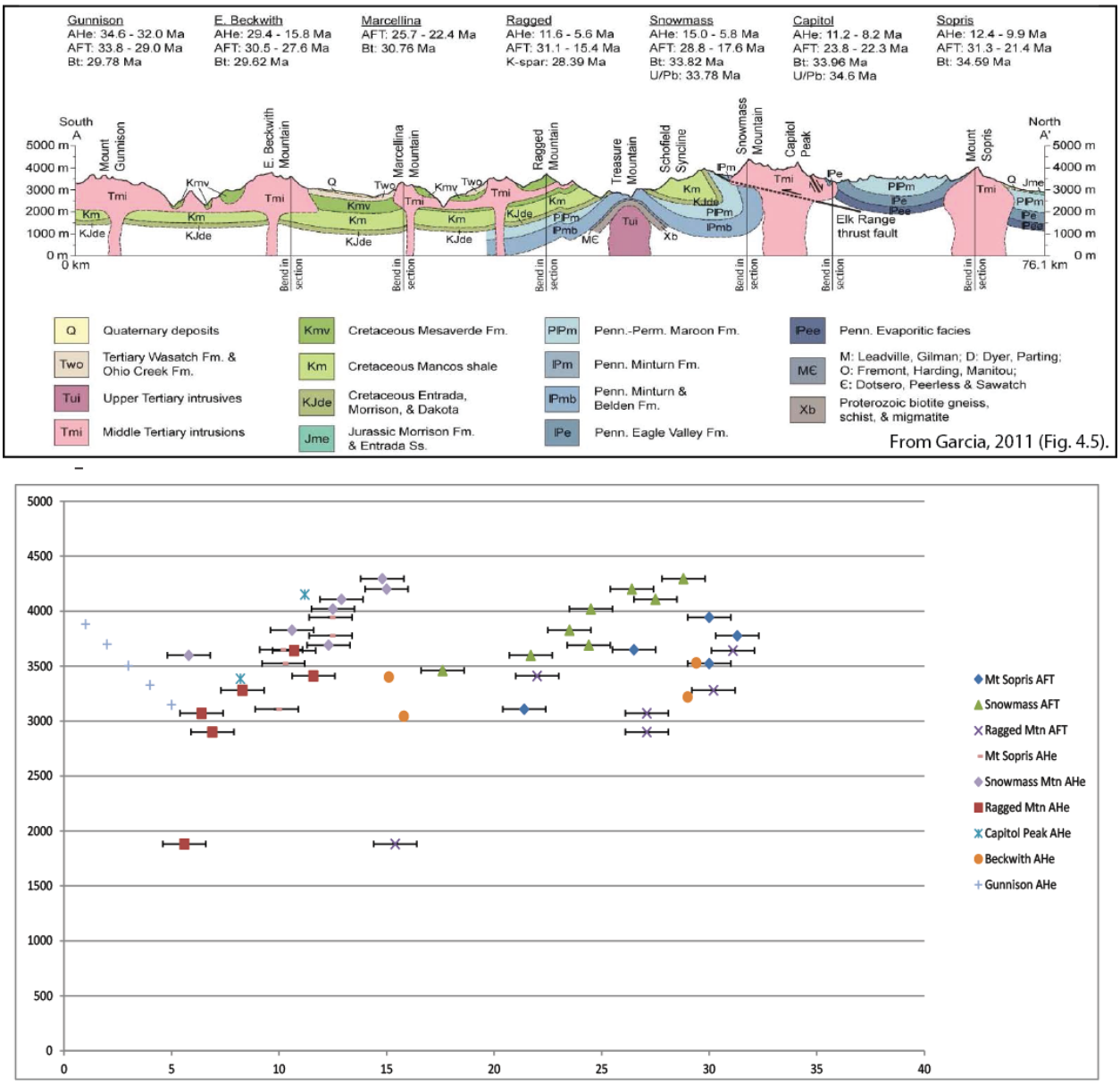

Figure 3-Error! No text of specified style in document.**-6** Cross section of Elk and West Elk mountains and age-elevation plot of AFT and AHe for these plutons (From Garcia, 2011).

^{40}Ar-^{39}Ar ages show a systematic southwest decrease in age of plutons from 35 to 30 Ma determined from combined U-Pb zircon (U-Pb), biotite Ar-Ar (b) and K-spar Ar-Ar (k) analyses. Mt. Sopris= 34.59 (b), Capitol Peak = 34.6 (U-Pb); 33.96 (b),

Snowmass Mountain= 33.78 (U-Pb), 33.82 (b), Ragged Mountain = 28.39 (K), Marcelina Mountain = 30.76 (b), East Mt. Beckwith= 29.62 (b), Mt. Gunnison= 29.78 (b). Younger plutonism is also present in associated with ~12 Ma Crystal Pluton & Redwell intrusion (18-16 Ma). The near concordance of U-Pb, Ar biotite, and Ar- K-spar ages shows rapid cooling of plutons from emplacement temperatures to < 175ºC within several million years in most cases, indicating that all plutons were emplaced into country rocks with ambient temperature < 175 º C, hence at depths shallower than 3.0-4.5 km (using 35-50 C/km geotherms), in agreement with probable stratal thicknesses in this part of the Rockies. Cooling through 110 ºC is more variable, depending on depth of emplacement, as discussed below.

Combined AFT and AHe analyses of elevation transects that span from summits (4-4.5 km) to lower elevations (3-3 km) are shown in Figs. 7-12. These show systematic decrease in both AFT and AHe ages with lower elevations. The slope of the regressed age-elevation line has units of m/Ma and is reported in Table 1 as an "apparent exhumation rate". Some peaks (e.g. Snowmass Mountain) give excellent age-elevation trends in both the AFT and AHe systems, in support of steady, denudationally –driven cooling at an apparent denudation rate of 70-79 m/Ma from ca. 30-5 Ma. Other plutons (e.g., Mt. Sopris and Ragged Mountain) also show progressive cooling in the AFT system from 35-15 Ma at rates of ~60-65 m/Ma, and accelerated cooling in the AHe system from 10-5 Ma at apparent rates of 195-850 m/Ma. The most southerly peaks have less data, but AFT and AHe ages overlap, compatible with rapid post-emplacement cooling.

The “offset” in AFT from AHe age at a given elevation can be considered a proxy for cooling rate. For example, at Mt Snowmass, cooling from 110º to 50ºC took about 10 Ma giving an “apparent cooling rate” of 4-5ºC/Ma. In this case, the combined data yield an apparent geothermal gradient of 55-65ºC/ km for this time interval.

HeFTy models for the Elk and West Elk Mountains (Figs. 7-12) were run on all samples to test possible validity of age-elevation estimates of cooling rates and patterns. Most models have 3 aliquots each with 3 apatite grains; thus, the points are averages of 3 grains. This method is non-ideal in terms of exploiting variations in eU to resolve cooling paths (Shuster and Farley, 2004). Rapidly cooled apatites from these Oligocene plutons have a narrow range of average eU (5-32 ppm overall, Fig. A), and the deeply emplaced northern plutons have an even narrower range of average eU (5-18 ppm). There is no observed eU-age relationship in these northern plutons. Southerly, shallower plutons have a wider range and somewhat higher eU and give older ages consistent with the RDAMM model. Northern plutons show no relationship of mean eU with mean radius; southern plutons show higher mean eU with smaller mean radius. Overall, our AHe models are preliminary and would be benefit from single grain aliquots in a future study.

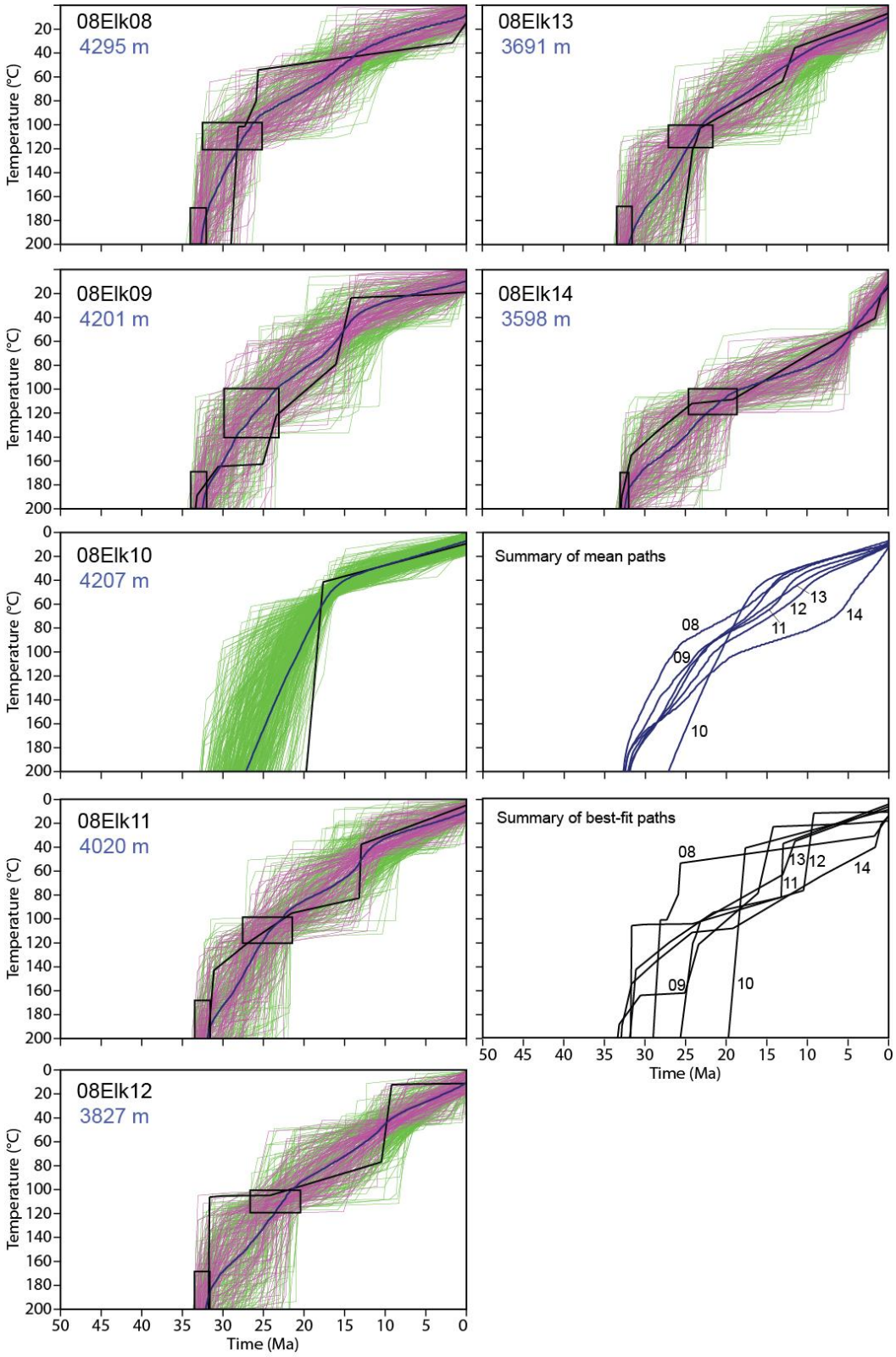

Figure Error! No text of specified style in document.**-7** HeFTy models for Snowmass Mountain.

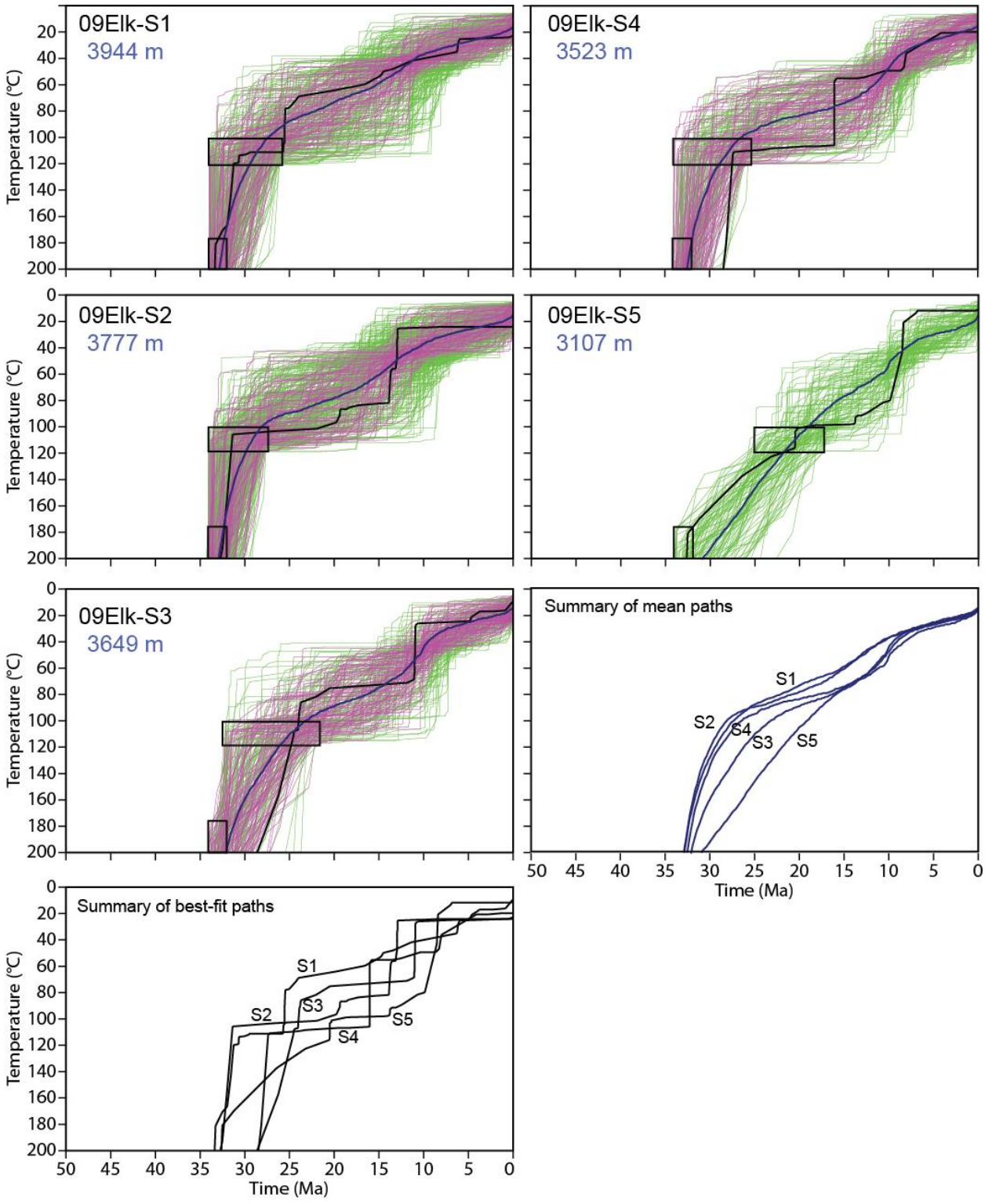

Figure 3-Error! No text of specified style in document.**-8** HeFTy models for Mt. Sopris.

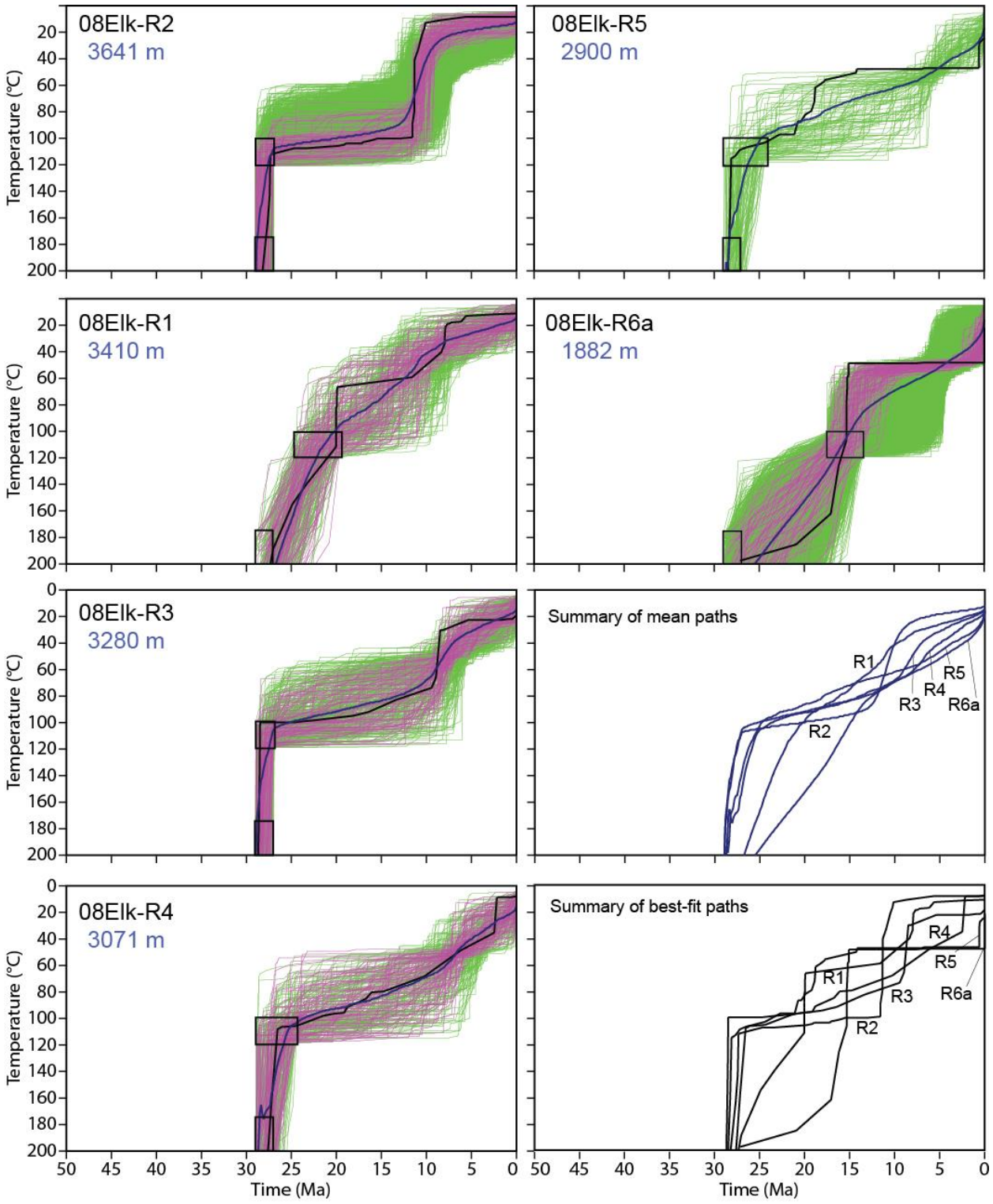

Figure Error! No text of specified style in document.**-9** HeFTy model for Mt. Ragged.

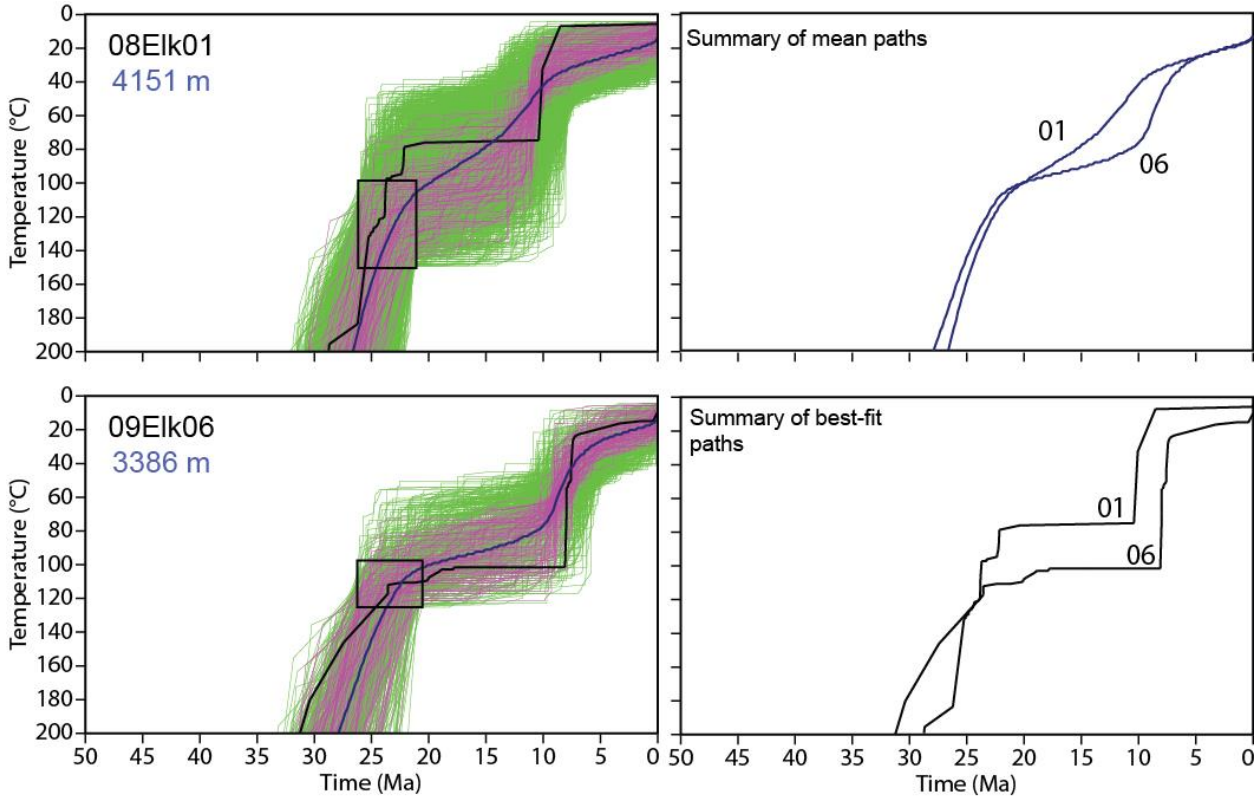

Figure 3-Error! No text of specified style in document.**-10** HeFTy model for Capitol Peak.

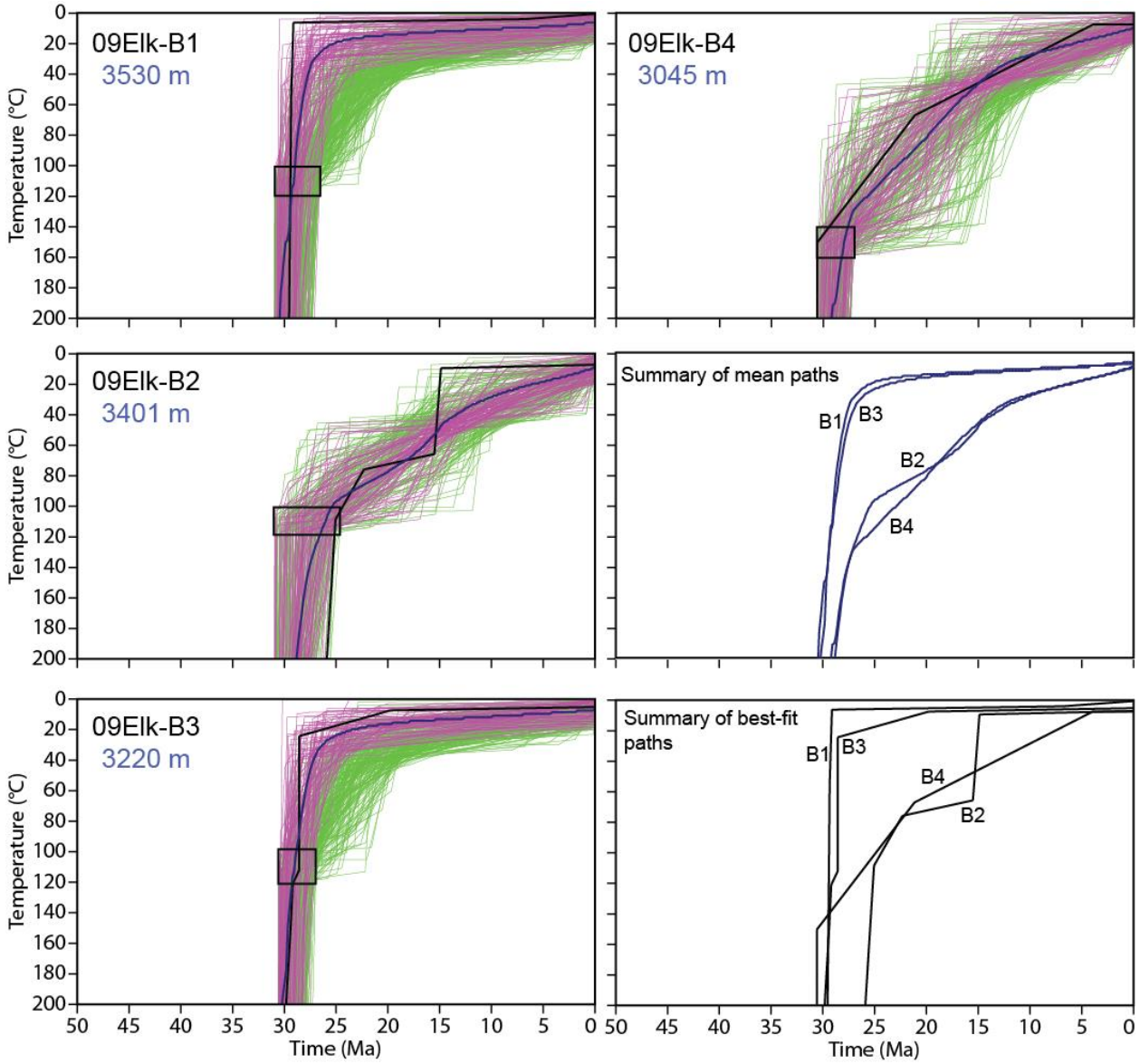

Figure 3-Error! No text of specified style in document.**-11** HeFTy models for East Mt. Beckwith.

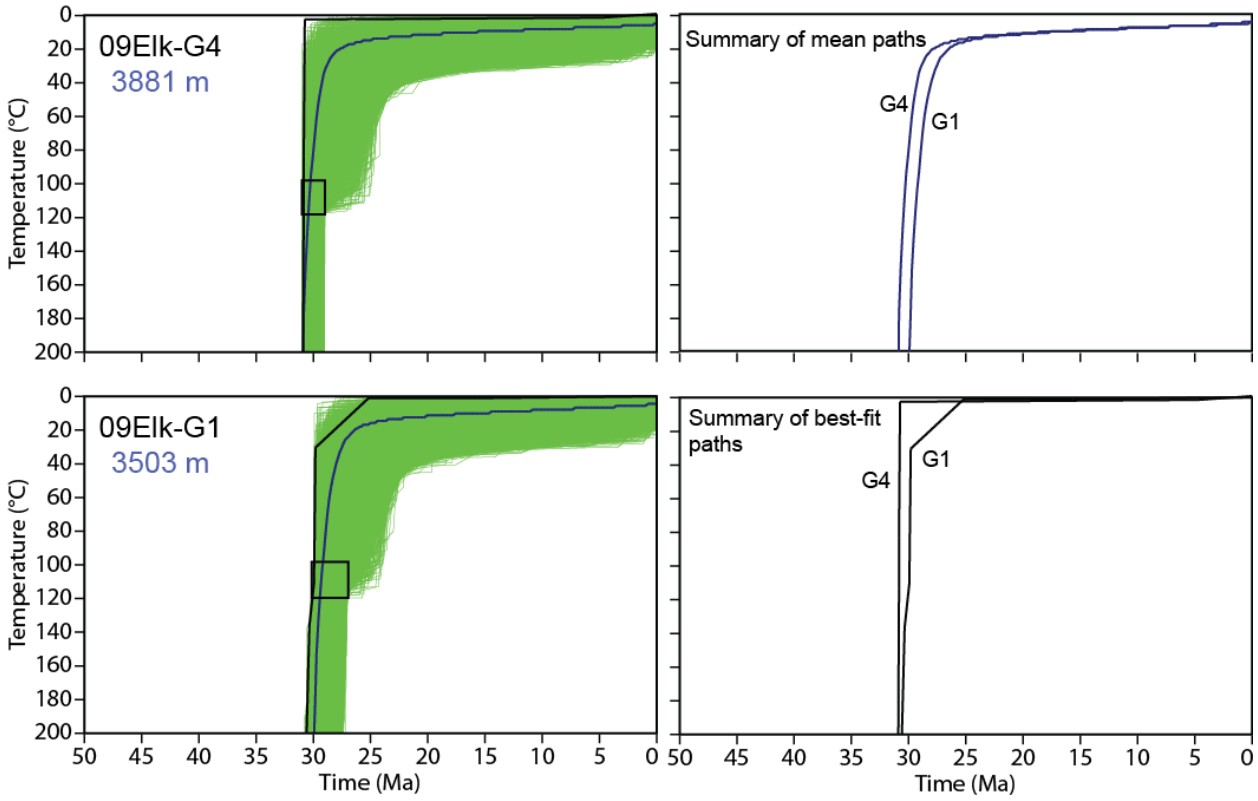

Figure 3-Error! No text of specified style in document.**-12** HeFTy models for Mt. Gunnison.

Similarly, our treatment of AFT data is preliminary in that the AFT data are incorporated only using the AFT age and uncertainty as a constraint box (100-120ºC for the period of age and 2 σ error) for the HeFTy AHe models that had 2-3 aliquots each. Future models can be improved by incorporating track lengths and angles directly into HeFTy modeling. Other constraints boxes imposed on the models include: Ar biotite age (±1 Ma geologic uncertainty) was assigned a temperature range of 300-350ºC, typical of rapidly cooled biotite Ar closure temperatures. When Ar K-spar ages were available for samples within the Garcia (2011) transect (and within about 1 km vertically of the sample being modeled), that age (± 1 ma) was assigned an age of 250-175ºC, the range of closure temperatures associated with domains of different retentivity in K-spar. Even

for the deepest plutons (Mt. Sopris), these constraints show rapid cooling from emplacement temperatures (> 700ºC to < 175ºC) within a few million years of emplacement.

Agreement between the age-elevation transects and HeFTy thermal models is reasonably good (Table 2). For samples from the deepest plutons (Snowmass and Sopris), models shows semi-steady cooling from 110º to 50ºC at rates of 3-5 ºC/Ma from 30 to 15 Ma. For a 30-50º C/km geothermal gradient, this would correspond to an exhumation rate of 100 m/Ma.

Table 2 Apparent exhumation rates, apparent cooling rates and apparent geothermal gradients for the Elk and West Elk Mountains.

Locality	Elevation (m)	AFT age	AHe Age	Apparent AFT Exhumation rate	Apparent AHe Exhumation rate	AFT-AHe offset	Apparent cooling rate#1	Apparent cooling rate #2	ACR/AER	Apparent geothermal gradient
				regressed elev-AFT age (from graph)	regressed elev-AHe age (from graph)	(column C-D)	AFT-AHe offset = 60º C per Ma to get from AFT->AHe or [60 C/ x Ma]	slope Hefty model	(º C/Ma)/(m/Ma)= c/m	(row J*1000) convert to ºC/km
Units	**m**	**Ma**	**Ma**	**m/Ma**	**m/Ma**	**Ma**	**ºC/Ma**	**(ºC/Ma)**	**(Ma/km)**	**(ºC/km)**
Mt Snowmass top	4295	28.8	14.8	79	71	14	4	6.5	0.054249548	54
Mt Snowmass mid	4020	24.5	12.9	79	71	11.6	5		0.065473592	65
Mt Snowmass base	3460	17.6	5.8	79	71	11.8	5	6.5	0.06436387	64
Sopris top	3777	31.3	12.4	66	195	18.9	3	5	0.048100048	48
Sopris mid	3523	30	10.2	66	195	19.8	3	5	0.045913682	46
Sopris base	3107	21.4	9.9	66	195	11.5	5	5	0.079051383	79
Ragged top	3640	31.1	10.7	62	85	20.4	3	5	0.034602076	35
Ragged mid	3071	27.1	6.4		85	20.7	3	5		

Locality	Elevation (m)	AFT age	AHe Age	Apparent AFT Exhumation rate	Apparent AHe Exhumation rate	AFT-AHe offset	Apparent cooling rate#1	Apparent cooling rate #2	ACR/AER	Apparent geothermal gradient
				regressed elev-AFT age (from graph)	regressed elev-AHe age (from graph)	(column C-D)	AFT-AHe offset = 60º C per Ma to get from AFT->AHe or [60 C/ x Ma]	slope Hefty model	(º C/Ma)/(m/Ma)= c/m	(row J*1000) convert to ºC/km
Ragged base	1882	15.4	5.6	848	85	9.8	6	5	0.072028812	72
Gunnison top	3881	33.8	34.6	100	70	-0.8	-75	3	-1.071428571	-1071
Gunnison mid	3698	32.5	32	100	70	0.5	120		1.714285714	1714
Gunnison base	3503	30.1		100		30.1	2	3		
Capitol top	4151	23.2	11.2		255	12	5	0.3	0.019607843	20
Capitol base	3386	23.8	8.2		255	15.6	4	0.3		
Beckwith top	3530	30.5	29.4	620	23	1.1	55	3	2.371541502	2372
Beckwith base	3220	30	15.8	620	23	14.2	4	3		

LOW-TEMPERATURE APATITE (U-TH)/HE ANALYSIS OF OLIGOCENE CONGLOMERATES: TELLURIDE CONGLOMERATE AND BLANCO BASIN FORMATION

This section addresses the thermal history of newly age-reassigned Oligocene conglomerates of the Telluride and Blanco Basin Formation that were deposited by rivers draining the San Juan Volcanic field (Donahue, Chapter 2). Data from this study are important for understanding the potential extent of the proposed volcaniclastic apron around the San Juan Mountains (e.g. Fig. 1 of Lipman, 2007 and Fig. 2 of Steven, 1975). The locations of these sedimentary units are shown in Fig. 1.

Background

The topography of the modern southern Rocky Mountains (SRM) began to take shape in the Laramide Orogeny (~70-45 Ma), which was characterized by fault-bounded, basement-cored uplifts and basins (Coney & Reynolds, 1978; Dickinson & Snyder, 1978) (Fig.1). The Oligocene ignimbrite flare-up (38-25 Ma), was characterized by large-volume volcanism ranging from Colorado to Mexico; these eruptions dramatically re-shaped SRM topography as the San Juan, Mogollon Datil, and Never Summer volcanic fields erupted voluminous ignimbrites from dozens of calderas in Colorado and New Mexico (Lipman, 2007).

The suite of deposits (Fig. 1) investigated in this study were historically given Eocene ages, though these ages have largely been revised to be Oligocene (Donahue, Chapter 2). The RMES bevels into basement, Mesozoic or Paleozoic strata. In key locations, gravels lie unconformably upon this RM surfaces (Donahue, Chapter 2). Basal

gravels are dominated by nonvolcanic clasts, but transition upsection to increasing volcanic clast content, and are capped by Tertiary volcanic flows. New AHe sample locations (Fig. 1) and dates are given in Table 1 and modeled cooling histories shown in Fig. 2, 3, 4, and 5 elucidate the burial and exhumation histories of these units. The samples that show post-depositional cooling ages are shown as stars and these were modeled and are discussed below in terms of their maximum post-depositional temperature and inferred depth of burial. Those samples containing solely detrital grains are shown with dots—these are discussed in term of the pre-30 Ma unroofing history of the San Juan Mountains. In the event of samples recording an exhumational history, we would expect to see ages reflecting post-volcanic material spanning some time as overlying insulating volcanics were gradually removed. The potential that young AHe ages are derived solely from reheating by overlying volcanics exists, in which case AHe cooling histories has very little to do with exhumation; in this scenario, we would expect to see AHe ages that cluster exclusively very near the age of volcanic material.

Widespread surfaces of gentle topography developed diachronously in the SRM region due to post-Laramide erosion (Epis and Chapin, 1975; Dickinson et al., 1988; Erslev, 1993; Pazzaglia and Kelley, 1998). The "late Eocene erosion surface" (Fig. 1) was defined in the classic Epis and Chapin (1975) paper that used geomorphic and geologic evidence (particularly the 36.7 Ma overlying Wall Mountain Tuff) to correlate many of the poorly preserved, extensively faulted and isolated segments of low relief erosion surfaces spanning approximately 10,000km^2 over the Front-, Rampart-, Sawatch-, Sangre de Cristo-, and Wet Mountain Ranges at elevations ranging from 2300-3800m (Pazzaglia and Kelley, 1998). The newer name, "Rocky Mountain Erosion

Surface" (RMES), was used to emphasize a diachronous origin for what was still considered a regional erosion surface (Evanoff, 1990; Chapin, C.E., Kelley, 1997; Cather et al., 2008). Pazzaglia and Kelley (1998) refer to the RMES as an "upland surface of low relief presumably formed by fluvial erosion following Laramide deformation."

The Rocky Mountain erosion surface is a composite, diachronous surface that formed in response to CMB, Laramide and Oligocene ignimbrite magmatism and associated mantle- driven epeirogenic uplift from 70-25 Ma and reflects the local-to-regional beveling of highlands (Chapter 2). Overlying conglomerates throughout southwestern CO and northern NM range in age from 70 to 26 Ma; thus, the RMES has different ages in different locations. Upon this diachronous surface, the Oligocene conglomerates of this study were deposited ca. 30 Ma, and were then quickly covered by volcaniclastic material.

The Telluride Conglomerate is a boulder-to-pebble conglomerate with interbedded sandstones and siltstones and preserves a regional unroofing sequence (Gonzales et al., 2005). Proximal debris flows in the unit contain poorly-sorted, matrix supported conglomerates and moderately sorted, grain supported sandstone lenses (Little Molas Lake, town of Telluride). Increasingly fine-grained fluvial characteristics with larger percentage of andesitic to rhyolitic clasts are found at more distal outcrops (Mt. Wilson; just north of Telluride). Upper sections of the Telluride Conglomerate at Mt. Wilson that are in contact with overlying volcanic units are metamorphosed. The overlying and widespread 32 Ma San Juan Formation (Lipman et al., 1970) is ~ 2,000 (615 m) in thickness, and consists largely of mudflow deposits, volcaniclastic rocks that

interfinger with lava flows (Luedke, 1968). The San Juan Formation is in turn overlain by volcanics of the 27.6-28.3 Ma Silverton and 29-35 Ma Uncompahgre calderas to an depth of >1 km.

The Blanco Basin Formation is exposed at 9,000-10,000 ft. (2743 -3048 m) elevation on the southern slopes of the San Juan Mountains (Fig. 7). The unit unconformably overlies the Cretaceous Mancos (90-85 Ma) or Paleocene-Cretaceous Animas Formations or Morrison Formation and is overlain by the 34 Ma Conejos Formation. (Brister, 1992; Lipman and McIntosh, 2008). The Conejos Formation is one of the early pre-caldera flows from the 28.3-27.8 Ma La Garita cluster; volcaniclastic units thin from ~1.3 km near caldera center to a preserved ~600 m thickness in more distal locations (Lipman, 2000, 2007).

The San Juan volcaniclastic apron of Lipman, 2007 (Fig. 1 – orange line), showed nearly all of the modern Colorado Rocky Mountains covered by voluminous ignimbrite material, a cover which perhaps extended westward onto the Colorado Plateau. The depth and true extent of this apron is unknown. One of the aspects of this study is to better constrain the depth of the San Juan volcanic field apron in the locations of these samples. The extent and volume of this volcaniclastic apron has important implications in better understanding post-depositional erosional history and regional isostatic rebound as the Rocky Mountain and Colorado Plateau regions have been denuded (e.g. Lazear et al., 2013).

In New Mexico, the Ritito Conglomerate and Galisteo Formation were investigated. The Ritito Conglomerate lies on unconformably on the El Rito Formation, Mesozoic or Permian sedimentary rocks or Proterozoic basement and is gradationally

overlain by the volcanic Los Pinos Formation(Koning et al., 2011) or Abiquiu Formations (Maldonado and Kelley, 2009). The unit has a maximum thickness of 210 m and clasts range from granule to boulder size (Maldonado and Kelley, 2009). A K-Ar age of ca. 27 Ma (Lipman et al., 1970)on a basalt near the base of the Ritito Conglomerate and an assumed ca. 27 Ma age on altered basalt interbedded with the Ritito Conglomerate (Moore, 2000) bracket the Oligocene age of the unit. The Ritito Conglomerate is dominated by Proterozoic basement clasts including quartzite, granite, metavolcanics, quartz schists and small amounts of Mesozoic sedimentary units. Cenozoic volcanic clasts sourced from the San Juan and Latir volcanic fields to the north are minor and found in the uppermost parts of the unit (Kelley, et al., 2013) where it transitions into the volcaniclastic dominated Los Pinos Formation (Aby, S.B., et al., 2011).

The late Paleocene-Eocene Galisteo Formation contains 37-40 Ma fossils (Lucas and Ingersoll, 1981; Williamson and Lucas, 1992; Ingersoll et al., 1990) and consists of two unconformity-bound tectonosequences (the lower Diamondtail Formation and the upper Galisteo Formation) representing the sedimentary response to two tectonic events (Lucas et al., 1982; Maynard, 2005). It is concordantly overlain by the ~4 km-thick 36-27 Ma volcaniclastic Espinaso Formation (Lisenbee, 1999; Connell et al., 2001) or is locally unconformably overlain by Santa Fe Group sequences (Cather, 1992).

New Low-Temperatures (U-Th)/He Results

New AHe dates are given in Table 2 (full data in Appendix 3) and modeled cooling histories are shown in Fig. 14-17 elucidate the burial and exhumation histories of these units.

Table 3 New (U-Th)/He data from this study.

Grain #	Mass (µg)	Radius (µm)	Length (µm)	U (ppm)	Th (ppm)	eU (ppm)	4He (pmol/g)	Ft	Raw date (Ma)	Corr date (Ma)	Error (Ma)
Telluride Conglomerate San Juan Mountains, CO											
Telluride Conglomerate – Mt. Wilson (MSD-CO-2011-17) UTM NAD83 13S E236328, N4191579											
a1	1.7	40.6	221.7	37.8	113.3	64.4	0.01	0.6	16.2	25.4	1.7
a2	1.0	32.0	205.5	2.5	3.4	3.3	0.46	0.6	na	na	0.0
a3	1.1	33.0	220.2	22.5	69.5	38.8	0.00	0.6	10.8	19.1	9.5
a4	0.4	25.7	107.3	38.9	88.3	59.7	0.00	0.5	7.5	15.8	4.4
a5	0.9	36.9	104.7	23.1	60.7	37.4	0.00	0.6	17.7	29.1	4.4
Telluride Conglomerate – Telluride (MS-10-10) UTM NAD83 13S E253999, N4203164											
a1	9.1	78.9	245.0	13.2	31.2	20.5	0.72	0.8	668.8	831.1	8.0
a2	11.6	88.6	191.0	5.9	24.7	11.7	0.07	0.8	86.3	105.0	1.0
a3	5.2	66.9	170.0	18.3	40.9	27.9	0.00	0.8	1.7	2.2	0.2
a4	3.8	60.9	144.0	4.6	45.6	15.3	0.05	0.7	151.1	204.1	1.9
a5	16.3	97.0	276.0	5.5	10.1	7.8	4.27	0.8	5608.0	6671.3	73.3
Telluride Conglomerate – Little Molas Lake (MS-10-9) UTM NAD83 13S E260912, N4182548											
a1	0.8	35.7	97.0	41.9	59.1	55.8	0.89	0.8	2923.4	4851.5	45.5
a2	1.0	38.7	94.0	5.7	8.2	7.7	0.00	0.8	8.5	13.6	0.7
a3	2.6	51.8	161.0	1.8	6.2	3.2	0.01	0.8	211.3	298.4	3.8
a4	3.6	58.5	166.0	4.3	17.4	8.4	0.00	0.7	21.1	28.6	0.6
a5	0.6	32.9	72.0	4.0	8.1	5.9	0.02	0.8	1032.5	1812.0	37.2
Blanco Basin Formation – North of Chama, NM (MSD-CO-2011-13) UTM NAD83 13S E363024, N4102024											
a1	0.6	27.1	190.0	7.2	26.7	13.5	0.89	0.5	1020.9	2095.3	1.6
a2	0.3	25.0	100.0	124.7	220.8	176.6	0.00	0.5	25.7	55.6	8.3
a3	0.5	28.8	130.0	27.6	24.1	33.3	0.01	0.5	20.2	38.4	1.8
a4	0.4	26.0	130.0	28.6	84.2	48.4	0.00	0.5	40.8	86.3	2.6
a5	0.8	30.3	200.0	15.5	32.6	23.2	0.02	0.5	46.3	85.8	3.6
Blanco Basin Formation – North of Chama, NM (MSD-CO-2011-14) UTM NAD83 13S E363101, N4102023											
a1	2.3	51.7	122.0	7.2	8.0	9.0	1.96	0.7	na	na	0.0
a2	4.6	64.6	156.0	11.0	15.1	14.6	0.02	0.8	53.3	69.4	1.7

Grain #	Mass (µg)	Radius (µm)	Length (µm)	U (ppm)	Th (ppm)	eU (ppm)	4He (pmol/g)	Ft	Raw date (Ma)	Corr date (Ma)	Error (Ma)
a3	5.5	69.2	146.0	4.6	9.3	6.8	0.01	0.8	67.3	86.3	2.1
a4	4.8	65.3	162.0	3.2	27.0	9.6	0.12	0.8	476.4	628.8	1.3
a5	5.5	67.8	188.0	15.2	26.4	21.4	0.03	0.8	53.5	68.9	1.4
Galisteo Formation – South of La Cienega, NM (MSD-NM-2011-23) UTM NAD83 13S E397607, N3935726											
a1	2.9	48.8	247.0	88.6	44.0	98.9	0.09	0.7	57.7	81.9	1.7
a2	1.3	38.3	170.0	101.0	132.0	132.0	0.04	0.6	48.0	76.5	1.6
a3	1.1	35.8	180.0	32.3	24.1	38.0	0.01	0.6	33.6	55.2	2.2
a4	0.4	23.5	150.0	4.9	26.5	11.2	0.00	0.4	30.9	73.7	6.8
a5	0.9	30.6	220.0	31.4	47.6	42.6	0.01	0.5	25.1	45.9	2.3
Ritito Formation – El Rito, NM (MS-11-4) UTM NAD83 13S E363998, N4001072											
a1	0.6	28.8	150.2	19.4	47.0	30.4	0.01	0.5	60.3	114.8	1.9
a2	0.3	22.0	139.7	218.4	97.2	241.3	0.03	0.4	83.0	202.8	1.4
a3	0.4	22.9	175.1	4.5	43.8	14.8	0.01	0.4	153.9	364.7	3.0
a4	0.5	28.1	130.9	95.0	59.2	108.9	0.05	0.5	150.0	305.5	1.6
a5	0.3	22.5	143.5	142.4	142.2	175.8	0.23	0.4	691.6	1661.7	1.3

Telluride Conglomerate. New (U-Th)/He indicate the upper section Little Molas Lake sample MS-10-9 shows AHe cooling ages of 13.58, 298.44, 28.63 Ma) (Fig. 2) , and the upsection sample from Mt. Wilson (MSD-CO-2011-17) (Fig. 3) returned cooling ages of 25.45, 19.06, 15.82, 29.06 Ma) (Table 2).

Telluride Conglomerate sample MS-10-10 from the basal section of near Little Molas Lake returned only detrital ages of 831.11, 105.05, 204.08 Ma, indicating no (or incomplete) resetting of the unit; this sample was not modeled in HeFTy.

Modeled cooling history for MS-10-9 indicates the unit - deposited just prior to eruption of the San Juan volcanic field - remained buried or thermally insulated for4-6

Ma until exhumation initiating at ~24 Ma with a slight acceleration in exhumation rate at ~4-6 Ma brought the unit to the surface (Fig. 2).

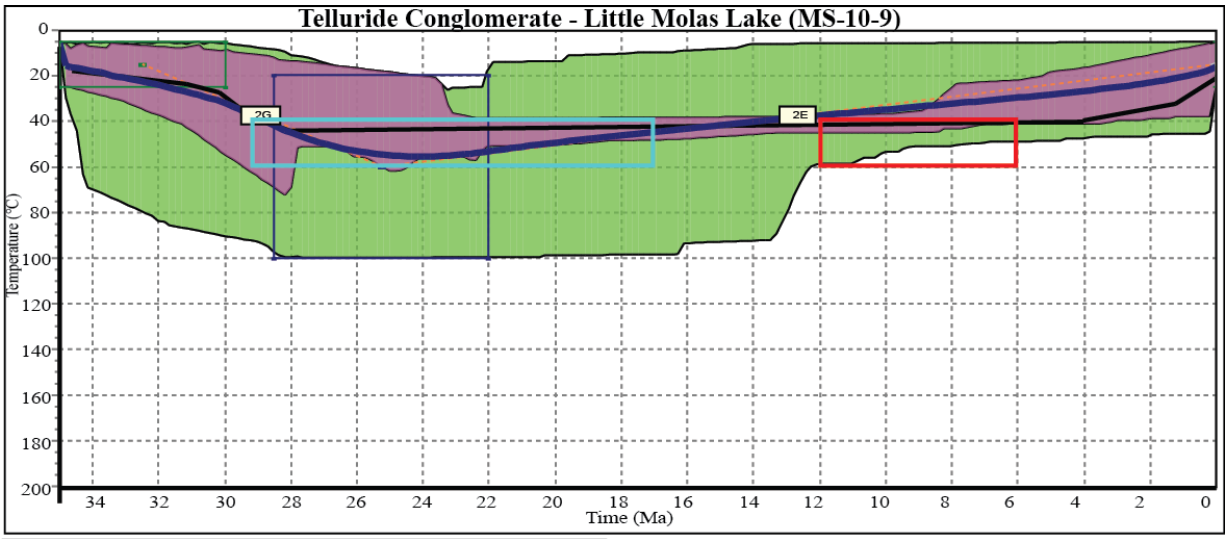

Path Information

10,000 paths tried
3793 acceptable paths
68 good paths

Blue path = weighted mean path
Black path = best-fit path

MS-10-9

Sample Location: 37.759°N, -107.711°W (Little Molas Lake)
Elevation: 3810 m
Rock Type: Conglomerate
Age: 33 Ma (this study)

HeFTy Model Description:
Thermal history model incorporates two single-grain apatites. Model required unit to be at surface temperatures (15° ± 10°C) at 34-29 Ma and then to temperatures of ≥20°C from 28.5-22 Ma to account for volcanic cover associated with eruption of the Silverton & San Juan Calderas. Overlying San Juan Formation volcanics are of 27.6 (Silverton) – 28.4 (San Juan) Ma (Lipman, 2007). Unit is forced to return to surface temperatures (15° ± 10°C) at present. Model used the Flowers et al., 2009 RDAAM (apatite) calibration

AHe Modeling Results

G2 input age (error): 8.7 ± 2.7
Corrected age: 13.5 ± 4.2
Model age: 13.7
GOF: 0.95

G4 input age: 21.0 ± 5.73
Corrected age: 26.6 ± 7.3
Model age: 19.8
GOF: 0.35

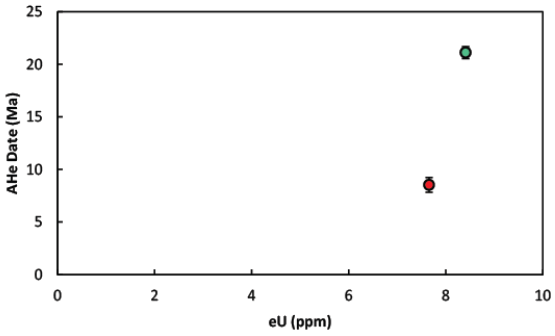

Figure 3-Error! No text of specified style in document.**-13** HeFTy models for Telluride Conglomerate at Little Molas Lake.

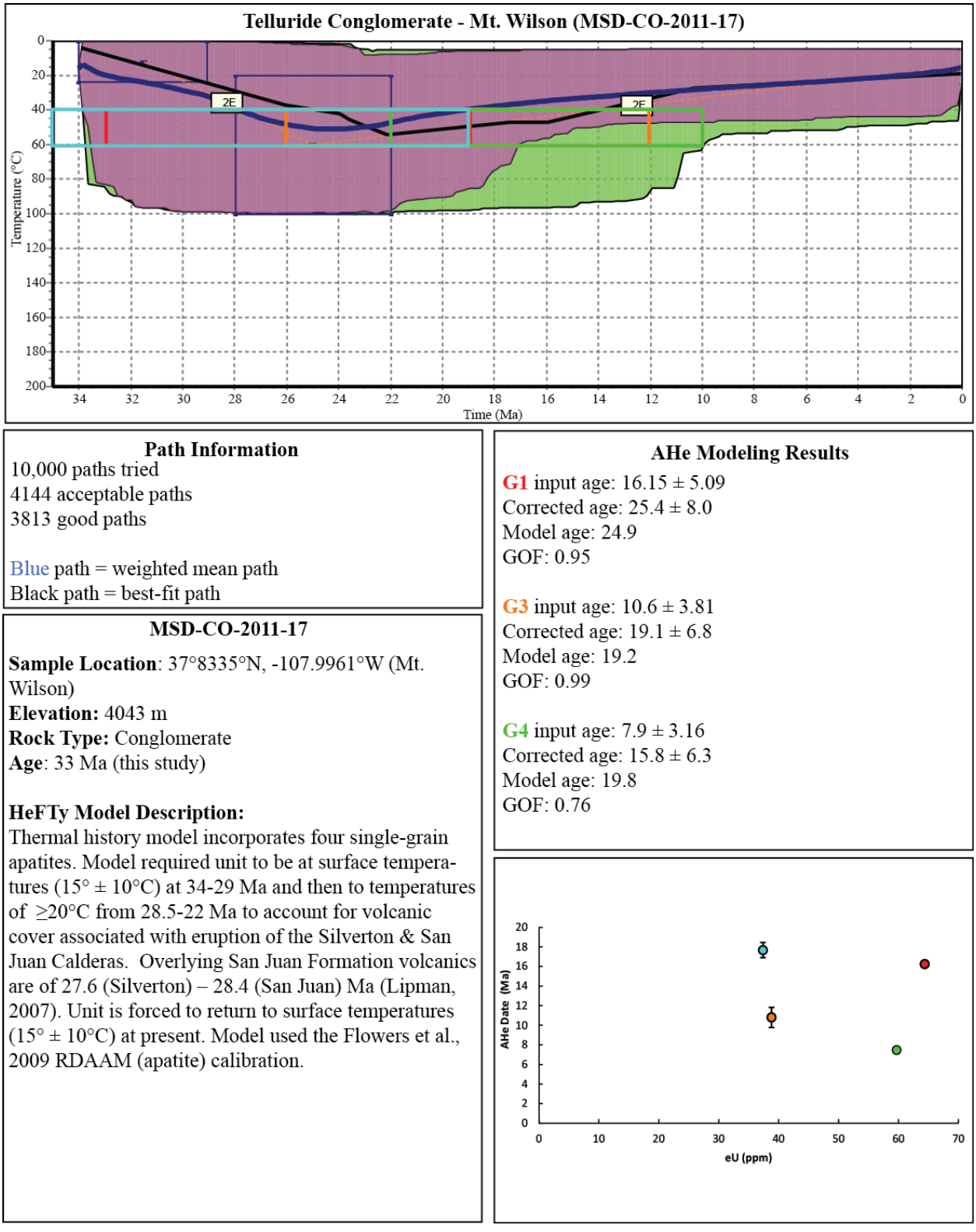

Figure 3-Error! No text of specified style in document.**-14** HeFTy models for Telluride Conglomerate at Mt. Wilson.

Blanco Basin Formation. Two samples of the Blanco Basin Formation were run for AHe analysis. The upper section sample (MSD-CO-2011-14) yielded only detrital grain ages of 69.38, 86.33, 628.84, 68.94 Ma and HeFTy modeling was not conducted on this sample suite. The lower-mid section sample (MSD-CO-2011-13) yielded cooling ages of 55.61, 38.38, 86.28, 85.77 Ma. Cooling models of this sample (Fig. 16) indicate that burial of the grain peaked at ~40-60º at ~25 Ma, after which the grain experienced gradual exhumation and cooling to present.

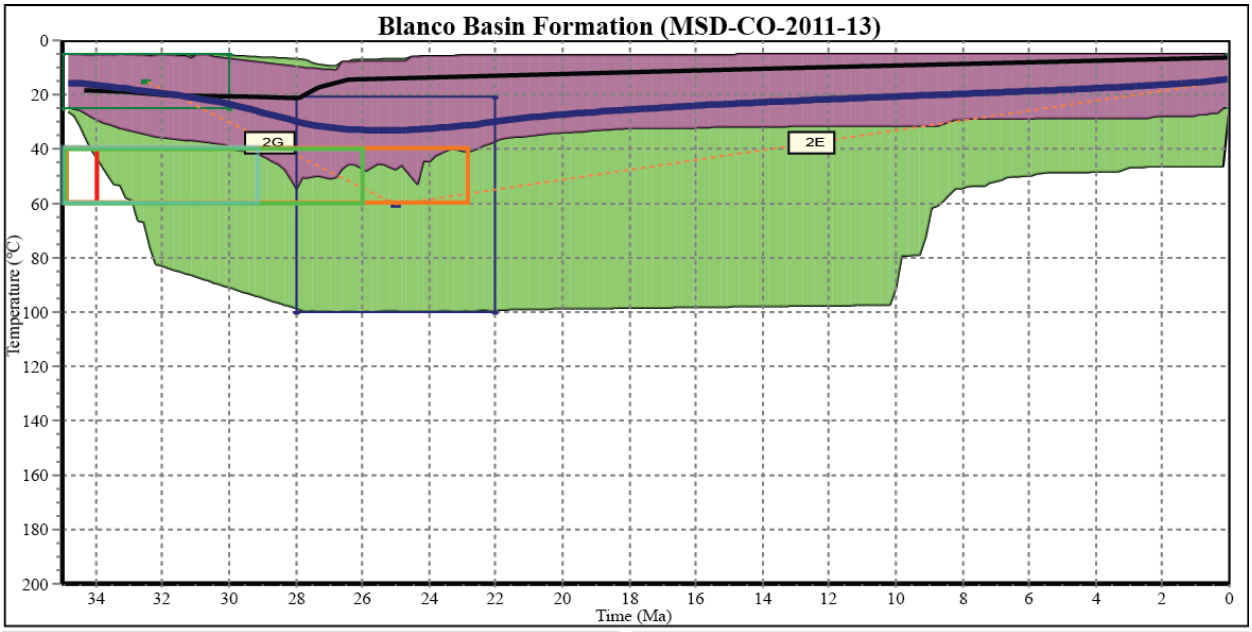

Path Information

10,000 paths tried
3022 acceptable paths
0 good paths

Blue path = weighted mean path
Black path = best-fit path

MSD-2011-CO-13

Sample Location: 37.0544°N, -106.5405°W
Elevation: 2870 m
Rock Type: Conglomerate, sedimentary
Age: 33 Ma (this study)

HeFTy Model Description:
Thermal history model incorporates four single-grain apatites. Grain #1 was excluded because of anomalously high He, not much U-Th, leading us to believe it is not an apatite, or has an implantation. Model required unit to be at surface temperatures (15° ± 10°C) at 35-30 Ma and then to temperatures of 20-100°C from 28-22 Ma to account for volcanic cover associated with eruption of the Summitville and Platoro Calderas. The unit is overlain by locally reworked Quaternary landslide deposits and Oligocene volcanic units, taking the form of bedded conglomerates and breccias. The unit is forced to return to surface temperatures (15° ± 10°C) at present. Model used the Flowers et al., 2009 RDAAM (apatite) calibration.

AHe Modeling Results

G2 input age: 27.8 ± 11.12
Corrected age: 55.6 ± 22.2
Model age: 34.6
GOF: 0.30

G4 input age: 43.15 ± 17.26
Corrected age: 86.3 ± 34.5
Model age: 33.7
GOF: 0.12

G3 input age: 19.5 ± 7.68
Corrected age: 38.3 ± 15.1
Model age: 33.4
GOF: 0.75

G5 input age: 46.0 ± 17.15
Corrected age: 85.7 ± 32.0
Model age: 33.1
GOF: 0.10

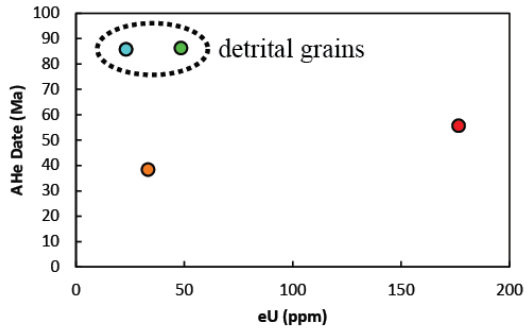

Figure 3-Error! No text of specified style in document.**-15** HeFTy models for Blanco Basin Formation, Chama, NM.

Ritito Conglomerate. (U-Th)/He raw ages for this unit are all detrital (Table 1). Ages of 114.81, 202.83, 364.74, 305.50, 1661.72 Ma were recorded; HeFTy models were run for this sample.

Galisteo Formation. (U-Th)/He ages for the Galisteo Formation (MSD-NM-2011-23; La Cienega Creek) are 81.85, 76.44, 55.15, 73.65, 45.93 Ma (Table 1). HeFTy models run on this sample agree with only very slight temperature reheating to 20-60º.

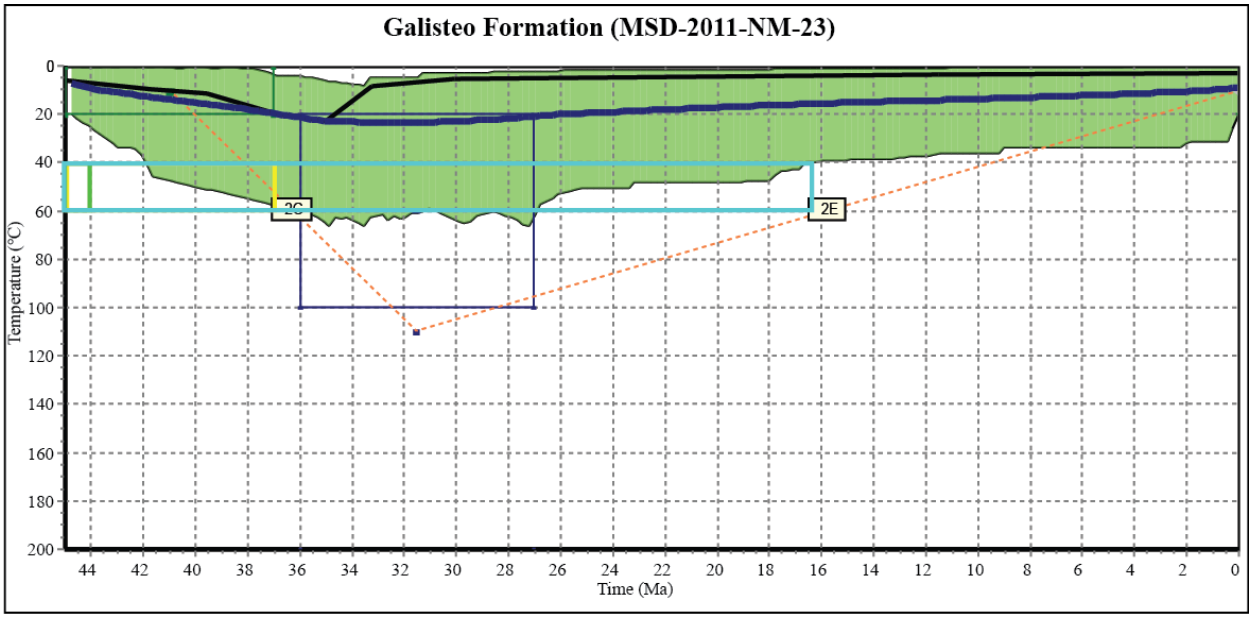

Path Information

10,000 paths tried
1293acceptable paths
0 good paths

Blue path = weighted mean path
Black path = best-fit path

MSD-2011-CO-23

Sample Location: 35.5599°N, -106.1298°W
Elevation: 1824m
Rock Type: Conglomerate, sedimentary
Age: 45-37 Ma (stratigraphic)

HeFTy Model Description:
Thermal history model incorporates five single-grain apatites. Model required unit to be at surface temperatures (10° ± 10°C) at 45-37 Ma and then to temperatures of ≥20°C from 36-27 Ma. The unit is overlain by 36-27 Ma Espinaso Formation. The unit is forced to return to surface temperatures (10° ± 10°C) at present. Model used the Flowers et al., 2009 RDAAM (apatite) calibration.

AHe Modeling Results

G1 input age: 59.15 ± 16.37
Corrected age: 81.9 ± 22.7
Model age: 44.8
GOF: 0.10

G2 input age: 47.97 ± 15.3
Corrected age: 76.5± 15.3
Model age: 44.8
GOF: 0.19

G3 input age: 34.25 ± 11.03
Corrected age: 55.1 ± 17.8
Model age: 44.3
GOF: 0.54

G4 input age: 36.8 ± 14.73
Corrected age: 73.6 ± 29.5
Model age: 42.8
GOF: 0.22

G5 input age: 45.9 ± 16.7
Corrected age: 73.6 ± 29.5
Model age: 44.2
GOF: 0.92

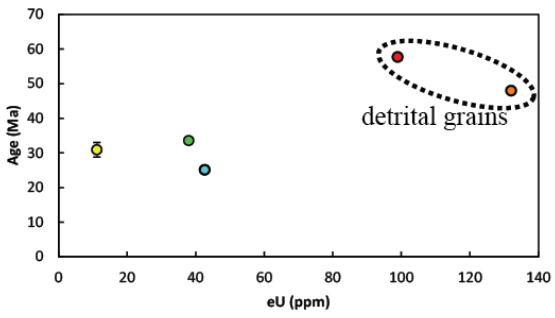

Figure 3-Error! No text of specified style in document.**-16** HeFTy model for the Galisteo Formation.

Miocene – Recent cooling: San Juan Mountains (McKeon, 2009)

Cooling ranged from ca. 3-40 Ma as recorded in AFT and AHe data from McKeon (2009). The range sections cooled differentially: in the NW parts of San Juan's cooling occurred between 3-10 Ma (AHe), and in the southern parts from 19-39 Ma. Erosion was driven by local tectonism rather than regional erosionally-induced isostatic rebound.

Additional discussion of joint AFT and AHe models will be included here after consultation with coauthors.

Interpretation of New Low-Temperatures (U-Th)/He Datasets

Telluride Conglomerate. We interpret this cooling model to indicate that the sample from Little Molas Lake (MS-10-9; Fig. 14) was shallowly buried to depths sufficient enough to raise to 20º -100º C or approximately 1-3 km. The cooling history from Mt. Wilson sample (MSD-Co-2011-17; Fig. 15) suggests a potentially slightly more prolonged burial history. Uplift and observed tilting of this unit from its presumed source area near Silverton (~ 2,800 m/9,300 feet elevation) to the west at Mt. Wilson (4267 m/ 14,000 feet elevation) requires several hundred meters of post-depositional and post-burial modification. Thermal histories suggest uplift initiating at ca. 20 Ma and steady, continued unroofing over the last 10-20 Ma. This uplift is potentially associated with the emplacement of the 26-25 Ma Wilson stock as well as post-10 Ma regional isostatic rebound associated with regional erosion (Lazear et al., 2013).

Blanco Basin Formation. Our interpretation is that the total original depth of volcaniclastic material ejected from the erupting San Juan volcanic vents in this region

was not significant enough to reset the thermal structure within the grains of the Blanco Basin and thus must have been less than 1-2 km of material likely buried by volcanic material from the Creede, La Garita, and/or the Summitville-Platoro caldera complexes at ~28 Ma, much of which has since been removed by erosion. From this, we conclude that grain ages are completely detrital from this unit.

El Rito Formation and Ritito Conglomerate Our interpretation is that both the El Rito Formation and Ritito Conglomerate underwent similar burial and exhumation histories and that neither unit has not been sufficiently reheated by burial to reset the inherited Laramide apatite signature of the grains of this unit.

Galisteo Formation. We interpret this to indicate that the unit barely if at all buried sufficiently to o reset the Laramide detrital signature (Fig. 17).

Additional discussion of joint AFT and AHe models will be included here after consultation with coauthors.

DISCUSSION: TIMING, SPATIAL DISTRIBUTION, UPLIFT RATES, AND MECHANISMS OF UPLIFT

The Cenozoic Rocky Mountain history is punctuated by periods of uplift and periods of slow cooling we interpret as periods of regional-scale tectonic quiescence or transition. This paper focuses on driving mechanisms and unique characteristics of each broad period within the SRM topographical history. We step through the major stages of SRM formation below.

Laramide (~70-45 Ma)

Cooling during this time largely reflects the uplift and erosion of these Laramide blocks. Sample ages are found in the hanging wall blocks in the WY Wind River,

Medicine Bow and Park, CO Front and Park, NM Nacimiento and Sangre de Cristo Ranges and some Colorado Plateau monoclines (Fig. 18). Laramide cooling is also observed in localized regions ("sky islands") throughout NM. Regional AERs from 70-45 Ma average at 70 m/Ma (r^2= 0.37 averaged for 5 AERs) (Figure 3; and in DR1 and DR2). Notably, the AERs from the Wind River Range, WY are much higher as we see rapid thrusting recorded during this time frame in thrust-front ranges. The continental expression of the Farallon slabs' collision with and subduction beneath North America (Ricketts et al., 2015; Humphreys and Coblentz, 2007), the Laramide Orogeny (~70-45 Ma) was characterized by the formation of fault-bounded, basement-cored uplifts and basins.

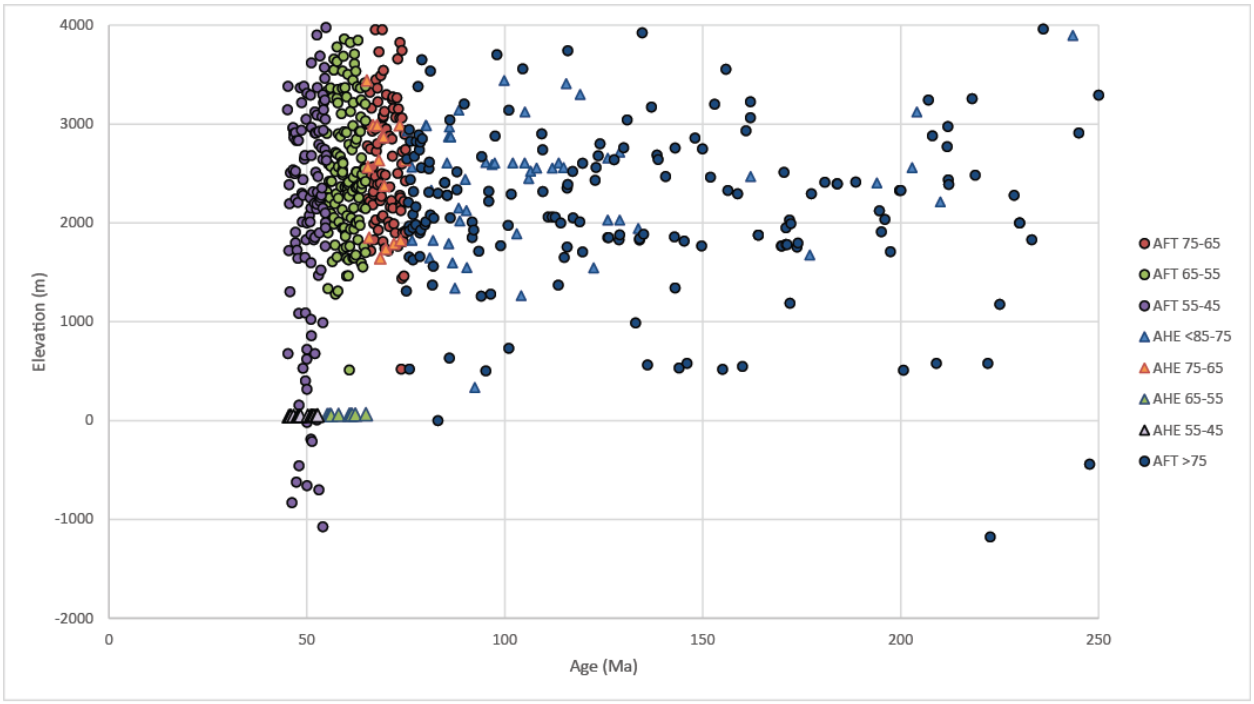

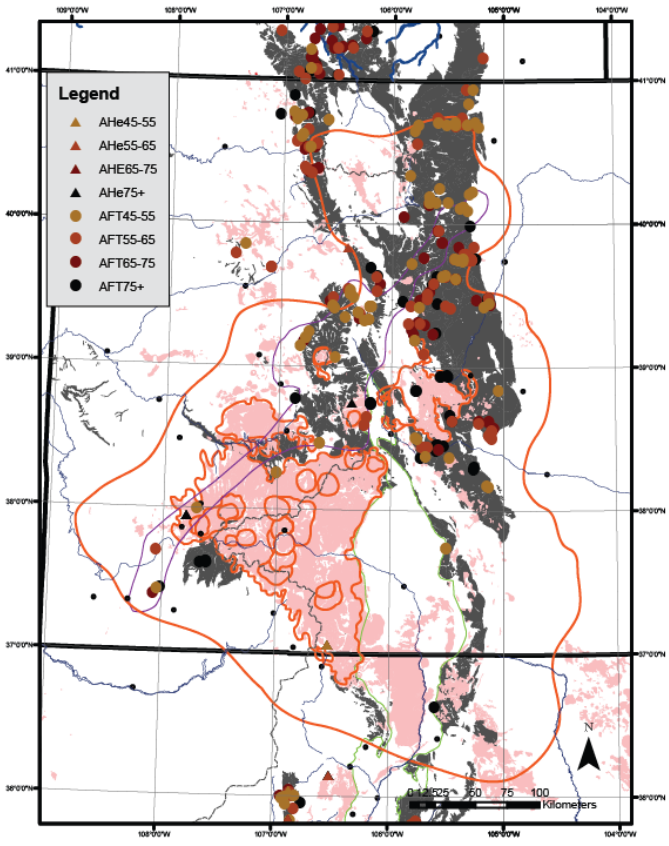

Figure 3-17 Laramide cooling. A. Age-elevation cloud broken into >75 Ma, 75-65 Ma, 65-55 Ma, 55-45 Ma. B. Spatial distribution of Laramide ages.

Fig. 4 transposes Laramide cooling ages with mantle temperature at 73 km depth(Hansen et al., 2013). We observe that areas dominantly of Laramide cooling age overlie cold crust whereas areas with younger (35-25 Ma) cooling ages tend to overlie warmer crust. We do observe that Laramide cooling ages are preserved throughout the region where not completely overprinted by younger heating events. This is suggestive that these preserved Laramide cooling ages reflect the pre- or syn -Laramide 110ºC isotherm preserved in the landscape and also that todays' crustal temperature structure has components inherited from ignimbrite flare up activity.

Rocky Mountain Erosion Surface (45-35 Ma)

Following the Laramide Orogeny, a period relative tectonic quiescence reigned in central North America. Regional isotherms were reset during this time to subhorizontal reflecting long-wavelength Laramide features (Jean Braun, 2005), by 40 Ma. Following the Laramide, the diachronous Rocky Mountain erosion surface began to form (Fig. 1 and Donahue, Chapter 2). Currently, this surface is an extensively faulted, discontinuous, and composite surface inferred from isolated segments spanning much of the Colorado Rocky Mountain Ranges at elevations ranging from 2300-3800 m. A range of sample elevations of the RMES are shown as green horizontal bars in Fig. 3.

Late Eocene-Oligocene (38-24 Ma)

Late Eocene-Oligocene ignimbrite volcanism broadly reheated and reset regional geotherms (Fig 1). While some cooling was due to cooling of erupted volcanic material, regional exhumation associated with regional doming due to regional volcanism was extremely important, and is recorded in AHe ages younger than ages of volcanism (Fig 6B). Ignimbrite volcanism from ~35-25 Ma is surficially expressed in the Never

Summer, San Juan, Mogollan-Datil volcanic fields, cooling of plutons (Lipman, 2007; Bryant and Naeser, 1980; Decker et al., 1988), and laccolithic intrusions in Elk Range, Colorado Plateau and eastern edge of the Great Plains.

Modeled cooling histories from Snowmass Mountain (after Garcia, 2011) using both AFT and AHe constraints give AERs of ~70 m/Ma, ACRs of 4-5ºC/Ma, and an AGG of 55-65ºC/km. These models also show semi-steady cooling at these rates from 30-5 Ma (Fig. 7). Within the same timeframe, the Sawatch Range (after Feldman, 2010) and Blanca Peak (Ricketts et al., 2015) show similar cooling histories, as do those of the western Gore Range (Landman and Flowers, 2013).

Miocene (25-10 Ma)

Thermochronology ages throughout the SRM region at ca. 20-10 Ma record a transition to Rio Grande rift activity (Landman and Flowers, 2013; Ricketts et al., 2015) and is also observed in non-rift cooling of plutons (Garcia, 2011) and distributed exhumation such as in the Needles Mountains of southern CO (Mckeon, 2009). Continued scouring of RMES and Oligocene volcanic deposits as well as surface uplift along rift flanks triggered a shift from regional inflation to one of extension during which we see the accumulation of large fluvial and eolian deposits into existing and forming basins (e.g. Cather et al., 2008). AERs during this interval are ~145 m/Ma (r^2=0.68)

Neogene (last 10 Ma)

Neogene cooling ages recorded in disparate groups with limited locality (Fig 1) and record extremely fast AERs of excess of 300 m/Ma (r^2 = 0.67). Some of these points clearly record young rift-related activity (e.g., Gore Range, NM rift flanks);

however some points cannot be explained by rifting activity due to their non-rift associated location (e.g., San Juan Range (McKeon, 2008; this study) and the MWX well (Kelley and Blackwell, 1990)). One instance that must be considered is young cooling and subsequent young reheating. This is especially possible in areas such as the southern Rockies where high heat flow (Reiter, 2008) and hydrothermal fluids may result in reset (young) cooling ages.

CONCLUSIONS: IMPLICATIONS FOR CENOZOIC LANDSCAPE EVOLUTION

Cenozoic history of Rocky Mountain uplift is punctuated by periods of exhumation with a period of relative thermal stability. Cooling during the Laramide Orogeny (75-45 Ma) at AERs of ~ 70 m/Ma were concentrated in uplifted Laramide fault-blocks and records slow cooling associated with modest surface uplift and exhumation following crustal thickening as the Farallon slab begins to impact the SRM region. A decrease in recorded cooling followed during a period of relative tectonic quiescence from 45-35 Ma, during which regional, diachronous beveling throughout the SRM region occurred. Driven by continued Farallon subduction and perhaps the delamination of the Farallon slab (and part of NA lithosphere; Karlstrom et al., 2012; Ricketts et al., 2015) beneath the San Juan and Mogollon Datil volcanic fields, Eocene-Oligocene ignimbrite volcanism (38-24 Ma), cooling occurred throughout the region both from regional inflation of landscape and associated erosion as well as cooling of plutons. Oligocene cooling rates range from 60-125 m/Ma. Local instances of Neogene (last 10 Ma) cooling ages recorded in short-wavelength uplifts driven by both young rifting/faulting events (e.g., Gore Range, Landman and Flowers, 2013) and also by

small-scale mantle convection acting upon a heterogeneous SRM crust at exceptionally fast AERs in excess of 300 m/Ma. These rates - faster than any others in Cenozoic SRM history – may be locally amplified by the integration of the Colorado and Rio Grande Rivers into the Gulf of California and ensuing accelerated incision, differential erosion due to isostatic rebound (Lazear et al., 2013), and an erosive late Cenozoic climate.

Thus, throughout the Cenozoic, we see mountain building and associated cooling reflecting multiple uplift or transitional events, each of which is characterized by distinct spatial distribution of cooling data and apparent exhumation rates from which unique driving mechanisms are inferred.

ACKNOWLEDGMENTS

This work was supported by the Colorado Rockies Experiment and Seismic Transects (CREST) experiment funded by the National Science Foundation Continental Dynamics Program under award EAR-0607808. Special thanks to reviewers for editorial comments, and for support from the Alfred P. Sloan Minority Ph.D. Program, Colorado Scientific Society, New Mexico Geological Society, Geological Society of America, and University of New Mexico Graduate & Professional Student Association.

REFERENCES CITED

Aby, S.B., Kempter, K., Koning, D., 2011, Recent mapping of the Oligo-Miocene Los Pinos Formation and associated units in the Tusas Mountains, New Mexico Scott, *in* New Mexico Geological Society 62nd Annual Fall Field Conference Guidebook, v. 62, p. 275–280.

Brister, B.S., 1992, The Blanco Basin Formation (Eocene), San Juan Mountains region, Colorado and New Mexico, *in* New Mexico Geological Society 43rd Annual Field COnference Guidebook, v. 43, p. 321–331.

Bryant, B., and Naeser, C.W., 1980, The significance of fission-track ages of apatite in relation to the tectonic history of the Front and Sawatch Ranges, Colorado:

Geological Society of America Bulletin, v. 91, p. 156–164.
Carter, L.S., Kelley, S.A., Blackwell, D.D., and Naeser, N.D., 1998, Heat Flow and Thermal History of the Anadarko Basin ,: v. 2, p. 291–316.
Cather, S.M., 1992, Suggested revisions to the Tertiary tectonic history of North-central New Mexico: New Mexico Geological Society Guidebook, 43rd Field Conference, v. 43, p. 109–122.
Cather, S.M., Chapin, C.E., and Kelley, S.A., 2012, Diachronous episodes of Cenozoic erosion in southwestern North America and their relationship to surface uplift, paleoclimate, paleodrainage, and paleoaltimetry: Geosphere, v. 8, p. 1177–1206, doi: 10.1130/GES00801.1.
Cather, S.M., Connell, S.D., Chamberlin, R.M., McIntosh, W.C., Jones, G.E., Potochnik, A.R., Lucas, S.G., and Johnson, P.S., 2008, The Chuska erg: Paleogeomorphic and paleoclimatic implications of an Oligocene sand sea on the Colorado Plateau: Geological Society of America Bulletin, v. 120, p. 13–33, doi: 10.1130/1326081.1.
Cerveny, P.F., and Steidtmann, J.R., 1993, Fission track thermochronology of the Wind River Range, Wyoming: Evidence for timing and magnitude of Laramide exhumation: Tectonics, v. 12, p. 77–91.
Chapin, C.E., Kelley, S. a, and Cather, S.M., 2014, The Rocky Mountain Front , southwestern USA: Geosphere, v. 10, p. 1043–1060, doi: 10.1130/GES01003.1.
Chapin, C.E., Kelley, S.A., 1997, The Rocky Mountain Erosion Surface in the Front Range of Colorado, *in* Colorado Front Range Guidebook, Rocky Mountain Association of Geologists, p. 101–113.
Coney, P.J., and Reynolds, S.J. Cordilleran Benioff zones: Nature, v. 270.
Connell, S.D., Lucas, S.G., Koning, D.J., Maynard, S.R., and Derrick, N.., 2001, First-day, Santo Domingo sub-basin: Hagan Embayment and northern flank of the Sandia Mountains:.
Decker, E.R., Heasler, H.P., Buelow, K.L., Baker, K.H., and James, S., 1988, Significance of past and recent heat-flow and radioactivity studies in the Southern Rocky Mountains region: Geological Society of America Bulletin, v. 100, p. 1851–1885, doi: 10.1130/0016-7606(1988)100<1851.
Dickinson, W.R., Klute, M.A., Hayes, M.J., Janecke, S.U., Lundin, E.R., McKittrick, M.A., and Olivares, M.D., 1988, Paleogeographic and paleotectonic setting of Laramide sedimentary basins in the central Rocky Mountain region: Geological Society of America Bulletin,.
Dickinson, W.R., and Snyder, W.S., 1978, Plate tectonics of the Laramide orogeny, *in* p. 355–366.
Epis, R.C., and Chapin, C.E., 1975, Geomorphic and tectonic implications of the Post-Laramide, Late Eocene Erosion Surface in the southern Rocky Mountains, *in* Curtis, G.F. ed., Cenozoic history of the southern Rocky Mountains, Geological Society of America Memoir 144, p. 45–74.
Erslev, E., 1993, Thrusts, back-thrusts, and detachment of Rocky Mountain foreland arches: Geological Society of America Special Paper, v. 280, p. 339–358.
Evanoff, E., 1990, Early Oligocene paleovalleys in southern and central Wyoming: Evindence of high local relief on the late Eocene unconformity: Geology, v. 18, p. 443–446.

Farley, K.A., Wolf, R.A., and Silver, L.T., 1996, The effects of long alpha-stopping distances on (U-Th)/He ages: Geochimica Cosmochimica Acta, v. 60, p. 4223–4229.
Feldman, J.D., 2010, The Emplacement and Exhumation History of the Twin Lakes Batholith and Implications for the Laramide Orogeny and Flat Slab Subduction.
Fitzgerald, P.G., Duebendorfer, E.M., Faulds, J.E., and O'Sullivan, P., 2009, South Virgin–White Hills detachment fault system of SE Nevada and NW Arizona: Applying apatite fission track thermochronology to constrain the tectonic evolution of a major continental detachment fault: Tectonics, v. 28, doi: 10.1029/2007TC002194.
Fleischer, R.L., Price, P.B., and Walker, R.M., 1975, Nuclear Tracks in Solids: Principles and Applications: University of California Press, Berkeley.
Flowers, R.M., Ketcham, R. a., Shuster, D.L., and Farley, K. a., 2009, Apatite (U–Th)/He thermochronometry using a radiation damage accumulation and annealing model: Geochimica et Cosmochimica Acta, v. 73, p. 2347–2365, doi: 10.1016/j.gca.2009.01.015.
Garcia, R., 2011, Cenozoic intrusive and exhumation hisotry of the West Elk Mountains, southwestern Colorado: New Mexico Institute of Minning and Technology, 143 p.
Gonzales, D.A., Kray, B., and Gianniny, G.L., 2005, Insight into the timing of the Cenozoic uplift in Southwestern Colorado from the Telluride Conglomerate: Geological Society of America Abstracts with Programs, v. 37, p. 16.
Hansen, S.M., Dueker, K.G., Stachnik, J.C., Aster, R.C., and Karlstrom, K.E., 2013, A rootless rockies-Support and lithospheric structure of the Colorado Rocky Mountains inferred from CREST and TA seismic data: Geochemistry, Geophysics, Geosystems, v. 14, p. 2670–2695, doi: 10.1002/ggge.20143.
Heller, P.L., Mathers, G., Dueker, K., and Foreman, B., 2013, Far-traveled latest Cretaceous-Paleocene conglomerates of the Southern Rocky Mountains, USA: Record of transient Laramide tectonism: Bulletin of the Geological Society of America, v. 125, p. 490–498, doi: 10.1130/B30699.1.
House, M. a., Kelley, S. a., and Roy, M., 2003a, Refining the footwall cooling history of a rift flank uplift, Rio Grande rift, New Mexico: Tectonics, v. 22, p. n/a–n/a, doi: 10.1029/2002TC001418.
House, M.A., Kelley, S.A., and Roy, M., 2003b, Refining the footwall cooling history of a rift flank uplift, Rio Grande rift, New Mexico: Tectonics, v. 22, p. 1–18, doi: 1060 10.1029/2002tc001418.
Humphreys, E.D., and Coblentz, D.D., 2007, North American dynamics and Western US tectonics: Reviews of Geophysics, v. 45, doi: Rg3001 10.1029/2005rg000181.
Humphreys, E.D., Hessler, E., Dueker, K., Farmer, C.L., Erslev, E., and Atwater, T., 2003, How Laramide-age hydration of North American lithosphere by the Farallon slab controlled subsequent activity in the western United States: International Geology Review, v. 45, p. 575–595.
Ingersoll, R. V., Cavazza, W., Baldridge, W.S., and Shafiqullah, M., 1990, Cenozoic sedimentation and paleotectonics of north-central New Mexico; Implications for initition and evolution of the Rio Grande rift: GSA Bulletin, v. 102, p. 1280–1296, doi: 10.1130/0016-7606(1990)102<1280:CSAPON>2.3.CO;2.
Jean Braun, 2005, Quantitative constraints on the rate of landform evolution derived from

low-temperature thermochronology, *in* Reiners, P.W. and Ehlers, T.A. eds., Low-temperature thermochronoogy: techniques, interpretations, and applications, Reviews in Mineralogy & Geochemistry, p. 351–374.

Karlstrom, K.E., Coblentz, D., Dueker, K., Ouimet, W., Kirby, E., Van Wijk, J., Schmandt, B., Kelley, S., Lazear, G., Crossey, L.J., Crow, R.S., Aslan, A., Darling, A., Aster, R., et al., 2012, Mantle-driven dynamic uplift of the Rocky Mountains and Colorado Plateau and its surface response: Toward a unified hypothesis: Lithosphere, v. 4, p. 3–22, doi: 10.1130/L150.1.

Kelley, S.A., 2005, The Rocky Mountain region—An evolving lithosphere: Tectonics, geochemistry, and geophysics, *in* Karlstrom, K.E. and Keller, R.G. eds., The Rocky Mountain region—An evolving lithosphere: Tectonics, geochemistry, and geophysics, p. 154.

Kelley, S.A., and Blackwell, D.D., 1990, Thermal history of the Multi-Well Experiment (MWX) site, Piceance Creek basin, northwestern Colorado, determined from apatite fission track analysis: Nuclear Tracks and Radiation Measurements, v. 17, p. 331–337.

Kelley, S.A., and Chapin, C.E., 2004, Denudation history and internal structure of the Front Range and Wet Moungains, Colorado, based on apatite-fission-track thermochonology: New Mexico Bureau of Geology & Mineral Resources, v. 160, p. 41–78.

Kelley, S.A., and Chapin, C.E., 1995, Fission-track thermochronology mapping in the Southern Rocky Mountains–Rio Grande Rift province: American Association of Petroleum Geologists Bulletin, v. 79, p. 920.

Kelley, S.A., Chapin, C.E., and Corrigan, J., 1992, Late Mesozoic to Cenozoic cooling histories of the flanks of the Northern and central Rio Grande rift, Colorado and New Mexico: New Mexico Bureau of Mines and Mineral Resources, Bulletin1, v. 145, p. 39.

Kelley, A., and Duncan, I.A.N., 1986, Late Cretaceous to Middle Tertiary Tectonic History of the Northern Rio Grande Rift, New Mexico: v. 91, p. 6246–6262.

Kelley, S.A., Kempter, K.A., McIntosh, W.C., Maldonado, F., Smith, G.A., Connell, S.D., Koning, D.J., and Whiteis, J., 2013, Syndepositional deformation and provenance of Oligocene to Lower Miocene sedimentary rocks along the western margin of the Rio Grande rift, Jemez Mountains, New Mexico, *in* Hudson, M.R., Grauch, V.J.S. ed., New Perspectives on Rio Grande Rift Basins: From Tectonics to Groundwater, Geological Society of America Special Paper 494, v. 494, p. 101–123, doi: 10.1130/2013.2494(05).

Ketcham, R. a., 2005, Forward and Inverse Modeling of Low-Temperature Thermochronometry Data: Reviews in Mineralogy and Geochemistry, v. 58, p. 275–314, doi: 10.2138/rmg.2005.58.11.

Ketcham, R.A., Gautheron, C., and Tassangot, L., 2011, Accounting for long alpha-particle 1388 stopping distances in (U-Th-Sm)/He geochronology: Refinement of the baseline case: Geochimica et Cosmochimica Acta, v. 75, p. 7779–7791.

Koning, D.J., Kempter, K., Peters, L., Mciintosh, W.C., and May, S.J., 2011, Miocene-Oligocene volcaniclastic deposits in the northern Abiquiu embayment and southern Tusas Mountains, New Mexico, *in* New Mexico Geological Society Guidebook

62nd Field Conference, p. 251–274.
Landman, R.L., and Flowers, R.M., 2013, (U-Th)/ He thermochronologic constraints on the evolution of the northern Rio Grande Rift , Gore Range , Colorado , and implications for rift propagation models to explain late Cenozoic elevation gain of the: Geosphere, v. 9, p. 170–187, doi: 10.1130/GES00826.1.
Lazear, G., Karlstrom, K., Aslan, A., and Kelley, S., 2013, Denudation and fl exural isostatic response of the Colorado Plateau and southern Rocky Mountains region since 10 Ma: Geosphere, v. 9, p. 792–814, doi: 10.1130/GES00836.1.
Lipman, P.W., 2000, Central San Juan caldera cluster: regional volcanic framework: Geological Society of America Special Paper 346, v. 346, p. 9–69.
Lipman, P., 2007, Incremental assembly and prolonged consolidation of Cordilleran magma chambers: Evidence from the Southern Rocky Mountain volcanic field: Geosphere2, v. 3, p. 42–70, doi: 10.1130/GES00061.1.
Lipman, P.W., and McIntosh, W.C., 2008, Eruptive and noneruptive calderas, northeastern San Juan Mountains, Colorado: Where did the ignimbrites come from? Geological Society of America Bulletin, v. 120, p. 771–795, doi: 10.1130/B26330.1.
Lipman, P.W., Steven, T.A., and Mehnert, H.H., 1970, Geological Society of America Bulletin Volcanic History of the San Juan Mountains , Colorado , as Indicated by Potassium − Argon Dating: Geological Society of America Bulletin, doi: 10.1130/0016-7606(1970)81.
Lisenbee, A.L., 1999, Preliminary Geologic Map of the Galisteo Quadrangle , Santa Fe County , New Mexico:.
Lucas, S.G., and Ingersoll, R.V., 1981, Cenozoic continental deposits of New Mexico: An overview: Geological Society of America Bulletin,.
Lucas, S.G., Wolberg, D.L., Hunt, A., and Schoch, R.M., 1982, A Middle Eocene Titanothere from the Baca Formation, South-Central new Mexico: Journal of Paleontology, v. 56, p. 542–545.
Luedke, R.G., 1968, Volcanism and cauldron developmen in the western San Juan Mountains, Colorado: Colorado School of Mines Quarterly, v. 63, p. 175–208.
Maldonado, F., and Kelley, S.A., 2009, Revisions to the stratigraphic nomenclature of the Abiquiu Formation , Abiquiu and contiguous areas , north-central New Mexico: New Mexico Geology, v. 31, p. 3–8.
Maynard, S., 2005, Laccoliths of the Ortiz porphyry belt, Santa Fe County, New Mexico: New Mexico Geology, v. 27, p. 3–21.
Mckeon, R.E., 2009, The interaction between tectonics, topography, and climate in the San Juan Mountains, southwestern Colorado: Montana State University, 77 p.
Moore, J.D., 2000, Tectonics and volcanism during deposition of the Oligocene–lower Miocene Abiquiu Formation in northern New Mexico: University of New Mexico, 147 p.
Naeser, C.W., Bryant, B., Kunk, M.J., Kellogg, K., Donelick, R.A., and Perry, W.J., 2002, Tertiary cooling and tectonic history of the White River uplift, Gore Range, and western Front Range, central Colorado: Evidence from fission-track and 39Ar/40Ar ages: Geological Society of America Special Paper 366, p. 31–53 ST – Tertiary cooling and tectonic history .
NAVDAT, 2015.

Omar, G.I., Lutz, T.M., and Giegengack, R., 1994, Apatite fission-track evidence for Laramide and post-Laramide uplift and anomalous thermal regime in the Beartooth overthrust, Montana-Wyoming: Geological Society of America Bulletin, v. 106, p. 74–85.

Painter, C.S., and Carrapa, B., 2013, Flexural versus dynamic processes of subsidence in the North American Cordillera foreland basin: Geophysical Research Letters, v. 40, p. 4249–4253, doi: 10.1002/grl.50831.

Pazzaglia, F.J., and Kelley, S., 1998, Large-scale geomorphology and fission-track thermochronology in topographic and exhumation reconstructions of the Southern Rocky Mountains: Rocky Mountain Geology, v. 33, p. 229–257.

Peyton, S.L., Reiners, P.W., Carrapa, B., and Celles, P.G.D., 2012, Low-temperature thermochronology of the northern Rocky Mountains, western U.S.A.: American Journal of Science, v. 312, p. 145–212, doi: 10.2475/02.2012.04.

Reiter, M., 2008, Geothermal anomalies in the crust and upper mantle along Southern Rocky Mountain transitions: Geological Society of America Bulletin, v. 120, p. 431–441, doi: 10.1130/B26198.1.

Ricketts, J.W., Kelley, S.A., Karlstrom, K.E., Schmandt, B., Donahue, M.S., and van Wijk, J., 2015, Synchronous opening of the Rio Grande rift along its entire length at 25–10 Ma supported by apatite (U-Th)/He and fission-track thermochronology, and evaluation of possible driving mechanisms: Geological Society of America Bulletin, p. B31223.1, doi: 10.1130/B31223.1.

Roy, M., Kelley, S., Pazzaglia, F., Cather, S., and House, M., 2004, Middle Tertiary buoyancy modification and its relationship to rock exhumation, cooling, and subsequent extension at the eastern margin of the Colorado Plateau: Geology, v. 32, p. 925, doi: 10.1130/G20561.1.

Shuster, D.L., and Farley, K.A., 2004, 4He/3He thermochronometry: Earth and Planetary Science Letters, v. 217, p. 1–17, doi: 10.1016/S0012-821X(03)00595-8.

Steidtmann, J.R., Middleton, L.T., and Shuster, M.W., 1989, Post-Laramide (Oligocene) uplift in the Wind River Range, Wyoming: Geology, v. 17, p. 38–41.

Steven, T.A., 1975, Middle Tertiary Volcanic Field in the Southern Rocky Mountains: Geological Society of America Memoir, v. 144, p. 75–94.

Tagami, T., and O'Sulllivan, P.B., 2005, Fundamentals of Fission-Track Thermochronology, *in* Reiners, P.W. and Ehlers, T.A. eds., Reivews in Mineraology & Geochemistry v. 58: Low-Temperature Thermochronology: Techniques, Interpretations, and Applications, Mineralogical Society of America Geochemical Society, p. 19–41.

Williamson, T.E., and Lucas, S.G., 1992, Stratigraphy and mammalian biostratigraphy of the Paleocene Nacimiento Formation, southern San Juan Basin: New Mexico Geological Society 43rd Annual Field COnference Guidebook, p. 265–296.

CHAPTER 4 THE *FIELD PLAY* MOBILE APPLICATION: AUGMENTED REALITY, LOCATION-AWARE CONTENT, AND THE CREATION OF AN INTERACTIVE, DATA-RICH DIGITAL EDUCATIONAL AND RESEARCH TOOL

Magdalena S. Donahue[1]
[1]Department of Earth and Planetary Sciences, Northrop Hall, University of New Mexico, Albuquerque, New Mexico 87131, USA

ABSTRACT

Digital technologies – web-based, mobile and wearable – are becoming increasingly used in geoscience education. Increases in access to technology and computing power are paired with a growing recognition of the need to diversify methods of teaching, research, data collection and management, and scientific communication both within geoscience communities and world populations. As digital tools and student populations evolve and diversify, traditional educational methods need updating. Digital technology is making inroads into the geosciences, and, as topics such as climate change, natural resources exploration, and funding cuts to research and educational institutions become increasingly part of our national discourse, the need to communicate with and educate the communities that support geoscience and environmental research is increasingly critical.

The Field Play project grew out of a recognized need to access multiple types of geologic information while in the field. The ongoing Field Play mobile device application seeks to create a data-rich and location-sensitive tool for geoscience education suitable for use by a range of audiences while in the field. The desire to create an educational tool suitable for use by an audience that ranges widely in skill mandates

the collection and streamlining of data from many sources and in many formats including maps, data tables, annotated photographs, etc. Field Play works to streamline the access to this range of tools using location, topic, and keyword search functions to direct a user through their educational experience. Field Play enhances the traditional field experience by enfolding tools such as location-triggered audio content, augmented reality-enhanced landscapes, multiple types of layered basemaps and location-specific data and references.

Field Play was originally deployed in the Albuquerque, NM, area. The application was also featured in the 2014 New Mexico Geological Society Fall Field Conference, located in the Sacramento Mountains of southern New Mexico. Demonstration trips have been created throughout the western US and Canada.

GEOSCIENCE EDUCATION: INTRODUCTION & BACKGROUND

Traditional Geoscience Field Education

Traditional undergraduate geoscience education seeks to introduce the broad fields of geoscience to the student, and traditional curriculums involve classroom, laboratory and field-based study (Whitmeyer et al., 2009). Students gain exposure to the major branches of geoscience (e.g., sedimentology, tectonics, hydrology, volcanology, mineralogy, etc.) through a structured classroom-based curriculum, while gaining skills such as map-making, rock and mineral identification, and mineral petrology in hands-on laboratories. Field-based education is an important component of geoscience education (Elkins and Elkins, 2007; Mgok and Goodwin, 2012; Petcovic et al., 2014). Field education expands upon classroom and laboratory work by placing students in the ‘real

world' where they are able to implement their knowledge to solve real geologic problems.

Multi-week field camps are often used as cap-stone courses for geoscience undergraduate degrees. Nearly 3,000 students attend field courses annually (Oleson, 2013). The intensive immersion into field study challenges students academically, socially, and physically. Participating in extensive field-based education can be problematic for many reasons: students' time commitments, camp tuition and associated costs, and family obligations all pose significant barriers to many potential geoscience students (Whitmeyer and Mogk, 2009).

Much of the work behind geologic field education is aimed at increasing the students' ability to visualize their world – both the visible, and the invisible, whether it is underground or has been removed through geologic processes. Traditional tools used in geoscience field education include paper maps, compasses, rulers, and colored pencils. More recently, the use of GPS has become ubiquitous as a location tool. More advanced field education courses utilize tablets for mapping and geographic information software such as ArcGIS to facilitate geologic mapping for both individuals and groups. Tablets and ArcGIS software allow the use and layering of basemaps including topographic maps, photo imagery, satellite imagery, and LiDAR, increasing information access and precision.

While many field-based courses are geared at general field skills, with the availability of technology and digital tools has come the interest in a more specific field education. As the branches of geoscience education require increasingly specific skill sets and background knowledge, many students desire to attend applied field education

courses that complement their career choices. These range from and include field-education courses dedicated to oil and gas exploration, geo-engineering, geothermal or alternative energy exploration and/or infrastructure, or environmental assessment. These opportunities allow for specialized training and job-skills cultivation with educators and working professionals.

Digital innovations in geoscience field education

Much of the interest in enfolding digital tools into geoscience education is to increase students' ability to visualize, understand, and interact with their environment – past, present, and future. One of the approaches that has gained popularity is the creation of virtual field trips (Caliskan, 2011; Whitmeyer et al., 2009; Meezan and Cuffey, 2012). The idea of creating a "virtual" trip is not a new one: geologists on early American scientific exploration parties, stunned by the amazing scenery and landscapes seen in the American West sought to express the new sceneries, geologic phenomena, and wildlife to people unfamiliar with and far from the remote wildernesses they explored. These expeditions accomplished this goal of transporting sceneries to the general population by bringing artists with them to capture the visual side of expeditions: the Hayden Geological survey of 1871 to what is now Yellowstone National Park included photographer William Henry Jackson and resulted in iconic paintings by Thomas Moran (Hayden, 1872), and the 1872 Powell expedition to the Grand Canyon included photographer John Hillers, artist Frederick Dellenbaugh, and again, Thomas Moran (Dutton, C.E., 1882). Since the time of these initial surveyors, scientists have been seeking ways of communicating the phenomena they observe and

ideas they formulate to people of both scientific and nonscientific backgrounds by blending science, graphic design, and emerging technologies.

The internet and digital field technologies have provided a phenomenal increase in ability to share and communicate scientific findings and have begun to be used to supplement traditional geoscience education (Whitmeyer, et al., 2011; Kelso and Brown 2008). Recently, "electronic" or "virtual" trips have been created by entities ranging from the National Park Service (Geology of the National Parks, 2014; National Parks Service, 2014), media sources and nonprofit foundations (Discovery Education, 2014; Electronic Field Trip, 2014), and many academic institutions (Roberts, et al., 2013, Virtual Field Trips, 2014; Geology Central, 2013) as educators attempt to bring "the field" to students, fellow geologists, and interested users around the globe. These trips are frequently structured so they provide a curated selection of annotated photographs, maps, and instructional text to users, which the user navigates in a method similar to a statically illustrated e-book or any website. Another approach to enhancing learning on geologic topics is the design of virtual environments. In this approach, high-resolution (usually LiDAR) data are used to create exceptionally detailed virtual environments that are accessed by users standing in a virtualization theater wearing 3D-glasses (Forte, et al., 2013). These environments allow for in-depth, immersive study of landscapes and geologic features in the section of data availability; however, drawbacks include very specific data collection, rarity of facilities supporting this visualization technique, the high amount of specialized equipment required, and an almost exclusively academic audience. Designers of these environments are working to increase their availability in widely-usable formats: Google Earth files and movies, some utilizing parts of data the

LiDAR data collection used in immersive environments, are increasingly available for public use as easily-accessible web-based virtual outcrops (Forte, et al., 2013; McCaffrey, et al., 2008) and the ability to collect georeferenced data and integrate with 3D visualization and geospatial anaylsis is growing (Wawrzyniec, et al., 2007) as a tool for increasing geologic learning in classroom settings.

Technological considerations for working in the field

Presenting digital content in the field offers a challenge that has been seen in the design of many technologies. Donald Norman, a cognitive scientist, has dedicated several books to the concept of user-centered design (Norman, 1988). Norman presents the idea of using design to serve the user, proposing that the product should serve the user, not that the user should not be slave to the product. In the context of field geology, the user should ideally spend a minimal amount of time trying to find content and maximal time engaging with the environment.

While Norman's philosophies can be applied to any user interface from a doorknob to a cabinet door, his work becomes critical when it comes to interacting with complex devices such as smart phones. Limited input options and the complexity of the phone can easily result in a complicated and demanding user experience. Human-Centered Computing aims to solve this problem by emphasizing the role the user takes as consumer of information (Sebe, 2010), and differs greatly from the process traditionally used in computer science whereby the algorithmic solution is often placed front and center. Location-aware applications help to improve the human-computer interface by allowing applications to become aware of human spaces.

Location aware educational applications are still in their infancy. Chen and Choi of Perdue University have experimented in creating a location aware application for the teaching of history (Chen, 2010). Their application incorporates 2D barcodes related to Google Earth locations and 3D models. Such tools are wonderful at creating an interactive educational experience, however, the interaction immerses users almost entirely in a virtual world as every bit of education takes place on the screen of the device.

Augmented reality (AR) takes location aware a step further by putting data as close to the source as possible. There have been a few gestures towards this approach in the geology discipline. A group from the University of Manchester created the Discovery Geology AR field trip, a concept program to highlight the advantages of using AR in the field using the Junaio application. Another interesting approach Mathiesen (2012) uses is overlaying 3D models onto a camera display.

Both of these approaches are wonderful demonstrations of the power of AR as an educational tool but each has significant limitations. Discovery Geology was implemented as demonstration project and is dependent on the Junaio application. Junaio is based on a streaming model that requires a constant connection to a network, which limits the use of Discovery Geology to locations with wireless connectivity. The Mathiesen approach shows great promise in enriching the AR experience, however, content creation is still dependent on knowledge of mobile application development.

THE FIELD PLAY APPLICATION

Introduction

The Field Play initiative has two themes: 1) AR field trips, and 2) geoscience outreach and education. The project works to address these themes by integrating field geology, geoscience education, and mobile device technology to create an interactive, data-rich, and user-friendly AR field trip experience available as a mobile device and web application.

The overall goal of the Field Play application ("app") is to provide accessible, personally interesting, interactive, and scientifically robust and relevant geoscience education to the public. Field Play provides users with AR field trips in which multiple data formats are streamlined into one interactive experience that enhances the traditional geological field trip.

The question of how to integrate and effectively use technology into geoscience education is of increasing importance and assumes global importance in the context of funding cuts, academic institutions curtailing field experiences, the large demographic of underserved or overcommitted students lacking funds or time to participate in important field-based education, and – critically – the need for scientific communication allowing for the accurate conveyance and productive discussion of scientific principles and findings with a diverse general public population.

Field Play was conceptualized as a means to help to alleviate some of the mystery and reduce the perceived difficulty and resulting intimidation many students associate with science education. By using familiar, widespread devices (e.g., smartphones, tablets) and navigational elements reminiscent to gaming controls, Field Play is designed to be a fluid, intuitive, engaging, and educational experience that fuses the best elements of field geology and with the added bonus of providing access to the

user to relevant background data (e.g., the vast font of published literature, photographs, and educational animations, etc.) to create an educational experience that is richer and more personally relevant than would be possible with either solely field or digital formats. The program is designed to offer a fluid scalability through ranges of users' intellectual levels, vastly increases the population that can be reached as it allows 'students' to interact with the information at their own educational and confidence levels. While previous digital education projects begin to bring images of the "field" to web users, no other project has attempted to achieve the level of personally-scalable interactive media, AR learning components, or data access that Field Play does.

The integration of technology into education evolves as rapidly as new technologies and innovative ideas emerge. The app is dynamic: content will increase and reflect topics of national (National Parks), regional (Field Conferences, key New Mexico geology locations), and political (e.g., hydrology in the southwest, local natural resource) importance. The growth and affordability of hardware is key in the development of Field Play: the prevalence and proliferation of data-enabled mobile platforms (Pew Research Center, 2015) allows access of this app to a wide, diverse, and growing segment of the population. Users learn more deeply if they are able to delve deeply into topics of personal interest in real-world context (Kelso, et al. 2008; Karlstrom, et al., 2008); although Field Play trips are designed to have a specified route and topical theme, they are also built to be completely self-directed such that users are able to dwell on topics of personal interest exploring material of increasing complexity, while skipping topics of lesser interest.

Access to technology and high-quality education is often a barrier to minority or underserved populations. Field Play is free and open-source, designed to run on any Android device or web browser. The code behind the field trip generator is available for download on the Field Play website (fieldplay.org, currently under construction), so that interested users can generate their own personal field trips using the Field Play code. With these open-access philosophies, I believe that Field Play will be able to provide quality geoscience education to a broader population than any other purely field or classroom format. Open access is especially critical in states such as New Mexico, where our population is diverse and our educational system can benefit from a flexible geoscience education model that will increase students' identity and understanding of their surrounding environment. The scalability of Field Play is principal in providing scientific educational materials to minority and underserved populations. The lack of minorities in the geosciences is well documented (Stokes, et al., 2014) and recognition of the need to increase geoscience education to students with diverse physical and mental needs is growing (Gilley et al., 2015). This app provides a means of accessing scientific education for underserved groups by providing educational material in a format that is familiar, not intimidating, can be explored individually or socially, and can provide learning from basic to advanced levels.

Role of Technology in Field Education Advances

Technology is often seen as a virtual world completely separate from our own, which we users engage with by removing oneself from the physical, "real" world. This presents a unique challenge when it comes to introducing technology into education in the geosciences. Students believe they must make the decision to engage their

technological device - where information lives and is accessible - or else they choose to engage the world around them that inspired that collected knowledge. This daunting and seemingly unbridgeable divide turns out to be a solvable UI (user interface) problem that works to minimize the gap between interaction with the real world and digital content. Mark Rolston, chief creative officer at Frog, talks of taking the computers out of computing so that we users do not have to stop our lives to operate a computer terminal (Rolston, 2011). Field Play brings powerful content into the field without sacrificing the attention of the participants by embedding knowledge and device use into the environment.

Many attempts to bring digital data into the field have relied on the user to discern, navigate and relate pertinent content into the context of the field experience. This requires the user to maintain a mental map of both the physical environment as well as the content layout.

For example, if a student is standing at a scenic viewpoint with typical digital information access, they first have to know where they are standing; next they must pull up the appropriate map or diagram to relate their vantage point to the available data categories; finally, they navigate through menus and submenus to pin point the data they wish to retrieve. Throughout this entire experience, the student is expending needless mental energy and time simply trying to access information. Many beginning geology students are intimidated and feel unqualified to pursue further study since they do not understand how the content is arranged; because they do not comprehend the organizational data structure, they become frustrated and feel they cannot understand geology. It is key to realize that in these situations, the stumbling point lies not with the

student, but rather in faults of the technology and its human interface. Donald Norman, author of Design of Everyday Things (Norman, 1988), puts it this way: "When you have trouble with things, whether it's figuring out whether to push or pull a door or the arbitrary vagaries of the modern computer and electronics industries, it's not your fault. Don't blame yourself: blame the designer."

The Field Play experience differs dramatically from the laborious process of data navigation. By pulling location and device orientation from a myriad of sensors, Field Play can deliver the necessary content when and where it is needed. As a user approaches a location, an audio file is played back that recites some of the more relevant features without user intervention. If the student wishes to view a map, they simply open the application where a map, automatically centered on their current location, is automatically displayed. When the student spots a physical feature they wish to know more about they point their camera at the feature in question and labels are superimposed on the moving camera feed. In Field Play, the variable data sources a geologist uses, which may have previously distracted from the new students' field experience, are now smoothly embedded into the environment, making content available as the students' needs change. Rather than a virtual experience separate from reality, the student now experiences what is known as an augmented reality.

While AR is not new, the solutions are often difficult to use and content generation is typically geared toward a more computer science oriented audience. In order for AR to be utilized for educational purposes, both the end user experience and the content generation must be simple and easy to use. The goal of Field Play is to make the

AR experience to enhance field geology, rather than to distract from the environment, the questions at hand, or the discussions that may be occurring between colleagues.

METHODS: APPLICATION CREATION

Field Play and the NMGS FFC:

In this section, I describe the specific steps required for the creation of the three-day Field Play trip used in the NMGS FFC from the perspectives of content and technological framework. This is an example of the process used for setting up a specific field trip. Apart from specific thematic and location information, the steps for an outside user to create a personalized field trip are streamlined within the Field Play programming, and advanced programming, troubleshooting, or other technical aspects are not required by the user.

Creation of Content:

Audio: Content to be included in audio portion of app will be selected from the NMGS 2014 FFC road log to highlight local and regionally important locations, ideas, concepts and debates with input from FFC trip coordinators. Content will be selected to highlight regional problems, topics of interest, and key points/locations. These will be georeferenced and will play automatically as users cross into the area.

Augmented reality: Locations will be selected based on FFC stops. A total of 6-9 AR stops are planned: 2-3 each day. AR will include relevant locations that will "float" during the "binoculars" feature of the Field Play app is and will include links to papers/abstracts and imagery including field photographs, figures, animations, and video. The accessible content during AR stops (and from the web/mobile searchable interface) can include papers, imagery, points of interest, and other relevant supplemental material

submitted by trip coordinators, NMGS staff, or NMGS FFC guidebook authors will be culled to ensure the learning experience is enhanced but does not overwhelm the user.

Video: Currently, approximately 5 videos for the 2014 NMGS FFC are planned: one general video which will provide an overview of the region and topics central to the FFC (7-10 minutes), and 3-6 key topic or concept explanation videos (2-5 minutes). Videos will be accessible in the field during the FFC and from the web (YouTube link) at any time. Videos will be created with the expertise of Brent Hall, UNM EPS M.S. student and amateur videographer. Opportunities for undergraduate mentorship exist in this location. I would enjoy employing an undergraduate student (from UNM or NMT) with crossover interests in videography, scientific communication, and the geosciences to help with the filming and production of these video lessons.

Content Submission: FFC road log content will need to be made available, as well as any supplementary content (e.g., photos, figures, etc.) authors choose to submit for inclusion in the digital format of the FFC. Content from authors will need to be submitted to app creators no later than June 30, 2014.

Technical Framework

Application Programming*:* Field Play is an Android application with a supporting website. All content is tailored to be network independent with the exception of video links. The Field Play application is currently in pre-prelease. Basic functionality has been implemented but not all features are in a usable state. The main features that still need work are: Incorporating alternative map layers, user-friendly control of audio playback and a reworking of content layout.

Augmented reality*:* The AR portion of the application is currently functioning but will require updating and troubleshooting before release. The AR portion relies heavily on onboard hardware that differs between devices. Testing this feature on a range of devices will be required.

Field testing*:* The Field Play app can largely be programmed in Albuquerque, but will require testing on several different Android devices and in locations throughout the FFC trip region. Troubleshooting will be conducted with content largely completely programmed. Field Play and the NMGS FFC trip will be tested by volunteer testers in addition to our troubleshooting prior to the FFC in September.

Web interface: The web interface is still in the planning stages. The planned web interface is an easy to use site that allows for the creation of fieldtrips, browsing and viewing of premade fieldtrips, and the download of fieldtrips to the user's device.

Apple IOS*:* Development for IOS platform is dependent upon interest and potential future funding.

FIELD DEPLOYMENT

Field Play will be deployed at the 2014 New Mexico Geological Society Fall Field Conference (NMGS FFC). Partnering with the NMGS for this conference provides the opportunity to utilize the expertise of NMGS scientists as well as being an opportunity in which I will be able to receive feedback from a cross-section of geoscientists ranging from interested hobbyists to students to experts and academic scientists on their impressions of the app, providing important feedback to help guide future app development. The end goal of Field Play is to create a personally-scalable educational experience, so partnering with the NMGS FFC will provide an excellent test

case in discovering what portions of the app are utilized or helpful to which segment of the population (e.g., does the hobbyist enjoy the audio road log, does the student find the background figures illustrating the background of a geologic process during an AR stop helpful in understanding the current discussions?). As a student from and educated in New Mexico, I am invested in working with the NMGS to create a globally-cutting edge educational tool to the New Mexico education and geological communities. In practice, the embedded GPS within mobile devices triggers location-aware interactive content to become available when the user was within a set proximity of the feature (e.g., audio alert when approaching a fault zone). Additionally, users are given the option to interactively explore topical and location-based sub-modules that include AR binoculars, informational text, audio, topographic and geologic maps, and short YouTube lessons while in the field.

Field Play content is both trip-specific and stand-alone. Content exists within the Field Play ecosystem at two levels: curated, scientific content created by Field Play, and crowd sourced data originated by users. Both of these data types are fully "mashable," and can be combined by users to create personal topical or location-based trips using our trip creation tool.

Field Play content can be accessed online as well as via mobile device. We are working to expand our curated and crowd-sourced content to provide the geologic and public communities with an up-to-date, easily accessible resource of reliable geologic and scientific information for recreational, educational or professional use.

FIELD PLAY FUTURE

As the Field Play project continues, the multi-level education scaling feature and interactive data collection ability will grow increasingly comprehensive. Progressively more available GPS and hardware developments will continue to increase field opportunities, and work to provide users the ability to geo-tag and annotate field photographs/sample locations, to easily share and communicate their findings with collaborators, and, importantly, to have the ability for educators to use Field Play in field classes to ensure students' confidence in collecting high-resolution, high-frequency, and in some cases real-time data (e.g., structural measurements, stream flow data, geophysical data, atmospheric monitoring, etc.) is planned.

CONCLUSIONS

Field Play is an augmented reality educational and experiential tool that integrates geoscience educational content with the physical world. Built to run on Android mobile devices, the Field Play system is based around the creation of a data-rich landscape through which users engage in location-aware content to explore their environment through geologic field trips. Field Play has two goals: 1) Improving access to abundant scientific information while in the field, and 2) Promoting scientific education on a large scale, in a way that is personal, relevant, and interest-driven.

Field Play was incorporated in the New Mexico Geological Society Fall Field Conference (Donahue and Donahue, 2014; September 2014). This three-day trip in southern New Mexico included AR stops, annotated photographs, audio content of critical features, and links to guidebook and other pertinent scientific publications. For this trip, Field Play created predetermined routes based off of conference road logs, as well as free-standing supplementary content.

Field Play is one attempt to bring evolving digital tools into a field-based science, and to do so in a way that benefits a range of audiences. As formal geoscience education grapples with the relevance and feasibility of field methods courses and as communication within and across an increasingly specific geoscience branches becomes increasingly critical in the world of large data sets and interdisciplinary science experiments, tools such as Field Play that facilitate exploration, learning, and communication are of vital importance.

REFERENCES

Discovery Education, 2014, Virtual Field Trip Series North America: http://www.discoveryeducation.com/northamerica/event.cfm (February 2014)

Donahue, M.S. and Donahue, J.P., 2014 Field Play and the 2014 New Mexico Geological Society Fall Field Conference: Incorporating augmented reality and location sensitive content to create an interactive, data-rich landscape: Geological Society of America Abstracts with programs, v. 46, no. 6, p.739.

Donahue, M.S. and Donahue, J.P., 2014, Field Play and the 2014 New Mexico Geological Society Fal Field Conference: Incorporating augmented reality geologic field trips and location-sensitive educational lessons for a personalized, interactive geoscience experience: New Mexico Geological Society Spring meeting: p.24.

Dutton, C.E., 1882, Tertiary History of the Grand Cañon District with Atlas: United States Geological Survey

Electronic Field Trip, 2014, National Parks Foundation virtual trips: http://www.nationalparks.org/our-work/programs/electronic-field-trip (February 2014)

Elkins, J.T., and Elkins, N.M.L., 2007, Teaching geology in the field: Significant geoscience concept gains in entirely field-based introductory geology courses: Journal of Geoscience Education, v. 55, p. 126–132.Forte, A., Kellogg, L.H., Kreylos, O., Yikilmaz, M.B., Oskin, M. Cowgill, E., Billen, M., Sumner, D., Elliott, A., 2013, Open-source virtual-reality based data visualization tools for research and teaching: 3D visualizer, Crusta and Lidarviewer at KekCaves: Geological Society of America Abstracts with Programs v. 45, no. 7, p. 503.

Geology Central, 2013, Virtual Field Trips http://homepage.smc.edu/robinsontirichard/Virtual%20Field%20Trips/tripstinationalparks.htm (February 2014).

Geology of the National Parks, 2014, Death Valley National Park Virtual Geology Field Trip: http://geomaps.wr.usgs.gov/parks/deva/devaft.html (February 2014).

Gilley, B., Atchison, C., Feig, A. and Stokes, A., 2015, Impact of inclusive field trips: Nature Geoscience, b. 8, no. 8, p.579-580, doi: 10.1038/ngeo2500.

Hayden, F.V., 1872, Preliminary Report of the United States Geological Survey of Montana and Portions of Adjacent Territories being a Fifth Annual Report of Progress. Washington, D.C.: U.S. Department of Interior.

Jaimes, A., Sebe, N., Ga_ca-Perez, D., 2006, Human-centered computing: a multimedia perspective. In Proceedings of the 14th annual ACM international conference on multimedia perspec_ve. In Proceedings of the 14th annual ACM international conference on Multimedia

Karlstrom, K., Semken, S., Crossey, L., Perry, D., Gyllenhaal, E.D., Dodick, J., Williams, M., Hellmich-Bryan, J., Crow, R., Bueno Watts, N., Ault, C., 2008, Informal geoscience education on a grand scale: the Trail of Time exhibition at Grand Canyon, Journal of Geoscience Education, v. 56, p. 354-361.

Kelso, P.R., and Brown, L.M., 2008, A geology curriculum for the 21st century: Leading Edge (Tulsa, Oklahoma), v. 27, p. 1334-1339.

Mogk, D.W., and Goodwin, C., 2012, Learning in the field: Synthesis of research on thinking and learning in the geosciences, in Kastens, K.A., and Manduca, C.A., eds., Earth and Mind II: A Synthesis of Research on Thinking and Learning in the Geosciences: Geological Society of America Special Paper 486, p. 131–164, doi: 10.1130/2012.2486(24).

MancOnline, 2013, Discovery Geology AR: http://manconline.wordpress.com/2013/08/15/discover-geology-ar/ (August 2013)

Mathiesen, D., Myers, T., Atkinson, I., Trevathan, J., 2012, Geological Visualisa_on with Augmented Reality: Proceedings of 15th Interna_onal Conference on Network-Based Informa_on Systems, pp.172-179.

McCaffrey K.J.W., Feely, M., Hennessey, R., Thompson, J., 2008, Visualization of folding in marble outcrops, Connemara, western Ireland: An application of virtual outcrop technology: Geosphere, v. 4, no. 3., p.588-599.

National Park Service, 2014, Glacier National Park: http://www.nps.gov/glac/forteachers/glacier-national-park-virtual-field-trip.htm (February 2014).

Norman, D. 1988. The Design of Everyday Things. London, MIT Press Chen, X., Choi, J., 2010, Desinging Online Collaborative Loca_on-aware Platform for History Learning: Journal of Educational Technology Development and Exchange, 3(1), 13-26.

Oleson, T., 2013, Mapping field camp's past and present: Exploring a mainstay of geoscience education: Earth Magazine, July.

Petcovic, H.L., Stokes, A., and Caulkins, J.L., 2014, Geoscientists' perceptions of the value of undergraduate field education: GSA Today, v. 24, no. 7, doi: 10.1130/GSATG196A.1.

Pew Research Center, 2015, U.S. Smartphone Use in 2015: http://www.pewinternet.org/2015/04/01/us-smartphone-use-in-2015/ (July 2015).

Roberts, T.M., 2013, Using technology for active learning in general education geology labs: Geological Socity of America Abstracts with Programs v. 45, no. 7, p. 504.
Virtual Field Trips, 2014, Geosc 101: https://www.e-education.psu.edu/geosc10/l9tip4.html (February 2014).
Wawrzyniec, T.F., Jones, R.R., McCaffrey, K.M., Imber, J., Holliman, N., Holdsworth, R.E., 2007, Introduction: Unlocking 3D earth systems – Harnessing new digital technologies to revolutionize multi-scale geological models: Geosphere, v. 3, no., 6., p. 406-407.
Whitmeyer, S.J., Mogk, D.W., Pyle, E.J., 2011, Field Geology Education: Historical Perspecives and Modern Approaches: Environmental and Engineering Geoscience, v. XVII, no. 2, p. 201-211.

APPENDICES

Appendix 1: U-Pb Detrital Zircon Data for Southwestern Colorado and New Mexico

Appendix 2: K-S Statistics for units of this Study

Appendix 3: New (U-Th)/He Data

Appendix 4: Compiled (U-Th)/He Data for Wyoming, Colorado, and New Mexico

Appendix 5: Compiled Apatite FissionTrack Data for Wyoming, Colorado, and New Mexico

Appendix 1: U-Pb Detrital Zircon Data for Southwestern Colorado and New Mexico

Appendix 1 is available electronically in supplementary materials.

Appendix 2: K-S Statistics for units of this Study

Table 2. K-S statistics by unit						
McDermott Member						
Analysis run on: Wednesday, Feb 10, 2016 @ 10:09:41 AM. Version: 1.0.						
	K-S P-values using error in the CDF					
	WP53	WP53B	MSD-10-02	MSD-10-04	WP56	
WP53		0.002	0.000	**0.097**	0.000	
WP53B	0.002		0.000	0.001	0.000	
MSD-10-02	0.000	0.000		0.000	**0.522**	
MSD-10-04	**0.097**	0.001	0.000		0.000	
WP56	0.000	0.000	**0.522**	0.000		
Baca Formation						
Analysis run on: Monday, Feb 8, 2016 @ 10:59:32 AM. Version: 1.0.						
	K-S P-values using error in the CDF					
	SCATH2012-1	MSD-NM-2012-1				
Sample A		0.010				
Sample B	0.010					
Galisteo Formation						
Analysis run on: Wednesday, Feb 10, 2016 @ 10:14:21 AM. Version: 1.0.						
	K-S P-values using error in the CDF					
	MSD-NM-2011-23	MSD-NM-2011-25	MSD-NM-2011-26			
MSD-NM-2011-23		0.001	**0.358**			
MSD-NM-2011-25	0.001		0.046			
MSD-NM-2011-26	**0.358**	0.046				
San Jose Formation						
Analysis run on: Wednesday, Feb 10, 2016 @ 09:58:27 AM. Version: 1.0.						
	K-S P-values using error in the CDF					
	WP46	WP32				
Sample A		0.000				

Sample B	0.000					
Ojo Alamo Formation						
Analysis run on: Wednesday, Feb 10, 2016 @ 10:19:36 AM. Version: 1.0.						
	K-S P-values using error in the CDF					
	WP27	WP36	WP63A			
WP27		**0.396**	**0.482**			
WP36	**0.396**		**0.509**			
WP63A	**0.482**	**0.509**				
Nacimiento Formation						
Analysis run on: Wednesday, Feb 10, 2016 @ 10:22:08 AM. Version: 1.0.						
	K-S P-values using error in the CDF					
	WP26	WP34				
WP26		0.000				
WP34	0.000					
Animas Formation						
Analysis run on: Wednesday, Feb 10, 2016 @ 10:29:14 AM. Version: 1.0.						
	K-S P-values using error in the CDF					
	WP44	WP45	WP57	WP57vc	WP57cc	
WP44		0.001	0.001	0.000	0.006	
WP45	0.001		**0.761**	**0.476**	**0.368**	
WP57	0.001	**0.761**		**0.320**	**0.426**	
WP57vc	0.000	**0.476**	**0.320**		**0.764**	
WP57cc	0.006	**0.368**	**0.426**	**0.764**		
Telluride Conglomerate						
Analysis run on: Monday, Feb 29, 2016 @ 11:38:59 AM. Version: 1.0.						
	K-S P-values using error in the CDF					
	MS-10-7	MS-10-9	MSD-CO-2011-17	MSD-CO-2011-18	WP42	WP43
MS-10-7		0.044	0.000	0.022	**0.058**	0.000
MS-10-9	0.044		**0.422**	**0.491**	**0.433**	0.000
MSD-CO-2011-17	0.000	**0.422**		**0.219**	0.037	0.000
MSD-CO-2011-18	0.022	**0.491**	**0.219**		**0.065**	0.000

WP42	**0.058**	**0.433**	0.037	**0.065**		0.000
WP43	0.000	0.000	0.000	0.000	0.000	
Wp52	0.000	0.006	0.010	0.003	0.008	**0.481**
Blanco Basin Formation						
Analysis run on: Monday, Feb 29, 2016 @ 11:43:52 AM. Version: 1.0.						
	K-S P-values using error in the CDF					
	MSD-Co-2011-13	MSD-CO-2011-14	DG-BristerE-PCA-2011	DG-BristerE-PC3B-2011	DG-BristerE-PC5-2011	
MSD-Co-2011-13		**0.078**	0.000	0.000	0.000	
MSD-CO-2011-14	**0.078**		0.000	0.000	0.000	
DG-BristerE-PCA-2011	0.000	0.000		**0.649**	**0.311**	
DG-BristerE-PC3B-2011	0.000	0.000	**0.649**		**1.000**	
DG-BristerE-PC5-2011	0.000	0.000	**0.311**	**1.000**		
El Rito-Ritito						
Analysis run on: Monday, Feb 29, 2016 @ 11:46:14 AM. Version: 1.0.						
	K-S P-values using error in the CDF					
	MS-11-1 El Rito	MS-11-5 El Rito	MS-11-2 Ritito	MS-11-4 Ritito		
MS-11-1 El Rito		0.002	0.000	0.002		
MS-11-5 El Rito	0.002		0.000	0.000		
MS-11-2 Ritito	0.000	0.000		0.000		
MS-11-4 Ritito	0.002	0.000	0.000			

Appendix 3: New (U-Th)/He Data

sample name	12B943_MS_10_9_Ap1	12B944_MS_10_9_Ap2	12B945_MS_10_9_Ap3	12B946_MS_10_9_Ap4	12B947_MS_10_9_Ap5	12B948_MS_10_10_Ap1
sample/run type	ap	ap	ap	ap	ap	ap
He date	10/11/2012	10/11/2012	10/11/2012	10/11/2012	10/11/2012	10/11/2012
pmol He	0.885332	0.00035	0.010016	0.003625	0.021349	0.71515
1s ± pmol He	0.0055	2.86E-05	0.000146	8.85E-05	0.000184	0.003826
% 1s ± He	0.621291	8.165174	1.456349	2.439802	0.861824	0.535063
U+Th date	10/25/2012	10/25/2012	10/25/2012	10/25/2012	10/25/2012	10/25/2012
(238/233)m	0.075002	0.014785	0.012574	0.036108	0.007697	0.263497
(238/233)m 1s ±	0.000227	0.000178	0.000156	0.000361	0.000495	0.000631
(232/229)m	0.091437	0.01676	0.031931	0.120344	0.010414	0.544139
(232/229)m 1s ±	0.000276	0.000168	0.000299	0.000436	0.000853	0.003569
(152/147)m	0.110843	0.027115	0.11035	0.46742	0.033444	0.418776
(152/147)m 1s ±	0.001127	0.000263	0.000668	0.001187	0.000173	0.001133
ng U	0.033424	0.005615	0.004594	0.015462	0.002342	0.120473
1s ± ng U	0.000475333	8.75557E-05	7.25593E-05	0.000231175	0.000107469	0.001709909
% 1s ± ng U	1.422132	1.559304	1.579442	1.495089	4.589307	1.419327
ng Th	0.047162	0.008099	0.016035	0.062283	0.00478	0.283964
1s ± ng Th	0.00067207	0.000121668	0.000238074	0.000889285	0.000210893	0.004113217
% 1s ± ng Th	1.425034	1.502218	1.484722	1.427822	4.412256	1.4485
ng Sm	0.237549	0.049347	0.236385	1.306992	0.062945	1.128205
1s ± ng Sm	0.003581	0.000746	0.003435	0.018696	0.000911	0.016144
% 1s ± ng Sm	1.50765	1.511199	1.452964	1.430431	1.446783	1.430913
Th/U	1.45	1.48	3.58	4.13	2.09	2.42
raw date (Ma)	2923.40	8.55	211.30	21.12	1032.48	668.79
1s ± date (Ma)	45.47	0.71	3.81	0.55	37.17	7.98
1s ± date %	1.56	8.25	1.80	2.62	3.60	1.19

sample name	12B949_MS_10_10_Ap2	12B950_MS_10_10_Ap3	12B951_MS_10_10_Ap4	*12B952_MS_10_10_Ap5*	12B953_MSD_11_4_Ap1	12B954_MSD_11_4_Ap2
sample/run type	ap	ap	ap	*ap*	ap	ap
He date	10/11/2012	10/11/2012	10/11/2012	*10/11/2012*	10/12/2012	10/12/2012
pmol He	0.065569	0.001313	0.048909	*4.273345*	0.006044	0.0345
1s ± pmol He	0.000388	0.000132	0.000284	*0.0255*	9.8E-05	0.000237
% 1s ± He	0.591703	10.03379	0.581047	*0.596729*	1.621196	0.68601
U+Th date	10/25/2012	10/25/2012	10/25/2012	*10/25/2012*	10/25/2012	10/25/2012
(238/233)m	0.150312	0.207172	0.040664	*0.195735*	0.027897	0.150067
(238/233)m 1s ±	0.000387	0.000827	0.000402	*0.000471*	0.000178	0.000446
(232/229)m	0.548708	0.40486	0.33333	*0.31671*	0.055382	0.059189
(232/229)m 1s ±	0.000954	0.001979	0.002615	*0.001432*	0.000049	0.000935
(152/147)m	0.855976	0.244247	0.29586	*0.288118*	0.060576	0.411992
(152/147)m 1s ±	0.002469	0.000569	0.001157	*0.000634*	0.000809	0.002683
ng U	0.068203	0.094462	0.017566	*0.08918*	0.01167	0.06809
1s ± ng U	0.000968512	0.001347687	0.000262095	*0.001265816*	0.0001692	0.000968
% 1s ± ng U	1.420042	1.426702	1.492036	*1.419396*	1.449833	1.421649
ng Th	0.286354	0.211109	0.173693	*0.164999*	0.028302	0.030293
1s ± ng Th	0.004067617	0.003029839	0.002538384	*0.002364119*	0.000401659	0.000482196
% 1s ± ng Th	1.420486	1.435201	1.461423	*1.432809*	1.419196	1.591761
ng Sm	3.407511	0.579681	0.728501	*0.705523*	0.122367	1.104278
1s ± ng Sm	0.04919	0.008274	0.010474	*0.010068*	0.001917	0.016258
% 1s ± ng Sm	1.443575	1.427287	1.437734	*1.426975*	1.566845	1.472274
Th/U	4.31	2.29	10.14	*1.90*	2.49	0.46
raw date (Ma)	86.32	1.68	151.08	*5607.96*	60.29	83.03
1s ± date (Ma)	0.97	0.17	1.85	*73.27*	1.16	1.17
1s ± date %	1.12	10.09	1.23	*1.31*	1.92	1.41

sample name	12B955_MSD_11_4_Ap3	12B956_MSD_11_4_Ap4	12B957_MSD_11_4_Ap5	12B958_MSD_2011_CO_13_Ap1	12B959_MSD_2011_CO_13_Ap2	12B960_MSD_2011_CO_13_Ap3
sample/run type	ap	ap	ap	ap	ap	ap
He date	10/12/2012	10/12/2012	10/12/2012	10/12/2012	10/12/2012	10/12/2012
pmol He	0.005065	0.046573	0.234501	0.053863	0.008259	0.001992
1s ± pmol He	0.000141	0.00045	0.001295	0.000457	0.000127	6.04E-05
% 1s ± He	2.788508	0.967151	0.552317	0.848317	1.533264	3.029332
U+Th date	10/25/2012	10/25/2012	10/25/2012	10/25/2012	10/25/2012	10/25/2012
(238/233)m	0.006561	0.109303	0.105581	0.012478	0.092166	0.035231
(238/233)m 1s ±	0.000091	0.000658	0.000323	0.000177	0.00036	0.000173
(232/229)m	0.035257	0.059992	0.092081	0.033414	0.141207	0.026444
(232/229)m 1s ±	0.000138	0.000524	0.000464	0.000224	0.000315	0.000253
(152/147)m	0.015805	0.14454	0.21512	0.230922	0.280005	0.031882
(152/147)m 1s ±	0.000148	0.000606	0.000547	0.001462	0.001464	0.000529
ng U	0.001817	0.049265	0.047546	0.00455	0.041351	0.015057
1s ± ng U	3.18515E-05	0.000710313	0.000676165	7.40402E-05	0.000589896	0.000216065
% 1s ± ng U	1.752868	1.441832	1.422136	1.627382	1.426575	1.434954
ng Th	0.017775	0.030713	0.047499	0.016811	0.073196	0.013165
1s ± ng Th	0.000254288	0.000452607	0.000682427	0.000244251	0.001040809	0.000196036
% 1s ± ng Th	1.430614	1.473652	1.436731	1.452951	1.421953	1.489096
ng Sm	0.025291	0.318715	0.500018	0.542866	0.681698	0.05958
1s ± ng Sm	0.000386	0.004581	0.007141	0.007925	0.009881	0.000989
% 1s ± ng Sm	1.527263	1.437325	1.428087	1.459802	1.449438	1.659348
Th/U	10.04	0.64	1.02	3.79	1.82	0.90
raw date (Ma)	153.87	149.96	691.61	1020.90	25.70	20.23
1s ± date (Ma)	4.64	2.36	9.19	14.21	0.48	0.66
1s ± date %	3.02	1.57	1.33	1.39	1.85	3.25

sample name	12B961_MSD_2011_CO_1 3_Ap4	12B962_MSD_2011_CO_1 3_Ap5	*12B963_MSD_CO_2011_1 4_Ap1*	12B964_MSD_CO_2011_1 4_Ap2	12B965_MSD_CO_2011_1 4_Ap3	12B966_MSD_CO_2011_1 4_Ap4
sample/run type	ap	ap	*ap*	ap	ap	ap
He date	10/12/2012	10/12/2012	*10/15/2012*	10/15/2012	10/15/2012	10/15/2012
pmol He	0.004678	0.004898	*1.958129*	0.019671	0.014351	0.123278
1s ± pmol He	9.5E-05	6.78E-05	*0.011731*	0.000259	0.000259	0.000836
% 1s ± He	2.031038	1.383427	*0.599102*	1.31721	1.805629	0.678359
U+Th date	10/25/2012	10/25/2012	*10/25/2012*	10/25/2012	10/25/2012	10/25/2012
(238/233)m	0.029362	0.030799	*0.038775*	0.111952	0.057452	0.036077
(238/233)m 1s ±	0.000111	0.00034	*0.000165*	0.000687	0.000299	0.000286
(232/229)m	0.070656	0.053495	*0.036788*	0.133605	0.09982	0.246482
(232/229)m 1s ±	0.000556	0.000285	*0.000458*	0.000511	0.000248	0.001728
(152/147)m	0.113046	0.043905	*0.181172*	0.421122	0.518694	0.338541
(152/147)m 1s ±	0.000564	0.000394	*0.00071*	0.001861	0.002266	0.001307
ng U	0.012347	0.013011	*0.016694*	0.050488	0.025319	0.015448
1s ± ng U	0.00017623	0.00019706	*0.000238697*	0.000728456	0.000363599	0.000226458
% 1s ± ng U	1.427327	1.514622	*1.429845*	1.442832	1.436061	1.465943
ng Th	0.036291	0.027315	*0.018576*	0.069219	0.051547	0.128264
1s ± ng Th	0.000530975	0.000393192	*0.000284527*	0.000989049	0.000733451	0.001863605
% 1s ± ng Th	1.463085	1.439483	*1.531725*	1.428864	1.422884	1.452949
ng Sm	0.242755	0.085636	*0.410821*	1.136535	1.510321	0.859592
1s ± ng Sm	0.003503	0.001277	*0.005899*	0.016431	0.02188	0.012363
% 1s ± ng Sm	1.443153	1.491376	*1.435864*	1.445686	1.44873	1.438196
Th/U	3.02	2.15	*1.14*	1.41	2.09	8.52
raw date (Ma)	40.75	46.25	*na*	53.27	67.35	476.44
1s ± date (Ma)	0.92	0.81	*211.77*	0.91	1.39	6.01
1s ± date %	2.26	1.76	*0.00*	1.71	2.07	1.26

sample name	12B967_MSD_CO_2011_14_Ap5	12B968_MSD_CO_17_Ap1	*12B969_MSD_CO_17_Ap2*	12B970_MSD_CO_17_Ap3	12B971_MSD_CO_17_Ap4	12B972_MSD_CO_17_Ap5
sample/run type	ap	ap	*ap*	ap	ap	ap
He date	10/15/2012	10/15/2012	*10/15/2012*	10/15/2012	10/15/2012	10/15/2012
pmol He	0.034813	0.010166	*0.457608*	0.002571	0.000912	0.003297
1s ± pmol He	0.000279	0.000137	*0.003758*	0.000243	3.92E-05	0.00014
% 1s ± He	0.800766	1.347486	*0.821208*	9.441229	4.300407	4.245868
U+Th date	10/25/2012	10/25/2012	*10/25/2012*	10/25/2012	10/25/2012	10/25/2012
(238/233)m	0.184097	0.145274	*0.00782*	0.055726	0.033878	0.047558
(238/233)m 1s ±	0.002368	0.000477	*0.00007*	0.000747	0.000256	0.000365
(232/229)m	0.28018	0.379402	*0.007596*	0.146302	0.063833	0.105561
(232/229)m 1s ±	0.000751	0.001565	*0.000066*	0.00089	0.000468	0.000487
(152/147)m	0.516136	0.759473	*0.013816*	0.477998	0.180627	0.299868
(152/147)m 1s ±	0.00308	0.002587	*0.000272*	0.002246	0.000611	0.001543
ng U	0.083805	0.065876	*0.002399*	0.024522	0.014432	0.02075
1s ± ng U	0.001282889	0.000937473	*3.68944E-05*	0.000379784	0.00021098	0.000303175
% 1s ± ng U	1.530796	1.423078	*1.538211*	1.54874	1.461845	1.461084
ng Th	0.145891	0.197792	*0.003306*	0.075861	0.032722	0.05455
1s ± ng Th	0.002076689	0.002829172	*4.99896E-05*	0.001095954	0.00047692	0.000782086
% 1s ± ng Th	1.423457	1.430376	*1.51225*	1.44469	1.45747	1.43371
ng Sm	1.499787	2.737181	*0.021092*	1.347633	0.40942	0.740491
1s ± ng Sm	0.022066	0.039598	*0.000395*	0.019555	0.005864	0.010732
% 1s ± ng Sm	1.471264	1.446686	*1.872805*	1.451036	1.432347	1.449244
Th/U	1.79	3.08	*1.41*	3.17	2.33	2.70
raw date (Ma)	53.54	16.23	*na*	10.80	7.46	17.67
1s ± date (Ma)	0.73	0.27	*377.08*	1.03	0.33	0.77
1s ± date %	1.37	1.66	*0.00*	9.50	4.42	4.37

sample name	12B973_MSD_2011_NM_23_Ap1	12B974_MSD_2011_NM_23_Ap2	12B975_MSD_2011_NM_23_Ap3	12B976_MSD_2011_NM_23_Ap4	12B977_MSD_2011_NM_23_Ap5	Nblk
sample/run type	ap	ap	ap	ap	ap	0
He date	10/17/2012	10/17/2012	10/17/2012	10/17/2012	10/17/2012	1/0/1900
pmol He	0.089851	0.043591	0.007853	0.000719	0.005383	#DIV/0!
1s ± pmol He	0.001052	0.000534	0.000145	4.84E-05	0.000104	#DIV/0!
% 1s ± He	1.170366	1.224064	1.849188	6.736963	1.934715	#DIV/0!
U+Th date	10/25/2012	10/25/2012	10/25/2012	10/25/2012	10/25/2012	10/25/2012
(238/233)m	0.554884	0.279964	0.08157	0.006707	0.065482	0.003148
(238/233)m 1s ±	0.002985	0.001127	0.000665	0.000065	0.001099	0.000075
(232/229)m	0.2433	0.321262	0.053347	0.0206	0.085239	0.001887
(232/229)m 1s ±	0.001204	0.001361	0.000076	0.000209	0.000648	0.000182
(152/147)m	0.666524	0.10871	0.152718	0.01419	0.116875	0.004006
(152/147)m 1s ±	0.002727	0.000646	0.000252	0.000201	0.000624	0.000281
ng U	0.255039	0.128078	0.036457	0.001885	0.029028	0.000241
1s ± ng U	0.003661583	0.00182744	0.000533908	2.9858E-05	0.000469332	1.58606E-05
% 1s ± ng U	1.435694	1.426819	1.464481	1.584371	1.616849	6.582711
ng Th	0.126599	0.16738	0.027237	0.010108	0.04392	0.000319
1s ± ng Th	0.001817584	0.002395291	0.000386809	0.000151677	0.000641159	4.35377E-05
% 1s ± ng Th	1.4357	1.431049	1.420141	1.500588	1.459845	13.63339
ng Sm	2.200946	0.232521	0.338919	0.021881	0.251837	0.00052
1s ± ng Sm	0.031956	0.003376	0.004828	0.000365	0.003642	0.000263
% 1s ± ng Sm	1.45192	1.451826	1.424437	1.667071	1.446246	50.47518
Th/U	0.51	1.34	0.77	5.50	1.55	1.36
raw date (Ma)	57.70	47.97	33.56	30.90	25.09	
1s ± date (Ma)	0.99	0.79	0.74	2.11	0.57	
1s ± date %	1.71	1.65	2.21	6.83	2.28	

Appendix 4: Compiled AFT Data for Wyoming, Colorado, and New Mexico

Appendix 4 is available electronically in supplementary materials.

Appendix 5: Compiled (U-Th)/He Data for Wyoming, Colorado, and New Mexico

Appendix 5 is available electronically in supplementary materials.